ROBUST WATERMARKING TECHNIQUES FOR SCALABLE CODED IMAGE AND VIDEO

submitted by

Deepayan Bhowmik

for the degree of

Doctor of Philosophy

of the

Department of Electronic and Electrical Engineering
The University of Sheffield

December, 2010

ABSTRACT

In scalable image/video coding, high resolution content is encoded to the highest visual quality and the bit-streams are adapted to cater various communication channels, display devices and usage requirements. These content adaptations, which include quality, resolution and frame rate scaling may also affect the content protection data, such as, watermarks and are considered as a potential watermark attack. In this thesis, research on robust watermarking techniques for scalable coded image and video, are proposed and the improvements in robustness against various content adaptation attacks, such as, JPEG 2000 for image and Motion JPEG 2000, MC-EZBC and H.264/SVC for video, are reported. The spread spectrum domain, particularly wavelet-based image watermarking schemes often provides better robustness to compression attacks due to its multi-resolution decomposition and hence chosen for this work. A comprehensive and comparative analysis of the available wavelet-based watermarking schemes, is performed by developing a new modular framework, Watermark Evaluation Bench for Content Adaptation Modes (WEBCAM). This analysis is used to derive a watermark embedding distortion model, that establishes a directly proportional relationship between the sum of energy of the selected wavelet coefficients and the distortion performance, *i.e.,* mean square error (MSE) in spatial domain. On the other hand, the improvements on robustness is achieved by modeling the bit plane discarding, which analyzes the effect of the quantization and de-quantization within the image coder and ranks the wavelet coefficients and other parameters according to their ability to retain the watermark data intact under quality scalable coding-based content adaptation. The work, then, extends these image watermarking models in video watermarking. But a direct extension of the image watermarking methods into frame by frame video watermarking without considering motion, results in flicker and other motion mismatch artifacts in the watermarked video. Motion compensated temporal filtering (MCTF) provides a good framework for accounting the motion. A generalized MCTF-based spatio-temporal decomposition domain (2D+t+2D) video watermarking framework is developed to address such issues. Improvements on imperceptibility and robustness are achieved by embedding the watermark in 2D+t compared to traditional t+2D MCTF based watermarking schemes. Finally, the research outcomes, discussed above, are combined to propose a novel concept of scalable watermarking scheme, that generates a distortion constrained robustness scalable watermarked media code stream which can be truncated at various points to generate the watermarked image or video with the desired distortion-robustness requirements.

Dedicated to my parents.

ACKNOWLEDGEMENTS

I am grateful to my parents to motivate and encourage me for this long and enduring journey, called PhD. I take this opportunity to express my sincere gratitude to Dr. Charith Abhayaratne for guiding and sailing me through the entire process. I feel fortunate to have him as my supervisor who helped me to learn not only the technical aspects but also the integrity of this degree. I wish to thank UK Engineering and Physical Sciences Research Council (EPSRC) for funding this work through an EPSRC-BP Dorothy Hodgkin Postgraduate Award (DHPA). I am specially thankful to Dr. Sanchita Bandyopadhyay, Dr. Subrata B. Ghosh, Ms. Ritu Sengupta, Mr. Subrato Chatterjee and Dr. Bala Amavasai for their encouragement and support. Finally, I like to thank Mr. James Screaton for the technical support, Mr. Mathew Oakes for helping me in proof reading, my colleagues in Visual and Information Engineering (VIE) lab and the last but not least, my friends in Sheffield.

Contents

List of Figures

List of Tables

List of Symbols and Acronyms

Symbols

Symbol	Description
Q	Quality scalability
S	Spatial scalability
T	Temporal scalability
$\zeta()$	Embedding function
$\varpi()$	Extraction function
I	Original host image
I'	Watermarked image
$X \times Y$	Image dimension
W	Watermark
W'	Extracted watermark
Ψ	Mother wavelet
C	Original wavelet coefficient
C'	Modified wavelet coefficient
Δ	Watermark modification
α	Watermarking weight factor for magnitude alteration based method
τ	Watermarking strength
v	HVS based weighting parameter
β	Fusion strength parameter
δ	Quantization step
$\hat{\delta}$	Reconstructed quantization step
γ	Watermark weighting parameter for re-quantization based method
H	Hamming Distance
S	Similarity Measure

Symbol	Description
L	Length of watermark sequence
x	Input signal
y	Transformed domain signal
$h'(z)$	Low pass filter coefficients
$g'(z)$	High pass filter coefficients
$W_t^{\Theta\Upsilon}$	Wavelet weighting parameter at Θ subband at Υ decomposition level
C_q	Quantized coefficient
$\hat{C}$	De-quantized coefficient
Q	Quantization factor
b	Binary bit $b \in \{0, 1\}$
b'	Recovered binary bit $b' \in \{0, 1\}$
T	Threshold parameter in magnitude alteration based watermark extraction
N	Number of bit planes assumed to be discarded
p	Number of bit plane actually being discarded
$\mathcal{V}$	Vertical displacement of motion block
$\mathcal{H}$	Horizontal displacement of motion block
λ	Binary tree quantizer
d	Depth of binary tree
Φ	Embedding distortion rate

Acronyms

Acronym	Description
AVC	Advanced Video Coding
DCT	Discrete Cosine Transform
DFT	Discrete Fourier Transform
DIA	Digital Item Adaptation
DWT	Discrete Wavelet Transform
FDWT	Forward Discrete Wavelet Transform
HVS	Human Visual System
IDWT	Inverse Discrete Wavelet Transform
JND	Just Noticeable Difference
JPEG	Joint Photographic Experts Group
MB	Macro-Block
MC-EZBC	Motion Compensated Embedded Zero Block Coding
MCTF	Motion Compensated Temporal Filtering
MMCTF	Modified Motion Compensated Temporal Filtering
MPEG	Moving Picture Experts Group
MSE	Mean Square Error
MV	Motion Vector
PSNR	Peak Signal to Noise Ratio
RMSE	Root Mean Square Error
SR	Search Range
SSIM	Structural Similarity Measure
SVC	Scalable Video Coding
UMA	Universal Media Access
WEBCAM	Watermarking Evaluation Bench for Content Adaptation Modes
WET	Watermark Evaluation Test bed
WO	Weak One
WZ	Weak Zero
CO	Cumulative One
CZ	Cumulative Zero
EO	Embedded One
EZ	Embedded Zero

Statement of Originality

The research conducted within the scope of this thesis produced the following novel and unique contributions towards robust watermarking techniques for scalable coded image and video:

Chapter 3

- State of the art analysis.

Chapter 4

- Generalization and dissection of wavelet based image watermarking schemes and the related parameters, *i.e.,* wavelet kernel, subband, host coefficients and embedding methods.
- Design and implementation of the modular and reconfigurable tool repository to develop WEBCAM framework.
- Providing evaluation platform for comparison of robustness performances against content adaptation attacks, including JPEG 2000.
- Comprehensive analysis and the comparison of various parametric inputs within WEBCAM framework.

Chapter 5

- Development of the watermark embedding distortion model.
- Relationships between the mean square error (MSE) and the wavelet coefficients to be embedded.
- Proof of concept of the model for non-blind and blind watermarking algorithms.
- Proof of concept of the model for orthonormal wavelet transforms.
- Proof of concept of the model for non-orthonormal wavelets by using weighting parameters for various wavelet kernels in different subbands.

Chapter 6

- Modeling of bit plane discarding, used in quality scalability, into the wavelet based watermarking.
- Establishing the relationship between watermark input parameters and bit plane discarding model.
- Design and implementation of enhanced robust watermarking algorithm for non-blind watermarking by coefficient ranking using the above model.
- Proof of concept to enhance the robustness in blind watermarking schemes, based on the bit plane discarding model.

Chapter 7

- Development of modified MCTF for video decomposition using lifting Haar.
- Design and implementation of generalized 2D+t+2D framework in wavelet domain.
- Comparative performance analysis of t+2D and 2D+t based watermarking.
- Robust video watermarking techniques against Motion JPEG 2000, MC-EZBC and H.264/SVC.

Chapter 8

- Defining common performance metric to represent data-capacity and embedding distortion.
- Design and implementation of scalable watermarking.
- Development of new binary tree-guided rules-based blind watermarking scheme.
- Scalable code stream generation using hierarchically nested joint distortion-robustness coding atoms.
- Proof concept of scalable watermarking by truncating the code-stream atom at any distortion-robustness atom level.
- Compliance of scalable watermarking with robust watermarking techniques for scalable coded image and video.

Chapter 1

Introduction

Recent years have seen the emergence of scalable coding standards for multimedia content coding: JPEG 2000 for images [1]; MPEG advanced video coding (AVC)/H.264 scalable video coding (SVC) extension for video [2]; and MPEG-4 scalable profile for audio [3]. The scalable coders produce scalable bit streams representing content in hierarchical layers according to audiovisual quality, spatio-temporal resolutions and regions-of-interests. The bit streams may be accordingly truncated in order to satisfy variable network data rates, display resolutions, display device resources and usage preferences. The new bit streams may be transmitted or further adapted or decoded using a universal decoder which is capable of decoding any original or adapted bit streams to display or play adapted versions of the original content in terms of quality or reductions. The multimedia usage framework standard, MPEG-21, standardizes the operation of a content-agnostic content adaptation engine as the part 7 of the standard: Digital Item Adaptation (DIA) [4]. Such bit stream truncation-based content adaptations also affect any content protection data, such as watermarks, embedded in the original content. This thesis considers the scalable coding based content adaptation as potential watermark attacks and present novel watermarking techniques, robust to such attacks particularly quality scalability. Within the scope of the thesis, this work focuses on the watermarking robustness of scalable coded image and extends those methods suitably in scalable coded video watermarking.

1.1 Scalable coded image watermarking

Influenced by its success in scalable image coding and multi-resolution decomposition capability, the DWT has been widely used in image watermarking [5–26]. Based on the embedding methodology, wavelet-based image watermarking can be categorized into two main classes: uncompressed domain algorithms [5–18] and joint compression-watermarking algorithms [19–26]. One of the main objectives of the latter class of algorithms is to accommodate watermarking algorithms within JPEG 2000 based scalable image coding as suggested by JPEG 2000 Part 8 (ISO/IEC 15444-8, T.807) Secure JPEG 2000 (JPSEC) [20] specification to secure JPEG 2000 bit streams. However the major drawbacks of the compression domain algorithms are its dependency on the specific coding scheme and the complexity to accommodate the algorithms within the coding pipeline. Therefore, uncompressed domain watermarking approaches, independent of the coding schemes, are considered here.

In order to propose robust watermarking techniques for scalable coded images, the objectives are broadly categorized as:

O.1 To analyze the existing schemes: The wavelet based watermarking schemes often share a common model. A comprehensive analysis of the existing schemes is presented by dissecting commonly used wavelet based watermarking algorithms into modular tool blocks and fitting them into a common wavelet-based watermarking framework, Watermark Evaluation Bench for Content Adaptation Modes (WEBCAM). Such analysis helps to develop models for embedding distortion and robust watermarking schemes.

O.2 To model watermarking robustness against scalable compression: To enhance the robustness against scalable compression such as JPEG 2000, the quantization process is analyzed in the context of watermarking. However the embedding distortion performance is also taken into account for the analysis, to balance imperceptibility and robustness. The research findings from these are used to propose a new scalable watermarking scheme later in this thesis. Hence objective O.2 is further categorized into following two sub-objectives:

O.2.1 To model embedding distortion: The embedding distortion and the robustness to scalable image coding are two complementary watermarking requirements. In order to increase the robustness often imperceptibility is compromised. The aim of this objective is to derive a model to find suitable relationships between the wavelet coefficients and the watermarking distortion in pixel domain.

O.2.2 To model quantization vs. watermarking robustness: The robustness performance deteriorates due to the scalable compression in content adaptation. The quantization process block within the scalable coding, is often responsible for the quality scaling. Here we aim to propose improved watermarking robustness by modeling the effect of quantization on the wavelet coefficients and rank them accordingly to embed the watermark.

1.2 Scalable coded video watermarking

As a successor of the wavelet based image watermarking, several attempts have been made to extend these image watermarking algorithms into video watermarking by using them either on frame-by-frame basis [27–30] or on 3D wavelet decompositions [9,31,32]. However, such video watermark embedding without considering motion, results in flicker and other motion mismatch artifacts in the watermarked video. Motion compensated temporal filtering (MCTF) provides a better framework for video watermarking by accounting object motion. Depending on the motion and texture characteristics of the video and the choice of spatial-temporal sub band for watermark embedding, MCTF has to be performed either on the spatial domain (t+2D) or in the wavelet domain (2D+t). In this thesis improved video watermarking schemes are proposed by offering a generalized motion compensated 2D+t+2D framework for watermark embedding. The watermarking algorithms derived for scalable coded images, as proposed in O.1 and O.2, are then extended to offer robust video watermarking schemes. Also an improved MCTF is used by modifying the MCTF update step to follow the motion trajectory in hierarchical temporal decomposition by using direct motion vector fields in the update step and implied motion vectors in the prediction step. In summary the main objectives of the robust video watermarking schemes are

O.3 To prepare 2D+t+2D framework: We aim to prepare a generalized modified MCTF based 2D+t+2D in order to analyze the motion and texture suitable for video watermarking.

O.4 To model the video watermarking schemes: The watermarking algorithms derived during robustness model for images are now extended to video watermarking within the generalized 2D+t+2D framework to offer a unique model for video watermarking, which is robust to content adaptation attacks, such as, scalable compression in Motion JPEG 2000, scalable video coder MC-EZBC [33] and H.264/SVC.

1.3 Scalable watermarking for image and video

Although, a wide variety of watermarking schemes have been offered to the date, a fundamentally traditional concept is still followed in almost all the schemes, including the robust watermarking techniques, proposed in previous objectives. With the increased use of scalable coded media, a need is realized for scalable watermarking. However, a little work has been proposed so far towards scalable watermarking [34–38]. The final part of this thesis aims to propose a novel concept of scalable watermarking as opposed to traditional watermarking schemes by creating hierarchically nested joint distortion-robustness coding atoms. The main objective of this part is:

O.5 To propose scalable watermarking: The research outcomes, proposed in different objectives above, are combined to model a novel concept of scalable watermarking scheme, that can generate a distortion constrained robustness scalable watermarked media code stream which can be truncated at various points to generate the watermarked image or video with the desired distortion-robustness requirements.

1.4 Thesis organization

Rest of the thesis is structured in eight different chapters, the contents of which are summarized as bellow:

Chapter 2 provides the background overview of content adaptation and digital watermarking. Scalabale coding structure, compression and application scenarios are briefed within the overview of content adaptation followed by a general discussion on digital watermarking, including, its properties, applications and attacks. Various wavelet transforms related to the proposed watermarking schemes are the discussed briefly to provide sufficient background of the work.

Chapter 3 presents the state-of-the-art analysis of the current literature on watermarking techniques for content adaptation attacks, which includes wavelet domain image and video watermarking, MCTF based video watermarking, compressed and uncompressed domain watermarking algorithms etc.

Chapter 4 offers a content adaptation test bed framework (WEBCAM), for evaluating the robustness of wavelet based watermarking. Overall, the framework facilitates and presents a parametric study of various variables in wavelet based watermarking

and proposes a watermark tweezing tool to balance the embedding distortion and the robustness to scalable coding-based content adaptation using the tools repository.

Chapter 5 presents a model for embedding distortion performance for wavelet based watermarking. The model derives the relationship between distortion performance metrics and the watermark embedding parameter, *i.e.,* wavelet coefficients and the related propositions are made separately for orthonormal and non-orthonormal wavelet bases.

Chapter 6 addresses the issues related to quality scalable content adaptation and proposes a new embedding criterion to ensure the robustness of the wavelet based image watermarking schemes for such adaptations. The quality scalable image coding is modeled using wavelet domain bit plane discarding to identify the effect of the quantization and de-quantization on wavelet coefficients and the data embedded within such coefficients.

Chapter 7 proposes improved video watermarking schemes by offering a generalized motion compensated 2D+t+2D framework for watermark embedding. An improved MCTF is used by modifying the MCTF update step to follow the motion trajectory in hierarchical temporal decomposition by using direct motion vector fields in the update step and implied motion vectors in the prediction step. The robust image watermarking schemes, described in previous chapter, are then extended in this framework to propose robust video watermarking to content adaptations.

Chapter 8 proposes a novel concept of scalable blind watermarking to generate a distortion constrained robustness scalable watermarked code stream which consists of hierarchically nested joint distortion robustness coding atoms. The code stream is generated using a new wavelet domain binary tree guided rules-based blind watermarking algorithm. The code stream can be truncated at any distortion-robustness atom level to generate the watermarked image with the desired distortion-robustness requirements.

Chapter 9 concludes this thesis by summarizing the research outcomes, *i.e.,* analysis, proposed models and new algorithms on robust watermarking to content adaptation attacks. Novel contributions of this work are also highlighted here along with the suggestions on new ideas for future research in this domain.

1.5 Publications and software releases

During various stages of the work, some of the research outcomes of this thesis have been published or are currently under review in the form of software and refereed publications, which are listed below:

Software Releases

S1. D. Bhowmik and C. Abhayaratne, Watermark Evaluation Bench for Content Adopted Modes (WEBCAM) v2.0 http://svc.group.shef.ac.uk/webcam.html

Book Chapter

B1. D. Bhowmik and C. Abhayaratne, A generalised model for distortion performance analysis of wavelet based watermarking, *Lecture Notes in Computer Science, Springer-Verlag, editor, Proceedings of International Workshop on Digital Watermarking (IWDW '08)*, vol. 5450, November 2008, Busan, South Korea, pp. 363-378.

Conference Proceedings

C9. D. Bhowmik and C. Abhayaratne, Distortion constrained robustness scalable image watermarking. (In preparation)

C8. D. Bhowmik and C. Abhayaratne, Video watermarking using motion compensated 2D+t+2D filtering, in *Proceedings of ACM Workshop on Multimedia and Security (ACM MM&Sec 2010)*, September 2010, Rome, Italy, pp. 127-136.

C7. D. Bhowmik , C. Abhayaratne and M. Oakes, Robustness analysis of blind watermarking for quality scalable image compression, in *Proceedings of 18th European Signal Processing Conference (EUSIPCO 2010)*, August 2010, Denmark, pp. 810-814.

C6. D. Bhowmik and C. Abhayaratne, The effect of quality scalable image compression on robust watermarking, in *Proceedings of Digital Signal Processing (DSP 2009)*, July 2009, Santorini, Greece, pp. 1-8.

C5. D. Bhowmik and C. Abhayaratne, Embedding distortion modeling for wavelet based watermarking schemes, in *Proceedings of Wavelet Applications in Industrial Processing VI , SPIE Electronic Imaging 2009*, vol. 7248, San Jose, CA, USA, January 2009, pp. 72480K (12 pages).

C4. D. Bhowmik and C. Abhayaratne, A framework for evaluating wavelet-based watermarking for scalable coded digital item adaptation attacks, in *Proceedings of Wavelet Applications in Industrial Processing VI , SPIE Electronic Imaging 2009*, vol. 7248, San Jose, CA, USA, January 2009, pp. 72480M (10 pages).

C3. D. Bhowmik and C. Abhayaratne, Evaluation of watermark robustness to JPEG2000 based content adaptation Attacks, in *Proceedings of IET 5th International Conference on Visual Information Engineering (VIE '08)*, July 2008, Xian, China, pp. 789-794.

C2. D. Bhowmik and C. Abhayaratne, A watermark evaluation bench for content adaptation modes, in *Proceedings of IET 4th European Conference on Visual Media Production (CVMP '07)*, November 2007, London, UK, pp. 1.

C1. D. Bhowmik and G. C. K. Abhayaratne, Morphological wavelet domain image watermarking, in *Proceedings of 15th European Signal Processing Conference (EUSIPCO 2007)*, September 2007, Poznan, Poland, pp. 2539-2543.

Chapter 2

Background Overview

Scalable coding-based content adaptation and wavelet-based image and video watermarking are two main components of this thesis. This chapter presents an overview of scalable coding-based content adaptation, digital watermarking and their applications and wavelet-based watermarking, of relevance to this thesis.

2.1 Scalable coding-based content adaptation

The universal media access (UMA) is an important requirement in modern multimedia usage chains. The UMA concept envisages seamless delivery of multimedia across the heterogeneous networks and various devices. This would require catering for different network bandwidths, transmission media, device capabilities, memory and power availability and most importantly the usage preferences. This can only be achieved by intelligent content-agnostic adaptations based on the scalable coded content representations. An example of scalable coding-based multimedia usage is shown in Figure 2.1.

2.1.1 Scalable coding modules

In scalable coding the input media is coded in a way that the main host server keeps bit streams that can be decodable to high quality full resolution content. When the content needs to be delivered to a less capable display or via a lower bandwidth network, the

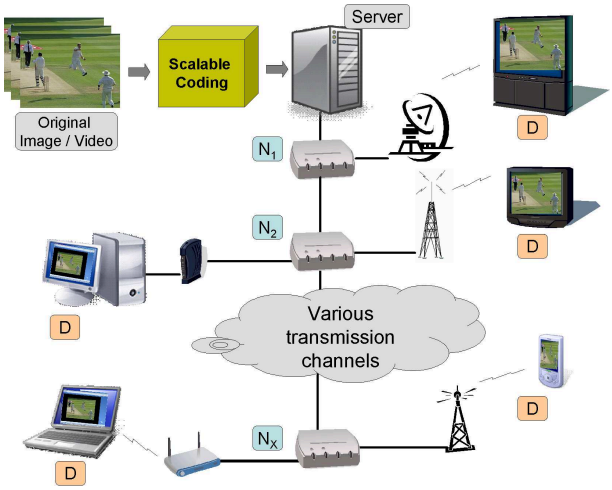

Figure 2.1: Universal multimedia usage scenarios using scalable coded content.

bit stream is adapted at different nodes (N_1, N_2, ... , N_x, as shown in Figure 2.1) using different scaling parameters to match those requirements. At each node the adaptation parameters may be different and a new bit stream may be generated. Finally the adapted bit streams are decoded using a universal decoder. The scalable coding-decoding process consists of three main modules [39]: encoder, extractor and decoder, as shown in Figure 2.2.

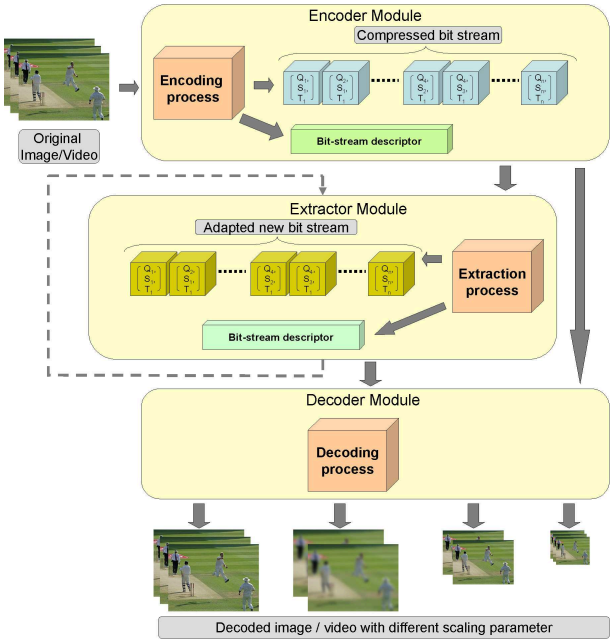

Figure 2.2: The scalable coding-decoding block diagram.

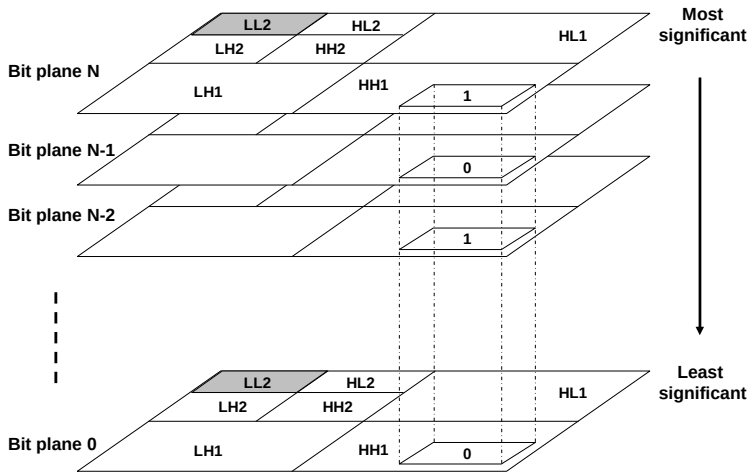

Figure 2.3: Quality scalable encoding process.

The **encoder module** is responsible for producing a full resolution, highest quality compressed bit stream from the original content. The bit stream generation normally focuses on three main functionalities: quality scalability (Q_i), spatial resolution scalability (S_i) and temporal resolution scalability (T_i : for video), where Q_i, S_i and T_i represent the scaling parameters for different quality-spatio-temporal layers with the layer index i. A bit stream descriptor is also generated along with the bit stream describing the location of these layers in the scalable bit stream.

The **extractor module** is part of a cross media engine that adapts the bit streams following the MPEG 21 part-7 DIA specifications. It truncates the scalable bit stream considering the context and produces the adapted bit-stream, which is also scalable and can be re-adapted at any following network node by using another extractor, and its new description.

The **decoder module** provides an universal decoder to decode any adapted bitstream to display the adapted content and may have full spatial, quality or temporal resolution or any combination of a lower resolution.

2.1.2 Scalable coding technique

The fundamental concept of spatio-temporal bitstream generation is shown in Figure 2.3, Figure 2.4 and Figure 2.5, for quality, spatial and temporal scalability, respectively with respect to wavelet decomposition. For quality scalable encoding process, firstly the images / video frames are wavelet decomposed and organized according to the bit plane significance as shown in Figure 2.3, where L and H corresponds to low

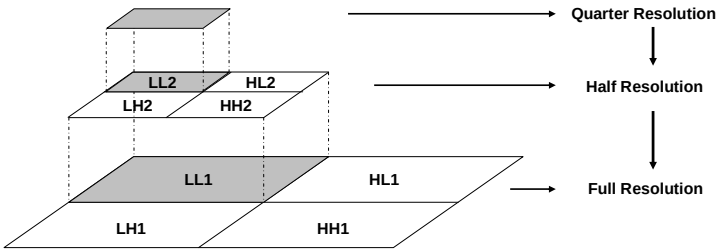

Figure 2.4: Spatial resolution scalable encoding process.

pass and high pass frequency decompositions, respectively. During the quality scaling, bit values from the selected bit planes are considered in a hierarchical order starting from most significant bit plane to least significant bit plane until the target bit rate is achieved. Similarly, for a resolution scaling process, hierarchically low frequency subbands are selected according to scaling requirements (Figure 2.4). To encode temporal scaling, the video frames are temporally decomposed and then organized in a hierarchical order as shown in Figure 2.5. The encoded bitstreams are generated by combining these three scalable coding schemes and putting them in individual concatenated packets in such a way that the extractor can truncate the bit stream at any point to fulfill the scaling requirements. Finally the decoder decodes the truncated bit stream and performs the inverse transform to reconstruct the scaled media.

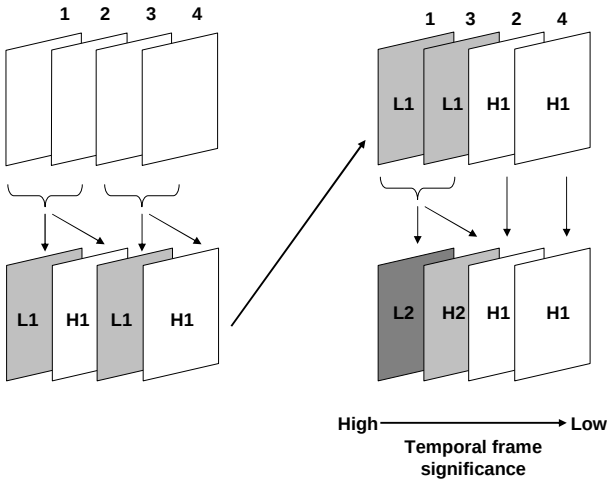

Figure 2.5: Temporal scalable encoding process.

Watermarking Applications		
Sl No.	**Name**	**Description**
1	Broadcast monitoring	Passive monitoring by the automatic watermark detection of broadcasted watermarked media.
2	Copyright identification	Resolving copyright issues of digital media by using watermark information as copyright data.
3	Content authentication	Authentication of original art work, performance and protection against digital forgery.
4	Access control	Access control applications, such as, Pay-TV.
5	Copy control	Disabling copy of CD / DVD etc. by watermarked permission.
6	Packaging and tracking	Transaction tracking and protection against forged consumable items including pharmaceutical products by embedding watermark on packaging.
7	Medical record authentication	Authentication of digitally preserved patient's medical record, including blood sample, X-ray, ECG etc.
8	Insurance / Banking document authentication	Digital authentication of insurance claim, banking, financial, mortgage and corporate documents.
9	Media piracy control	Tracking of the source of media piracy.
10	Ownership identification	Supproting legitimate claim, such as, royalty by the media owner.
11	Transaction tracking	Tracking of media ownership in a buyer-seller scenario.
12	Meta-data hiding	Hiding meta-data within the media instead of a big header.
13	Video summary creation	Instant retrieval of video summary by embedding the summary within the host video.
14	Video hosting authentication	Piracy control by video authentication at video hosting servers, including youtube, megavideo etc.

Figure 2.6: Watermarking applications.

2.2 Digital watermarking

2.2.1 Definition, properties, applications and attacks

By definition a digital watermark is the copyright or author identification information which is embedded directly in the digital media in such a way that it is imperceptible, robust and secure. The watermarking research is considerably mature by now, after its major inception in mid nineties and offers digital protection to a wide spectrum of application as shown in Figure 2.6. It comprises elements from a variety of disciplines including image processing, video processing, telecommunication, computer science, cryptography, remote sensing and geographical information systems etc. Watermarking systems are often characterized by a set of common properties and the importance of each property depends on the application requirements. A list of such properties and corresponding example applications [40, 41] are shown in Figure 2.7, where last column of the figure shows the associated applications' number from Figure 2.6.

Based on the embedding method, the watermarking techniques can be categorized [42] as shown in Figure 2.8. The watermark embedding can be done in the spatial domain or in the frequency domain. The latter have been a much popular choice as frequency

General Properties of Digital Watermarking		
Properties	Description	Applications
Imperceptibility	The watermark should not noticeably distort or degrade the host data in order to preserve the quality of the marked document.	1, 2, 3, 4, 14.
Robustness	To measure robustness the watermark must be reliably detectable against signal processing schemes including data compression.	
Fragility	These kinds of watermark are embedded in host data in such a way that they do not survive in the case of any modification even copying.	7, 8.
Tamper-resistance	The tamper-resistance property is focused on the intentional attacks in contrast to robustness.	3, 5, 9, 10, 11, 14.
False positive rate	The probability of identifying an un-watermarked piece of data as containing a watermark by a detector is called the false positive rate.	6.
Data payload	The amount of information present in watermarked media is called data payload.	12, 13.

Figure 2.7: Watermarking properties and associated applications.

decomposition characterizes the host media to represent the human eye characteristics and eye perception towards the media. Therefore frequency domain watermarking can provide better insight to reduce embedding distortion or increase the robustness [30]. Now, depending on the type of host media, watermarking can be divided into four different categories: audio, image and video watermarking. Again, based on the human perception the watermarking schemes can be categorized as visible or imperceptible (invisible) watermarking and the latter can also be categorized as robust, fragile or semi-fragile watermarking. In case of a robust watermarking scheme, the watermark is expected to be sustained even after a compression or any other intentional attack, whereas in the case of a fragile scheme [43] the watermark information is usually destroyed to any alteration or attack to the media, in order to authenticate the image integrity. A semi-fragile scheme [44] represents properties from both the above mentioned categories and the watermark information is robust to certain type of attacks while fragile to other type of attacks.

Watermark represents the owner's identity. Hence the selection of the watermark is considered important and varies according to application requirements. Early days of watermarking scheme often used a pseudo-random number to embed the watermark and authenticity of the media is examined by the presence or absence of the watermark. In recent literature a message or logo based watermark [15] has been preferred by the researchers and in this case authentication is done by extracting the hidden message or

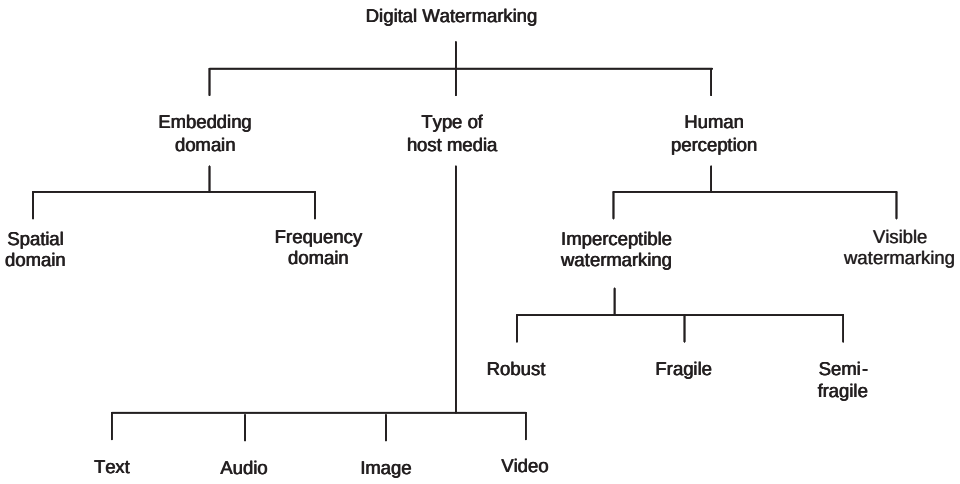

Figure 2.8: Types of watermarking techniques.

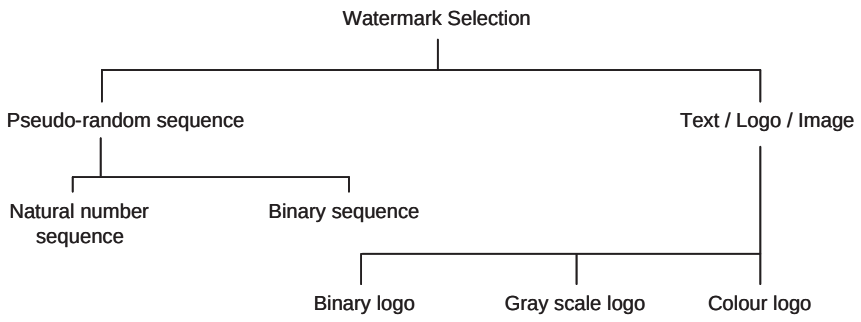

Figure 2.9: Watermark types.

logo to identify the legitimate owner. Figure 2.9 shows the different types of watermark used in this field.

Main requirements of the watermarking schemes are either 1) to retain the watermark information after any intentional attacks or natural image/video processing operation, or 2) to identify any tampering (fragile watermarking) of the target media. Any process that modifies the host media affecting the watermark information, is called attack on watermarking. Various types of attacks can be grouped together as follows: 1) signal processing, 2) geometric, 3) enhancement, 4) printing-scanning-capturing, 5) oracle, 6) chrominance, 7) transcoding attacks etc. The attack characterization with respect to image and video watermarking and related applications are shown in Figure 2.10.

Watermarking schemes in general are evaluated in terms of imperceptibility, robustness or capacity, while few research have been reported in the literature [45, 46] on the security of the watermarks. The security of the watermark can be defined as the

Watermarking attack characterisation													
Applications / Attacks	Comm. n/w adaptation	Display device adaptation	Image editing	Medical record	Intentional Attacks	Packaging / Tracking	Broadcast monitoring	Copy control	Meta-data hiding	Video editing	Video summary	Insurance / Banking document	Video hosting authentication
Image:													
Signal Processing													
JPEG	■	■							■				
JPEG 2000	■	■							■				
Geometric													
Horizontal Flip			■						■				
Rotation			■						■				
Cropping			■		■				■				
Scaling			■		■				■				
Row / Column removal					■				■				
Enhancement													
Low pass filtering			■		■				■			■	
Shrpening			■		■				■				
Histogram modification			■		■				■				
Gamma correction			■		■				■				
Color quantisation			■		■				■				
Restoration			■		■				■				
Noise addition			■		■				■				
Printing-Scanning					■	■						■	
Printing-Capturing						■						■	
Oracle Attack					■	■		■				■	
Fragile watermarking				■								■	
Semi-Fragile watermarking				■	■		■	■					■
Video:													
Signal Processing													
Motion JPEG 2000	■	■					■		■	■	■		
MPEG-2	■	■					■		■	■	■		
MPEG-4	■	■					■		■	■	■		
MC-EZBC	■	■					■		■	■	■		
H.264/AVC	■	■					■		■	■	■		
H.264/SVC	■	■					■		■	■	■		
H.264/MVC	■	■					■		■	■	■		
Linear / Non-linear adaptive filtering										■	■		
Geometric													
Desynchronisation					■				■	■	■		■
Cropping					■					■	■		■
Row / Column removal					■								
Chrominance attack					■					■			■
Trasncoding										■	■		■

Figure 2.10: Attack characterization.

ability to properly conceal the watermark information in such way that it is secret to the unauthorized users. The security of the watermarking schemes are usually implemented using two different approaches [47]:

- *Asymmetric watermarking* which uses two different keys for watermark embedding and detection and
- *Zero-knowledge watermark detection* using cryptographic techniques where the watermark detection process is substituted by cryptographical protocol.

Cryptographical scrambling of the watermark logo is also used in order to secure the

watermark [15] in addition to the other security measures, such as, key based coefficient selection, random filter parameter selection etc. These are particularly useful when the attacker has access to the watermark detector. The security of the watermark is intend to make the scheme robust against intentional attacks whereas this thesis considers watermarking robustness to natural signal processing attacks such as compression. Therefore the security aspects of the watermarking techniques have not been analyzed further.

The scalable content adaptation, which compresses image and video during the scaling operation, is considered as a type of signal processing attack to watermarking. Considering the nature of UMA application scenario, watermarking schemes for scalable coded media focuses on two main properties: 1) imperceptibility and 2) robustness, which are complementary to each other. This thesis provides an insight on the effects of content adaptation on watermarking within the scalable coded media and suggested robust watermarking techniques accordingly.

2.2.2 Watermarking process

The watermarking procedure, in its basic form, consists of two main processes: 1) Embedding and 2) Extraction and authentication. At this point, for simplicity, we describe these processes with reference to the image watermarking.

2.2.2.1 Embedding

This process insert or embed the watermark information within the host image by modifying all or selected pixel values (spatial domain); or coefficients (frequency domain), in such a way that the watermark is imperceptible to human eye and is achieved by minimizing the embedding distortion to the host image. The system block for the embedding process is shown in Figure 2.11 amd can be expressed as:

$$I' = \zeta(I, W), \tag{2.1}$$

where I' is the watermarked image, I is the original host image, W is the watermark information and $\zeta()$ is the embedding function. The embedding function can further be categorized in sub-processes: 1) forward transform (for frequency domain), 2) pixel / coefficient selection, 3) embedding method (additive, multiplicative, quantization etc.) and 4) inverse transform.

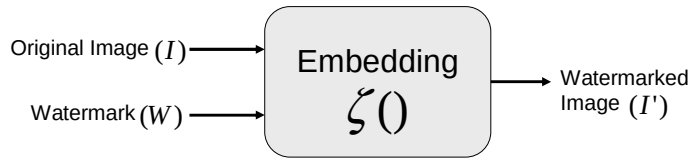

Figure 2.11: Watermark embedding process.

Finally the performance of the watermark embedding is measured by comparing the watermarked image (I') with the original unmarked image (I) and is calculated by various metrics: 1) peak signal to noise ratio (PSNR), 2) weighted PSNR (wPSNR) [48], 3) structural similarity measure (SSIM) [49], 4) just noticeable difference (JND) [50] and 5) subjective quality measurement [51].

PSNR: This is one of the most commonly used visual quality metric which is based on the root mean square error (RMSE) of the two images with dimension of $X \times Y$ as in Eq. (2.2) and Eq. (2.3).

$$PSNR = 20 \log_{10} \left(\frac{255}{RMSE} \right) \quad dB. \tag{2.2}$$

$$RMSE = \sqrt{\frac{1}{X \times Y} \sum_{m=0}^{X-1} \sum_{n=0}^{Y-1} (I(m,n) - I'(m,n))^2}. \tag{2.3}$$

wPSNR: On contrary to error measurement in spatial domain as in the previous metric, this metric measures PSNR in wavelet transform domain with weighting factors at different frequency decomposition level. The host and processed images are firstly wavelet decomposed and then squared error is computed at every subband. Finally wPSNR is calculated using cumulative squared error with weighting parameters for each subband. The weights for various subbands are adjusted in such way that wPSNR has the highest correlation with the subjective score.

SSIM: This quality measurement metric assumes that human visual system is highly adapted for extracting structural information from a scene. Unlike PSNR, where average error between two images taken into consideration, SSIM focuses on a quality assessment based on the degradation of structural information. The structural information in the scene is calculated using local luminance and contrast rather an average luminance and contrast.

JND: In this metric the host and test images are DCT transformed and Just Noticeable Differences are measured using thresholds. The thresholds are decided based on 1) luminance masking and 2) contrast masking of the transformed images. The threshold for luminance pattern relies on the mean luminance of the local image region, whereas

the contrast masking is calculated within a block and particular DCT coefficient using a visual masking algorithm.

Subjective: Although various objective metrics have been proposed to measure the visual quality, often by modeling the human visual system or subjective visual tests, the subjective test offers best visual quality measurement. Subjective tests procedures are recommended by ITU [51] which defines the specification of the screen, luminance of the test room, distance of the observer from the screen, scoring techniques, test types such as double stimulus continuous quality test (DSCQT) or double stimulus impairment scale test (DSIST) etc. The tests are carried out with multiple viewer and the mean opinion score (MOS) represents the visual quality of the test image. However the subjective tests are often time consuming and difficult to perform and hence researchers prefer objective metrics to measure the visual quality.

Among these metrics, due its simplicity, the most common method of evaluating the embedding performance in watermarking research is PSNR. It is also observed that most of the metrics behaves in a similar fashion when compared with any embedding distortion measured by PSNR of $35dB$ or above. Therefore, this thesis have also used PSNR as the visual quality metric in the following chapters.

2.2.2.2 Extraction and authentication

As the process name suggested, it consists of two subprocess: 1) extraction of watermark and 2) authentication of the extracted watermark. The watermark extraction follows a reverse embedding algorithm, but with a similar input parameter set. Now based on the watermark extraction criteria any watermarking method can be categorized in: 1) non-blind type and 2) blind type. For the first category, a copy of the original un-watermarked image is required during extraction whereas in the latter case, the watermark is extracted from the test image itself. The extraction process can be written in the simplified form as:

$$W' = \varpi(I', I), \tag{2.4}$$

where W' is the extracted watermark, I' is the test image, I is the original image and $\varpi()$ is the extraction function.

Once the watermark is extracted from the test image, the authentication is performed by comparing with the original input watermark information. Common authentication methods are defined by finding the closeness between the two in a vector space, by

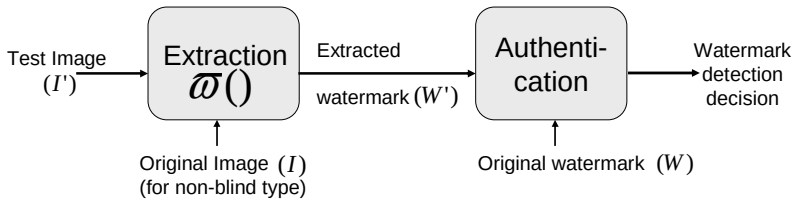

Figure 2.12: Watermark extraction and authentication process.

calculating the similarity correlation or Hamming distance. A complete system diagram of extraction and authentication process is shown in Figure 2.12.

2.2.3 Wavelet-based watermarking

Embedding watermark information by modifying direct pixel values, can be referred as the simplest form of the watermarking process. But eventually, the frequency domain watermarking schemes received more attention due its ability to decompose the media information in various frequency spaces. Research conducted by Cox *et al.* [30] indicates that in order to increase the robustness and reliability, the watermark should be embedded in the significant part such as low frequency components of the host media. The frequency domain watermarking schemes are exploited using different frequency domain analysis, namely, discrete Fourier transform (DFT) [52], fractal transform [53], discrete cosine transform (DCT) [54–56], digital wavelet transform (DWT) [5–11]. Due to its efficient multi-resolution spatio-frequency representation of signals, the DWT has become the main transform used in image watermarking.

An extension of image watermarking to video is the easiest option for any video watermarking scheme. Frame-by-frame video watermarking [27, 30] and 3D wavelet based video watermarking schemes [9, 32] are available in the literature. However a direct extension of the image watermarking schemes without consideration of motion, produces flicker and other motion related mismatch. The watermarking algorithms along with MCTF, which decomposes motion information, provides a better solution to this problem [57].

Therefore, this thesis focuses on wavelet based image watermarking research and extends the outcomes to video watermarking scenario using a motion compensated video decomposition. But before continuing with the wavelet based watermarking schemes and MCTF based video watermarking algorithms, here we like to discuss the background of the wavelet transform, various wavelet implementations and finally MCTF concept.

2.2.4 Wavelet transform

Wavelets can described as a class of function used to localize a time domain input signal in both space and scaling. A family of wavelets can be developed by defining the *mother wavelet*, $\Psi(t)$, which is confined in a finite interval. The family members, often referred as *daughter wavelets* can be defined as:

$$\Psi_{(a,b)}(t) = \frac{1}{\sqrt{a}}\Psi\left(\frac{t-b}{a}\right), \tag{2.5}$$

where $a > 1$ is the change of scale and $b \in \mathcal{R}$ is the translation in time [58,59]. Therefore a continuous input signal $f(t)$ can be represented in wavelet transform as a linear combination of *daughter wavelets*, $\Psi_{a,b}(t)$ and the corresponding wavelet coefficients $f_{(a,b)}$ can be defined as:

$$f_{(a,b)} = \int_{-\alpha}^{\alpha} \Psi_{(a,b)} f(t)dt, \tag{2.6}$$

$$= \langle \Psi_{(a,b)}, f(t) \rangle. \tag{2.7}$$

The above defined Continuous Wavelet Transform (CWT) can be extended to Discrete Wavelet Transform (DWT), which is used in image and video coding applications, including watermarking. In case of DWT, usually the wavelet function ($\Psi_{(a,b)} : a, b \in \mathcal{Z}$) follows dyadic translation (by power of 2) and dilation in Hilbert space and Eq. (2.5) is modified to:

$$\Psi_{(a,b)}(t) = 2^{a/2}(2^a t - b). \tag{2.8}$$

The implementation of DWT is adapted primarily by two different methods: 1) Filter bank approach and 2) Lifting based approach. The first one is more widely used for many applications where as the latter one is more popular in recent image and video coding schemes.

2.2.4.1 Filter bank approach

This approach consists of two filter banks, one each for the analysis (forward transform) and the synthesis (inverse transform) as shown in Figure 2.13. During the analysis, the input signal is passed through two separate channels, using a high pass filter (g) and a low pass filter (h) followed by a down sampling operation by a factor of 2, in each

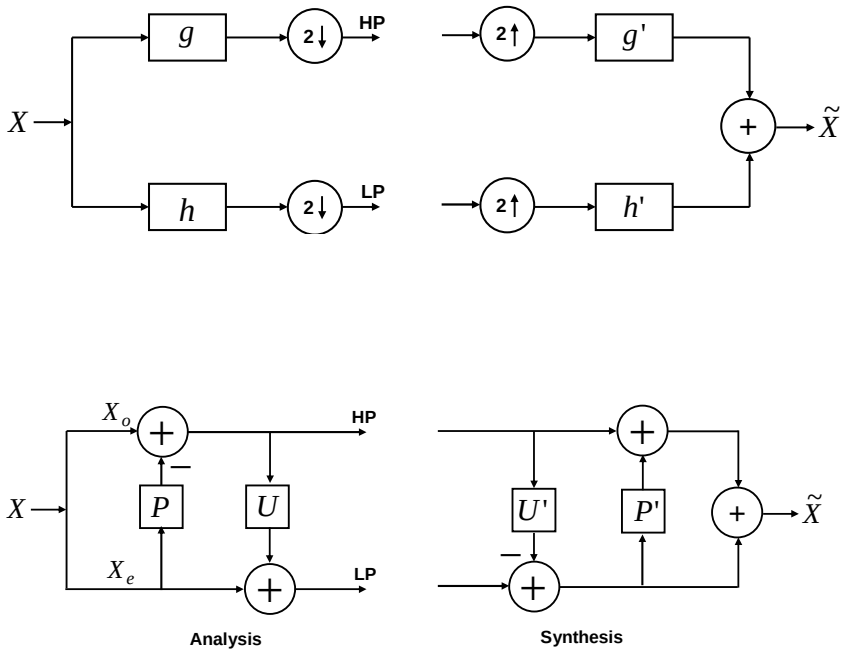

Figure 2.14: The lifting approach for DWT.

channel. The low pass filter data contains the coarse grain information while the high passed data retains the fine-grained or detailed information of the input signal. To reconstruct the signal data, the transformed coefficients are first interpolated by an up sampling operation with a factor of 2 and then convolved with synthesis filter banks, g' and h'. The filter coefficients of g' and h' are obtained from corresponding analysis filters g and h, respectively, to eliminate the aliasing.

2.2.4.2 Lifting based approach

In this alternative DWT implementation, the input signal is first decomposed into odd (o) and even (e) samples. Then a predict (P) and update (U) lifting functions are operated sequentially on the odd and even samples, respectively, to obtain the wavelet coefficients [60] as shown in Figure 2.14. The predict function approximates the data set and the difference between the approximation and the odd samples creates the detailed information of the input signal (equivalent to high pass subset in filter bank). Then the update step modifies the even sample using the predicted samples from the previous step and generates the average of the input signal (low pass subset). The inverse transform (synthesis) of the lifting scheme is a mirror of the forward transform, followed by a merging step to reconstruct the input signal.

2.2.5 2D wavelet

The wavelet decomposition of image requires 2D transform and it is achieved by performing 1D DWT separately on rows and columns of 2D signals. At each stage of the transform one low pass (L) and one high pass (H) coefficient subsets are generated and as a result an one level 2D wavelet transform creates four subbands, namely, LL, LH, HL and HH as shown in Figure 2.15.a). The LL subband represents the original image in half resolution and contains smooth spatial data with high spatial correlation. The HH subband contains the noise and edge information while HL and LH subbands consists of vertically and horizontally oriented high frequency details, respectively. The 2D wavelet transform can repeatedly be applied on LL subband from previous decomposition to create hierarchy of the wavelet coefficients. An example of 2 level 2D wavelet decomposition is shown in Figure 2.15.b).

Based on the orthogonality property, the wavelets are often designed as 1) orthogonal kernels (Haar, Daubechies etc.) and 2) bi-orthogonal kernels (9/7, 5/3 etc.) The above mentioned wavelets retains linearity property while non-linear wavelets, such as, Morphological Haar (M-Haar) and Median lifting on quincunx sampling (M-QC) are obtained by replacing the linear operations, such as weighted averaging, in lifting steps with non-linear operations. They can modify only the lifting step(s) affecting the low pass sub band (known as update step) [61], only the lifting step(s) affecting the high pass subbands (known as prediction step) [62] and the both types of lifting steps [63].

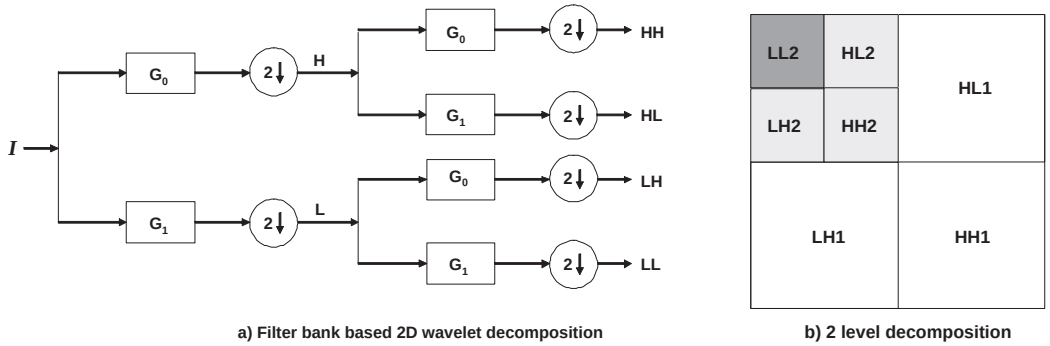

Figure 2.15: 2D wavelet transform operation.

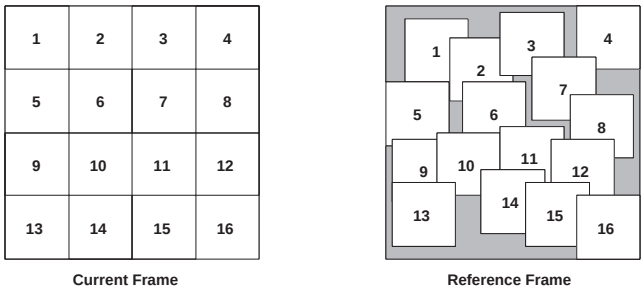

Figure 2.16: The block based motion estimation.

2.2.6 Motion compensated temporal filtering

In the case of video decomposition, a temporal dimension has to be added and the same can be achieved by extending previously discussed 2D wavelet transforms in 3D transform. But for video, object motion between frames is important and therefore translational motion information in temporal direction is required to be incorporated during temporal decomposition. Motion Compensated Temporal Filtering (MCTF) [64] provides such temporal decomposition solution using a block based motion estimation as shown in Figure 2.16. The 1D lifting based wavelet transform can also be used to adopt the motion model within its prediction and update steps to provide MCTF decomposition. More about MCTF and related wavelet decomposition is discussed in Chapter 7.

2.3 Conlcusions

In this chapter, overview and background of the scalable coding based content adaptation and digital watermarking are presented. Firstly, the content adaptation is described according to MPEG 21 part-7 DIA specification. Then the basic properties and applications of digital watermarking are briefed along with the probable attacks on watermarking including scalable compression in content adaptation. To propose robust watermarking techniques against such content adaptation, wavelet-domain watermarking schemes are selected. In the next chapter the state-of-the-art study on wavelet based watermarking schemes related to image and video watermarking are discussed and analyzed.

Chapter 3

State-of-the-art

Image and video watermarking can be performed either in the pixel domain or in the frequency domain. Frequency domain watermarking, more recently wavelet domain watermarking schemes are preferred due to its increased robustness and reliability by choosing important frequency components. At the same time scalable image and video coding schemes, *i.e.,* JPEG 2000, Motion JPEG 2000, MC-EZBC, and H.264/SVC uses wavelets and related transforms for progressive transmission of media data with low bit-rate, resolution, quality or a temporal scalability. Therefore an increased interest in wavelet domain watermarking is noticed in the recent literature. Due to its multi-resolution anlysis and compliance with image and video coding schemes, DWT is a natural choice for robust watermarking research for scalable coded image and video, in this thesis. This chapter discusses about the state-of-the-art researches, published in this domain.

3.1 Image watermarking

3.1.1 Wavelet-based image watermarking

Due to its ability for efficient multi-resolution spatio-frequency representation of signals, the DWT has become the major transform for spread spectrum watermarking. The wavelet domain watermarking algorithms often share a common model. Based on the embedding methodology, wavelet-based image watermarking can be categorized into two main classes: uncompressed domain algorithms and joint compression-

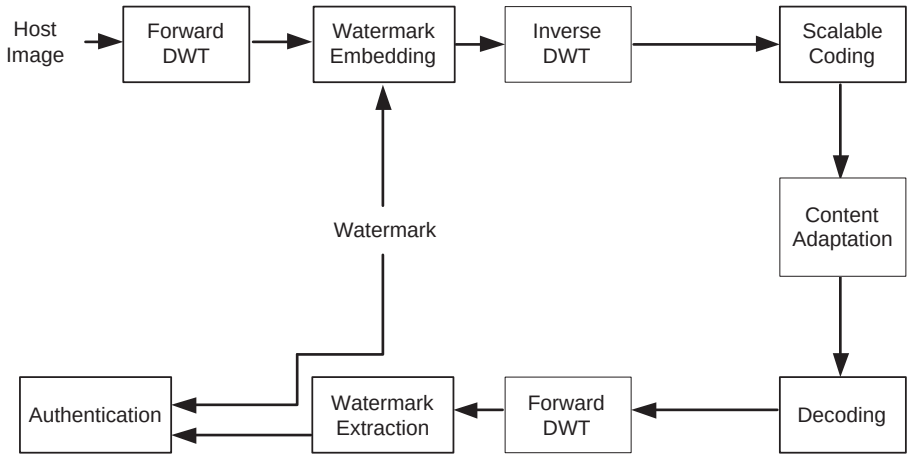

Figure 3.1: Uncompressed domain image watermarking and content adaptation attack.

watermarking algorithms.

3.1.1.1 Uncompressed domain watermarking algorithms

Watermark embedding is performed independent of and prior to compression. There are many algorithms of this type of watermarking, presented in the literature [5–8, 10–18, 65, 66]. A system block diagram in the context of scalable coding-based content adaptation is shown in Figure 3.1. The major steps for embedding include the forward DWT (FDWT) and coefficient modification followed by the inverse DWT (IDWT). Then the content is scalable coded and may be adapted during usage. Watermark authentication includes the FDWT and recovery of the watermark as blind or non-blind extraction and comparison with the original watermark.

3.1.1.2 Joint compression-watermarking algorithms

As scalable image coding is mainly based on the DWT, joint compression-watermarking algorithms [19–25] incorporated into JPEG 2000 are also becoming more efficient way of image watermarking. A general system block diagram is shown in Figure 3.2. In most cases the watermark is embedded by modifying the quantized wavelet coefficients. The watermark extraction is done during the decoding operation. The main difference in this type of algorithms compared to the previous type is that the embedding DWT kernel and the compression DWT kernel are the same in this case. The use of JPEG 2000 lossless mode in a joint watermarking-compression scheme results in an uncompressed-domain watermarking algorithm that uses the same DWT kernel for both compression

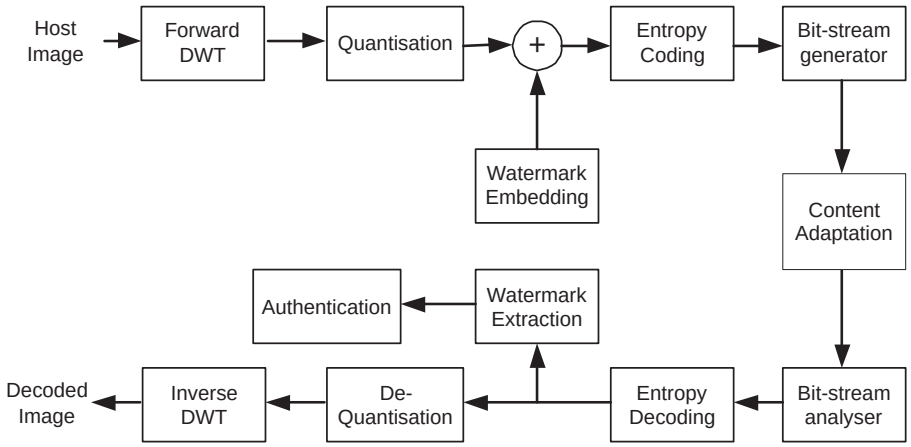

Figure 3.2: Joint compression-watermarking and content adaptation attack.

and watermark embedding.

3.1.2 Dissection of wavelet-based image watermarking algorithms

In both algorithm types, the watermark embedding algorithm considers different options for the choice of embedding subbands, for the selection of embedding coefficients and the modification methodology. In addition to above three parameters for the uncompressed domain algorithms, the choice of wavelet kernels is also regarded as a design parameter. In this section the well-known wavelet-based algorithms are dissected in terms of these four parameters to accumulate different options that have been used so far in current watermarking algorithms. Currently used different options are listed as follows:

3.1.2.1 Wavelet kernel

Early work on wavelet-based watermarking used mainly Haar or other Daubechies family orthogonal wavelets [5–15]. Then with the success of biorthogonal wavelets in image coding, they have been used in watermarking algorithms [16–18]. Further, joint compression-watermarking algorithms are also considered as biorthogonal wavelet domain watermarking. With the introduction of lifting-based wavelet design, lifting-based integer-to-integer Haar transform [10] and lifting-based non-linear wavelets [16] have been used in watermarking algorithms. In a recent work [67], the effect of different wavelet kernels on watermark embedding distortion performance and robustness to scalable coding-based content adaptation attacks is presented.

3.1.2.2 Subband

Wavelet-based watermarking algorithms also vary in terms of the number of wavelet decomposition levels used and the subbands chosen for watermark embedding. There have been algorithms using two [5, 6, 10–12], three [16–18] and four [8, 14, 15] levels of wavelet decompositions. Joint compression-watermarking algorithms used the same number of levels of decompositions used in the compression algorithm. The choice of subbands for watermark embedding is often driven by the imperceptibility and robustness criteria. Algorithms intending to meet low embedding distortion and imperceptibility requirements use high frequency subbands for embedding [6, 7, 10–15, 20]. On the other hand, algorithms designed to achieve high robustness against compression use low frequency subbands for embedding [5, 8, 16]. Finally, algorithms aiming to meet a balance between these two criterions use all subbands resulting in spread spectrum embedding [17–19, 22].

3.1.2.3 Hosting coefficient

The selection of wavelet coefficients to host the watermark can be classified into three methods: choosing all coefficients in a subband [11–15, 19, 21]; using a threshold based on their magnitude significance [10,17,18,20] or the just noticeable difference (JND) [16]; and based on the median of a 3x1 non-overlapping window, which can be based on the same subband (Intra-band) [5, 22] or spanning three high frequency subbands in the same decomposition level (Inter-band) [6, 7]. Some of the all-coefficients-based algorithms use a Human Visual System (HVS)-based mask [13, 14] or a fusion rule-based mask for refining the selection of host coefficients [15] or key-based random sequence for ordering host coefficients [8].

3.1.2.4 Embedding method

The host wavelet coefficient modification methods used in wavelet-based watermarking algorithms can be generalized as follows:

$$C'_{m,n} = C_{m,n} + \Delta_{m,n}, \tag{3.1}$$

where $C'_{m,n}$ is the modified coefficient at (m, n) position, $C_{m,n}$ is the original value of the host coefficient and $\Delta_{m,n}$ is the amount of modification due to watermark embedding. The modification methods can be categorized into two classes: modification based on

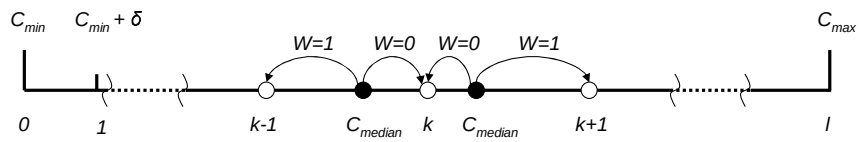

Figure 3.3: Re-quantisation-based modification.

magnitude alteration [10–21]; and re-quantization of a coefficient with respect to a group of coefficients within a given window [5–8, 22].

Further, for magnitude alteration algorithms, the way $\Delta_{m,n}$ in Eq. (3.1) is modified can be mapped into a generalized form consisting of four sub-classes of methods as follows:

$$\begin{aligned} \Delta_{m,n} &= a_1 A_1 + a_2 A_2 + a_3 A_3 + a_4 A_4, \qquad (3.2) \\ \text{where} & \\ A_1 &= \alpha C_{m,n}^{\tau} W_{m,n}, \\ A_2 &= v_{m,n} W_{m,n}, \\ A_3 &= \beta_{m,n} w_{m,n} \text{ and} \\ A_4 &= f(C_{m,n}, W_{m,n}). \end{aligned}$$

A_1 corresponds to direct modification of the host coefficient $C_{m,n}$ with a watermark value $W_{m,n}$ according to the user specified parameters (α and $\tau = 1, 2, ...$) to vary the watermark weight and the strength, respectively [11, 16–19]. A_2 corresponds to the HVS driven modification using a weighting parameter ($v_{m,n}$) which is a function of $C_{m,n}$ and the pixel masking process in the HVS model [13, 14, 20]. A_3 corresponds to fusion-based methods where the host wavelet coefficients are fused with the watermark wavelet coefficients $w_{m,n}$ using an HVS-based fusion strength parameter, $\beta_{m,n}$ [15]. With A_4, all other magnitude alteration algorithms are represented based on any function, $f(C_{m,n}, W_{m,n})$. Concluding this analysis a binary vector $< a_1, a_2, a_3, a_4 >$ is used to represent different magnitude alteration for watermark embedding by setting the corresponding vector element to one in our proposed WEBCAM framework.

Similarly the re-quantization-based modifications are mapped into Eq. (3.1) as follows: Such algorithms change the median coefficient of a group of coefficients to the kth quantisation step position by a modification value $\Delta_{m,n}$, where $|\Delta_{m,n}| \leq \delta$, which is based on the new quantization step δ as shown in Figure 3.3. Different functions are suggested in the literature to find the value of δ and such functions normally use the minimum (C_{min}) and the maximum (C_{max}) coefficient values in the coefficients group.

They can be generalized into the following form:

$$\delta = f(\gamma, C_{min}, C_{max}), \tag{3.3}$$

where γ is the user defined weighting factor. As $\Delta_{m,n}$ depends on the step size δ and the user defined γ, the modification value $\Delta_{m,n}$ is typically a function of C_{min} and C_{max} for each group of coefficients. Details of the embedding procedures can be found in [5] and [7].

The above parametric dissection of state-of-the-art wavelet-based watermarking algorithms, in terms of wavelet kernel, subband, host coefficient and embedding method, is used to design and implement the tools repository and the modular and reconfigurable wavelet-based watermarking implementation is presented as WEBCAM framework in Chapter 4. The comparative study of various input parameters, as mentioned above, are also performed in Chapter 4 by experimental simulations.

3.2 Video watermarking

3.2.1 Uncompressed and compressed domain video watermarking

Video watermarking at its simplest form can be proposed by extending image watermarking algorithms in the individual video frames considering the video as a collection of frames. However frame-by-frame video watermarking without considering the temporal correlation in video often suffers from flickering problem and poor robustness performance against various video processing attacks, such as, collusion, de-synchronization and compression. Solutions are proposed in the literature by proposing 3D wavelet decomposition, watermarking in compressed domain etc. Similar to the state of the art image watermarking techniques, these video watermarking algorithms can be categorized in 1) Uncompressed domain and 2) Compressed domain algorithms.

3.2.1.1 Uncompressed domain algorithms

Similar to the uncompressed domain image watermarking, the algorithms in this category embed the watermark in video before video encoding and the embedding algorithms are independent of the video coding algorithms. Many such algorithms, offered in the literature [9, 27, 28, 30–32, 57, 68–81], often, extend the image watermarking

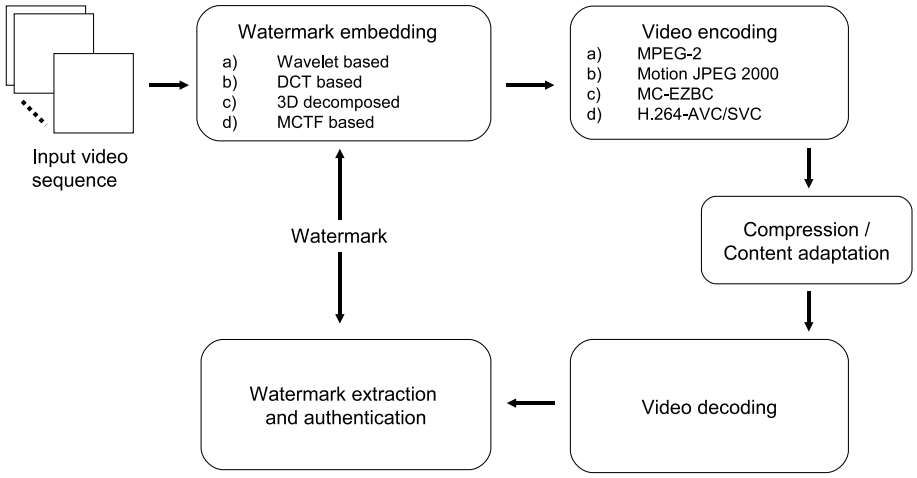

Figure 3.4: Uncompressed domain video watermarking and compression / content adaptation attack.

schemes into video which also consider temporal decomposition and motion information of the host video sequence. A system block diagram of uncompressed domain video watermarking schemes are shown in Figure 3.4. Firstly the video frames are either individually decomposed in 2D or 3D space using wavelet, DCT or other spread spectrum algorithms or temporally filtered using motion information and then decomposed. Then the watermark is embedded using various algorithms, similar to the image watermarking algorithms as described in Section 3.1. An inverse transform generates the watermarked video which is then content adapted by various encoding schemes, such as, MPEG-2, Motion JPEG 2000, MC-EZBC or H.264-AVC/SVC etc. The watermark extraction and authentication is done by forward transform similar to the one used during embedding, followed by a blind or non-blind recovery of the watermark.

3.2.1.2 Compressed domain algorithms

With the evolution of hybrid video coders, namely, from MPEG-2 to H.264-AVC/SVC various joint compression domain schemes are proposed in the literature [82–98]. A generic schematic block diagram of such system is shown in Figure 3.5. In these algorithms, the watermark embedding is usually performed either on motion compensated intra frames or residual frames (*Option 1*); on motion vector (*Option 2*) or by modifying the encoded bit streams (*Option 3* in the figure). Joint compression domain watermarking schemes are offered by modifying video coding pipeline and inserting the embedding modules within it. Therefore, these schemes are always associated to and dependent on a given video coding algorithms and offer lesser flexibility.

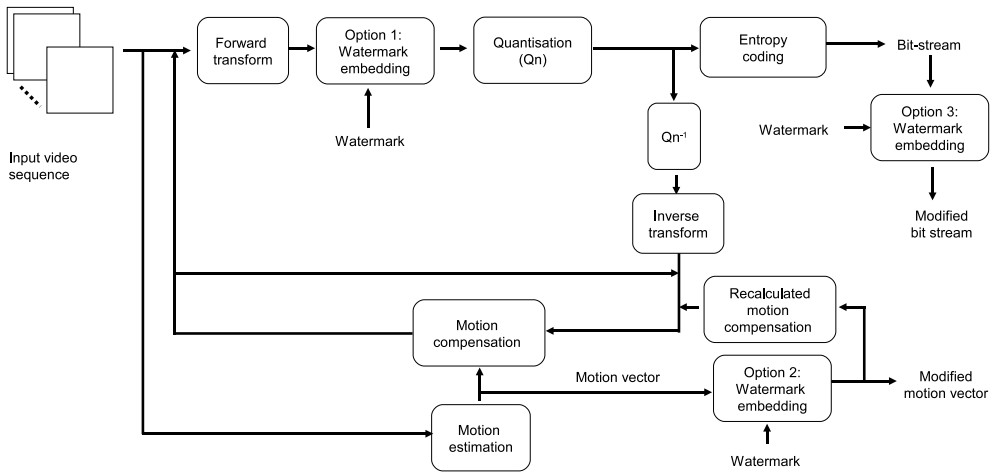

Figure 3.5: Generic scheme for joint compression domain video watermarking.

3.2.2 Dissection of the video watermarking algorithms

In Section 3.1.2, the image watermarking algorithms were dissected in terms of wavelet kernels, subbands, hosting coefficients and embedding algorithms. On the other hand, the video watermarking schemes exploited the temporal dimension and motion information of host video sequences. In most of the cases, the image watermarking embedding methods are adopted within the video decomposition schemes. In video watermarking more focus has been given to various motion and temporal dimension related decompositions of the host video and such video watermarking algorithms, available in the literature, can be categorized as follows: 1) Frame-by-frame, 2) 3D decomposed, 3) Motion compensated, 4) Bit stream domain and 5) Motion vector based watermarking.

3.2.2.1 Frame-by-frame

Frame-by-frame video watermarking can be defined as the extension of image watermarking algorithms into individual video frames. The initial attempts to video watermarking were made by this approach due to its simplicity in implementation using comparatively matured image watermarking algorithms. Many such algorithms are available in the literature [27, 28, 30, 68–73]. However frame-by-frame watermarking schemes often suffer from flickering problem and robustness issues, including, compression in hybrid video coding, collusion, frame dropping and de-synchronization.

3.2.2.2 3D decomposed

In order to overcome the weaknesses, as indicated in frame-by-frame video watermarking, new algorithms are proposed considering the temporal dimension in video sequences. These algorithms decompose the video by performing spatial 2D transform on individual frames followed by 1D transform in the temporal domain. Various transforms are proposed in 3D decomposed watermarking schemes, such as, 3D DFT domain watermarking [74]; 3D DCT domain [75] and more popular multi-resolution 3D DWT domain watermarking [9, 31, 32, 76–78]. A multi-level 3D DWT is performed by recursively applying the above mentioned procedure on low frequency spatio-temporal subband. Various watermarking methods similar to image watermarking are then applied to suitable subbands to balance the imperceptibility and robustness. Although 3D decomposition based methods overcome issues, such as, temporal de-synchronization, video format conversion, video collusion; 3D decomposition without considering motion often creates flickering problem and fragile to video compression attacks which considers motion trajectory during encoding.

3.2.2.3 Motion compensated

Motion compensated decomposition is one of the primary features of the hybrid video coding schemes, *i.e.,* MPEG-x and H.26x. To offer robust watermarking schemes against collusion attack and compression attacks in hybrid video coding, motion compensated video watermarking algorithms are proposed in the literature. The account for motion in these schemes also helps to remove the flicker problem, indicated in the previous subsections. Various such schemes are proposed in the literature as uncompressed domain [57,79–81] or joint compression domain within MPEG-2 encoder [82–84] and H.264/AVC encoder [85–87]. In these schemes object motion within the frames are tracked by motion estimation and motion compensation followed by the transform. The watermark embedding is usually done on transform coefficients before or after the quantization process on intra frames or prediction frames.

3.2.2.4 Bit stream domain

In this category the watermark embedding is done on partially decoded bit streams. Many such algorithms are proposed for MPEG-2 bit streams [88–91] and more recent H.264/AVC bit stream [92, 93]. The major advantage of bit stream domain watermark-

ing is that the computational complexity is much lower which leads to a faster watermark detection for real time applications. It also prevents the decoding and re-encoding data loss, when compared to joint compression domain watermarking schemes. In bit stream domain schemes, usually, the bit-stream is partially decoded by entropy decoding followed by the de-quantization process and the watermark embedding is performed on the transform coefficients. However any error due to embedding modification in the bit stream propagates and causes distortion. Various drift compensation algorithms are suggested in these algorithms to counter such error propagation.

3.2.2.5 Motion vector based

Video watermarking within motion vector can be defined as special case of bit stream domain watermarking. One of the major motivations of these schemes is that for any video encoder motion vector is always preserved and encoded with higher priority and hence less affected by compressions. Therefore any watermark embedding within motion vector is robust to compression and other attacks. But at the same time any small change in motion vector can cause a significant distortion in the host video. However, a careful choice of motion vector to embed the watermark can reduce the embedding distortion while keeping high robustness. Few such algorithms are proposed in the literature for MPEG-2 motion vector [94–96] and H.264/AVC motion vector [97, 98]. To avoid significant embedding distortion, in all the cases the watermark capacity is kept small and various algorithms adopted different methods to select the motion vectors to be embedded, such as, higher magnitude based [96, 97]; motion estimation mode selection based [98]; texture based [95] and phase angle based [94].

3.3 Conclusions

In this chapter various image and video watermarking schemes are discussed and broadly categorized in uncompressed domain and compressed domain. Uncompressed domain schemes are generally independent of any image and video encoding schemes and hence more flexible compared to compressed domain algorithms. Therefore in this thesis we choose to analyze and propose new uncompressed domain image watermarking and video watermarking schemes based on a motion compensated framework. From the state of the art analysis, it is evident that although many image watermarking schemes are proposed towards robustness against JPEG 2000, a little work has been done on robust video watermarking against scalable coded video and related attacks.

Again, within image watermarking schemes a gap is identified to model scalable compression within the watermarking algorithm. Hence, within the scope of this thesis, we aim to propose improved image watermarking schemes to enhance the robustness and robust video watermarking techniques to quality scalable content adaptation.

Chapter 4

Watermarking Evaluation Bench for Content Adaptation Modes

In the previous chapters, the content adaptation scenario and the state-of-the-art digital watermarking schemes in such scenario were discussed. In the state-of-the-art analysis different wavelet-based image and video watermarking schemes are dissected and categorized into common system blocks. Based on dissection, in this chapter a novel modular framework, Watermarking Evaluation Bench for Content Adaptation Modes (WEBCAM) is presented for evaluating image watermark robustness against scalable coding based content adaptation attacks. The various stages of the development of the proposed framework have been previously presented in different publications [99–101]. The framework is also available for download from the framework's web pages [102].

4.1 Introduction

Currently, a few good watermarking evaluation tools are available in the watermarking research community. These evaluation tools have proven very useful to measure the performance of the watermarking algorithms against different intentional attacks (including cropping, average filtering, scanning etc.) and unintentional attacks (natural image processing tasks, such as compression, rotation, scaling etc.). Examples of such evaluation tools include Stirmark [103], Checkmark [104], Optimark [105] and Watermark Evaluation Test bed (WET) [106]. Stirmark, for a given watermarked image, applies different attacks including cropping, filtering, rotation, JPEG compression to

generate a number of modified images which are used to verify the existence of the watermark. In addition to the attacks considered in Stirmark, Checkmark includes wavelet-based compression and helps to evaluate and rate the watermarking schemes. The Optimark evaluation bench provides performance metrics such as receiver operating characteristics curve, equal error rate, probability of false detection and rejection etc. WET provides a facility to test the robustness performance of different algorithms against usual attacks.

In the proposed test bed, Watermark Evaluation Bench for Content Adaption Modes (WEBCAM), the main aim is to address the evaluation of watermarking schemes for robustness against scalable coding-based content adaptation attacks. However, another important requirement of watermarking, the imperceptibility, is often complementary in nature to robustness to content adaptation and is evaluated in this framework. For example, in order to lower the embedding distortion, one may choose low significant frequencies or low significant bit plane which often forms the low significant portions of the scalable bit streams which may be discarded during content adaptations.

As stated before, due to the use of digital wavelet transform (DWT) as the underlying technology of JPEG 2000 compression standard and its success in image coding, recent years have seen wide use of wavelet-based techniques for image watermarking [5–25,66]. These algorithms are different to each other in terms of the wavelet kernel, number of wavelet decomposition levels, wavelet sub band choices for embedding, wavelet coefficient choices for embedding and the coefficient modification method for embedding. Therefore it is important to study the effect of above parametric choices in terms of balanced embedded distortion and robustness to content adaptation attacks performances.

Overall, the proposed WEBCAM framework provides a tool repository for wavelet-based watermarking, facilitates a parametric study of various design choices in wavelet-based watermarking and proposes a watermark tweezing tool to balance the embedding distortion and the robustness to scalable coding-based content adaptation. The current version of the framework provides tools for wavelet-based image watermarking, JPEG 2000-based scalability attacks and emulation of multiple node multimedia content adaptation chains covering various networks and devices. In summary, the main objectives of this chapter are:

1. To provide tools to emulate multiple node multimedia content adaptation chains and to perform scalable coding-based content adaptation (MPEG-21 Part-7) attacks for evaluation of robustness of image watermarks to such attacks.

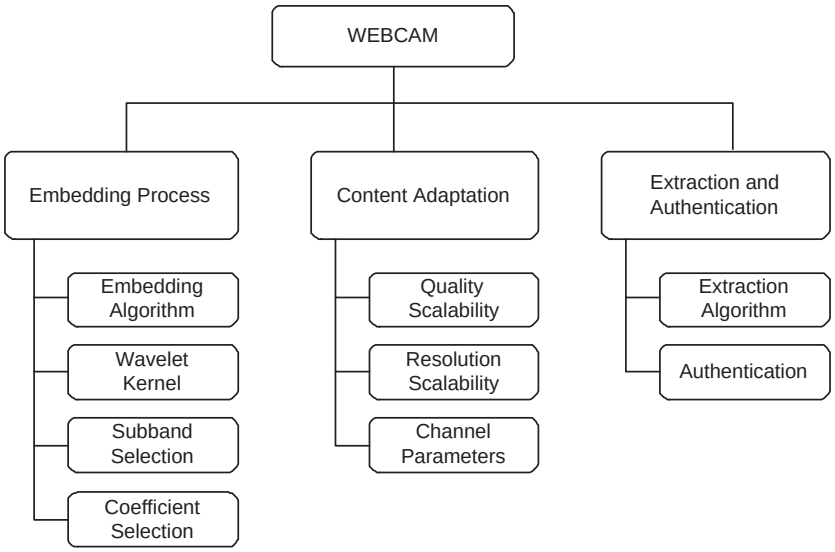

Figure 4.1: WEBCAM modules and input/output parameter blocks

2. To provide a tool repository for wavelet-based watermarking enabling controlled experimentation for their parametric evaluation, in terms of both embedding distortion and robustness to content adaptation attacks. This is achieved by dissecting commonly used wavelet based watermarking algorithms into modular tool blocks and fitting them into a common wavelet-based watermarking framework.

3. To facilitate tools for developing new watermarking schemes by choosing various modules and parameters from this common framework which can also be used as a research and learning tool for wavelet-based watermarking.

4. To provide a comparative parametric study of wavelet based watermarking algorithms using the framework.

4.2 WEBCAM system architecture

WEBCAM architecture for image consists of three main functional modules: 1) Watermark embedding; 2) Scalable coding-based content adaptation; and 3) Watermark extraction and authentication. The high-level block diagram of WEBCAM with main modular input/output parameters is shown in Figure 4.1. WEBCAM can operate on two modes: as a full system using all three modules or as a scalable coding-based content adaptation attack emulator for any watermarked image by just using the module 2.

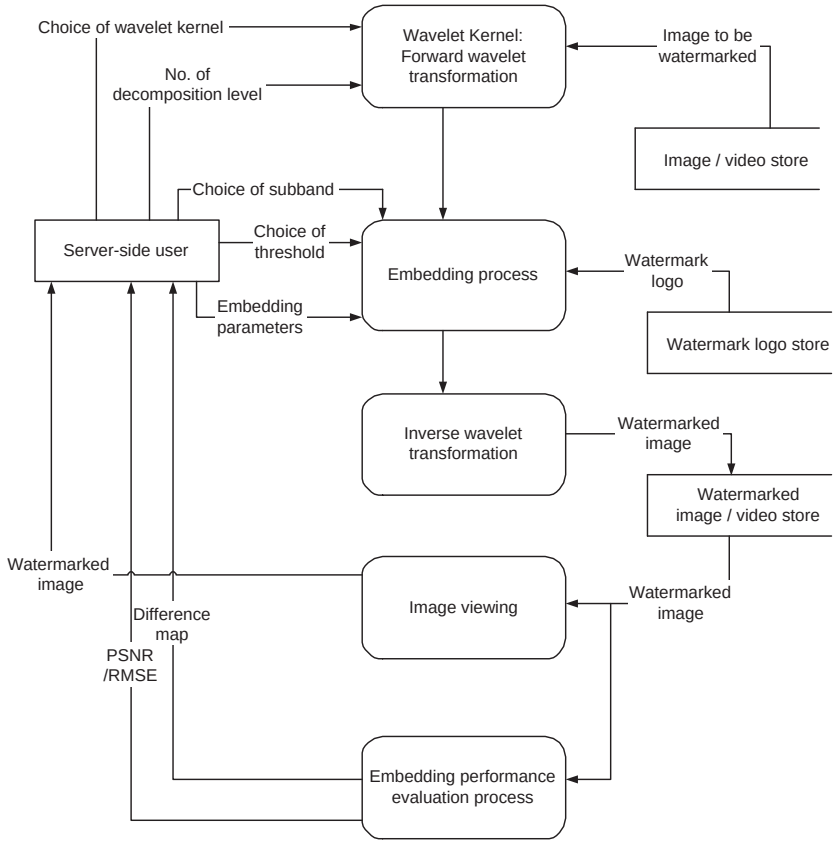

Figure 4.2: Flow diagram of the watermark embedding module in WEBCAM.

4.2.1 Watermark embedding tools

Following the dissection of wavelet-based watermarking shown in Chapter 3, the watermark embedding module of WEBCAM facilitates a common framework consisting of a tool repository for implementing those wavelet-based watermarking algorithms as well as a research platform for designing new algorithms. The block diagram of the watermark embedding module consisting all input parameters, the sub module functional blocks, embedding performance evaluation, output parameters and their interconnected flow is shown in Figure 4.2. The sub modules include the FDWT, watermark embedding, the IDWT, image display and embedding performance evaluation.

The input parameters to this module are three folds: operational; systems-related; and user-defined. Operational inputs are the host image and the watermark logo. The systems-related input parameters are related to the tools repository and consist of wavelet kernel choice, number of wavelet decomposition levels, host subband choice, host coefficient selection method and embedding procedure choice. The user-defined input parameters include embedding parameters, such as, thresholds, water-

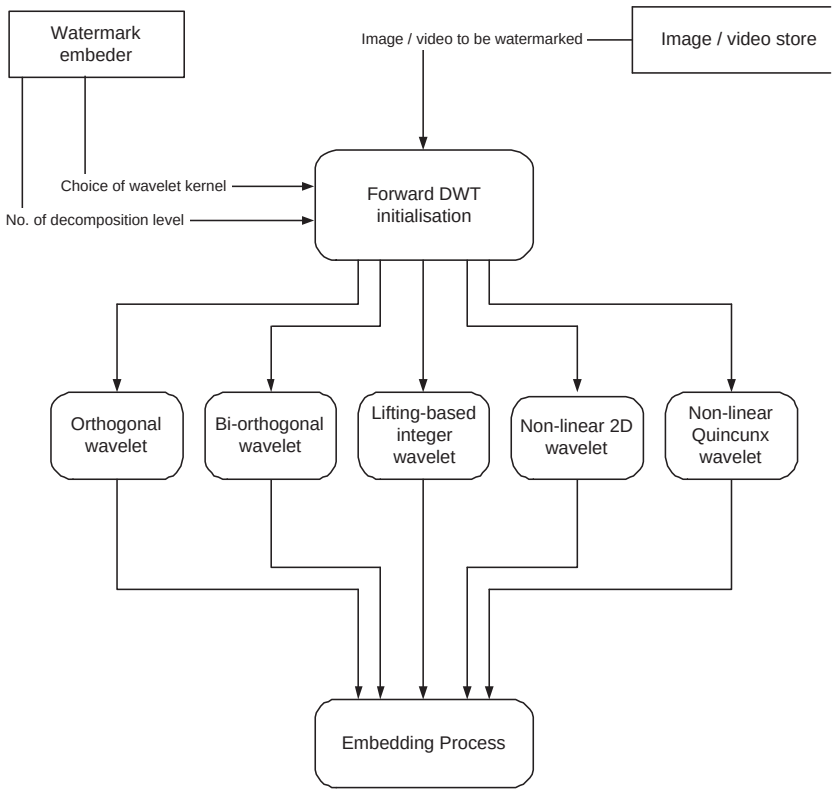

Figure 4.3: The FDWT submodule with choices wavelet kernels.

mark strengths etc. The output parameters include the watermarked image and embedding performance evaluation metrics, such as, the Peak Signal to Noise Ratio (PSNR) and the data hiding capacity.

The FDWT submodule with its choices for the wavelet kernel is shown in Figure 4.3. Currently available choices include orthogonal wavelets (Haar and Daubechies orthogonal), biorthogonal (9/7 and 5/3), lifting-based integer wavelets [60], separable non-linear wavelets [62,63] and Quincunx sampling-based non-linear wavelets [61,63]. WEBCAM allows any number of wavelet decomposition levels permitting the image dimensions. It also facilitates choosing any single or a group of subbands as the host subbands, followed by coefficient selection based on the realization of the embedding methods discussed in Chapter 3. For the embedding methods, WEBCAM provides both magnitude alteration and re-quantization schemes with flexibility of the binary input vector $< a_1, a_2, a_3, a_4 >$ for choosing different options for the former and options of inter and intra band coefficient selection for the latter.

4.2.2 Content adaptation tools

We aim to implement the emulation of a heterogenous communication system, where the content is encoded using the scalable coders to produce scalable bit streams followed by channel coding and transmitted along various types of networks, such as, optical, wired or wireless networks to reach the final user to display the content using devices with various display resolutions and resources availability. Such content may be adapted to address the varying network bandwidths, quality of services, display resolutions and usage requirements at various nodes of the network. These bit streams are adapted in terms of reducing quality, spatial resolutions and frame rates just by truncating various layers of the bitstream, resulting in low data rates to be streamed.

The flow diagram depicting the functionality of the content adaptation tools of WEBCAM, emulating a heterogenous communication system, is shown in Figure 4.4. The content adaptation tools in WEBCAM are two fold: channels-related tools and MPEG-21 DIA-related content adaptation rules. The channel-related tools consists of channel coding and channel models. The content adaptation module consists of a media adaptation engine. The adaptation engine is fed with the quality reduction, resolution reduction and frame rate reduction parameters translated from the network, device and usage requirements. Then the adaptation engine first adapts the bit stream description (if available) and then based on the new description adapts the scalable bitstream to produce the new bitstream, which is also scalable. This process may be carried out repeatedly at the successive nodes.

WEBCAM also provides the facility to decode a bitstream and extract the watermark at any node. An example of repeated node adaptations is shown in Figure 4.5. In this thesis WEBCAM provides JPEG 2000-based content adaptation and excludes the channel related modules as the present focus is on image watermarking schemes and their evaluation against content adaptation attacks. Although, the wavelet-based watermarking is considered in this framework, the content adaptation module in WEBCAM can be used as a stand alone tool for emulating the scalable coding-based content adaptation attack on any image watermarking scheme.

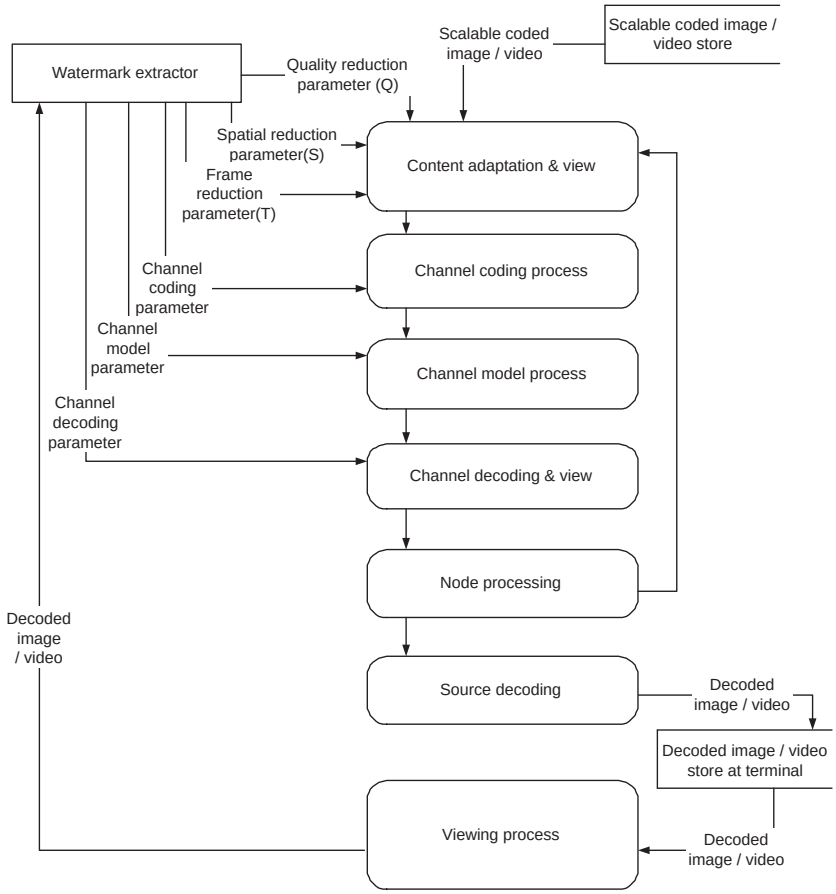

Figure 4.4: The flow diagram content adaptation tools in WEBCAM.

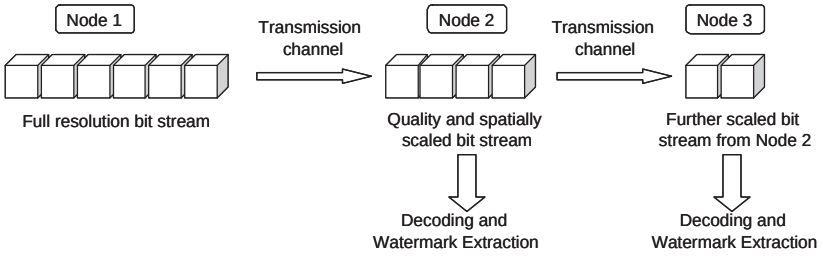

Figure 4.5: Content adaptation at nodes.

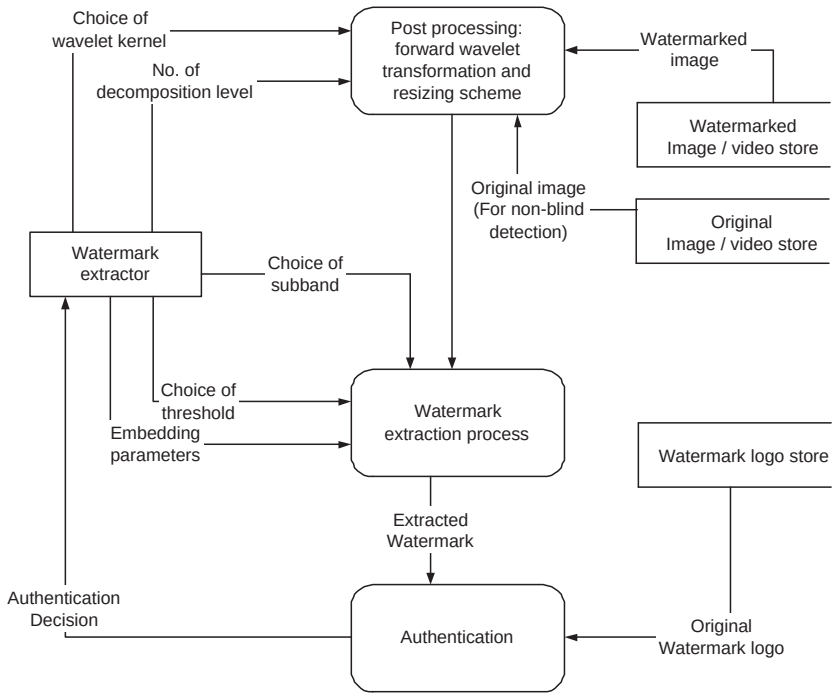

Figure 4.6: Flow diagram of watermark extraction and authentication in WEBCAM.

4.2.3 Watermark extraction and authentication tools

4.2.3.1 Watermark extraction

The watermark extraction process can be either blind or non-blind depending on the coefficient selection and modification process used in the embedding algorithm. In this test bed, the schemes associated with magnitude alteration algorithms are non-blind, whereas, re-quantization-based modifications are blind. In general, watermark extraction (as shown in Figure 4.6) includes the FDWT followed by the finding of $\Delta_{m,n}$ either as $C'_{m,n} - C_{m,n}$ from Eq. (3.1) or as $f(\gamma, C_{min}, C_{max})$ from Eq. (3.3) to find the watermark information $W_{m,n}$. In addition to watermark extraction, WEBCAM includes tools for postprocessing of the decoded image and the watermark authentication.

4.2.3.2 Postprocessing

WEBCAM addresses the situations where the resolution of the image of the decoded image is smaller than the original image due to resolution scalability-based content adaptation. The resizing scheme used in WEBCAM follows three steps. Firstly, the decoded image is decomposed into $(M_1 - M_2)$ levels using the FDWT employed in the

compression algorithm, where M_1 is the number of wavelet decomposition levels used in the embedding algorithm and M_2 is the number of levels discarded due to content adaptation. Secondly, the normalization of all coefficients are adjusted by multiplying with 2^{M_2}. Finally the dimensions are extended to those of the original by zero padding the current matrix and the IDWT is applied to obtain the full resolution image.

4.2.3.3 Watermark authentication

The authentication process verifies the extracted watermark with the original watermark. Two commonly used authentication metrics are Hamming Distance (H) (often referred as Bit Error Rate (BER) in communication systems) and correlation similarity measure (S). The former is widely used for a binary watermark detection while the latter is commonly used for pseudo-random sequence-based watermark data or for a gray scale logo [15, 17]. Using these metrics, a watermark is said to be detected if the Hamming Distance is lower than a specific threshold value or the correlation similarity measure is higher than a given threshold. WEBCAM is equipped with both of these metrics which are computed as follows:

$$H(W, W') = \frac{1}{L}\sum_{i=0}^{L-1} W_i \oplus W'_i, \tag{4.1}$$

$$\begin{aligned} S(W, W') &= \frac{W.W'}{\sqrt{W'.W'}} / \frac{W.W}{\sqrt{W.W}} \times 100, \\ &= \frac{W.W'}{\sqrt{W'.W'}\sqrt{W.W}} \times 100, \end{aligned} \tag{4.2}$$

where W and W' are the original and the extracted watermarks, respectively. L is the length of the sequence and $\oplus$ represents the XOR operation between the respective bits.

4.3 Experimental simulations and comparative study

WEBCAM provides a tools repository for evaluating scalable coding-based content adaptation attacks, implementing wavelet-based image watermarking schemes by dissecting major algorithms into design tools and designing new tools. This section demonstrates the achievement of objectives with experimental simulations and corresponding comparative study.

Table 4.1: Realization of major wavelet-based watermarking algorithms using combinations of options for submodules in WEBCAM.

Wavelet Kernel	Decom- -position Levels	Subband Choice	Host Coefficient Selection	Embedding Method	The Resulting Algorithm
Orthogonal	2	Low	Median	Intra Re-quantization	[5]
Orthogonal	2	High	Median	Inter Re-quantization	[6]
Orthogonal	2	High	Threshold	$< 1, 0, 0, 0 >(\tau = 1)$	[10]
Haar	2	High	All	$< 1, 0, 0, 0 >(\tau = 2)$	[11]
Orthogonal	2	High	All	$< 0, 0, 0, 1 >$	[12]
Orthogonal	3	High	All	$< 0, 1, 0, 0 >$	[13]
Orthogonal	4	High	HVS	$< 0, 1, 0, 0 >$	[14]
Orthogonal	4	High	Fusion rule	$< 0, 0, 1, 0 >$	[15]
Haar	1	High	Median	Inter Re-quantization	[7]
Orthogonal	4	Low	Key based random sequence	Intra Re-quantization	[8]
Biorthogonal	3	Low	JND	$< 1, 0, 0, 0 >(\tau = 1)$	[16]
Biorthogonal	3	All	Threshold	$< 1, 0, 0, 0 >(\tau = 1)$	[17]
Biorthogonal	3	All	Threshold	$< 1, 0, 0, 0 >(\tau = 1)$	[18]
Biorthogonal	5	All	All	$< 1, 0, 0, 0 >(\tau = 1)$	[19]
Biorthogonal	5	All	Median	Intra Re-quantization	[22]
Biorthogonal	5	High	Threshold	$< 0, 1, 0, 0 >$	[20]

4.3.1 Different wavelet-based watermarking algorithm realization

With the provided tools repository, different wavelet-based watermarking algorithms can be realized by combining various options for the WEBCAM submodules, namely, the wavelet kernel, wavelet decomposition, subband choice, host coefficient choice and embedding method, and using a set of user-defined parameters. A few examples of realization of major wavelet-based watermarking algorithms in WEBCAM are shown in Table 4.1. In addition to these existing algorithms one can pick and mix different parameters and design new algorithms to cater their application requirements.

4.3.2 Robustness to content adaptation attacks

Next, the use of content adaptation tools are demonstrated in WEBCAM to evaluate the robustness of watermarking against the MPEG-21 DIA attacks, such as, JPEG 2000-based quality scalable adaptations and JPEG 2000-based resolution scalable adaptations.

Figure 4.7: The test image set.

4.3.2.1 The experimental setup

For these experiments, the Kodak test image set and other popular test images are used, as shown in Figure 4.7, and a binary logo as the watermark data is used. The PSNR is used for setting the host image distortion level to an acceptable level for embedding a given amount of watermarking data for robustness evaluation experiments. The Hamming distance is used as the authentication measure. The results show the mean value of the Hamming distance for the test image set and the error bars corresponding to 95% confidence level. The robustness against different compression ratios for the quality scalability attacks on the full resolution and joint resolution-quality scalability attacks (on half resolution) is evaluated.

1) The choice of logo

The experimental observations show that the choice of logo has no effect on the robustness performance of a given watermarking algorithm. As an example, Figure 4.9 shows the robustness performance for a watermarking algorithm, when used for five different logos as shown in Figure 4.8. Irrespective of the used watermark logo, the

Logo 1 (40x40) Logo 2 (70x74) Logo 3 (64x64) Logo 4 (64x64) Logo 5 (76x77)

Figure 4.8: The test logo set.

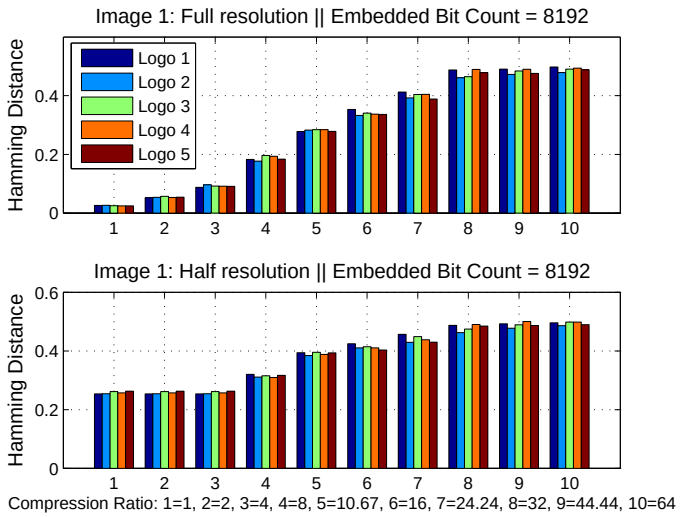

Figure 4.9: An example of comparing the choice of logo with the same bit count (8192) being embedded using the intra re-quantization-based embedding on robustness to - *Row 1*: Quality scalability attack on full resolution; and *Row 2*: Joint resolution-quality scalability attack (half resolution).

trend of robustness under different resolution-quality scalability attacks remains the same. Therefore, in this work results are shown using one logo (*Logo 3*).

2) On the use of PSNR in embedding distortion evaluations

In these experiments, the embedding performance is measured using the PSNR against data capacity. In robustness evaluation tests, this measure is used to ensure that either the distortion or data capacity is maintained constant for different watermarking algorithms, so that a fair comparison can be made for robustness under different embedding scenarios. Initial experiments suggest that for most host images, the PSNR greater than 35dB, provides acceptable image quality in naked human eye.

As an example of the embedding distortion, Figure 4.10 shows the performance of three types of wavelet kernels: orthogonal, bi-orthogonal and non-linear, using the Haar (HR)

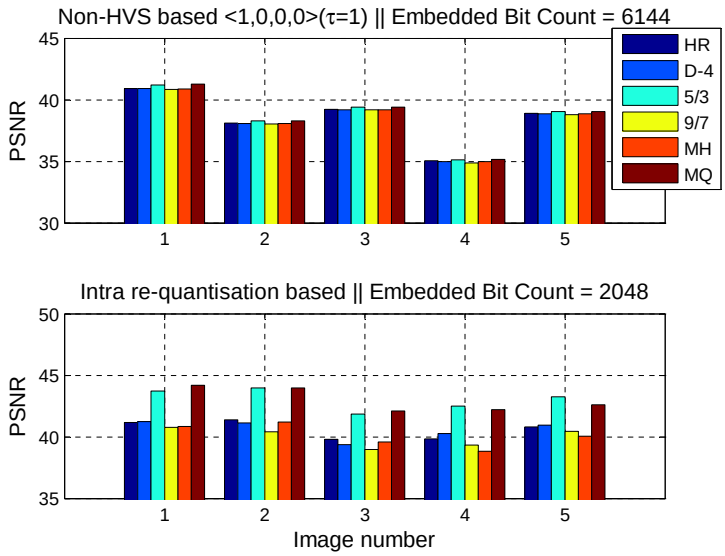

Figure 4.10: Capacity-distortion plots. Numbers 1 to 5 represent the five images from the test image set. Two different category of algorithms: 1) non-blind (non-HVS based <1,0,0,0>(τ=1)) and 2) blind (intra re-quantization based), are shown in each row for six different wavelet kernels: HR, D-4, 5/3 9/7, MH and MQ.

and Daubechies-4 (D-4) for orthogonal, 5/3 and 9/7 for bi-orthogonal and Morphological Haar (MH) and Quincunx domain Morphological (MQ) wavelets for non-linear types, respectively. The experiment considered two different categories of embedding algorithms, namely, the non-blind algorithm (non-HVS-based (<1,0,0,0>(τ=1))) and the blind algorithm (intra re-quantization-based). A comprehensive study on the effect of wavelet kernel and other parameters on embedding performance is discussed in Chapter 5.

3) Hamming distance interpretation

The Hamming distance is used as the authentication measure for robustness evaluation. Figure 4.11 shows the visual quality corresponding to different Hamming distance values. It is evident from these figures that after about 0.25 Hamming distance, the visual quality of logos becomes poor and difficult to compare with the original logo. Based on the visual significance, one can define a threshold value of the Hamming distance to ensure the extracted watermark is visually comparable with the original logo. Based on the experiments a generalized threshold of 0.20 ± 0.02 hamming distance can be set.

Using the above discussed experimental set up, three different scenarios are considered to compare and evaluate the robustness against content adaptation. With the shown set of experiments, it is also demonstrated how the full features of WEBCAM can be

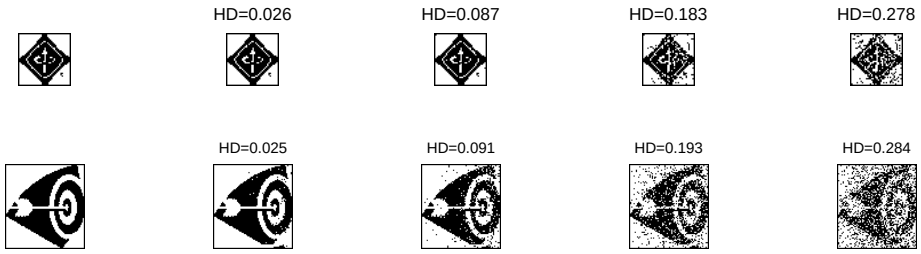

Figure 4.11: Original and extracted watermark logo and corresponding to different Hamming distances (HD).

used for evaluating the effect of different options chosen for submodules in wavelet-based watermarking algorithms. This is carried out by setting all but one submodules setting as common and fixed choices. The scenarios, considered here are as follows:

4.3.2.2 The effect of wavelet kernel choice on robustness

The contribution of the choice of wavelet kernel on the robustness to content adaptation is evaluated by considering non-blind and blind extraction algorithms. The other parameters, namely, the embedding subband and the host coefficient selection are set to low frequency and thresholds-based (<1,0,0,0>(τ=1) for the non-blind case and intra re-quantization-based for the blind algorithm, respectively. In all the cases, three level decomposition has been performed by trading of between complexity, data capacity and the robustness. Lesser number of decomposition level often lacks required robustness specially in the case of resolution scalability, whereas a higher number of decomposition adds complexity and reduces watermarking data capacity. The watermark strength parameter, α and γ, has been set to 0.08 for all wavelet kernel choices. A set of six different wavelet kernels representing three different wavelet classes, namely, orthonormal (HR and D-4), bi-orthogonal (5/3 and 9/7) and non-linear (MH and MQ) have been used for the comparisons. The results are shown in Figure 4.12 (for the non-blind algorithm) and Figure 4.13 (for the example blind algorithm). For the full resolution quality scalability as well as joint resolution-quality scalability attacks, the longer bi-orthogonal wavelets performed better compared to other wavelet kernels. Particularly bi-orthogonal 9/7 wavelet which is also used in JPEG2000 compression here, provides best result due to close approximation between watermarking wavelet and compression wavelet kernels. Therefore for further experimental set 9/7 is used as the watermarking wavelet transform.

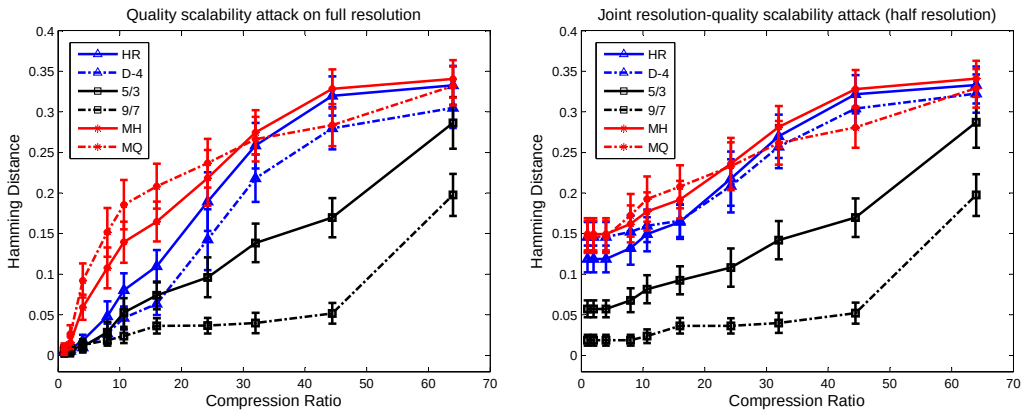

Figure 4.12: An example of evaluating the effect of the wavelet kernel for $< 1, 0, 0, 0 >$ ($\tau = 1$) direct modification-based embedding on robustness to - *Column 1*: Quality scalability attack on full resolution; and *Column 2*: Joint resolution-quality scalability attack (half resolution).

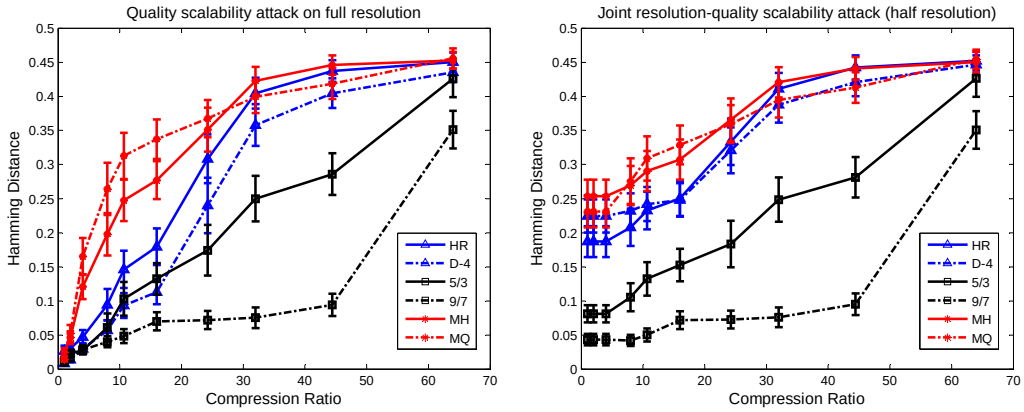

Figure 4.13: An example of evaluating the effect of the wavelet kernel for intra re-quantization-based embedding on robustness to - *Column 1*: Quality scalability attack on full resolution; and *Column 2*: Joint resolution-quality scalability attack (half resolution).

4.3.2.3 The effect of subband choice

The contribution of the choice of subbands for the robustness of a watermarking algorithm is compared by setting all other choices to fixed. In this set of experiments, the wavelet kernel and decomposition levels are set to 9/7 and three, respectively. Figure 4.14 shows the robustness performance for non-blind extraction that uses threshold-based (<1,0,0,0>(τ=1)) embedding method, while Figure 4.15 shows the robustness performance for blind extraction that uses intra re-quantization-based embedding. In plots, low, high and all frequency subband selection refers to the lowest frequency

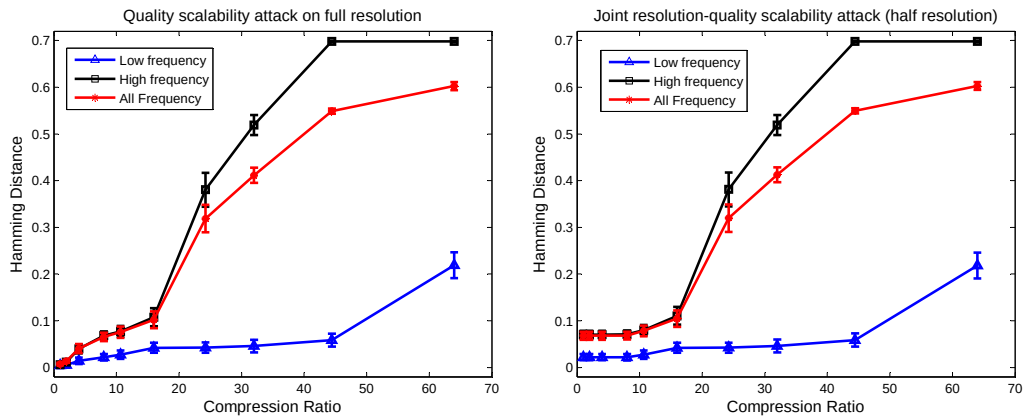

Figure 4.14: An example of evaluating the effect of the subband choice for $< 1, 0, 0, 0 >$ ($\tau = 1$) direct modification-based embedding on robustness to - *Column 1*: Quality scalability attack on full resolution; and *Column 2*: Joint resolution-quality scalability attack (half resolution).

subband, three high frequency subbands in the third decomposition level and all four frequency subband in the third decomposition level, respectively. For non-blind and blind embedding cases, an average PSNR range of $32.75 \sim 33.75db$ and $39 \sim 40$dB, respectively is maintained for all three different subband selection modes by tuning the watermark weight parameter α and γ. In both cases, embedding in low frequency subbands results in the highest robustness, compared to other two choices. This is mainly due to the high energy concentration in low frequency subband of the host image and the content scalability treatments used in JPEG 2000 quality scalability and resolution scalability.

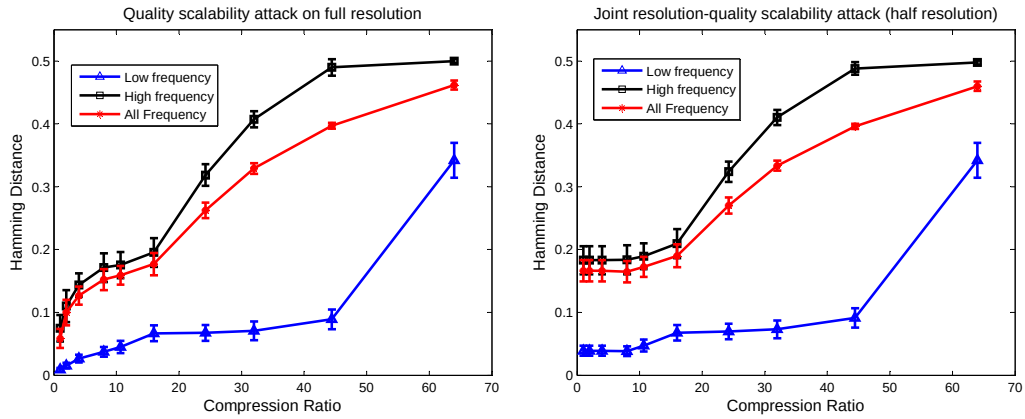

Figure 4.15: An example of evaluating the effect of the subband choice for intra requantization-based embedding on robustness to - *Column 1*: Quality scalability attack on full resolution; and *Column 2*: Joint resolution-quality scalability attack (half resolution).

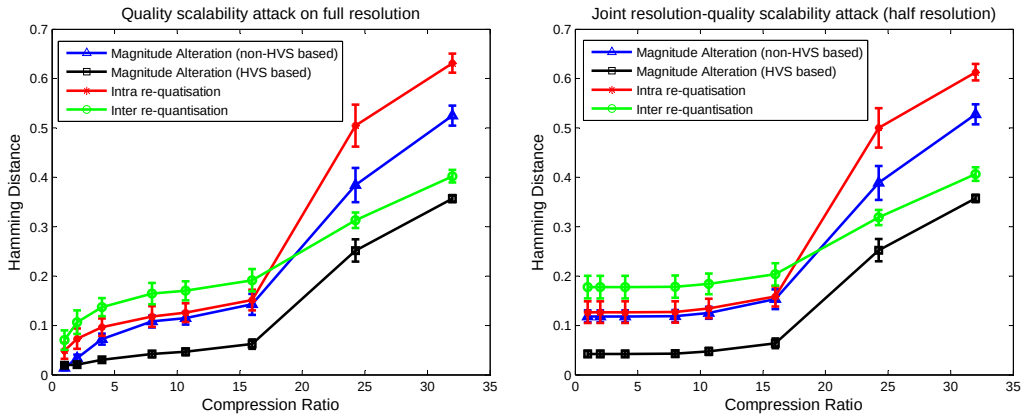

Figure 4.16: An example of evaluating the effect of different embedding methods on robustness to - *Column 1*: Quality scalability attack on full resolution; and *Column 2*: Joint resolution-quality scalability attack (half resolution).

4.3.2.4 The effect of the choice of embedding method and host coefficient selection

In this experiment set, two different embedding methods, namely, magnitude alteration and re-quantization are considered. For magnitude alteration, two cases are considered: HVS-based and all coefficient selection. For re-quantization-based methods also two cases are considered : inter and intra subband coefficient selection. The other parameters, the wavelet kernel, decomposition levels and the embedding subband are set to 9/7, three and high frequency subbands in the third decomposition level, respectively. For a fair comparison, the average PSNR are adjusted within the range of 38 $\sim$ 40dB for each algorithm by tuning the watermark weight parameter α and γ. It is evident from Figure 4.16, for all different content adaptation scenarios, the HVS-based direct modification combination shows the highest robustness. This is mainly due to the efficiency in the coefficient selection method, enabling to choose a higher value for the watermark strength parameter, yet resulting in distortion performance in the specified range. However, HVS-based model [14] and inter re-quantization based model [7] are only intended for high frequency subband embedding. Whereas non-HVS based and intra re-quantization based algorithms are independent of the subbands and hence used in the thesis for further research.

4.4 Conclusions

Although there are few watermarking toolboxes available in the literature, most of them rely on various attacks to evaluate the watermarking algorithms. On the contrary in this chapter we proposed WEBCAM framework to provide a common control experimental environment to compare the effect of various input parameters for various wavelet based algorithms. A modular test bed consisting of a repository of tools is presented for emulating MPEG-21 DIA content adaptation attacks, wavelet-based watermarking, extraction and authentication. The parametric dissections of the wavelet based watermarking algorithms from the previous chapter are used to design and implement the tools repository and its modular and reconfigurable wavelet-based watermarking implementation within WEBCAM framework. WEBCAM provides a formal evaluation platform to compare the performances of different schemes under a controlled experimental environment for various combinations of choices for those functional submodules and a comparative study of the same is provided here. It also facilitates the development of new algorithms and can also be used as an educational tool for wavelet-based watermarking algorithm design. The content adaptation tools repository provides a new set of attacks that are emerging in modern multimedia usage within the heterogeneous networks.

Chapter 5

Embedding distortion analysis and modeling

5.1 Introduction

Embedding performance and robustness are the two main but complementary properties of robust watermarking applications. The various contributing parameters on imperceptibility and robustness performances are studied in the previous chapters. The state of the art review and a generalization of the wavelet based watermarking schemes are proposed in Chapter 3 and Chapter 4. Though many independent algorithms are available in the literature, a gap has been identified which requires a generalized mathematical analysis to identify the relationship between distortion performance and various input parameters, responsible for embedding distortion. There are very little or no research have been done to establish a relationship between an objective metric for embedding distortion and watermarking input parameters. Few attempts [107] have been made towards this problem but they mainly focused on their own algorithms. In this chapter a mathematical model is derived to establish the relationship between embedding distortion performance metric, such as mean square error (MSE) and watermarking input parameters including wavelet kernels, subband selection and coefficient selection. Although many objective metrics are presented in the literature (as discussed in Chapter 2), most of the watermarking algorithms to date, due its simplicity, used PSNR to measure the embedding distortion. In this chapter MSE has been used instead of PSNR to represent the embedding distortion in a linear scale. However similar mathematical modeling can be developed using other objective

metrics and that is considered as a future work in this thesis.

The main objective of the work in this chapter, is to derive a generalized model for distortion performance analysis of wavelet based watermarking. In order to achieve the same, first a proposition is made to show the relationship between the noise power in the transform domain and the input signal domain. Then using the above proposition a relationship is established between the distortion performance metrics and the input parameters of a given wavelet based watermarking scheme. The proposed model is derived in two parts: 1) Initial propositions are made using orthonormal wavelet bases, which conserves energy in the signal domain as well as in the transform domain; 2) Extension of the same into non-orthonormal bases, including bi-orthogonal and non-linear wavelet kernels, to give a universal acceptance of the model.

5.2 Embedding distortion model for orthonormal wavelet bases

5.2.1 Preliminaries

The embedding distortion performance is measured by MSE, which can be defined as follows:

Definition 5.2.1 *The Mean Square Error (MSE) or average noise power in pixel domain between original image I and watermarked image I' is defined by:*

$$MSE = \frac{1}{X \times Y} \sum_{m=0}^{X-1} \sum_{n=0}^{Y-1} (I(m,n) - I'(m,n))^2, \tag{5.1}$$

where X and Y are the image dimension and m and n indicate each pixel position.

In order to formulate the model the transformation of noise energy from frequency domain to the signal domain is shown using *Parseval's equality.*

Definition 5.2.2 *In the Parseval's Equality, the energy is conserved between an input signal and the transform domain coefficient in the case of an orthonormal filter bank wavelet base [59]. Assuming the input signal $x[n]$ with the length of $n \in \mathcal{Z}$ and the*

corresponding transformed domain coefficients of $y[k]$ where $k \in \mathcal{Z}$, according to energy conservation theorem,

$$\|x\|^2 = \|y\|^2. \tag{5.2}$$

5.2.2 The model

Based on these primary definitions the model is built which consists of the following propositions and its proof.

Proposition 5.2.1 *Sum of the noise power in the transform domain is equal to sum of the noise power in the input signal for orthonormal transforms. If the input signal noise is defined by $\Delta x[n]$ and the noise in transform domain is $\Delta y[k]$ then,*

$$\sum_n |\Delta x[n]|^2 = \sum_k |\Delta y[k]|^2, \tag{5.3}$$

where $n \in \mathcal{Z}$ is the length of the input signal and $k \in \mathcal{Z}$ is the length in the transform domain, respectively.

Proof: As discussed in Chapter 2, DWT can be realized with a filter bank or lifting scheme based factoring. In both the cases the wavelet decomposition and the reconstruction can be represented by a polyphase matrix [60]. The inverse DWT can be defined by a synthesis filter bank using the polyphase matrix $M'(z) = \begin{pmatrix} h'_e(z) & h'_o(z) \\ g'_e(z) & g'_o(z) \end{pmatrix}$ where $h'(z)$ represents the low pass filter coefficients and $g'(z)$ is the high pass filter coefficients and the subscripts e and o denote even and odd indexed terms, respectively. Now the transform domain coefficient y can be re-mapped into input signal x as bellow:

$$\begin{pmatrix} x_e(z) \\ x_o(z) \end{pmatrix} = \begin{pmatrix} h'_e(z) & h'_o(z) \\ g'_e(z) & g'_o(z) \end{pmatrix} \begin{pmatrix} y_e(z) \\ y_o(z) \end{pmatrix}. \tag{5.4}$$

Assuming Δy is the noise introduced in wavelet domain and Δx is the modified signal after the inverse transform, the relationship between the noise in the wavelet coefficient and the noise in the modified signal can be defined using the following equations. From Eq. (5.4) we can write

$$\begin{pmatrix} x_e(z)+\Delta x_e(z) \\ x_o(z)+\Delta x_o(z) \end{pmatrix} = \begin{pmatrix} h'_e(z) & h'_o(z) \\ g'_e(z) & g'_o(z) \end{pmatrix} \begin{pmatrix} y_e(z)+\Delta y_e(z) \\ y_o(z)+\Delta y_o(z) \end{pmatrix}. \tag{5.5}$$

From Eq. (5.4) and Eq. (5.5) using the *Linearity* property of the Z-transform of the filter coefficients and signals in the polyphase matrix we can get,

$$\begin{aligned}
x_e(z) + \Delta x_e(z) &= h'_e(z)(y_e(z) + \Delta y_e(z)) \\
&\quad + h'_o(z)(y_o(z) + \Delta y_o(z)), \\
h'_e(z)y_e(z) + h'_o(z)y_o(z) + \Delta x_e(z) &= h'_e(z)y_e(z) + h'_e(z)\Delta y_e(z) \\
&\quad + h'_o(z)y_o(z) + h'_o(z)\Delta y_o(z), \\
\Delta x_e(z) &= h'_e(z)\Delta y_e(z) + h'_o(z)\Delta y_o(z). \qquad (5.6)
\end{aligned}$$

Similarly $\Delta x_o(z)$ can be obtained and written as

$$\Delta x_o(z) = g'_e(z)\Delta y_e(z) + g'_o(z)\Delta y_o(z). \qquad (5.7)$$

Combining Eq. (5.6) and Eq. (5.7), finally we can write the polyphase matrix form of the noise in the output signal:

$$\begin{pmatrix} \Delta x_e(z) \\ \Delta x_o(z) \end{pmatrix} = \begin{pmatrix} h'_e(z) & h'_o(z) \\ g'_e(z) & g'_o(z) \end{pmatrix} \begin{pmatrix} \Delta y_e(z) \\ \Delta y_o(z) \end{pmatrix}. \qquad (5.8)$$

Recalling the Parseval's energy conservation theorem as stated in *Definition 5.2.2*, from Eq. (5.8) it can be concluded that

$$\begin{aligned}
\sum |\Delta x_e|^2 + \sum |\Delta x_o|^2 &= \sum |\Delta y_e|^2 + \sum |\Delta y_o|^2 , \\
\sum_n |\Delta x[n]|^2 &= \sum_k |\Delta y[k]|^2. \qquad (5.9)
\end{aligned}$$

■.

Using the generalized framework, the *Proposition 5.2.1* can be applied to build the relationship between the modification energy in the coefficient domain to embed the watermark and the distortion performance metrics. In this model propositions are made for two different categories of embedding schemes, discussed in Chapter 3.

Proposition 5.2.2 *In a wavelet based watermarking scheme, the mean square error (MSE) of the watermarked image is directly proportional to the sum of the energy of the modification values of the selected wavelet coefficients. The modification value itself is a function of the wavelet coefficients and therefore two different cases are proposed based on the categorization.*

Case A: Non-blind model. *For the magnitude alteration based embedding method (non-blind algorithm), the modification is a function of the selected coefficient to be*

watermarked and the relationship between (MSE) and the selected coefficient ($C_{m,n}$) is expressed as:

$$MSE \propto \sum |f(C_{m,n})|^2. \tag{5.10}$$

Case B. Blind model. *For the re-quantization based method (blind algorithm), the modification is a function of the neighboring wavelet coefficients of the selected median coefficient to be watermarked and the relationship between MSE and the wavelet coefficients C_{min} and C_{max} is expressed as:*

$$MSE \propto \sum |f(C_{min}, C_{max})|^2. \tag{5.11}$$

Proof: In a wavelet based watermark embedding scheme the watermark information is inserted by modifying the wavelet coefficients. This watermark insertion can be considered as introducing noise in the transform domain. Hence the sum of the energy of the modification value due to watermark embedding in the wavelet domain is equal to the sum of the noise energy in the transform domain as stated in *Proposition 5.2.1.* From Eq. (3.1) and Eq. (5.3), the energy sum of the modification value $\Delta_{m,n}$ can be defined as:

$$\sum_{m,n} |\Delta_{m,n}|^2 = \sum_{k} |\Delta y[k]|^2. \tag{5.12}$$

Similarly, the pixel domain distortion performance metrics which is represented by MSE is considered as the noise error created in the signal due to the noise in wavelet domain. Therefore, the sum of the noise energy in the input signal is equal to the sum of the noise error energy MSE in the pixel domain:

$$MSE.(X \times Y) = \sum_{n} |\Delta x[n]|^2, \tag{5.13}$$

where X and Y are the image dimensions. Now the relationship between the distortion performance metrics MSE of the watermarked image and the coefficient modification value which is normally a function of the selected wavelet coefficients can be decided using the *Proposition 5.2.1.* Thus from Eq. (5.12) and Eq. (5.13) we can write:

$$MSE.(X \times Y) = \sum_{m,n} |\Delta_{m,n}|^2, \tag{5.14}$$

where X and Y are the image dimensions. Hence for any watermarked image, the average noise power MSE is proportional to the sum of the energy of the modification values of the selected wavelet coefficients:

$$MSE \propto \sum_{m,n} |\Delta_{m,n}|^2. \tag{5.15}$$

Now with the help of the categorization in the generalized form of the popular wavelet based watermarking schemes as discussed in Chapter 3, a relationship is established between the error energy of the watermarked image and the selected wavelet coefficient energy of the host image. For a magnitude alteration based algorithm, which is a category of non-blind watermarking algorithm, the mean square error MSE is directly proportional to the sum of the energy of the modification value Δ which is a function of wavelet coefficient value as stated below:

$$MSE \propto \sum |f(C_{m,n})|^2. \tag{5.16}$$

Similarly for the re-quantization based method (blind watermarking) the mean square error depends on the neighboring wavelet coefficient values. In this case the modification energy $|\Delta_{m,n}|^2$ hold an inequality due the modification range $-\delta \leq \Delta_{m,n} \leq \delta$:

$$|\Delta_{m,n}|^2 \leq |\delta|^2. \tag{5.17}$$

Therefore the upper bound of the mean square error MSE is defined by:

$$MSE \propto \sum |f(C_{min}, C_{max})|^2. \tag{5.18}$$

■.

5.2.2.1 An example of non-blind model

Considering a specific case of the non-blind algorithm in [17] the modification value Δ is a direct function of wavelet coefficient ($\Delta_{m,n} = \alpha C_{m,n} W_{m,n}$). Hence Eq. (5.16) can be modified and the MSE can be expressed as:

$$MSE \propto \sum_{k=1}^{l} |C(k)|^2, \tag{5.19}$$

where $C(k)$ is the selected coefficients to be watermarked and l is the number of such selected coefficients.

Table 5.1: Correlation coefficient values between sum of energy and the MSE for different wavelet kernel in various subbands.

	Non-blind model				Blind model			
	HR	D4	D8	D16	HR	D4	D8	D16
LL3	0.81	0.81	0.81	0.81	0.66	0.68	0.68	0.73
LH3	0.93	0.94	0.96	0.97	0.78	0.68	0.61	0.58
HL3	0.98	0.99	0.99	0.99	0.78	0.92	0.94	0.97
HH3	0.96	0.97	0.98	0.98	0.82	0.81	0.73	0.72
LH2	0.98	0.98	0.99	0.99	0.80	0.82	0.75	0.81
HL2	0.99	0.99	0.99	0.99	0.92	0.92	0.94	0.97
HH2	0.99	0.99	0.99	0.99	0.83	0.80	0.85	0.89
LH1	0.99	0.99	0.99	0.99	0.89	0.90	0.89	0.90
HL1	0.99	0.99	0.99	0.99	0.84	0.90	0.96	0.94
HH1	0.99	0.99	0.99	0.99	0.90	0.91	0.93	0.96

5.2.2.2 An example of blind embedding model

In an blind embedding algorithm suggested in [5], the quantization step δ is defined as:

$$\delta = \gamma \frac{C_{max} + C_{min}}{2}, \tag{5.20}$$

where γ is the user defined watermark weighting factor. As the modification value Δ depends on δ, with reference to Eq. (5.18), the relationship between the maximum limit of MSE and wavelet energy is defined by the following equation:

$$MSE \propto \sum_k (C(k)_{max} + C(k)_{min})^2, \tag{5.21}$$

where $C(k)_{max}$ and $C(k)_{min}$ are the neighborhood coefficients of the median value and k is the number of such selected median value.

5.2.3 Experimental simulations and result discussion

The propositions made in the previous section are verified in the experimental simulations. The sum of the energy of the selected wavelet coefficients and the MSE of the watermarked image have been calculated for the test images with a combination of different input parameters. As the wavelet coefficients varies greatly in different subbands the performances of all subbands are considered separately after a 3 level wavelet decomposition. After three level of wavelet decompositions, ten subbands are

created, such as, LL3, HL3, LH3 and HH3 at 3rd decomposition level, HL2, LH2 and HH2 at 2nd decomposition level and HL1, LH1 and HH1 at 1st decomposition level. Also a set of different wavelet kernels having various filter lengths are selected to perform the simulations. The performance of different wavelet kernels such as Haar (HR), Daubechies-4 (D4), Daubechies-8 (D8) and Daubechies-16 (D16) are simulated and studied in order to verify the proposed model. A set of 20 images have been considered as shown in Figure 4.7. Two different sets of results are obtained for each non-blind and blind model, and displayed to verify the effects of different input parameters which are responsible for embedding distortion performance. These two sets of experimental arrangements and resulting plots are discussed separately as follows:

5.2.3.1 Non-blind model

In experiment *Set 1*, the non-blind type watermark embedding model is considered as described in Section 5.2.2.1. The sum of energy of the selected wavelet coefficients to be modified and MSE of the watermarked image have been calculated using $\alpha = 0.5$ and the binary watermark logo for each selected method. Various wavelet kernels are used and the results are observed for each selected subbands. The correlation coefficients are also calculated and presented in Table 5.1.

In another representation a set of graphs are plotted in Figure 5.1 to present the average values of the MSE and the sum of energy for the test image set for four different wavelet kernels. The error bars denote the accuracy up to the 95% confidence interval. For display purposes the sum of energy values were scaled, so that they can be shown on the same plot for comparing the trend.

In the experiment *Set 2*, the performance for ten different subbands are plotted for each wavelet kernel in a similar fashion as mentioned in experiment *Set 1* in order to observe the trend. The results are shown in Figure 5.2. As earlier, a 95% confidence interval is considered which is denoted by the error bars and the LL3 values are scaled suitably in all cases to observe the trends.

5.2.3.2 Blind model

The experimental simulations for the blind model are conducted as described in Section 5.2.2.2. A similar set of experimental set up is followed as in non-blind model with $\gamma = 0.04$ and 0.2 for LL3 subband and other high frequency subbands, respectively.

The correlation coefficients, average pattern graphs for various wavelet kernels and ten different subbands are presented in Table 5.1, Figure 5.3 and Figure 5.4, respectively.

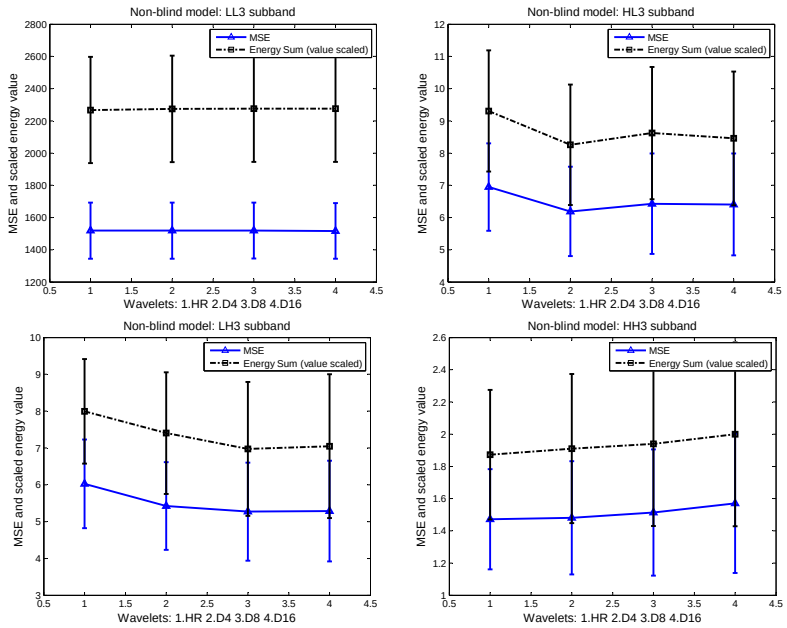

Figure 5.1: Watermark embedding (non-blind) performance graph for different subbands. Four different wavelet kernels used here: 1. HR, 2. D4, 3. D8 and 4. D16, respectively. Subbands are shown left to right and top to bottom: LL3, HL3, LH3, HH3, respectively.

The simulation results show a strong correlation between MSE of the watermarked image and the energy sum of the selected wavelet coefficients to be modified. It is observed that for the non-blind model, the correlation coefficient value is more than 0.80 and more than 0.58 in the case of blind model, for different wavelet kernels and various selected subbands. On the other hand, a similar graph patterns are observed in Figure 5.1, Figure 5.2, Figure 5.3 and Figure 5.4, which show the proportionality trend between MSE and the energy sum as proposed in the model. Lower correlation coefficients are observed for blind model due to the reason that the proportionality relationship only defines the upper bound in Eq. (5.18) and Eq. (5.21).

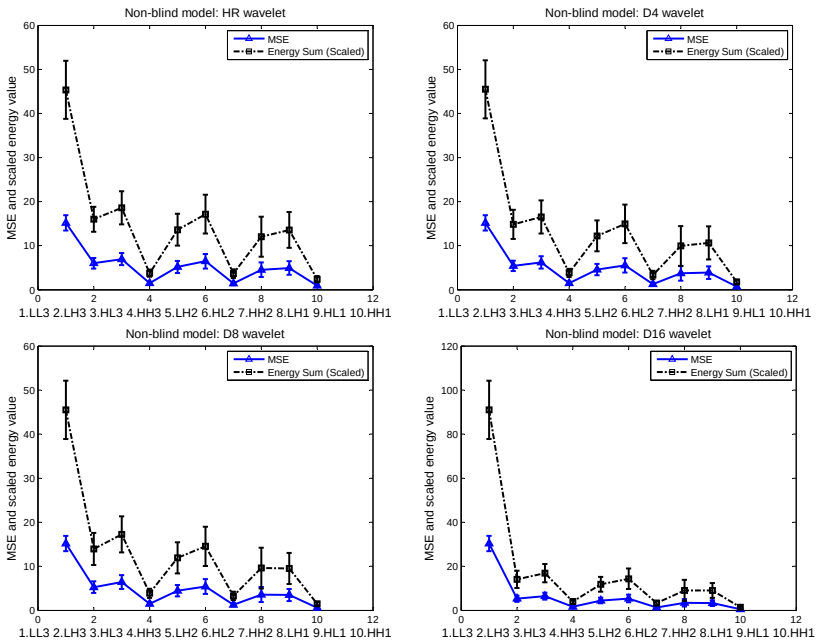

Figure 5.2: Watermark embedding (non-blind) performance graph for various wavelets in different subband. Wavelet kernels are shown left to right and top to bottom: HR, D4, D8 and D16, respectively.

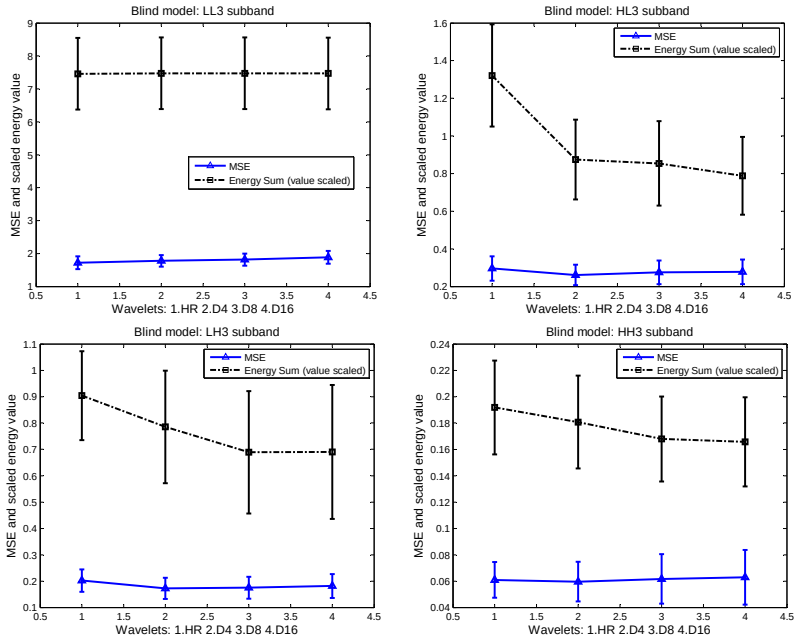

Figure 5.3: Watermark embedding (blind) performance graph for different subbands. Four different wavelet kernels used here: 1. HR, 2. D4, 3. D8 and 4. D16, respectively. Subbands are shown left to right and top to bottom: LL3, HL3, LH3, HH3, respectively.

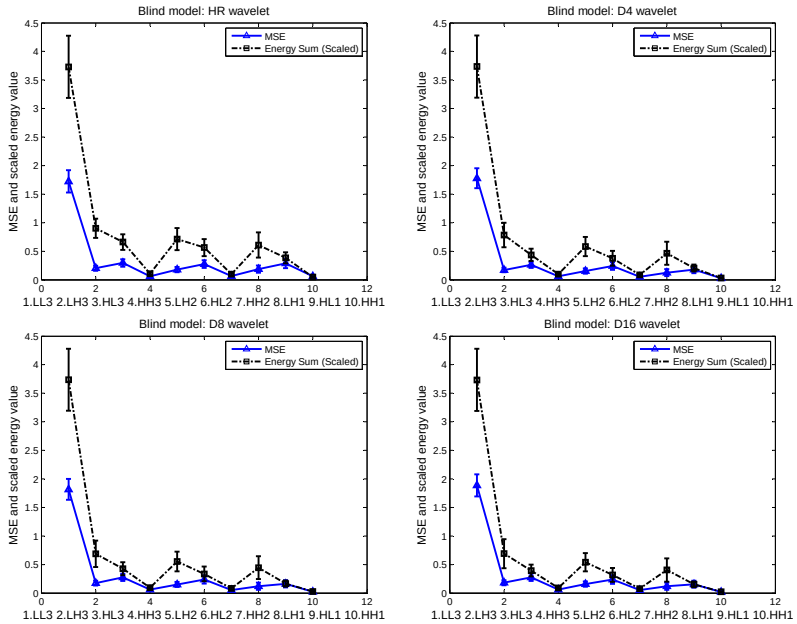

Figure 5.4: Watermark embedding (blind) performance graph for various wavelets in different subband. Wavelet kernels are shown left to right and top to bottom: HR, D4, D8 and D16, respectively.

5.3 Embedding distortion model for non-orthonormal wavelet bases

5.3.1 Preliminaries

Recalling *Parseval's Equality* in *Definition 5.2.2*, Eq. (5.2) is true for orthonormal transforms where energy is conserved between transforms. On the contrary, non-orthonormal wavelets such as biorthogonal wavelets do not hold conservation of energy. But for a stable expansion, the transform domain coefficients have to satisfy the Eq. (5.22) [59].

$$A \sum_k |y[k]|^2 \leq \|x\|^2 \leq B \sum_k |y[k]|^2, \tag{5.22}$$

where A and B are the orthonormality correction factor.

Based on the discussed propositions and the definitions we shall build the extended model and make the new propositions. As suggested in Eq. (5.22), for a non-orthonormal wavelet base an orthonormality correction factor is required and we shall call this as a

weighting factor W_t which is defined as follows:

$$W_t = \frac{\|x\|^2}{\sum_k |y[k]|^2}, \tag{5.23}$$

where x and y is the input signal and the transform domain coefficients, respectively.

Therefore at this point *Proposition 5.2.1* can be extended to a more generalized form. In a polyphase decomposition we use different low pass and high pass filter banks. Hence at each of the different transform points, we receive different weighting factors W_t^g and W_t^h, corresponding to high or low pass filters, respectively. Now the *Proposition 5.2.1* can be extended as follows, accommodating the weighting factors for non-orthonormal transforms:

$$\begin{aligned}\sum(|\Delta x_e|^2 + |\Delta x_o|^2) &= W_t^g \sum(|\Delta y_e|^2 + |\Delta y_o|^2) + W_t^h \sum(|\Delta y_e|^2 + |\Delta y_o|^2),\\ \sum_n |\Delta x[n]|^2 &= W_t^g \sum(|\Delta y_e|^2 + |\Delta y_o|^2) + W_t^h \sum(|\Delta y_e|^2 + |\Delta y_o|^2).\end{aligned} \tag{5.24}$$

Now using the generalized framework, Eq. (5.24) can be applied to build the relationship between the modification energy in the coefficient domain to embed the watermark and the distortion performance metrics for orthonormal as well as non-orthonormal wavelet bases.

Proposition 5.3.1 *In a wavelet based watermarking scheme, the mean square error (MSE) of the watermarked image is directly proportional to the weighted sum of the energy of the modification values of the selected wavelet coefficients.*

$$MSE \propto W_t^{\Theta\Upsilon} \sum |\Delta_{m,n}|)|^2, \tag{5.25}$$

where W_t is the weighting parameter at each subband and Θ represents the subband number at Υ decomposition level.

Proof: In order to prove this proposition, we recall Eq. (5.12) and Eq. (5.13) to combine them with Eq. (5.24) and the combined form can be written as:

$$\begin{aligned} MSE.(X \times Y) &= \sum_n |\Delta x[n]|^2,\\ &= W_t^g \sum_n |\Delta y[n]|^2 + W_t^h \sum_n |\Delta y[n]|^2,\\ &= W_t^g \sum_{m,n} |\Delta_{m,n}|^2 + W_t^h \sum_{m,n} |\Delta_{m,n}|^2. \end{aligned} \tag{5.26}$$

Hence for any watermarked image, the average noise power MSE is proportional to the sum of the weighted energy of the modification values of the selected wavelet coefficients:

$$MSE \propto W_t^g \sum_{m,n} |\Delta_{m,n}|^2 + W_t^h \sum_{m,n} |\Delta_{m,n}|^2. \tag{5.27}$$

Now in the case of 2-D wavelet decompositions, the wavelet kernel transfer function, for each subband at each decomposition level are different and so that the weighting factors are. Hence the Δ in Eq. (5.27) are associated with a corresponding weighting parameter for each subband at each decomposition level. We define the weighting parameter as $W_t^{\Theta\Upsilon}$ at each subband and Θ represents the subband number at Υ decomposition level and therefore Eq. (5.27) can be re-written as:

$$MSE \propto W_t^{\Theta\Upsilon} \sum |\Delta_{m,n}|)|^2. \tag{5.28}$$

■.

Therefore, using Eq. (5.28), the Eq. (5.10) and Eq. (5.11) can be extended for non-blind and blind model to Eq. (5.29) and Eq. (5.30), respectively, as follows:

$$MSE \propto \sum W_t^{\Theta\Upsilon} |f(C_{m,n})|^2. \tag{5.29}$$

$$MSE \propto \sum W_t^{\Theta\Upsilon} |f(C_{min}, C_{max})|^2. \tag{5.30}$$

Hence the above equation can universally used for various wavelet kernels, where for orthonormal wavelet kernels the value of the weighting parameters are equal to unity. For non-orthonormal wavelet kernel, different weighting parameter values are suggested in next section for different subbands at each decomposition level.

5.3.2 Experimental simulations and discussion

Experimental simulations have been carried out to verify the propositions made in the previous section. There are two different parts of the experiment conducted: calculation of the weighting parameters and simulation of the propositions.

Table 5.2: Weighting parameter values of each subband at each decomposition level for various non-orthonormal wavelets.

	9/7	5/3	MH	MQ
LL1	1.00 ± 0.00	0.99 ± 0.00	1.00 ± 0.00	0.99 ± 0.00
LH1	1.22 ± 0.04	1.31 ± 0.03	1.00 ± 0.00	0.94 ± 0.02
HL1	1.09 ± 0.02	1.31 ± 0.03	1.00 ± 0.00	1.97 ± 0.03
HH1	1.34 ± 0.04	2.43 ± 0.08	1.02 ± 0.00	1.64 ± 0.05
LL2	1.00 ± 0.00	0.99 ± 0.00	1.00 ± 0.00	0.98 ± 0.00
LH2	1.22 ± 0.06	0.69 ± 0.03	1.00 ± 0.00	0.31 ± 0.01
HL2	1.07 ± 0.03	0.74 ± 0.04	1.00 ± 0.00	0.52 ± 0.00
HH2	1.17 ± 0.05	0.81 ± 0.03	1.01 ± 0.00	0.41 ± 0.01
LL3	1.00 ± 0.00	0.98 ± 0.00	1.00 ± 0.00	0.98 ± 0.01
LH3	1.37 ± 0.08	0.57 ± 0.03	1.00 ± 0.00	0.15 ± 0.01
HL3	1.13 ± 0.02	0.57 ± 0.03	1.00 ± 0.00	0.17 ± 0.00
HH3	1.31 ± 0.06	0.53 ± 0.02	1.00 ± 0.00	0.12 ± 0.00

5.3.2.1 Calculation of the weighting parameters

The weighting parameters are calculated for each subband at each decomposition level for various wavelet kernels. A three level decomposition is done and the weighting parameter values are calculated for each of the ten subbands. A set of different non-orthonormal wavelet kernels including bi-orthogonal 5/3 and 9/7, are chosen for the experimental simulations. Although the propositions made here assumed *Linearity* property of wavelet kernels, we have experimentally simulated and observe the similar proposition on non-linear wavelets, such as, Morphological Haar (MH) and Quincunx domain Morphological wavelets (MQ). While calculating the weighting parameters, the energy ratios are considered for each subband one at a time while keeping other subband values to zero in Eq. (5.31).

$$W_t^{\Theta\Upsilon} = \frac{\|x\|^2}{\sum |y^{\Theta\Upsilon}|^2}, \tag{5.31}$$

where $W_t^{\Theta\Upsilon}$ is the weighting parameter at Θ subband at Υ decomposition level, $y^{\Theta\Upsilon}$ is the coefficient value at Θ subband at Υ decomposition level and x is the output pixel values after the inverse wavelet transform. The weighting parameters are calculated for the experimental image set and generalized by averaging them. It is observed that these parameters are image independent. The corresponding weighting parameters for different subbands at each decomposition levels are calculated and shown Table 5.2 along with the error. The errors presented here display accuracy up to the 95% confidence interval.

5.3.2.2 Simulations of the propositions

The simulations of the proposed embedding distortion model for non-orthonormal wavelet kernels are performed using a similar set up as used in the simulations of the embedding models for orthonormal wavelets. The same test image set is used, with three level wavelet decomposition. Four different non-orthonormal wavelet kernels, namely, bi-orthogonal 9/7 and 5/3 and non-linear Morphological Haar (MH) and Quincunx domain Morphological wavelets (MQ), are simulated and studied here. For each simulations, first, results are shown without considering the weighting parameters ($W_t^{\Theta\Upsilon}$) and then the corresponding results using weighting parameters from Table 5.2:

Non-blind model: The experimental simulations for non-blind model as described in Eq. (5.29) is performed and the correlation coefficients are calculated and represented in Table 5.3. The average values of the MSE and the sum of energy are shown in Figure 5.5. *Column 1* and *Column 2* represent the results without and with considering the weighting parameter, while calculating the energy sum, respectively. The error bars denote the accuracy up to the 95% confidence interval. For display purposes the sum of energy value was scaled, so that they can be shown on the same plot for comparing the trend.

In the other experiment set the subbands are compared and the results are shown in Figure 5.6. Here *Column 1*, *Column 2* and *Column 3* represent the MSE, energy sum without and with weighting parameters, respectively. As earlier the LL3 values are scaled suitably in all cases to observe the trends.

Blind model: A similar experimental set, as in non-blind model, is used for the blind model for non-orthonormal wavelet kernels as described in Eq. (5.30). The correlation coefficients, average pattern graphs for various wavelet kernels and ten different subbands are presented in Table 5.3, Figure 5.7 and Figure 5.8, respectively, without and with consideration of the weighting parameters.

It is observed that bi-orthogonal wavelets strongly support the propositions, whereas an occasional deviation is noticed for MH and MQ wavelet kernels due its non-linear activity within the transform. However, the general behavioral pattern is maintained in all four non-orthonormal wavelets, ensures the propositions' realization in embedding distortion performance of the generalized watermarking schemes.

Table 5.3: Correlation coefficient values between sum of energy and the MSE for different wavelet kernel in various subbands.

	Non-blind model				Blind model			
	9/7	5/3	MH	MQ	9/7	5/3	MH	MQ
LL3	0.80	0.81	0.81	0.81	0.77	0.82	0.43	0.78
LH3	0.95	0.90	0.93	0.97	0.78	0.51	0.73	0.86
HL3	0.99	0.97	0.98	0.95	0.96	0.94	0.73	0.92
HH3	0.95	0.94	0.95	0.96	0.80	0.84	0.69	0.83
LH2	0.97	0.97	0.98	0.99	0.81	0.81	0.70	0.94
HL2	0.99	0.99	0.99	0.99	0.96	0.97	0.90	0.86
HH2	0.99	0.99	0.99	0.98	0.89	0.88	0.84	0.93
LH1	0.99	0.99	0.99	0.97	0.88	0.87	0.90	0.89
HL1	0.97	0.97	0.98	0.99	0.75	0.91	0.91	0.95
HH1	0.99	0.99	0.99	0.99	0.95	0.89	0.88	0.94

5.4 Conclusions

A gap is identified in the literature to mathematically relate the embedding distortion performance metric and watermarking input parameters. A universal embedding distortion performance model for wavelet based watermarking schemes is presented in this chapter to address such gap. First we have proposed models for orthonormal wavelet bases, which is then extended to non-orthonormal wavelet kernels such as biorthogonal and non-linear wavelets. The current model suggests that the MSE of the watermarked image is directly proportional to the weighted sum of energy of the modification values of the selected wavelet coefficients and this proposition is valid for orthonormal as well as non-orthonormal wavelet kernels. In the case of the non-orthonormal wavelet bases a weighting parameter is introduced and it is computed experimentally for different non-orthonormal wavelet bases whereas in the case of orthonormal wavelets, these weighting parameters are set to unity. This universal model is verified by extensive experimental simulations with a wide range of wavelet kernels. Such a model is useful to optimize the input parameters, *i.e.,* wavelet kernel or subband selection or the host coefficient selection in wavelet based watermarking schemes.

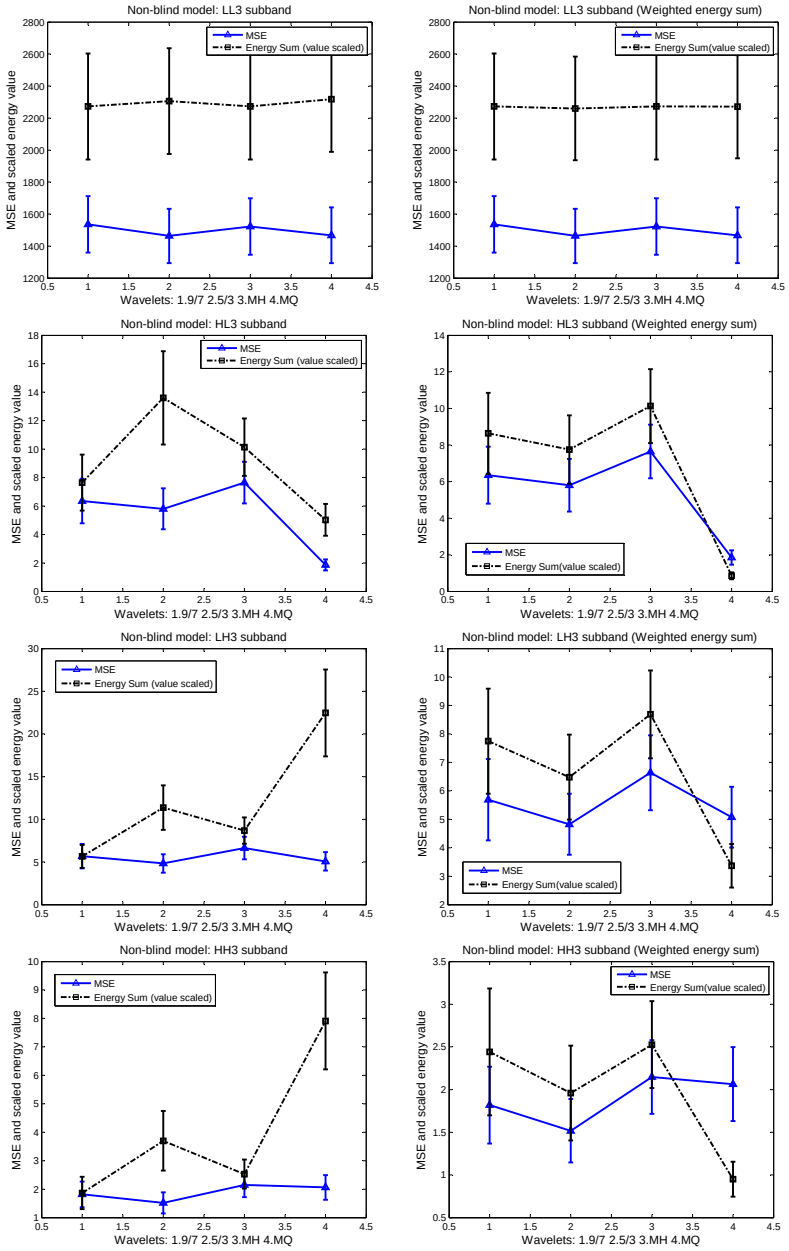

Figure 5.5: Watermark embedding (non-blind) performance graph for different subbands. Four different wavelet kernels used here: 1. 9/7, 2. 5/3, 3. MH and 4. MQ, respectively. Subbands are shown left to right and top to bottom: LL3, HL3, LH3, HH3, respectively.

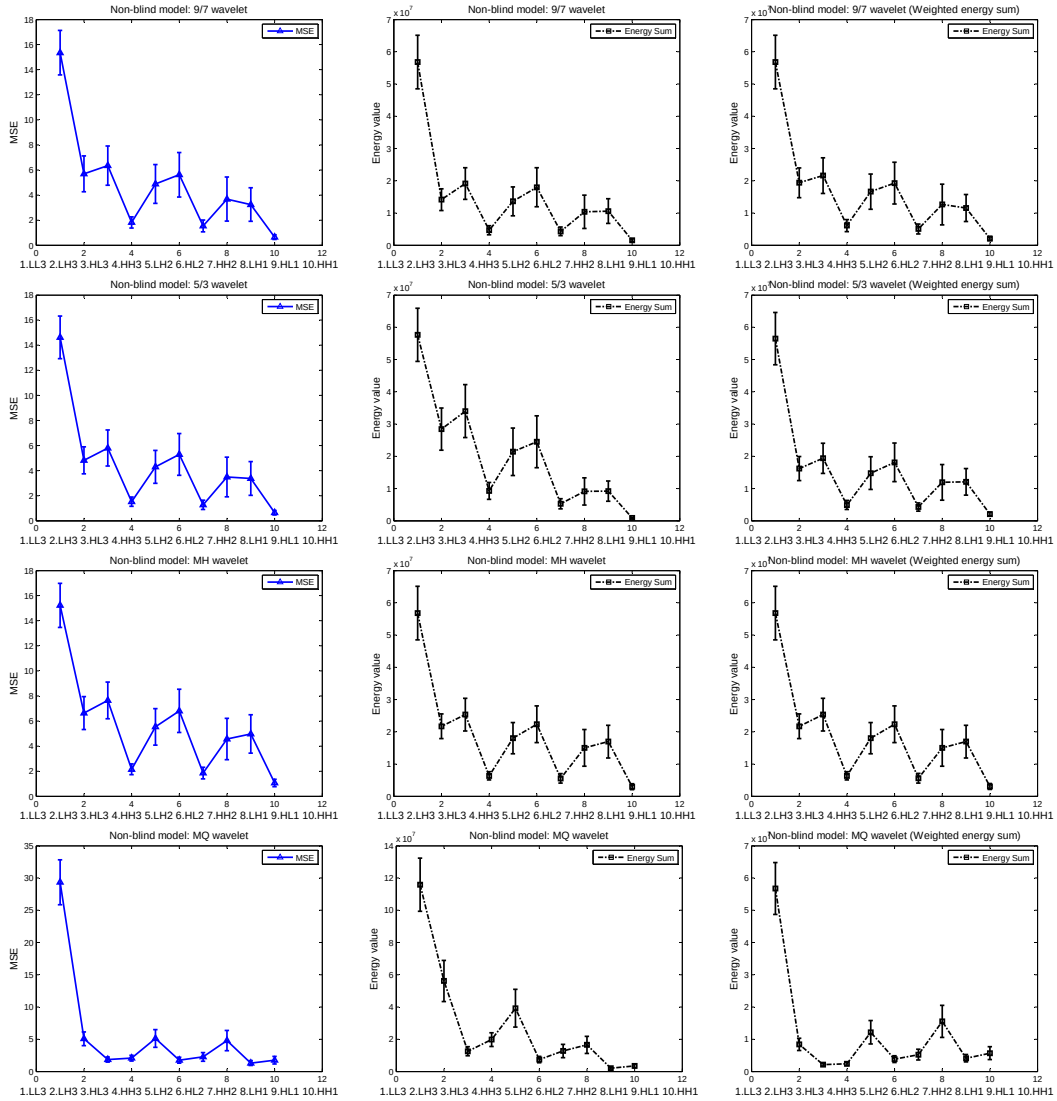

Figure 5.6: Watermark embedding (non-blind) performance graph for various wavelets in different subband. Wavelet kernels are shown left to right and top to bottom: 1. 9/7, 2. 5/3, 3. MH and 4. MQ, respectively.

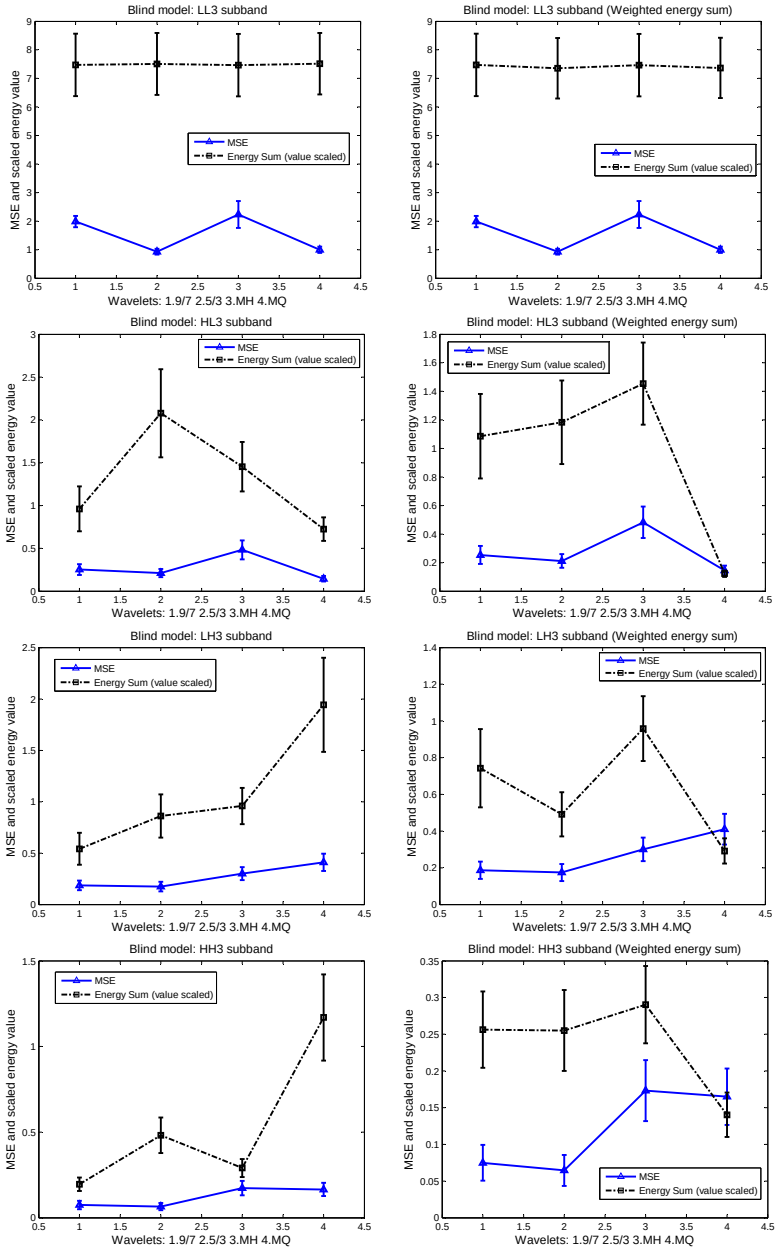

Figure 5.7: Watermark embedding (blind) performance graph for different subbands. Four different wavelet kernels used here: 1. 9/7, 2. 5/3, 3. MH and 4. MQ, respectively. Subbands are shown left to right and top to bottom: LL3, HL3, LH3, HH3, respectively.

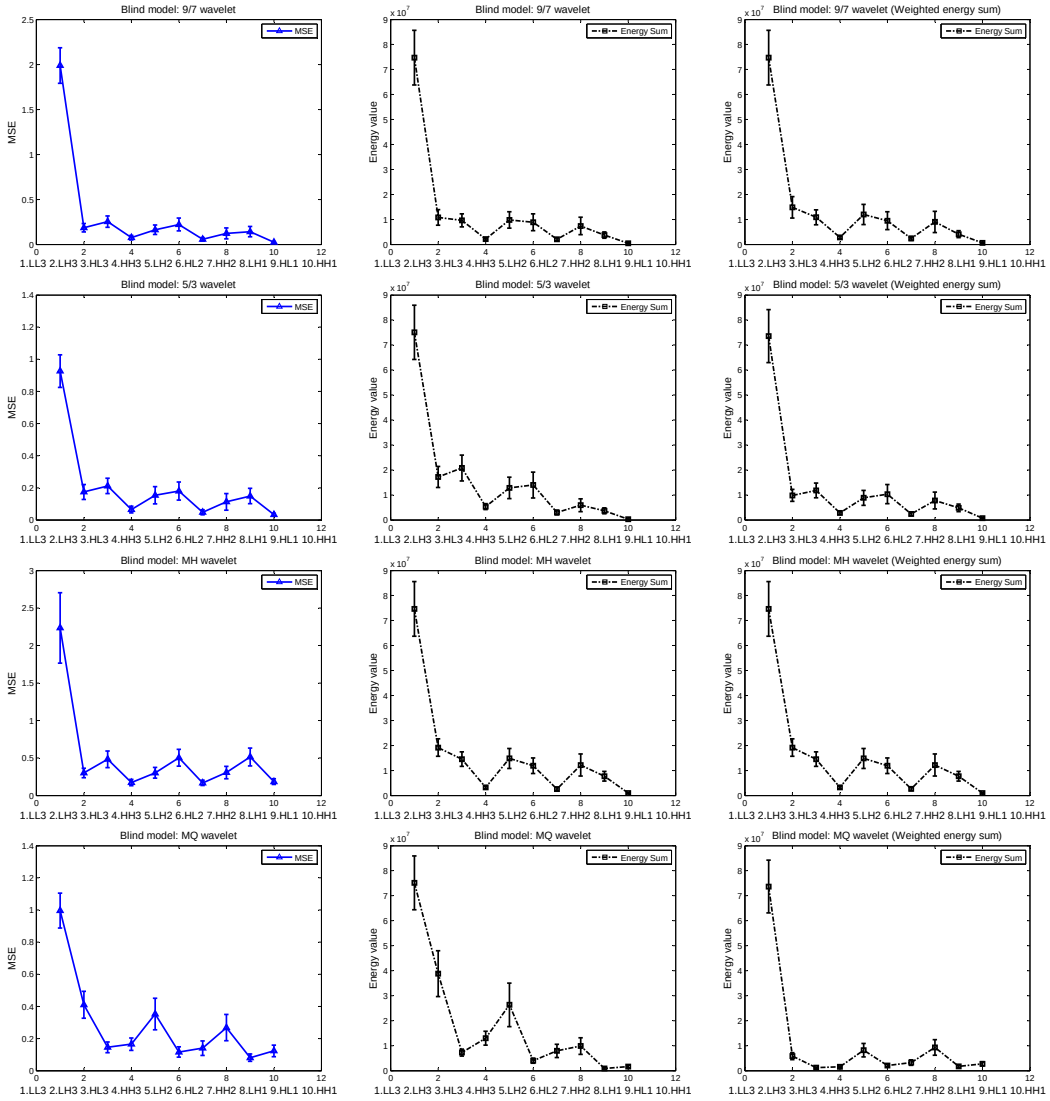

Figure 5.8: Watermark embedding (blind) performance graph for various wavelets in different subband. Wavelet kernels are shown left to right and top to bottom: 1. 9/7, 2. 5/3, 3. MH and 4. MQ, respectively.

Chapter 6

Robustness analysis and modeling

6.1 Introduction

Scalable image coding consists of multi-resolution decomposition of images, such as, the discrete wavelet transform (DWT), followed by hierarchical layered representation considering the scalability requirements. For the quality scalability driven content adaptations, the corresponding insignificant quality layers are discarded. Such content adaptations result in loss of watermark data embedded within the affected coefficients, thus, diminishing the robustness of the watermarking schemes. The watermarking literature often focuses only on the robustness to attacks, such as, image processing, JPEG-based compression and geometric adaptations [107]. This chapter proposes a novel approach enhancing the robustness of wavelet-based image watermarking for scalable coding-based content adaptation attacks.

As discussed in Chapter 3, based on the embedding methodology, wavelet-based image watermarking can be categorized into two main classes: uncompressed domain algorithms [5–18] and joint compression-watermarking algorithms [19–26]. One of the main objectives of the latter class of algorithms is to enhance the robustness to JPEG 2000-based compression, although in most cases the effect of full capabilities of JPEG 2000 compression and associated content adaptations has not been considered in the proposed solutions. However, JPEG 2000 Part 8 (ISO/IEC 15444-8, T.807) Secure JPEG 2000 (JPSEC) [20] specifies the framework, concepts, and methodology for securing

JPEG 2000 bit streams considering the full capabilities of JPEG 2000. One of the underlying techniques in JPSEC is watermarking [26,108], proposed as joint compression domain embedding within the coding pipeline.

The work, here, focuses on the uncompressed domain watermarking algorithms considering the sequence of events as watermarking, JPEG 2000 compression, content adaptation and watermark authentication for the decoded image. We model quality scalability by bit plane discarding and propose the choice of embedding coefficients and watermarking parameters to minimize the effect of bit plane discarding on the watermarked data. The proposed model addresses both non-blind and blind watermark extraction scenarios.

6.2 Quality scalability in content adaptation

In universal media access (UMA) application scenario for images, the resolution-quality layers in the scalable bit stream lead into two types of content adaptation: quality scalability and resolution scalability. The present work focuses only on the quality scalability, available in JPEG 2000 scalable image coding. The simplest form of quality layers used in JPEG 2000 coding corresponds to bit plane-based coding of wavelet coefficients. Choosing certain quality layers up to some bit planes corresponds to quantization of the wavelet coefficients. In general, the coefficient quantization due to bit plane discarding, in its simplest form, can be formulated as follows:

$$C_q = \frac{C}{|C|} \left\lfloor \frac{|C|}{Q} \right\rfloor, \tag{6.1}$$

where C_q is the quantized coefficient, C is the non-zero original coefficient, Q is the quantization factor and $\lfloor x \rfloor$ denotes rounding of x to the largest integer smaller than x (called downward rounding). Embedded quantizers often use $Q = 2^N$, where N is a non-negative integer that corresponds to the number of bit planes being discarded.

At the decoder side, the reverse process of the quantization (de-quantization) is followed by multiplying by the quantization factor Q and allowing for the uncertainty due to downward rounding as follows:

$$\hat{C} = C_q Q + \frac{C}{|C|} \left(\frac{Q-1}{2} \right), \tag{6.2}$$

where $\hat{C}$ is the de-quantized coefficient. The outcome of the combined quantization

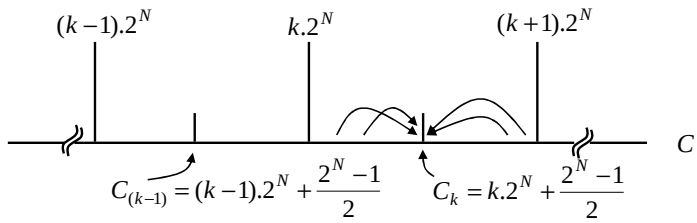

Figure 6.1: The effect of quantization and de-quantization processes in wavelet domain considering discarding of N bit planes.

and de-quantization processes is

$$\hat{C} = \frac{C}{|C|}\left(\left\lfloor \frac{|C|}{Q} \right\rfloor Q + \frac{Q-1}{2}\right). \tag{6.3}$$

Thereby, one can show that the original coefficient values in the range $kQ \leq C < (k+1)Q$, where $k \in \{0, \pm 1, \pm 2, ...\}$, are quantized using N bit plane discarding, *i.e.,* $Q = 2^N$, are mapped to $\hat{C} = C_k$, which is the center value of the region marked by kQ and $(k+1)Q$ as shown in Figure 6.1. Thus, the center value, C_k, is given by

$$C_k = k2^N + \frac{k}{|k|}\left(\frac{2^N-1}{2}\right). \tag{6.4}$$

This relationship is further exploited in Section 6.3 and Section 6.4 in order to model the watermark robustness to bit-plane discarding driven quality scalable decoding in content adaptations.

6.3 Robustness model for non-blind extraction using magnitude alteration

6.3.1 Preliminaries

For magnitude alteration algorithms Eq. (3.1) and Eq. (3.2) are combined considering $< 1, 0, 0, 0 >$ $(\tau = 1)$, ignoring the index subscripts (m, n), to get

$$\begin{aligned} C' &= C + \alpha C w_b, \\ &= C(1 + \alpha w_b), \end{aligned} \tag{6.5}$$

where the watermark W in Eq. (3.2) is replaced with w_b ($b \in \{0, 1\}$) for a binary watermark logo. The two values, w_0 and w_1, are usually chosen as $w_1 > w_0 > 0$. From Eq. (6.5), the relationship between C' and C is

$$C = \frac{C'}{1 + \alpha w_b}. \tag{6.6}$$

Since $(1+\alpha w_b) > 0$, both C and C' share the same sign. The corresponding modification Δ is

$$\Delta = C' - C = \alpha C w_b. \tag{6.7}$$

Thus, the extracted watermark value, w'_b, is computed as

$$w'_b = \frac{C' - C}{\alpha C}. \tag{6.8}$$

Then the recovered watermark value, b', is

$$b' = \begin{cases} 1 & : \quad w'_b \geq T, \\ 0 & : \quad w'_b < T, \end{cases} \tag{6.9}$$

where the threshold $T = \frac{w_0 + w_1}{2}$.

6.3.2 The model

Now considering the quantization and de-quantization processes in the compression and decompression, let $\hat{C}'$ be the reconstructed watermarked coefficient after decompression. As shown in Eq. (6.4) in Section 6.2, for discarding N bit planes, $\hat{C}'$ represents re-mapping of the original watermarked coefficients, C', to the center points, C_k, of the corresponding coefficient cluster, $[k2^N, (k+1)2^N)$, *i.e.,*

$$\hat{C}' = C_k, \quad \forall \quad k2^N \leq C' < (k+1)2^N. \tag{6.10}$$

The proposed model aims to identify coefficients with magnitude values that fall into regions where the accurate watermark extraction is possible after the quantization and de-quantization processes as follows:

Proposition 1 *The original wavelet coefficients, C, for embedding a bit with value $b = 1$ and retain intact when N bit planes are discarded are in the range*

$$\frac{k.2^N}{1+\alpha w_1} \leq C \leq \frac{C_k}{1+\alpha T},$$

with $k \in \{0, \pm 1, \pm 2, \pm 3, ...\}$.

Proof : To extract $b = 1$ accurately, we need $w'_b \geq T$. That means

$$\frac{C' - C}{\alpha C} \geq T. \tag{6.11}$$

Since both C' and C share the same sign and $|C'| > |C|$,

$$C' \geq C(1 + \alpha T). \tag{6.12}$$

If there is no compression, the value of C' is given by Eq. (6.5). But due to compression, only the reconstructed coefficients, $\hat{C}'$, are available. The correct extraction of $b = 1$ is possible if

$$\hat{C}' \geq C'. \tag{6.13}$$

Considering the values in the region, $k2^N \leq C' < (k+1)2^N$,

$$\begin{aligned} \forall \quad k2^N \leq C' \leq C_k, \quad \hat{C}' = C_k \Rightarrow \hat{C}' \geq C', \\ \forall \quad C_k < C' < (k+1)2^N, \quad \hat{C}' = C_k \Rightarrow \hat{C}' < C'. \end{aligned} \tag{6.14}$$

Therefore, the condition in Eq. (6.13) is true when

$$k2^N \leq C' \leq C_k, \tag{6.15}$$

which in terms of the original coefficients, C, is

$$\begin{aligned} k2^N \leq C(1 + \alpha w_1) \leq C_k, \\ \tfrac{k2^N}{1+\alpha w_1} \leq C \leq \tfrac{C_k}{1+\alpha w_1}. \end{aligned} \tag{6.16}$$

However, even if $\hat{C}' < C'$, the correct extraction of $b = 1$ is still possible if (by considering Eq. (6.12))

$$C_k - C \geq \alpha C T. \tag{6.17}$$

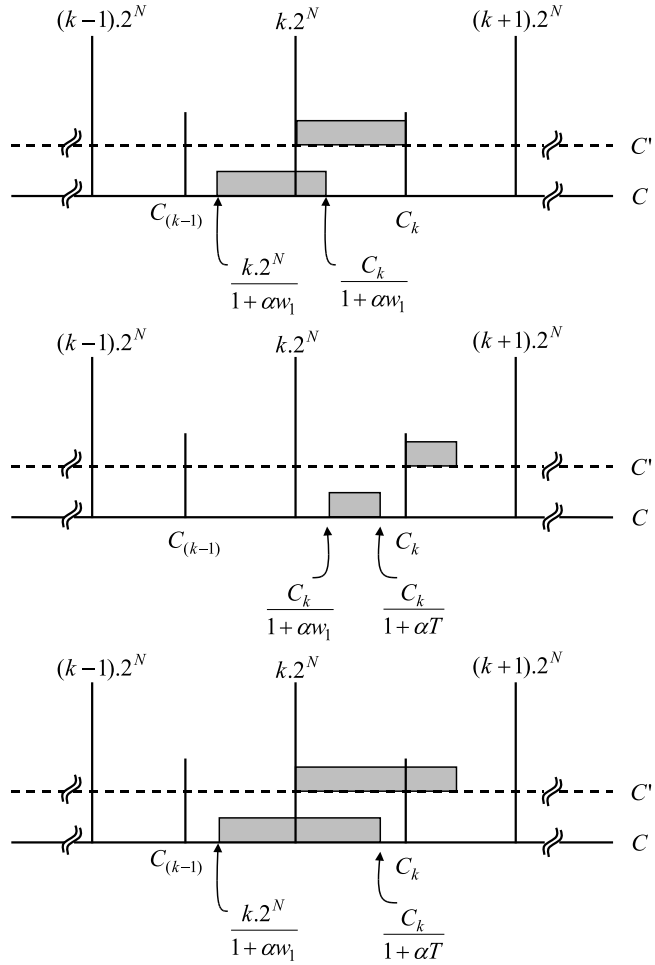

Figure 6.2: The range of C capable of robust extraction of $b = 1$. *Row 1*: $\hat{C}' \geq C'$; *Row 2*: $\hat{C}' < C'$; *Row 3*: The total range.

This means,

$$C_k \geq C(1 + \alpha T),$$
$$C \leq \tfrac{C_k}{1+\alpha T}. \tag{6.18}$$

We know that $w_1 > T$. Therefore, $\frac{1}{1+\alpha T} > \frac{1}{1+\alpha w_1}$ and thus we can merge the ranges in Eq. (6.16) and Eq. (6.18), as summarized in Figure 6.2, to get the range of original coefficients capable of robust extraction of $b = 1$ to

$$\frac{k2^N}{1 + \alpha w_1} \leq C \leq \frac{C_k}{1 + \alpha T}. \tag{6.19}$$

■.

Proposition 2 *The original wavelet coefficients, C, for embedding a bit with value $b = 0$ and retain intact when N bit planes are discarded are in the range*

$$\frac{C_{(k-1)}}{1+\alpha T} < C < \frac{k.2^N}{1+\alpha w_0},$$

with $k \in \{0, \pm 1, \pm 2, \pm 3, ...\}$.

Proof : To extract $b = 0$ accurately, we need $w'_b < T$. That means

$$\tfrac{C'-C}{\alpha C} < T, \tag{6.20}$$

$$C' < C(1+\alpha T). \tag{6.21}$$

The correct extraction of $b = 0$ from the reconstructed coefficients, $\hat{C}'$, is possible if

$$\hat{C}' < C'. \tag{6.22}$$

Therefore, considering the values in the region, $(k-1)2^N \leq C' < k2^N$,

$$\begin{aligned} \forall \quad (k-1)2^N \leq C' \leq C_{k-1}, \quad \hat{C}' = C_{k-1} \Rightarrow \hat{C}' \geq C', \\ \forall \quad C_{k-1} < C' < k2^N, \quad \hat{C}' = C_{k-1} \Rightarrow \hat{C}' < C'. \end{aligned} \tag{6.23}$$

Therefore, the condition in Eq. (6.22) is true when

$$C_{k-1} < C' < k2^N, \tag{6.24}$$

which in terms of the original coefficients, C, is

$$\begin{aligned} C_{k-1} < C(1+\alpha w_0) < k2^N, \\ \tfrac{C_{k-1}}{1+\alpha w_0} < C < \tfrac{k2^N}{1+\alpha w_0}. \end{aligned} \tag{6.25}$$

However, even if $\hat{C}' \geq C'$, the correct extraction of $b = 0$ is still possible if

$$C_{k-1} - C < \alpha C T, \tag{6.26}$$

as suggested by Eq. (6.21). This means,

$$\begin{aligned} C_{k-1} &< C(1+\alpha T), \\ C &> \frac{C_{k-1}}{1+\alpha T}. \end{aligned} \tag{6.27}$$

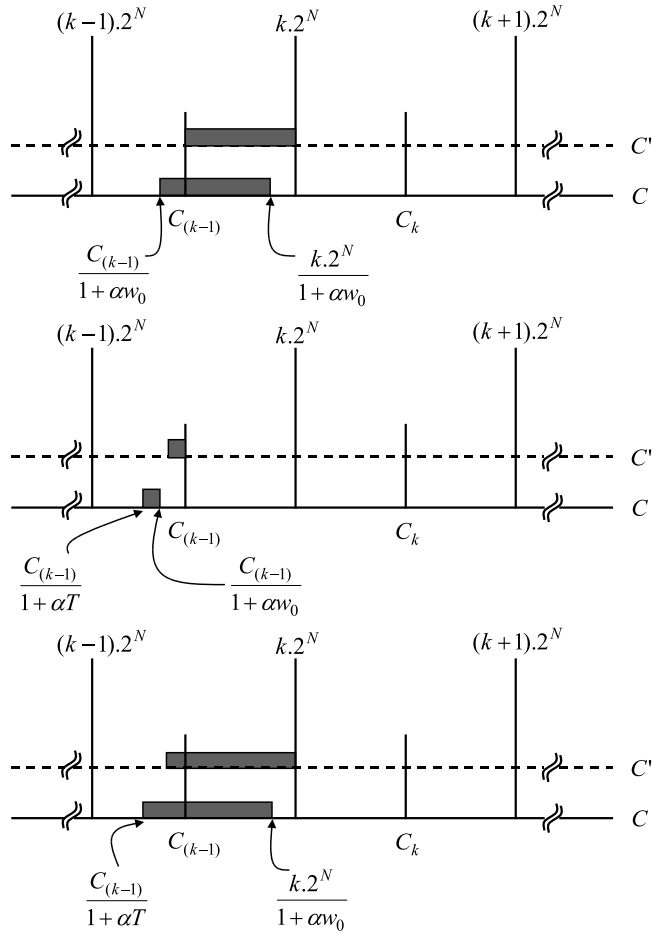

Figure 6.3: The range of C capable of robust extraction of $b = 0$. *Row 1*: $\hat{C}' < C'$; *Row 2*: $\hat{C}' \geq C'$; *Row 3*: The total range.

Since $w_0 < T$, we can write $\frac{1}{1+\alpha T} < \frac{1}{1+\alpha w_0}$. Thus we can merge the ranges in Eq. (6.25) and Eq. (6.27), as summarized in Figure 6.3, to get the range of original coefficients capable of robust extraction of $b = 0$ to

$$\frac{C_{(k-1)}}{1+\alpha T} < C < \frac{k.2^N}{1+\alpha w_0}. \tag{6.28}$$

■.

Finally, as shown in Figure 6.4, the above two results in Eq. (6.19) and Eq. (6.28) are combined to derive the region of coefficient magnitudes that are capable of retaining both $b = 1$ and $b = 0$ when N bit planes are discarded as follows:

$$\frac{k.2^N}{1+\alpha w_1} \leq C < \frac{k.2^N}{1+\alpha w_0}. \tag{6.29}$$

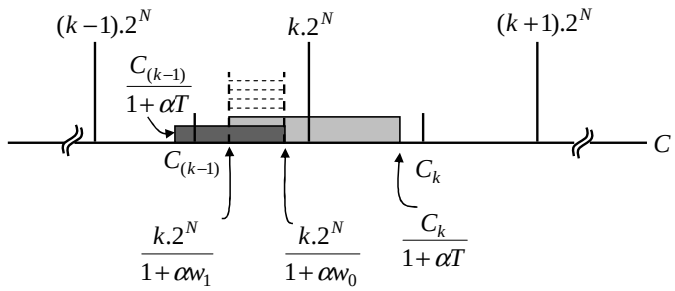

Figure 6.4: The combined range of C capable of robust extraction of both $b = 1$ and $b = 0$.

6.3.3 Examples

As an example, we choose $w_1 = 0.8$, $w_0 = 0.3$, the threshold $T = 0.55$ and a data set containing coefficient values, C from -512 to 512, and show the ranges of coefficient values that can robustly retain the embedded watermark bits after discarding $N = 7$ bit planes in Table 6.1. Two scenarios of $\alpha = 0.5$ and $\alpha = 0.05$ are shown. First, the coefficient selection for embedding $b = 1$ using Eq. (6.19) are shown followed by the coefficient selection for embedding $b = 0$ using Eq. (6.28). Finally the common region is found for embedding any value of b as shown in Eq. (6.29).

Figure 6.5 shows the robustness ability of wavelet coefficients for two different subbands (LL and HL after a single level of decomposition) for given numbers of bit plane discarding. In this figure the gray scale is quantized into 7 levels with black representing robustness to $N = 0$ bit plane discarding (*i.e.,* the least robust) and white representing robustness up to $N = 6$ bit plane discarding (*i.e.,* the most robust), with other intermediate grey levels corresponding to coefficients robust up to discarding of $N = 1, ..., 5$ bit planes, respectively.

6.4 Robustness model for blind extraction using re-quantization-based modifications

6.4.1 Preliminaries

Recalling Section 3.1.2.4, in re-quantization-based modification (*e.g.,* [5,6,22]), a group of coefficients (usually three coefficients) are ranked ordered to identify the minimum

Table 6.1: Data value (C) ranges for retaining the watermark data, $b = 1$ and $b = 0$ for discarding $N = 7$ bit planes.

(a) $\alpha = 0.5$

	$k \rightarrow$	-5	-4	-3	-2	-1	0	1	2	3	4	5
$b = 1$	min	-512	-460	-358	-256	-153	0	91	183	274	366	457
	max	-457	-366	-274	-183	-91	51	153	256	358	460	512
$b = 0$	min	-512	-445	-334	-223	-111	-51	51	153	256	358	460
	max	-460	-358	-256	-153	-51	0	111	223	334	445	512
$b = 1$ and	min	-512	-445	-334	-223	-111		91	183	274	366	460
$b = 0$	max	-460	-366	-274	-183	-91		111	223	334	445	512

(b) $\alpha = 0.05$

	$k \rightarrow$	-4	-3	-2	-1	0	1	2	3	4
$b = 1$	min	-512	-437	-312	-187	0	123	246	369	492
	max	-492	-369	-246	-123	62	187	312	437	512
$b = 0$	min	-504	-378	-252	-126	-62	62	187	312	437
	max	-437	-312	-187	-62	0	126	252	378	504
$b = 1$ and	min	-504	-378	-252	-126		123	246	369	492
$b = 0$	max	-492	-369	-246	-123		126	252	378	504

(C_1), the maximum (C_3) and the median (C_2) coefficients. Then C_2 is modified to obtain C_2' as follows:

$$C_2' = f(\gamma, C_1, C_3, b), \tag{6.30}$$

where b is binary watermark bit, $b \in \{0, 1\}$, γ is a parameter corresponding to the watermark strength and $f()$ is a non-linear transformation process which is described as follows. This process first partitions the coefficient range, r, where

$$r = C_3 - C_1, \tag{6.31}$$

by the quantization bin size, δ, defined by

$$\delta = \gamma \frac{|C_1| + |C_3|}{2}, \tag{6.32}$$

into quantization bins with indexes, $i = 0, 1, ..., \frac{r}{\delta} - 1$. Then in order to embed a watermark bit b, the original value, C_2, is modified to C_2' by choosing any value that comes from the quantization bin index, i, where $b = i\%2$, *i.e.,*

$$C_2' \in \left\{ C : \quad \frac{C - C_1}{\delta} \% 2 = b \right\}, \tag{6.33}$$

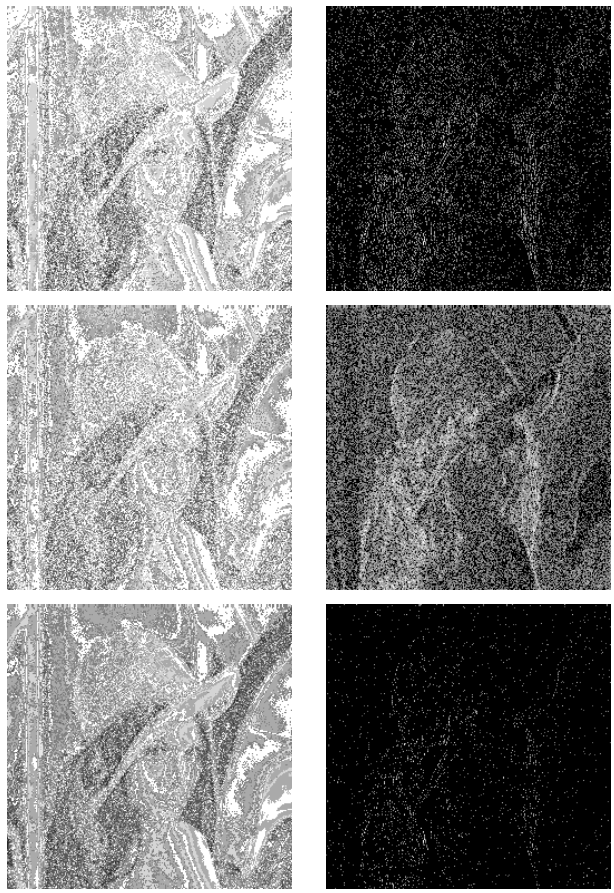

Figure 6.5: Coefficients' robustness rank maps for discarding up to N bit planes shown using 7 gray scales corresponding to $N = 0, ..., 6$. *Left*: LL subband; *Right*: HL subband; *Row 1*: Embedding $b = 1$; *Row 2*: Embedding $b = 0$; *Row 3*: Embedding any value of b.

where % denotes the modulo operator as shown in Figure 3.3. To extract the watermark bit, b, back from C_1, C_2' and C_3,

$$b = \left(\frac{C_2' - C_1}{\delta} \right) \%2. \tag{6.34}$$

6.4.2 The model

After compression and decompression, only the reconstructed coefficients, $\hat{C}_1$, $\hat{C'}_2$ and $\hat{C}_3$, are available to the watermark extraction process. In order for the successful extraction, *i.e.,* to maintain the robustness to quality scalable compression, the relationship,

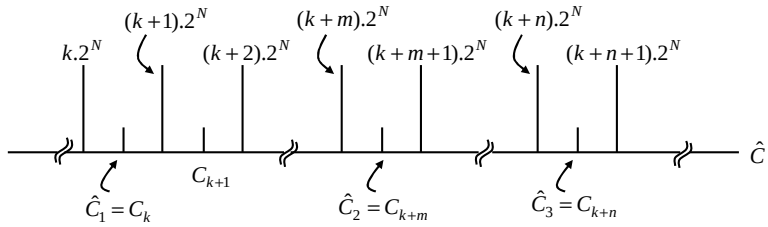

Figure 6.6: Mapping of coefficients after quantization and de-quantization processes considering the discarding of N bit planes.

$\hat{C}_1 \leq \hat{C}'_2 \leq \hat{C}_3$, must be remained intact while $\hat{C}_1 \neq \hat{C}'_2 \neq \hat{C}_3$ and

$$\hat{b} = \left(\frac{\hat{C}'_2 - \hat{C}_1}{\hat{\delta}} \right) \%2, \tag{6.35}$$

where

$$\hat{\delta} = \gamma \frac{|\hat{C}_1| + |\hat{C}_3|}{2}. \tag{6.36}$$

As discussed earlier, the original coefficient values in the range $kQ \leq C < (k+1)Q$, where $k \in \{0, \pm 1, \pm 2, \pm 3, ...\}$ are quantized using N bit plane discarding *i.e.,* $Q = 2^N$, are mapped to $\hat{C} = C_k$, which is the center value of the region marked by kQ and $(k+1)Q$ as shown in Figure 6.1. The center value, C_k, of the clusters is given by Eq. (6.4). In line with this definition, we assume that the mapped three values, $\hat{C}_1$, $\hat{C}'_2$ and $\hat{C}_3$, are C_k, C_{k+m} and C_{k+n}, where $m, n \in \{0, 1, 2, ...\}$ and $0 \leq m \leq n$, respectively as shown in Figure 6.6. Therefore, the robustness model needs to estimate the extracted watermark bit, $\hat{b}$, as a function of m, with respect to discarding N bit planes at the time of embedding the watermark.

Proposition 3 *The estimated extracted watermark bit, $\hat{b}$, with respect to discarding N bit planes, is given by*

$$\hat{b} = \left(\frac{2m + z}{\gamma(|k| + |k+n| + 1)} \right) \%2,$$

where $z = 0$, if C_k and C_{k+m} have the same sign and $z = 2 - 2^{1-N}$, if otherwise.

Proof : C_k in Eq. (6.4) can be represented in the sign magnitude form as follows:

$$C_k = \frac{k}{|k|} \left(|k| 2^N + \frac{2^N - 1}{2} \right). \tag{6.37}$$

With reference to Eq. (6.36), the reconstructed watermark quantization step value, $\hat{\delta}$, after discarding N bit planes can now be defined as:

$$\begin{aligned}
\hat{\delta} &= \gamma\frac{|\hat{C}_1| + |\hat{C}_3|}{2}, \\
&= \gamma\frac{|C_k| + |C_{k+n}|}{2}, \\
&= \frac{\gamma}{2}\left(|k|2^N + \frac{2^N - 1}{2} + |k+n|2^N + \frac{2^N - 1}{2}\right), \\
&= \gamma 2^{N-1}(|k| + |k+n| + 1) - \frac{\gamma}{2},
\end{aligned} \tag{6.38}$$

The usual values of γ are in the range, $0.05 \leq \gamma \leq 0.1$. Therefore, $\frac{\gamma}{2} << \gamma 2^{N-1}(|k| + |k+n| + 1)$. thus, Eq. (6.38) can be re-written as

$$\hat{\delta} = \gamma 2^{N-1}(|k| + |k+n| + 1). \tag{6.39}$$

Using Eq. (6.37) and Eq. (6.39) in Eq. (6.35), the estimated extracted watermark bit, $\hat{b}$, with respect to discarding N bit planes, can be formulated as,

$$\begin{aligned}
\hat{b} &= \left(\frac{\hat{C}_2 - \hat{C}_1}{\hat{\delta}}\right)\%2, \\
&= \left(\frac{C_{k+m} - C_k}{\hat{\delta}}\right)\%2, \\
&= \left(\frac{(k+m)2^N + \frac{(k+m)}{|k+m|}\frac{(2^N-1)}{2} - k2^N - \frac{k}{|k|}\frac{(2^N-1)}{2}}{\gamma 2^{N-1}(|k| + |k+n| + 1)}\right)\%2, \\
&= \left(\frac{m2^N + \left(\frac{(k+m)}{|k+m|} - \frac{k}{|k|}\right)\left(\frac{2^N-1}{2}\right)}{\gamma 2^{N-1}(|k| + |k+n| + 1)}\right)\%2, \\
&= \left(\frac{2m + \left(\frac{(k+m)}{|k+m|} - \frac{k}{|k|}\right)\left(1 - 2^{-N}\right)}{\gamma(|k| + |k+n| + 1)}\right)\%2.
\end{aligned} \tag{6.40}$$

Now considering the two cases: k and $k+m$ have the same sign (Case 1) and k and $k+m$ have different signs (Case 2),

$$\hat{b} = \begin{cases} \left(\frac{2m}{\gamma(|k|+|k+n|+1)}\right)\%2 & : \text{ Case 1}, \\ \left(\frac{2m+2-2^{1-N}}{\gamma(|k|+|k+n|+1)}\right)\%2 & : \text{ Case 2}. \end{cases} \tag{6.41}$$

■.

Thus, using Eq. (6.41), it is possible to predict $\hat{b}$ for a given number of discarded bit

Table 6.2: Values of m and corresponding $\hat{b}$ for different modifications of C_2' for $k = 1$, $k + n = 6$ and $N = 5$.

C_2' values range	$\hat{C}_2$	m	$\hat{b}$
35-63	47.5	0	0
64-95	79.5	1	1
96-127	111.5	2	1
128-159	143.5	3	0
160-191	175.5	4	0
192-203	207.5	5	1

planes, N, for particular modifications of C_2 to C_2' during embedding. This relationship is used for identifying the ranges of values for C_2', *i.e.,* the value of C_2 after embedding the watermark bit, b, by considering the value of m for given k, n and N. Similarly the optimal values of C_2' for other $N - u$, where $u \in \{1, 2, 3...N - 1\}$ lower bit-planes being discarded are calculated to maintain the robustness for discarding of any bit plane up to the Nth bit plane.

6.4.3 Examples

Let $C_1 = 35$, $C_2 = 181$ and $C_3 = 203$ are the three coefficients concerned. Set $\gamma = 0.1$ and consider $N = 5$ bit planes are being discarded. Then $k = \lfloor 35/32 \rfloor = 1$ and $k+n = \lfloor 203/32 \rfloor = 6$. Thus, Eq. (6.41) is simplified to $\hat{b} = (2.5m)\%2$. A look-up table, as shown in Table 6.2, of $\hat{b}$ for different $\hat{C}_2$ and corresponding m is derived. Thus, in this example, for robustly embedding a watermark bit, $b = 0$, C_2 can be modified to any value in the regions, $35 \leq C_2' \leq 63$ and $128 \leq C_2' \leq 191$. Similarly, for robustly embedding a watermark bit, $b = 1$, C_2 can be modified to any value in the regions, $64 \leq C_2' \leq 127$ and $192 \leq C_2' \leq 203$. However, a value close to the original value, C_2, within these ranges is chosen in order to minimize the amount of distortion.

Similar computations are carried out for $N = 1, 2, 3, 4...$ to obtain the corresponding robust ranges for C_2' The common range for all N values ensures correct watermark extraction when N or any lower number of bit planes are discarded. The extension of the previous example for $N = 1, 2, 3, 4$ to find the value ranges of C_2' to embed the watermark bits, $b = 1$ or $b = 0$, is shown in Table 6.3.

Table 6.3: Ranges of C_2' to embed watermark bits, $b = 1$ and $b = 0$, for different N

	Embedding $b = 0$	
	Robustness for discarding N bit planes	Robustness for discarding up to N bit planes
$N = 1$	172-184 & 196-203	-
$N = 2$	168-180 & 192-203	172-180 & 196-203
$N = 3$	176-184 & 200-203	176-180 & 200-203
$N = 4$	176-192 & -	176-180
$N = 5$	128-192	176-180
	Embedding $b = 1$	
	Robustness for discarding N bit planes	Robustness for discarding up to N bit planes
$N = 1$	160-172 & 184-196	-
$N = 2$	156-168 & 180-192	160-168 &184-192
$N = 3$	160-176 & 184-200	160-176 &184-192
$N = 4$	144-176 & 192-203	160-176
$N = 5$	192-203	-

6.5 Performance evaluation

This section presents the results of experimental validation of the proposed two models by simulating wavelet domain bit plane discarding and their performance against JPEG 2000 quality scalability-based content adaptation. The experimental set up includes the test image set as shown in Figure 4.7.

In the experiments, firstly the watermark data is embedded by considering different values of N, *i.e.,* the maximum number of bit planes that can be discarded without affecting the robustness. The case, $N = 0$, corresponds to not using the model. Then for each case of N, the robustness to different compression ratios using different quantization factors, Q, where $Q = 2^p$ and p is the corresponding number of bit planes actually being discarded, is evaluated. Finally, JPEG 2000 quality scalability-based content adaptation experiments are performed using WEBCAM framework to evaluate the performance of the proposed models in actual quality scalability scenarios. The extracted watermark data is compared with the original watermark data by comparing the Hamming distance. The lower the Hammming distance, the higher the robustness.

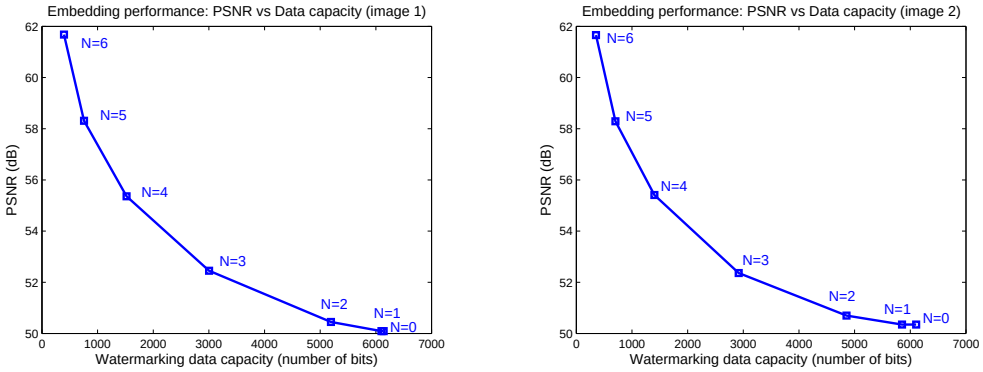

Figure 6.7: Embedding performance of the model for non-blind watermarking considering different values of N at embedding. *Column 1*: Image 1; and *Column 2*: Image 2.

6.5.1 Evaluation of the model for non-blind watermarking

The proposed model for non-blind watermarking is evaluated using one of the magnitude alteration algorithms [17] as the control algorithm. Similar such algorithms are discussed in the literature and categorized in Chapter 3 and Chapter 4 as shown in Table 4.1. The proposed robustness model is incorporated into the algorithm for choosing the coefficients for embedding the watermark and the robustness performance for quality scalability content adaptation attacks are compared with the original algorithm that does not use the proposed model. The experimental set up includes the 9/7 wavelet, 3 levels of decomposition and embedding within the low-low (LL) frequency subbband using $\alpha = 0.01$ and considering different values for N, *i.e.,* the maximum number of bit planes that can be discarded without affecting the robustness. The case, $N = 0$, corresponds to the control algorithm that does not use the model. For completeness, the embedding performance is first shown in Figure 6.7 for different values of N. The watermark embedding performance was measured by the watermark data count and the corresponding peak signal to noise ratio (PSNR) of the watermarked image with respect to the original image. Since a fewer number of coefficients are able to robustly retain the watermark data for large N values considered in the model, the amount of watermark data embedded is smaller for larger N, consequently, resulting in higher PSNR values for such cases.

6.5.1.1 Simulations with bit plane discarding

Figure 6.8 shows the robustness performance for various compression steps achieved by a quantization factor $Q = 2^p$, where p is the corresponding number of bit planes actually being discarded for each different embedding model values of N. The figure shows the robustness plots for embedding scenarios that use different embedding model values of N. The first two graphs in each column correspond to the Image 1 and Image 2 from the test image set, respectively. The third row shows the average performance with error bars corresponding to 95% confidence intervals for the entire image set. For better visualization, we have grouped the plots into two sets: viz., *Column 1* with $N = 1, 3, 5$ and *Column 2* with $N = 2, 4, 6$. In the plots, the x-axis represents the number of bit planes being discarded (p) during compression while the y-axis shows the robustness performance in terms of Hamming distance.

The simulations verify the high robustness performance of the proposed model. It is also evident that the robustness remains high for any $p \leq N$ number of bit planes being discarded.

For further clarification of the proposed model's behavior, in Figure 6.9, we show $|C' - C|$ and $|\hat{C}' - C|$ for the LL subband coefficients chosen using the two embedding model scenarios, $N = 0$ and $N = 5$, and two bit plane discarding scenarios, $p = 0$ and $p = 5$. For $N = 0$ all coefficients are chosen for watermark embedding, while for $N = 5$ only some of the coefficients are chosen by the model. The non-chosen coefficients are shown in black in Figure 6.9.b and Figure 6.9.d. For the chosen coefficients, the absolute magnitude differences due to embedding and compression are added with a bias value and displayed in gray scale for clear distinction between the chosen and non-chosen coefficients. The results show a greater similarity between Figure 6.9.b and Figure 6.9.d (where $p \leq N$) compared to that between Figure 6.9.a and Figure 6.9.c (where $p > N$). The consideration of more bit plane discarding ($N = 5$ here) during embedding helps to select the optimum set of coefficients to embed the watermark in such a way that it can retain the watermarks after the said number of bit plane discarding ($p = 5$ here) during compression, hence high robustness.

6.5.1.2 Experiments with JPEG 2000 quality scalability

Figure 6.10 shows the robustness performance of the proposed embedding modelwhen the JPEG 2000 quality scalability-based content adaptations are used. For better visualization, we have grouped the plots into two sets: viz., *Column 1* with $N = 1, 3, 5$

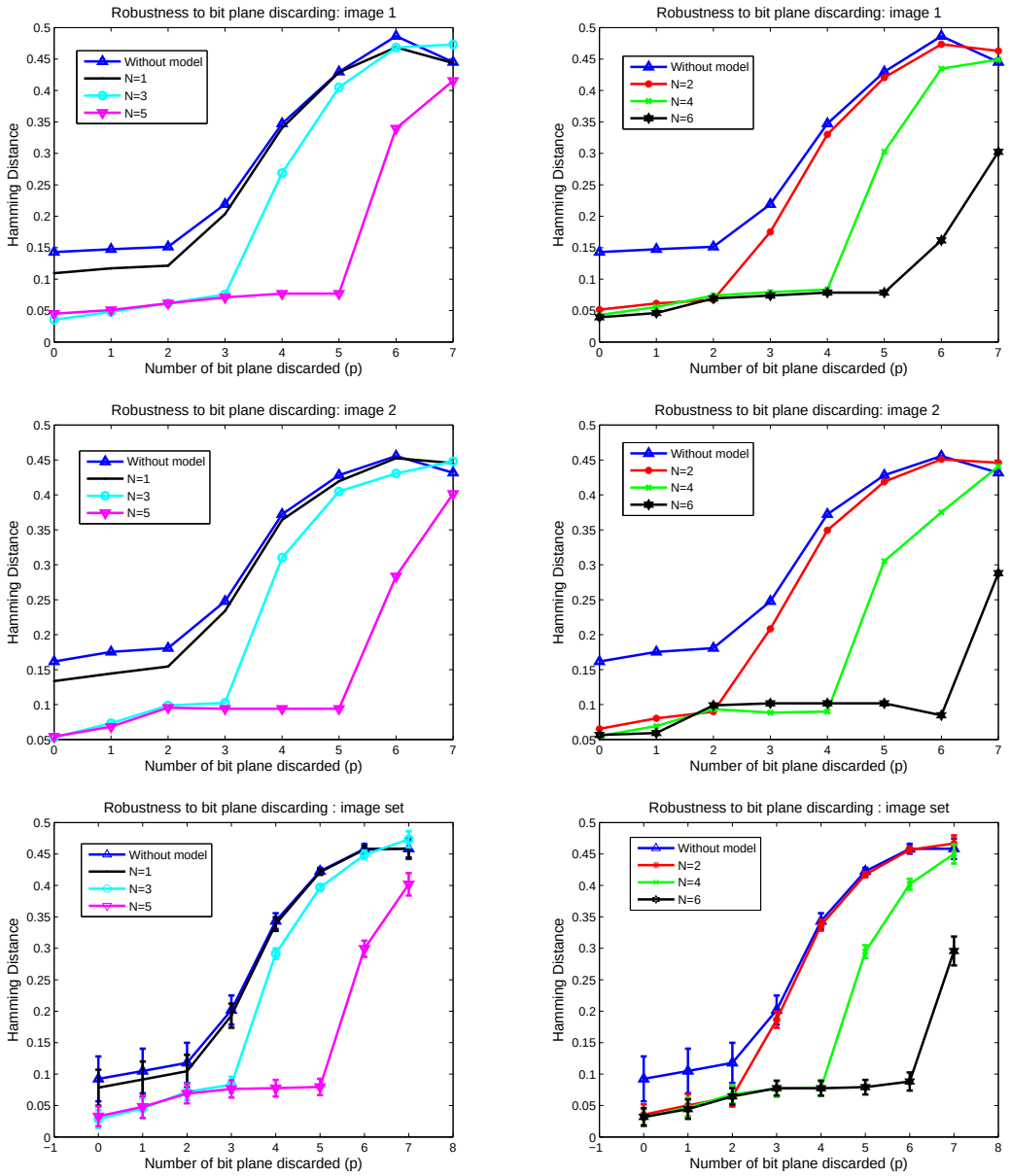

Figure 6.8: Non-blind model evaluation: Robustness performance against discarding of p bit planes for the embedding models that consider $N = 1, 3, 5$ (*Column 1*) and $N = 2, 4, 6$ (*Column 2*) bit planes to be discarded. $N = 0$ corresponds to algorithm without model. *Row 1*: Image 1; and *Row 2*: Image 2; *Row 3*: The entire image set.

and *Column 2* with $N = 2, 4, 6$. In the plots, the x-axis shows the compression ratio while the y-axis shows the robustness performance in terms of Hamming distance. The first two rows show the results for two of the test images while the third row shows the average performance with error bars corresponding to 95% confidence intervals for the entire image set. It is evident from these plots, that the higher the value of N considered in the embedding model, the higher the watermarking robustness. With the

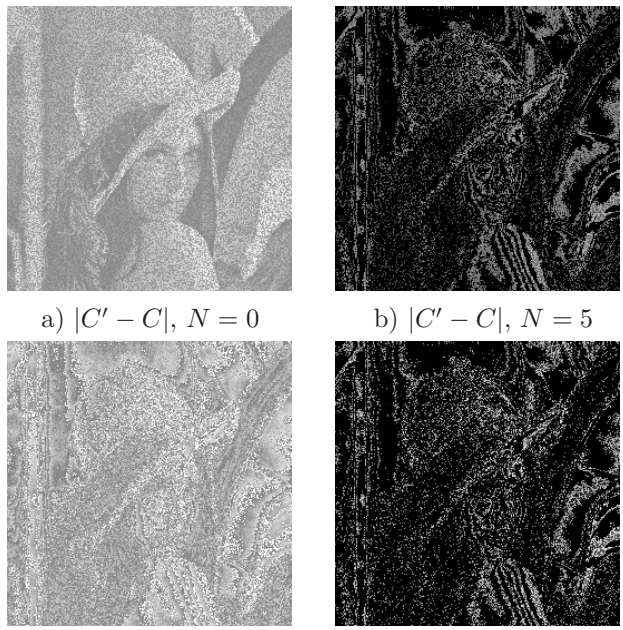

a) $|C' - C|$, $N = 0$ b) $|C' - C|$, $N = 5$

c) $|\hat{C}' - C|$, $N = 0$, $p = 5$ d) $|\hat{C}' - C|$, $N = 5$, $p = 5$

Figure 6.9: Non-blind model evaluation. a) and b) represent the difference images $|C' - C|$ in for using the embedding model with $N = 0$ and $N = 5$, respectively. c) and d) show the corresponding difference images $|\hat{C}' - C|$ at the decoder after discarding $p = 5$ bit planes.

higher order models, coefficients for embedding watermark data are chosen accurately according to their ability to retain the correct watermark data under compression. The improvement in robustness over the original algorithm [17], *i.e.,* without using the model ($N = 0$), is achieved by more than 30% at various compression ratio using the non-blind model at $N = 6$.

6.5.2 Evaluation of the model for blind watermarking

In this case, the re-quantization based blind watermarking schemes discussed in Chapter 3 and Chapter 4 are evaluated here and as an example, the algorithm presented in [5] is used as control algorithm to verify and evaluate the model proposed for blind watermarking algorithms. In this model, unlike the non-blind one, number of coefficients to be embedded are constant for any value of N, as no reference image is available at the decoder. Due to the nature of the model, for a given N, all selected coefficients may not satisfy the conditions in Eq. (6.41), particularly when m is small and can not provide any suitable value to embed 0 or 1. This situation is possible when C_1 and C_2 are very close to each other. Therefore, the algorithmic implementation first attempts

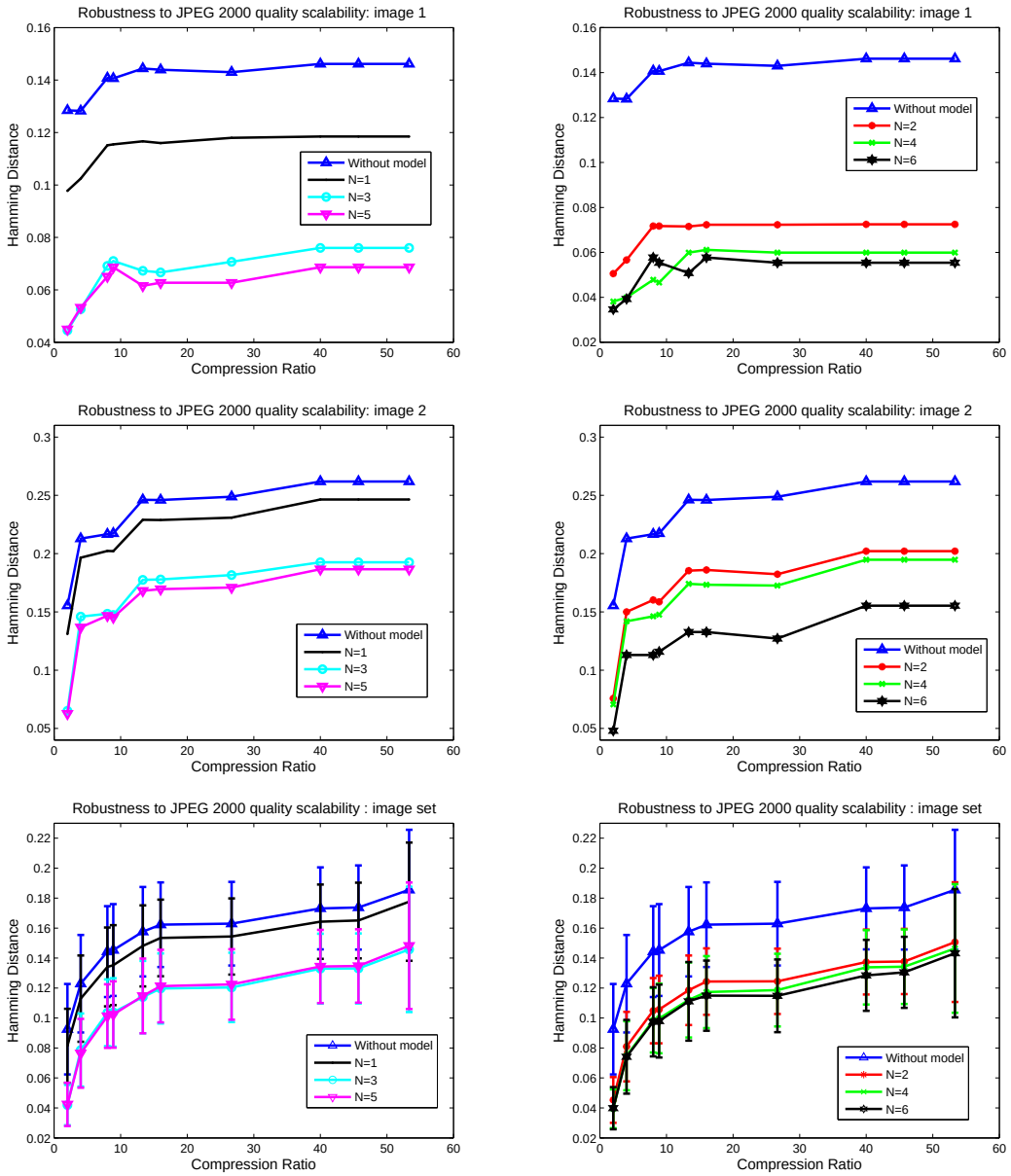

Figure 6.10: Non-blind model evaluation: Robustness performance against JPEG 2000 quality scalability for the embedding models that consider $N = 1, 3, 5$ (*Column 1*) and $N = 2, 4, 6$ (*Column 2*) bit planes to be discarded. $N = 0$ corresponds to algorithm without model. *Row 1*: Image 1; and *Row 2*: Image 2; *Row 3*: The entire image set.

to calculate and modify the the coefficient C_2 according to given N using Eq. (6.41). In case, the required m is unavailable, it attempts to calculate and modify C_2 considering $N-1$. This process continues until a suitable m is available with the condition $N \geqslant 0$.

Here, the experimental set up includes the 9/7 wavelet, 3 levels of decomposition and embedding within the low-low (LL) frequency subbband using $\gamma = 0.02$ and considering

Figure 6.11: Embedding performance of the model for blind watermarking considering different values of N at embedding for image 3 and image 4.

different values for N, *i.e.,* the maximum number of bit planes that can be discarded without affecting the robustness. The case, $N = 0$, corresponds to the control algorithm that does not use the model. In this case also for completeness, the embedding performance is first shown in Figure 6.11 for different values of N. In this type of blind watermarking, the modification value often increases with the higher N values whilst keeping the same watermark bit count. As a result more embedding distortion is introduced as shown in Figure 6.11. Hence the optimal N can be decided depending on tolerable PSNR value for a given application.

6.5.2.1 Simulations with bit plane discarding

Figure 6.12 shows the robustness performance for various compression steps achieved by a quantization factor $Q = 2^p$, where p is the corresponding number of bit planes actually being discarded for each different embedding model values of N. The first two graphs correspond to the Image 3 and Image 4 from the test image set, respectively. The third graph shows the average performance with error bars corresponding to 95% confidence intervals for the entire image set. The simulations verify the enhanced robustness performance of the proposed model. It is also evident that the robustness remains high for any $p \leq N$ number of bit planes being discarded.

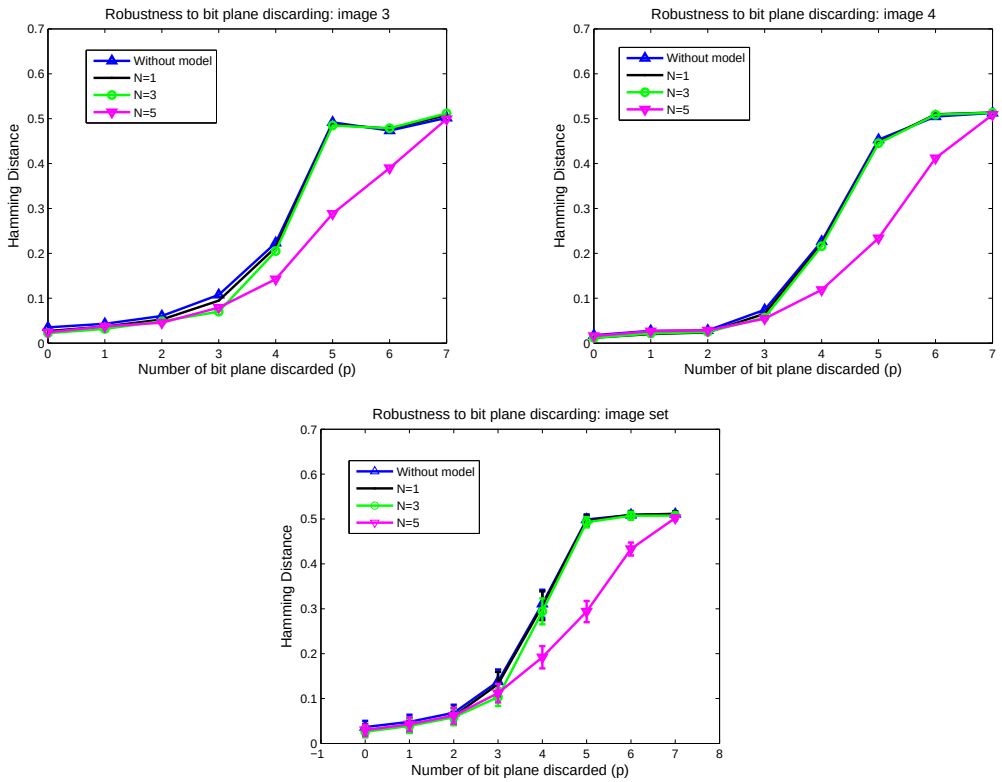

Figure 6.12: Blind model evaluation: Robustness performance against discarding of p bit planes for the embedding models that consider $N = 0, 3, 4, 5$ bit planes to be discarded. $N = 0$ corresponds to algorithm without model. *Row 1, Column 1*: Image 3; and *Row 1, Column 2*: Image 4; *Row 2*: The entire image set.

6.5.2.2 Experiments with JPEG 2000 quality scalability

Similarly, Figure 6.13 shows the robustness performance of the model for actual JPEG 2000 quality scalability-based content adaptations for Image 3, Image 4, and the entire image set (Figure 4.7). Plots show the robustness to different compression ratio points for different embedding model values of N and compares with the case for $N = 0$, where the model is not used. It is evident from these plots, that high values of N considered in the embedding model lead to enhanced robustness of the blind watermarking scheme. Similar to the non-blind model, the improvement over the original algorithm [5], in robustness is achieved by more than 15% at various compression ratio using the blind model at $N = 5$.

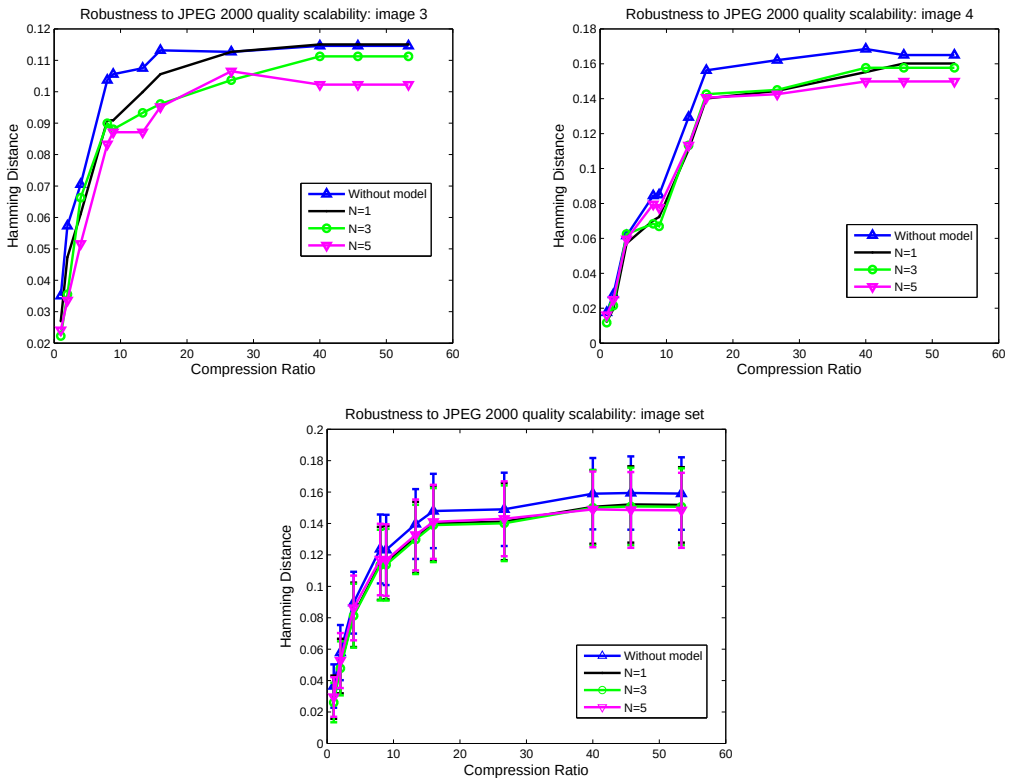

Figure 6.13: Blind model evaluation: Robustness performance against JPEG 2000 quality scalability for the embedding models that consider $N = 0, 3, 4, 5$ bit planes to be discarded. $N = 0$ corresponds to algorithm without model. *Row 1, Column 1*: Image 3; and *Row 1, Column 2*: Image 4; *Row 2*: The entire image set.

6.6 Conclusions

In this chapter the models have been presented for enhancing the robustness of non-blind and blind watermarking algorithms against quality scalability-based content adaptation. The proposed model for non-blind watermarking specifies the range of coefficient magnitudes that are capable of correctly extracting the embedded watermark bit under compression by considering wavelet domain bit plane discarding and ranks the coefficients accordingly. Similarly for blind algorithms, the proposed model specifies the range of magnitudes for the modified coefficient in order to extract the watermark data under compression. The simulations show the proposed models outperforming the robustness performance of the existing watermarking methods, where the model was not used. The proposed models result in scalable robustness performance where the robustness remained high for any, $p \leq N$, number of bit planes being discarded. The high robustness of the models was experimentally verified for the JPEG 2000 quality scalability.

Chapter 7

Motion Compensated Video Watermarking Techniques

So far in this thesis, we have discussed, analyzed and proposed models to enhance the watermarking robustness for images and evaluated the performances against scalable compression, *i.e.,* JPEG 2000. In this chapter the research findings are extended in video watermarking scenario. Inline with the thesis objectives, this chapter focuses on robust watermarking techniques for scalable coded video compression, such as, Motion JPEG 2000, wavelet based MC-EZBC [33] and more recent H.264/SVC. In order to account the motion information, we have proposed Motion Compensated Temporal Filtering (MCTF) based video watermarking algorithms here. Firstly the generalized MCTF based video watermarking schemes are proposed and evaluated and then robustness models, derived in Chapter 6 are applied within MCTF framework for enhanced robustness in video watermarking.

7.1 Introduction

MCTF has been successfully used in wavelet based scalable video coding reseach [33, 109]. The idea of MCTF is evolved from 3D subband wavelet decomposition, which is merely an extension of spatial domain transform into temporal domain [110]. But 3D wavelet decomposition alone does not decouple motion information and it is addressed by using temporal filtering along the motion trajectories. This MCTF based video decomposition technique motivates a new avenue in transform domain video wa-

termarking.

Often video watermarking schemes are developed by extending image watermarking algorithms. Transform domain, especially, wavelet based image watermarking has been very successful in imperceptibility as well as robustness performance against various image processing attacks. As a successor of the same, several attempts have been made to extend these image watermarking algorithms into video watermarking by using them either on a frame-by-frame basis [27–30] or based on 3D wavelet decompositions [9, 31, 32].

The frame-by-frame video watermarking considers embedding on selected frames located at fixed intervals to make them robust against frame dropping based temporal adaptations of video. In this case each frame is treated separately as an individual image, hence any image watermarking algorithm can be adopted to achieve the intended robustness. But frame-by-frame watermarking schemes often perform poorly in terms of robustness against various video processing attacks including temporal desynchronization, video collusion, video compression attacks etc. In order to address these issues, the video temporal dimension is exploited by the spread spectrum domain i.e. DCT and more recently wavelet based 3D decomposition of the host video. In 3D wavelet-based watermarking approaches [9,31,32], video is composed into 3D subbands by using separable 3D wavelet transform with shorter mother wavelets, such as Haar. Unfortunately, such naive subband decomposition-based embedding strategies, that do not consider the motion element of the sequence when embedding the watermark, often result in unpleasant flickering visual artifacts. The amount of flickering in watermarked sequences varies according to the texture, color and motion characteristics of the video content as well as the watermark strength and the choice of frequency subband used for watermark embedding. At the same time, these schemes are also fragile to video compression attacks which consider motion trajectory during compression coding.

The aim of this chapter is to address the consideration of motion and texture characteristics of the video sequence for extending image watermarking techniques into video. The new proposed approach is evolved from the MCTF based wavelet domain video decomposition concept, as briefed at the beginning of the chapter. Few attempts have already been made to investigate the effect of motion in video watermarking attempts on incorporating motion compensation into video watermarking [57, 79, 80]. In these investigations the sequence is first temporally decomposed into Haar wavelet subbands using MCTF and then spatially decomposed using the 2D DCT transform resulting in the decomposition scheme widely known as t+2D. Here we aim to advance further by investigating along the line of MCTF based wavelet coding to improve the robust-

ness while keeping the imperceptibility or vice versa. Apparent problems of direct use of MCTF and t+2D decompositions in watermarking are three-fold and alternative solutions are offered to address the same.

1. In scalable video coding research it has been evident that video with different texture and motion characteristics leading to its spatial and temporal features perform differently on t+2D domain [33] and its alternative 2D+t domain [111], where MCTF is performed on the 2D wavelet decomposition domain. Further, in 3D subband decomposition for video watermarking, the consideration of motion, thus the use of MCTF, is only required for subbands where the watermarks are embedded. Therefore fixed architectures, such as t+2D or 2D+t, add unnecessary complexity in terms of motion estimation and compensation into the watermarking algorithm.

2. The conventional MCTF is focused on achieving higher compression and thus gives more attention on the prediction lifting step in MCTF. However, for watermarking it is necessary to follow the motion trajectory of content into low frequency temporal subband frames, in order to avoid motion mismatch in the update step of MCTF when these frames are modified due to watermark embedding.

3. t+2D structure offers better energy compaction in the low frequency temporal subband, while keeping majority coefficient values to very small or nearly zero in high frequency temporal subbands. This is very useful during compression but leaves very little room for watermark embedding in high frequency temporal subbands. Therefore, for a robust algorithm most of the MCTF domain watermarking schemes, as mentioned before, embed the watermark in the low-pass temporal frames. On the other hand 2D+t provides more energy in high frequency subbands, which enables the possibility to embed and recover the watermark robustly using high-pass temporal frames which improves the overall imperceptibility of the watermarked video.

To overcome these shortcomings, MCTF based 3D wavelet decomposition schemes are proposed for video sequences and a flexible 2D+t+2D generalized motion compensated temporal-spatial subband decomposition scheme is offered using a modified motion compensated temporal filtering (MMCTF) scheme for video watermarking. Using the proposed decompositions within the framework we study and analyze the merits and the demerits of watermark embedding using various combinations of 2D+t+2D structure and propose new video watermarking schemes to improve the imperceptibility

and the robustness performance against scalable coded video attacks, such as, Motion JPEG 2000, MC-EZBC and H.264-SVC. The issues related to motion estimation from watermarked video without any prior knowledge of original motion information are also addressed in the case of a blind watermarking method.

7.2 Motion compensated 2D+t+2D filtering

The generalised spatio-temporal decomposition scheme consists of two modules: *1) MCTF* and *2) 2D spatial frequency decomposition.* To capture the motion information accurately, the commonly used lifting based MCTF is modified by tracking inter-frame pixel connectivity and the 2D wavelet transform is used for spatial decomposition. In this section the modified motion compensated temporal filtering (MMCTF) is described first and then the 2D+t+2D general framework is proposed based on MMCTF.

7.2.1 MMCTF

The MMCTF scheme is formulated by giving more focus into the motion trajectory-based update step as follows. Let I_t be the video sequence, where t is the time index in display order. We consider two consecutive frames I_{2t} and I_{2t+1}, as the current frame (c) and the reference frame (r), respectively, following the video coding terminology. The I_{2t} frame is partitioned into non-overlapping blocks and for each block, vertical and horizontal displacements are quantified and represented as motion vector fields $\mathcal{V}^{c\rightarrow r}$ and $\mathcal{H}^{c\rightarrow r}$, respectively. In the I_{2t} frame, each block can be one of two types, namely inter and intra blocks, where the motion is only estimated for the former block type only. Similarly, as far as the I_{2t+1} frame is concerned any pixel can be one of three types, namely, one-to-one connected, one-to-many connected and unconnected (as shown in Figure 7.1), depending on their connectivity to pixels in the I_{2t} frame following the implied motion vector vector fields $\mathcal{V}^{c\leftarrow r}$ and $\mathcal{H}^{c\leftarrow r}$, which are simply the directional inverse of the original motion vector fields, $\mathcal{V}^{c\rightarrow r}$ and $\mathcal{H}^{c\rightarrow r}$.

Considering these block and pixel classifications, the lifting steps for pixels at positions $[m, n]$ in frames I_{2t} and I_{2t+1} (*i.e.,* $I_{2t}[m, n]$ and $I_{2t+1}[m, n]$) performing the temporal motion compensated Haar wavelet transform are defined as follows:

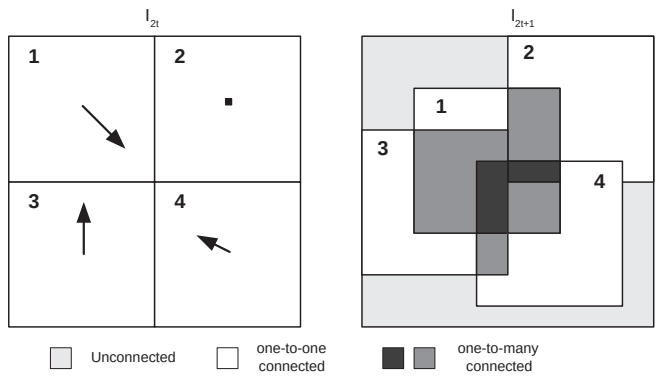

Figure 7.1: Pixel connectivity in I_{2t} and I_{2t+1} frames.

The prediction step:

For one-to-one connected pixels:

$$I'_{2t+1}[m,n] = I_{2t+1}[m,n] - I_{2t}[m + \mathcal{H}^{c\to r}, n + \mathcal{V}^{c\to r}]. \tag{7.1}$$

For one-to-many connected pixels:

$$I'_{2t+1}[m,n] = I_{2t+1}[m,n] - \frac{1}{J}\sum_{i=0}^{J-1} I_{2t}[m + \mathcal{H}_i^{c\to r}, n + \mathcal{V}_i^{c\to r}], \tag{7.2}$$

where J is the total number of connections. For unconnected pixels:

$$I'_{2t+1}[m,n] = I_{2t+1}[m,n]. \tag{7.3}$$

The above case is similar to the no prediction case as in intra blocks used in conventional MCTF.

The update step:

For inter blocks: Every pixel in an inter block is one-to-one connected with a unique pixel in I_{2t+1}. Then the update step is computed as

$$I'_{2t}[m,n] = I_{2t}[m,n] + \frac{1}{2} I'_{2t+1}[m - \mathcal{H}^{c\leftarrow r}, n - \mathcal{V}^{c\leftarrow r}]. \tag{7.4}$$

For intra blocks: As there are no motion compensated connections with I_{2t+1},

$$I'_{2t}[m,n] = I_{2t}[m,n]. \tag{7.5}$$

Finally these lifting steps are followed by the normalization step.

$$I''_{2t}[m,n] = \sqrt{2}I'_{2t}[m,n], \tag{7.6}$$

$$I''_{2t+1}[m,n] = \frac{1}{\sqrt{2}}I'_{2t+1}[m,n]. \tag{7.7}$$

The temporally decomposed frames I''_{2t} and I''_{2t+1} are the first level low and high pass frames and are denoted as L and H temporal subbands. These steps are repeated for all frames in L to obtain LL and LH sub bands and continued to obtain the desired number of temporal decomposition levels. For the inverse transform, the order of operation of steps is reversed and the first operand in lifting steps is changed to subject variable in above equations.

7.2.2 2D+t+2D framework

As discussed earlier in Section 7.1, in a 3D video decomposition scheme, t+2D is achieved by performing temporal decomposition followed by a spatial transform where as in case of 2D+t, the temporal filtering is done after the spatial 2D transform. Due to its own merit and demerit, it is required to analyse both the combinations in order to enhance the video watermarking performance. A common flexible reconfigurable framework, which allows to create such possible combinations, are particularly useful for applications like video watermarking. Here the 2D+t+2D framework is proposed by combining the modified motion compensated temporal filtering with spatial 2D wavelet transformation.

Let $(s_1 t s_2)$ be the number of decomposition levels used in the 2D+t+2D subband decomposition to obtain a 3D subband decomposition with motion compensated t temporal levels and s spatial levels, where $s = s_1 + s_2$. In such a scheme, first the 2D Discrete Wavelet Transform (DWT) is applied for an s_1 level decomposition. As a result a new sequence is formed by the low frequency spatial LL subband of all frames. Then the sequence of spatial LL subbands are temporally decomposed using the MMCTF into t temporal levels. Finally each of the temporal transformed spatial LL subbands are further spatially decomposed into s_2 wavelet levels.

For a t-s motion compensated temporal subband decomposition, the values of s_1 and s_2 are determined by considering the context of the choice of temporal-spatial subbands used for watermark embedding. For example, (032) and (230) parameter combinations result in t+2D and 2D+t motion compensated 3D subband decompositions, respec-

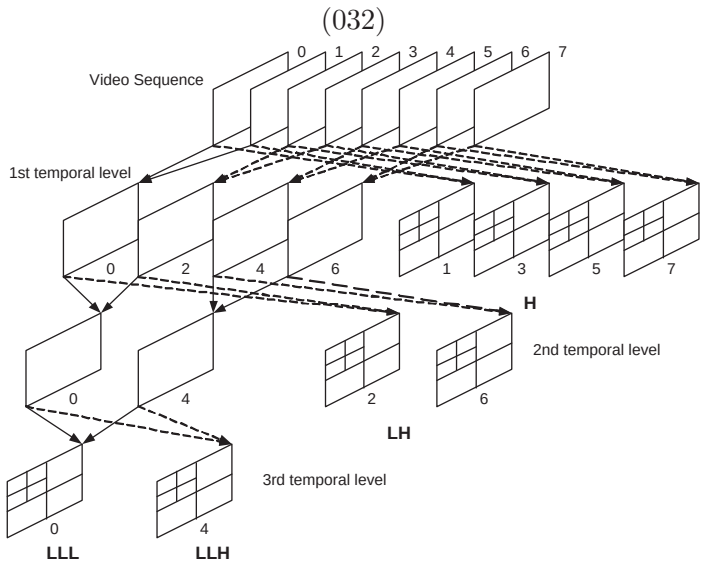

Figure 7.2: Realization of 3-2 temporal schemes using the 2D+t+2D framework with different parameters: (032).

tively. The same amount subband decomposition levels can be obtained by also using the parameter combination (131) using the proposed generalized scheme implementation. The combination (002) allows 2D decomposition of all frames for frame by frame watermark embedding. The realization of these examples are shown in Figure 7.2, Figure 7.3, Figure 7.4 and Figure 7.5. We use the notation (LLL, LLH, LH, H) to denote the temporal subbands after a 3 level decomposition. The use of this framework is described in combination with watermarking algorithms, in the next section.

7.3 Video watermarking in 2D+t+2D spatio-temporal decomposition

We propose a new video watermarking scheme by extending the wavelet based image watermarking algorithms into 2D+t+2D framework. At this point we recall the generalized wavelet based image watermarking schemes as described in Chapter 3 and Chapter 4. In this section those watermarking algorithms are extended into MCTF based framework to propose new video watermarking schemes. Then various combinations in the proposed video decomposition framework are analyzed to decide on unique video embedding parameters, such as, 1) choice of temporal subband selection and 2) motion estimation parameters to retrieve the motion information from watermarked video.

(230)

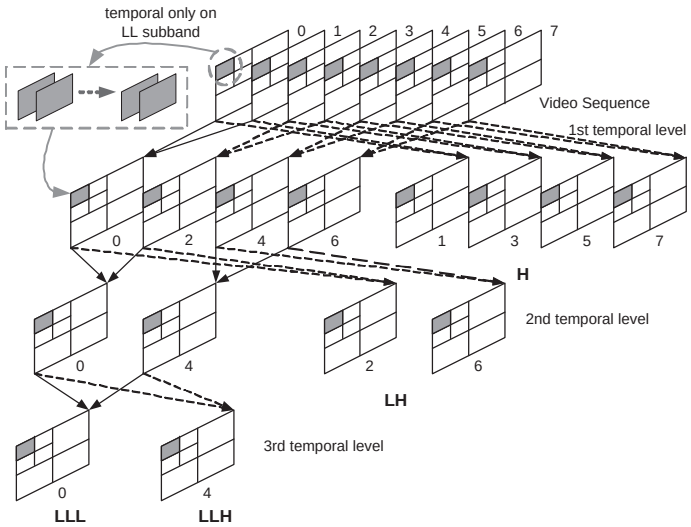

Figure 7.3: Realization of 3-2 temporal schemes using the 2D+t+2D framework with different parameters: (230).

(131)

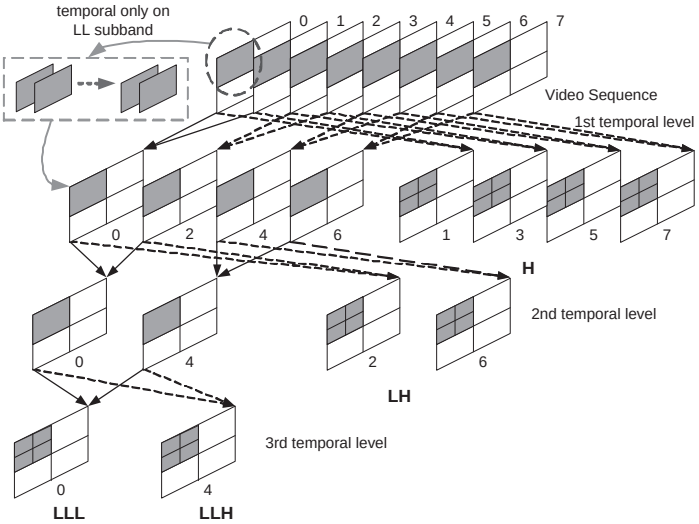

Figure 7.4: Realization of 3-2 temporal schemes using the 2D+t+2D framework with different parameters: (131).

7.3.1 Proposed video watermarking scheme

The new video watermarking scheme uses the image watermarking algorithms on spatial-temporal decomposed video. The system block diagrams for watermark embedding, a non-blind extraction and a blind extraction are shown in Figure 7.6, Figure 7.7

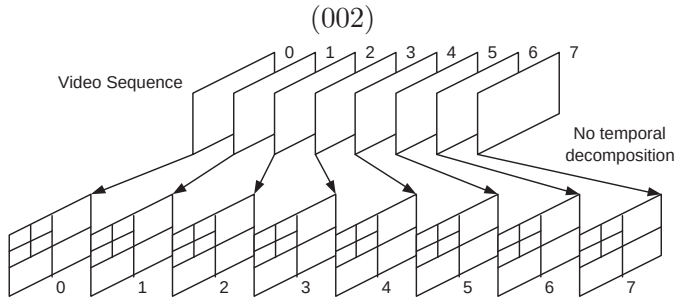

Figure 7.5: Realization of spatial 2D frame-by-frame scheme using the 2D+t+2D framework with different parameters: (002).

and Figure 7.8, respectively.

7.3.1.1 Embedding

To embed the watermark, first spatio-temporal decomposition is performed on the host video sequence by applying spatial 2D-DWT followed by temporal MMCTF for a 2D+t (230) or temporal decomposition followed by spatial transform for a t+2D (032). In both the cases, the motion estimation (ME) is performed to create the motion vector (MV) either on the spatial domain (t+2D) or in the frequency domain (2D+t) as described in Section 7.2.2. Other combinations, such as, 131 and 002 are achieved in a similar fashion. After obtaining the decomposed coefficients, the watermark is embedded either using magnitude alteration (Eq. (3.2)) or a re-quantisation based modification algorithm (Eq. (3.3)) by selecting various temporal low or high pass frames (i.e. LLL or LLH etc.) and spatial subband within the selected frame. Once embedded, the coefficients follow inverse process of spatio temporal decomposition in order to reconstruct the watermarked video.

7.3.1.2 Extraction and authentication

The extraction procedure follows a similar decomposition scheme as in embedding and the system diagram for the same is shown in Figure 7.7 and Figure 7.8. The watermark coefficients are retrieved by applying 2D+t+2D decomposition on watermarked test video. At this point we need to specifically mention about the motion information retrieval. For a non-blind algorithm the original video sequence is available at the decoder and hence the motion vector is obtained from the original video. After spatio-temporal filtering on test and original video, the coefficients are compared to extract

the watermark. On the other hand, in case of a blind watermarking scheme, the motion estimation is performed on the test video itself without any prior knowledge of original motion information. The temporal filtering is then done by using the new motion vector and consequently the spatio-temporal coefficients are obtained for the detection. The authentication is then done by measuring the Hamming distance (H) between the original and the extracted watermark using Eq. (4.1).

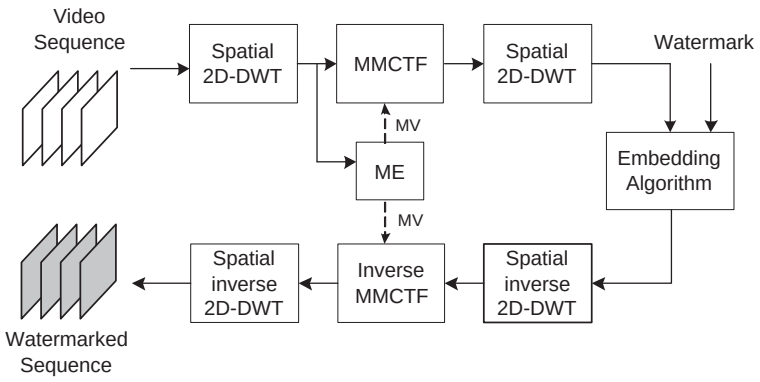

Figure 7.6: System blocks for watermark embedding scheme in 2D+t+2D spatio-temporal decomposition.

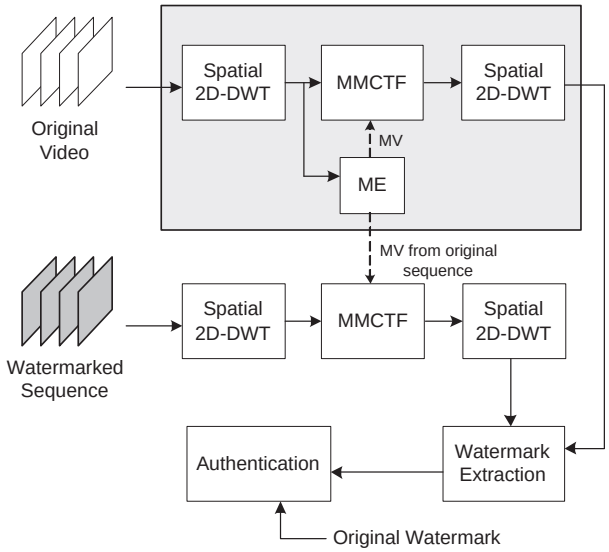

Figure 7.7: System blocks for non-blind watermark extraction scheme in 2D+t+2D spatio-temporal decomposition.

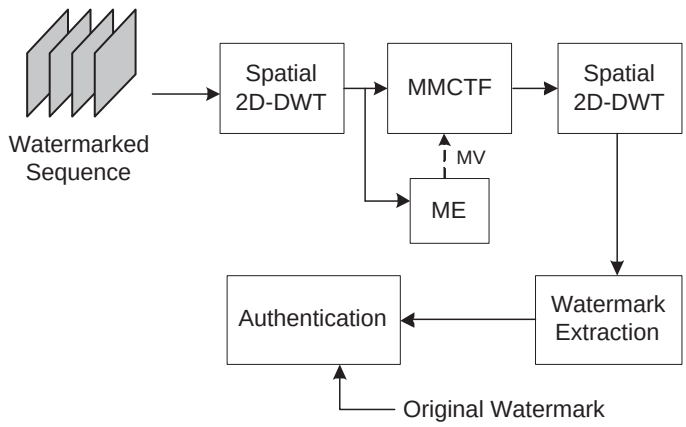

Figure 7.8: System blocks for blind watermark extraction scheme in 2D+t+2D spatio-temporal decomposition.

7.3.2 The framework analysis in video watermarking context

Before approaching to the experimental results, in this sub section we aim to address the issues related to MMCTF based video watermarking of the proposed framework. Firstly to improve the imperceptibility, an investigation is made about the energy distribution of the host video in different temporal subbands, which is useful to select the temporally decomposed frames during embedding. Then an insight is given to motion retrieval for a blind watermarking scheme, where no prior motion information is available during watermark extraction and this is crucial for the robustness performance.

7.3.2.1 On improving imperceptibility

In wavelet domain watermarking research, it is well known fact that embedding in high frequency subbands offers better imperceptibility and low frequency embedding provides better robustness. Often wavelet decompositions compact most of the energy in low frequency subbands and leave lesser energy in high frequencies and due to this reason, high frequency watermarking schemes are less robust to compression. Therefore, increase in energy distribution in high frequency subbands can offer a better watermarking algorithm.

In analyzing the framework, the research findings shows that different 2D+t+2D combinations can vary the energy distribution in high frequency temporal subbands and this is independent of video content. To show an example, *Foreman* and *Crew* sequences are used and decomposed using 032, 131, 230 and 002 combinations in the framework

Table 7.1: Sum of energy of coefficients at LL_s for first two GOP each with 8 temporal low and high frequency frames of *Foreman* sequence.

Temporal frames	Sum of Energy (GOP 1)			
	032	131	230	002
LLL	1.82×10^8	1.82×10^8	1.82×10^8	1.83×10^8
LLH	4.66×10^7	6.45×10^7	8.26×10^7	1.82×10^8
LH1	3.68×10^7	5.54×10^7	7.54×10^7	1.82×10^8
LH2	3.03×10^7	4.32×10^7	6.55×10^7	1.83×10^8
H1	3.15×10^7	4.32×10^7	5.58×10^7	1.82×10^8
H2	2.51×10^7	3.69×10^7	5.17×10^7	1.82×10^8
H3	2.85×10^7	3.84×10^7	5.69×10^7	1.83×10^8
H4	3.48×10^7	4.89×10^7	5.47×10^7	1.83×10^8
Temporal frames	Sum of Energy (GOP 2)			
	032	131	230	002
LLL	1.84×10^8	1.84×10^8	1.84×10^8	1.84×10^8
LLH	4.93×10^7	6.34×10^7	9.08×10^7	1.85×10^8
LH1	3.32×10^7	4.79×10^7	8.65×10^7	1.85×10^8
LH2	4.01×10^7	7.06×10^7	1.06×10^8	1.85×10^8
H1	2.51×10^7	5.08×10^7	6.49×10^7	1.84×10^8
H2	2.82×10^7	5.45×10^7	6.50×10^7	1.85×10^8
H3	3.78×10^7	5.62×10^7	7.62×10^7	1.85×10^8
H4	3.80×10^7	4.34×10^7	8.18×10^7	1.85×10^8

and the sum of energy are calculated for first two GOP each with 8 temporal frequency frames, namely, LLL, LLH, $LH1$, $LH2$, $H1$, $H2$, $H3$ and $H4$. In all cases the energy is calculated for the low frequency (LL_s) subband of spatial decomposition. Other input parameters are set to 8×8 macro block, a fixed size block matching (FSBM) motion estimation with ± 16 search window. The results are shown in Table 7.1, Table 7.2 and the histograms of the coefficients for 032, 131 and 230 of LLL and LLH are shown in Figure 7.9 and Figure 7.10 for *Foreman* and *Crew* sequences, respectively. The inner graphs in Figure 7.9 and Figure 7.10 represent the zoomed version of the local variations by clipping the y-axis to show the coefficient distribution more effectively. From the results, the energy distribution in high frequency temporal subbands can be ranked as: (002) > (230) > (131) > (032). This analysis guides us to select optimum spatio-temporal parameter in the framework to improve the robustness while keeping better imperceptibility.

Table 7.2: Sum of energy of coefficients at LL_s for first two GOP each with 8 temporal low and high frequency frames of *Crew* sequence.

Temporal frames	Sum of Energy (GOP 1)			
	032	131	230	002
LLL	6.47×10^7	6.46×10^7	6.45×10^7	6.54×10^7
LLH	2.70×10^7	2.67×10^7	3.86×10^7	6.32×10^7
LH1	1.04×10^7	2.49×10^7	3.01×10^7	6.57×10^7
LH2	6.75×10^7	7.20×10^7	7.79×10^7	8.46×10^7
H1	6.44×10^7	6.85×10^7	7.78×10^7	8.33×10^7
H2	1.50×10^7	1.19×10^7	1.88×10^7	6.53×10^7
H3	1.49×10^7	1.45×10^7	1.66×10^7	6.22×10^7
H4	4.38×10^7	5.38×10^7	5.99×10^7	6.24×10^7
Temporal frames	Sum of Energy (GOP 2)			
	032	131	230	002
LLL	6.06×10^7	6.04×10^7	6.06×10^7	6.24×10^7
LLH	1.94×10^7	2.23×10^7	2.40×10^7	6.00×10^7
LH1	1.79×10^7	1.67×10^7	2.34×10^7	5.97×10^7
LH2	3.62×10^7	3.70×10^7	4.24×10^7	6.60×10^7
H1	1.39×10^7	1.38×10^7	1.67×10^7	6.04×10^7
H2	1.13×10^7	1.05×10^7	1.50×10^7	5.97×10^7
H3	1.36×10^7	1.37×10^7	1.39×10^7	6.10×10^7
H4	2.86×10^7	3.09×10^7	3.91×10^7	6.80×10^7

7.3.2.2 On motion retrieval

In an MCTF based video watermarking scheme motion information contributes at large for temporal decomposition along motion trajectory. The watermarking embedding modification in the temporal domain causes motion mismatch which affects the decoder performance. While original motion information is available for a non-blind watermarking scheme, a motion estimation must be done in the case of a blind video watermarking scheme. In this case, the motion vector is expected to be retrieved from the watermarked video without any prior knowledge of the original motion vector (MV). Our study shows that, in such a case, a more accurate motion estimation is possible by choosing the right 2D+t+2D combination along with an optimum choice of macro block (MB) size. At the same time we investigate the performance based on motion search range (SR) and effectively SR has lesser contribution towards motion retrieval. The experiment set is organized by studying the watermarking detection performance by measuring Hamming distance of a blind watermark embedding at LL_s spatial subband on LLL and LLH temporal frames. The watermark extraction is done by using various combinations of MB and SR to find the best the motion retrieval parameters.

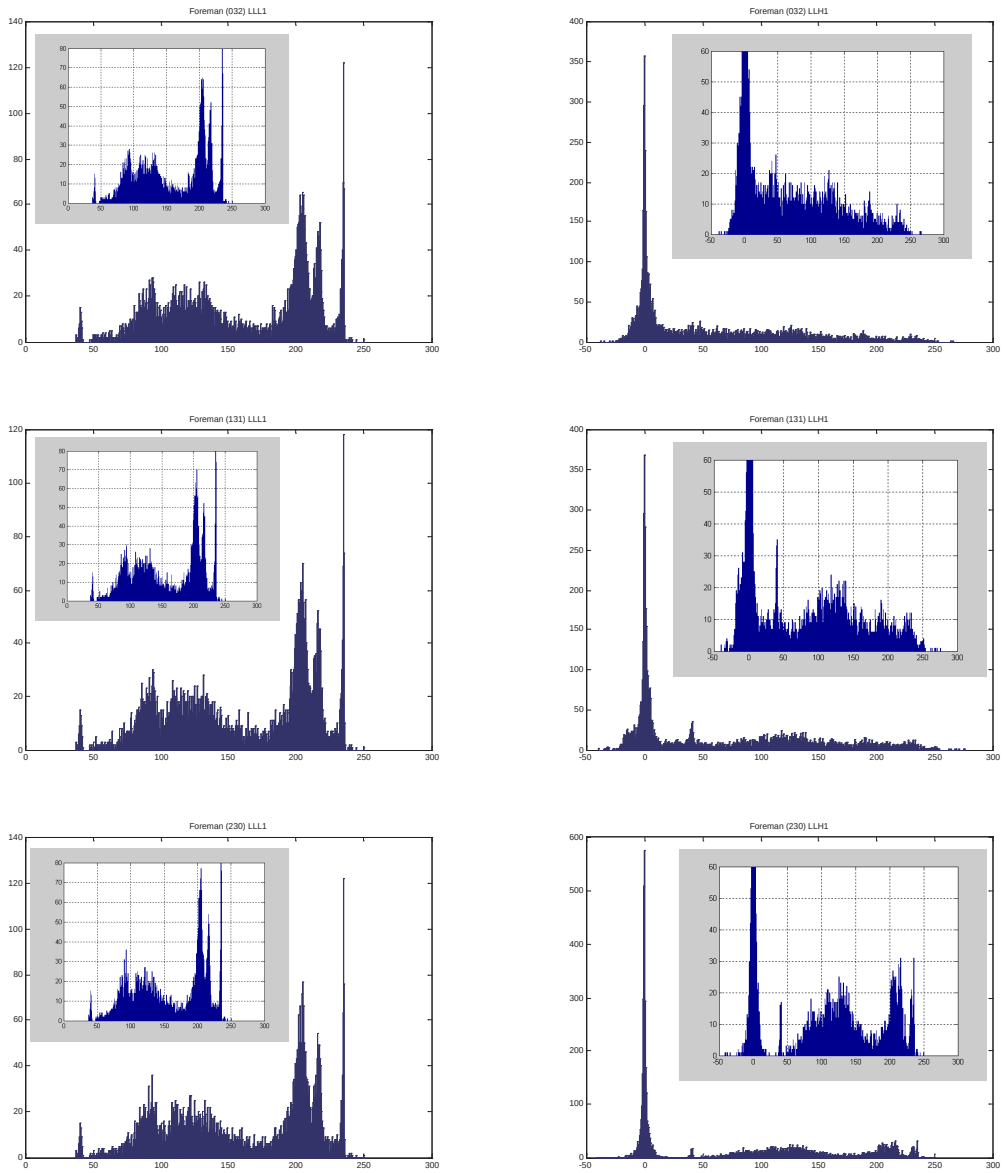

Figure 7.9: Histogram of coefficients at LL_s for 3rd level temporal low and high frequency frames (GOP 1) for *Foreman* sequence. *Column 1) & 2)* represents LLL and LLH temporal frames, respectively and *Row 1), 2) & 3)* shows 032, 131 and 230 combinations of 2D+t+2D framework.

The results are shown in Table 7.3 and Table 7.4 using average of first 64 frames from *Foreman* and *Crew* CIF size video sequence, respectively, for 032, 131 and 230 spatio-temporal decompositions. The motion is estimated using a fixed size block motion algorithm. Due to the limitations in macro-block size and integer pixel motion search, 32×32 MB search is excluded for 131 decomposition and 32×32, 16×16 MB searches are excluded for 230 decomposition.

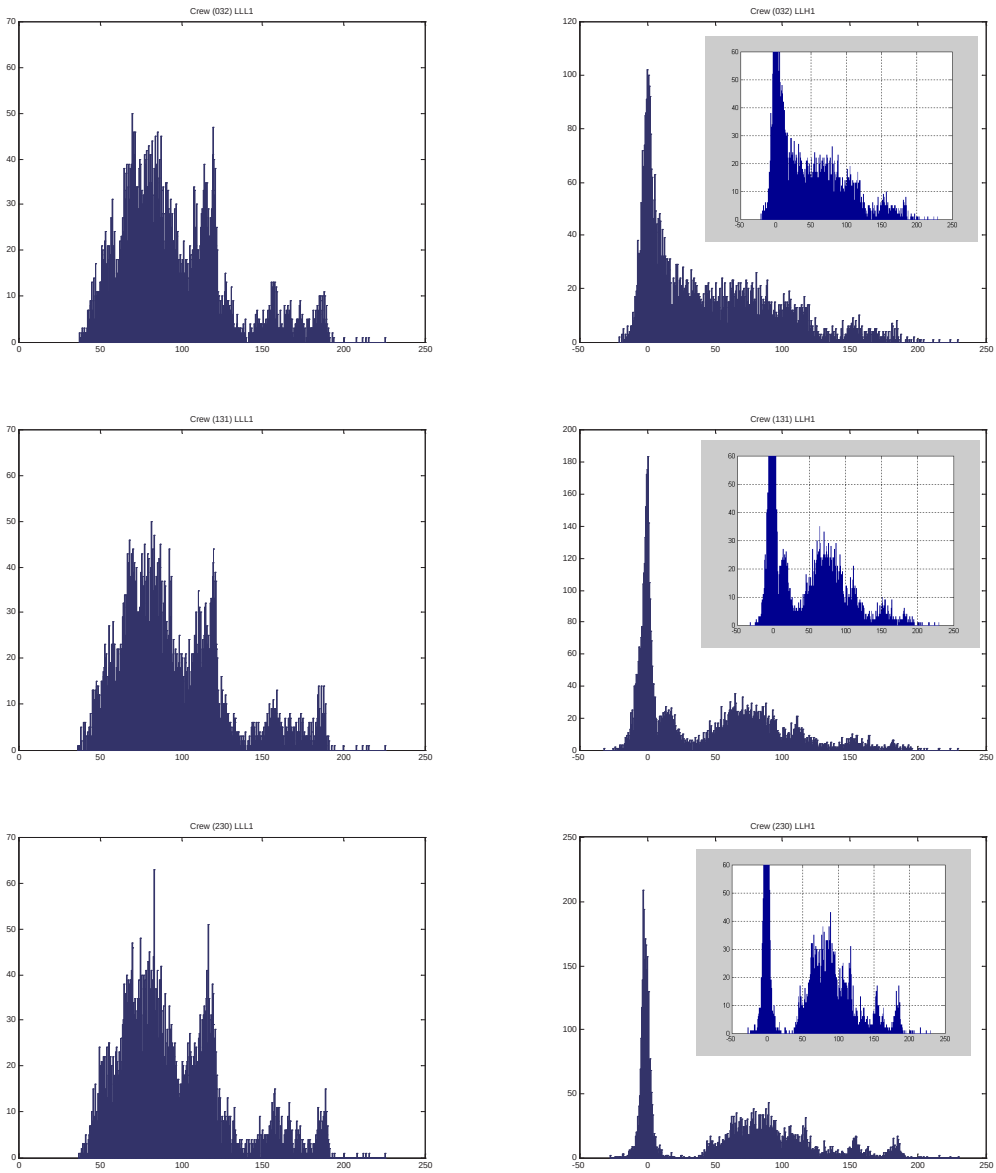

Figure 7.10: Histogram of coefficients at LL_s for 3rd level temporal low and high frequency frames (GOP 1) for *Crew* sequence. *Column 1) & 2)* represents LLL and LLH temporal frames, respectively and *Row 1), 2) & 3)* shows 032, 131 and 230 combinations of 2D+t+2D framework.

The results show that for a MB size of 8×8 or more, 2D+t outperform t+2D. In this context the spatio-temporal decompositions can be ranked as (230) > (131) > (032). In the case of 131 or 230, the motion is estimated in hierarchically down sampled low frequency subband. Therefore number of motion vector reduces accordingly for a given macro block size. As a result for a blind motion estimation less number of motion vector needs to be estimated at the decoder resulting in more accurate motion estimation and

Table 7.3: Hamming distance for blind watermarking by estimating motion from watermarked video using different macro block size (MB) and search range (SR). Embedding at LL_s on frame: a) LLL and b) LLH on *Foreman* sequence (average of first 64 frames).

(a) LLL

	MV from watermarked video: MB/SR						
	32×32 / ± 64	16×16 / ± 64	16×16 / ± 32	8×8 ± 32	8×8 / ± 16	4×4 / ± 16	4×4 / ± 8
032	0.02	0.03	0.02	0.03	0.03	0.04	0.04
131	-	0.02	0.03	0.03	0.03	0.08	0.07
230	-	-	-	0.03	0.03	0.08	0.07

(b) LLH

	MV from watermarked video: MB/SR						
	32×32 / ± 64	16×16 / ± 64	16×16 / ± 32	8×8 ± 32	8×8 / ± 16	4×4 / ± 16	4×4 / ± 8
032	0.15	0.29	0.29	0.40	0.39	0.49	0.49
131	-	0.22	0.21	0.29	0.28	0.44	0.44
230	-	-	-	0.23	0.22	0.30	0.30

better robustness. It is evident from Table 7.3 and Table 7.4, that if same number of motion vectors are considered, *i.e.,* 32×32 MB for 032, 16×16 MB for 131 and 8×8 MB for 230, the robustness performance are comparable for all three combinations. However in LLL subband of 2D+t, for a smaller MB, such as, 4×4, more motion mismatch is observed as motion estimation is done in a spatially decomposed region. Now, using the analysis, above, the experiments are designed to verify the proposed video watermarking schemes for improved imperceptibility as well as robustness against scalable video compressions.

7.4 Experimental results and discussion

The following experimental setups are used for the simulation of watermark embedding using the proposed generalized 2D+t+2D motion compensated temporal-spatial subband scheme. In order to make the watermarking strength constant across subbands, the normalization steps in the MCTF and the 2D DWT were omitted.

There are two different sets of result obtained for luma component of 8 test video sequences ($4:2:0$ YUV sequences) as shown in Figure 7.11 to show the embedding distortion and the robustness performance. One non-blind and one blind watermarking schemes are used as example cases, described in Section 7.3.1. For the simulations

Table 7.4: Hamming distance for blind watermarking by estimating motion from watermarked video using different macro block size (MB) and search range (SR). Embedding at LL_s on frame: a) LLL and b) LLH on *Crew* sequence (average of first 64 frames).

(a) LLL

	MV from watermarked video: MB/SR						
	32×32 / ± 64	16×16 / ± 64	16×16 / ± 32	8×8 ± 32	8×8 / ± 16	4×4 / ± 16	4×4 / ± 8
032	0.03	0.06	0.05	0.09	0.09	0.09	0.09
131	-	0.03	0.03	0.07	0.07	0.14	0.13
230	-	-	-	0.03	0.03	0.15	0.12

(b) LLH

	MV from watermarked video: MB/SR						
	32×32 / ± 64	16×16 / ± 64	16×16 / ± 32	8×8 ± 32	8×8 / ± 16	4×4 / ± 16	4×4 / ± 8
032	0.17	0.24	0.23	0.36	0.36	0.48	0.47
131	-	0.16	0.16	0.23	0.23	0.41	0.38
230	-	-	-	0.17	0.17	0.28	0.27

shown in this work the four combinations (032), (230), (131) and (002) were used. In each case, the watermark embedding is performed on the low frequency subband (LL_s) of 2D spatial decompositions due to its improved robustness performance against compression attacks in image watermarking. In these simulations the 9/7 bi-orthogonal wavelet transform was used as the 2D decompositions.

Based on the analysis in the previous section, here we explored the possibility of watermark embedding in high frequency temporal subband and investigate the robustness performance against compression attacks, as high frequency subband can offer improved imperceptibility. In the experiment sets, 3rd temporal level high pass (LLH) and low pass (LLL) frames are chosen to embed the watermark. Other video decomposition parameters are set to: *1)* Eight groups of picture (GOP) size of 8 frames each, *2)* 8×8 macro block size and *3)* a search window of ± 16. The choice of macro block size and search window are decided by referring the motion retrieval analysis in Section 7.3.2.2.

For embedding distortion measure, Mean Square Error (MSE) is used here along with the amount of flicker introduced due to watermark embedding by using the flicker metric in the MSU Quality Measurement Tool [112]. The flicker metric compares the flicker content in the watermarked video with respect to the original video. In both metrics the lower values correspond to the better distortion performance. On the other hand the watermarking robustness is represented by Hamming distance as mentioned in Eq. (4.1) and lower Hamming distance corresponds a better detection performance. Various

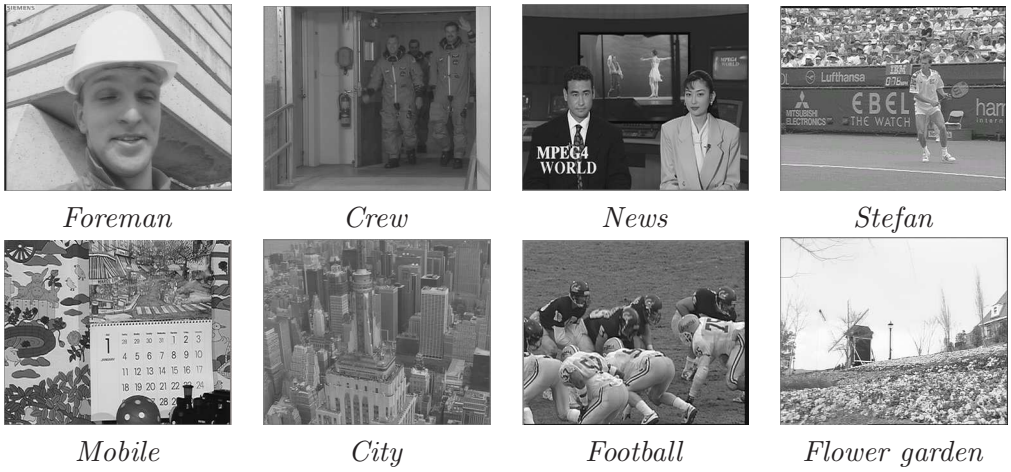

Foreman *Crew* *News* *Stefan*

Mobile *City* *Football* *Flower garden*

Figure 7.11: The test video sequence set.

wavelet scalable coded quality compression attacks are considered, such as, Motion JPEG 2000 (using *Open JPEG* software code) and MC-EZBC scalable video coding (an RWTH Aachen University implementation). We have also reported the preliminary robustness performance against H.264-SVC (scalable extension) using JSVM software (Release 9.15). The results show the mean value of Hamming distance for average of first 64 frames of test video set.

The experiments are divided into two sets, one for embedding distortion analysis and the other for robustness evaluation. In all the experimental set up, two example watermarking algorithms, one each from non-blind [17] and blind [5] category are considered. The weighting parameter α and γ are set to 0.1. In case of non-blind algorithm a level adaptive threshold selection method [17] is used to choose the coefficients to embed the watermark. The watermarking data capacity is set to 2000 bits and 2112 bits using a binary logo for all combinations and every sequences for non-blind and blind watermarking methods, respectively.

7.4.1 Embedding distortion analysis

The embedding distortion results are shown in Figure 7.12 for *LLL* and *LLH* frames for *News* sequence; Figure 7.13 for *LLL* and *LLH* frames for *Foreman* sequence; Figure 7.14 for *Crew* sequence for non-blind watermarking method and embedding distortion results for blind watermarking methods are shown in Figure 7.15 for *LLL* and *LLH* frames for *News* sequence; Figure 7.16 for *LLL* and *LLH* frames for *Foreman* sequence; Figure 7.17 for *Crew* sequence. In each of the figures *y-axis* in a) and c) rep-

resents the MSE and b) and d) represents flicker metrics for LLL and LLH subband, respectively. The *x-axis* of the figures presents first 64 frames of the test sequences with the size of 8 frames per GOP.

From the results for LLL subband, it is evident that although the MSE performances are comparable, proposed MCTF based methods ((032), (131) and (230)) outperform the frame-by-frame embedding (002) with respect to embedding distortion performance to address the flickering problem. In all four combinations the sum of energy in LLL subband are similar and resulting in comparable MSE. However in the proposed methods the error (*i.e.,* MSE) is propagated along the GOP due to due to hierarchical temporal decomposition along the motion trajectory and the error propagation along the motion trajectory addressed the issues related to flickering artifacts.

On the other hand for LLH subband, due to temporal filtering the sum of energy is lesser and the four combinations can be ranked as $032 < 131 < 230 < 002$. Hence the MSE and flickering performance for this temporal subband can be ranked as $032 > 131 > 230 > 002$. Therefore while choosing a temporally filtered high frequency subband, such as LLH, LH or H, the proposed MCTF approach also outperform the frame by frame embedding in terms of MSE while addressing the flickering issues.

To evaluate the embedding performance we chose three video sequences from different motion activity, with very low motion (*News*), medium motion (*Foreman*) and high motion (*Crew*). It is evident that flickering due to frame-by-frame embedding is increasingly prominent in the sequences with lower motion and is successfully addressed by the proposed MCTF based watermarking approach.

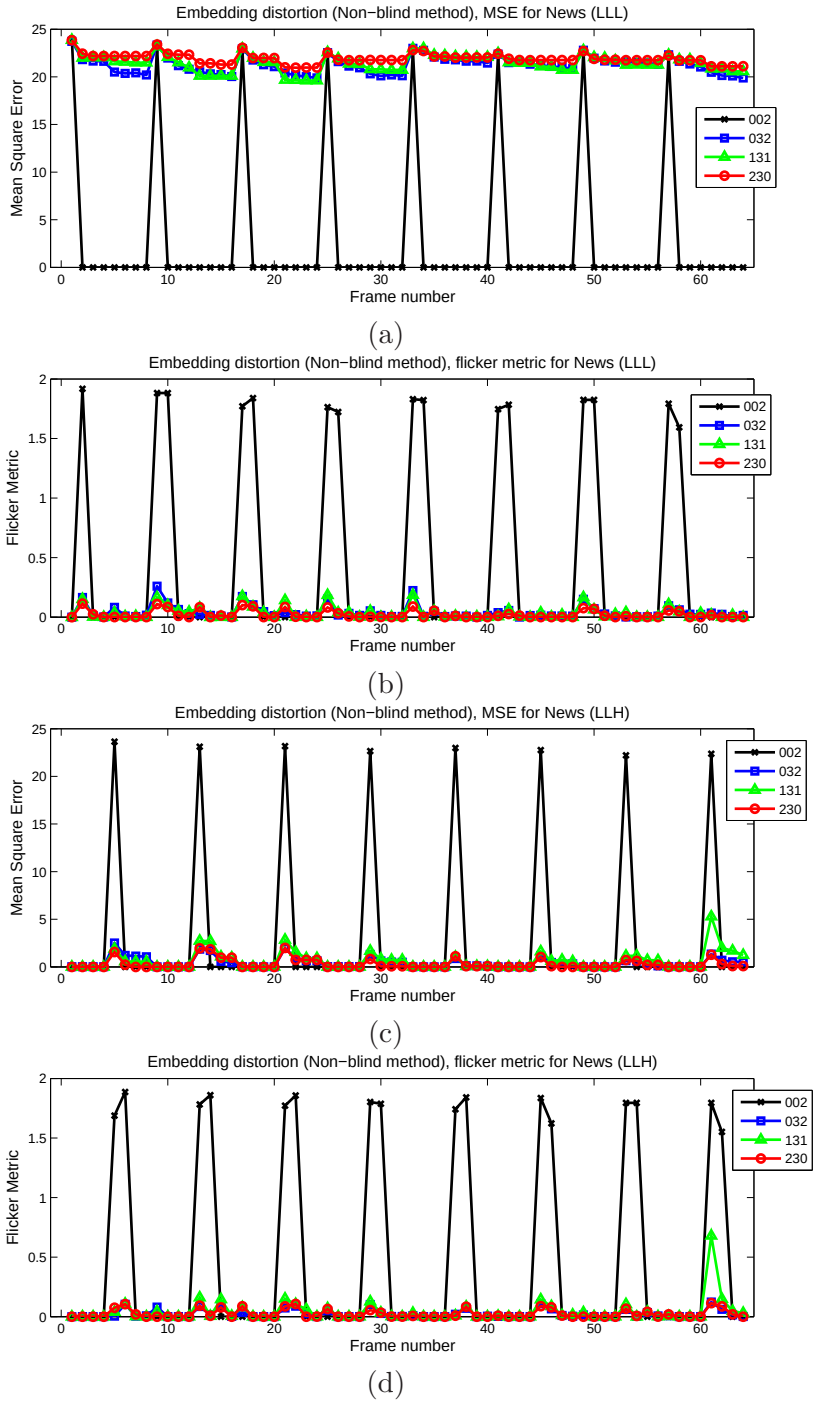

Figure 7.12: Embedding distortion performance for non-blind watermarking on LLL and LLH temporal subbands for *News* sequence. a) and c) represents MSE and b) and d) represents Flicker metric for LLL and LLH, respectively.

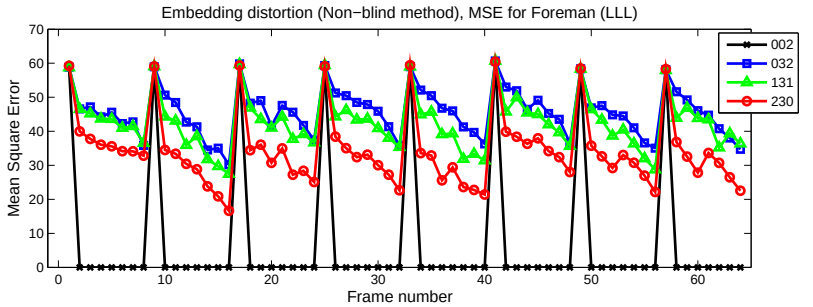

(a)

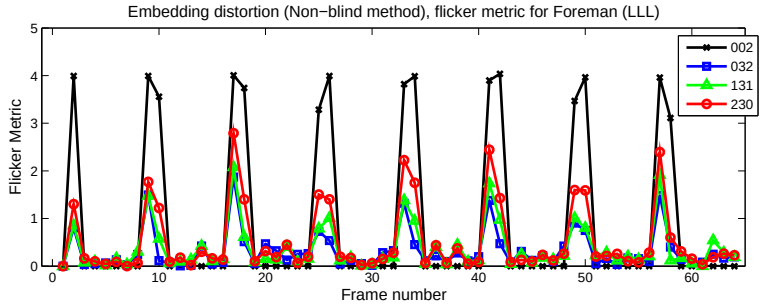

(b)

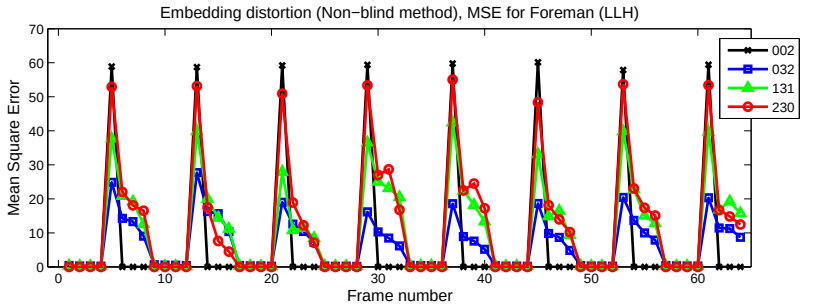

(c)

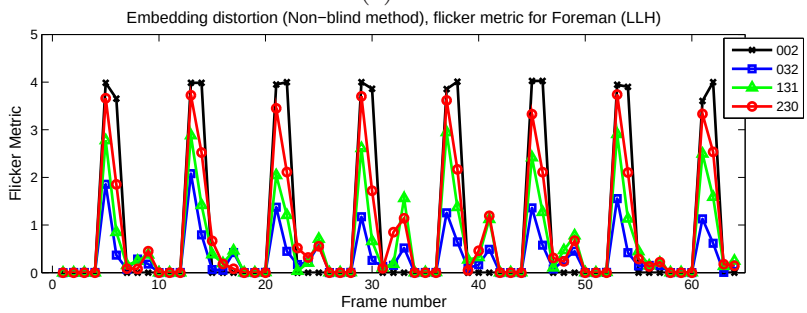

(d)

Figure 7.13: Embedding distortion performance for non-blind watermarking on LLL and LLH temporal subbands for *Foreman* sequence. a) and c) represents MSE and b) and d) represents Flicker metric for LLL and LLH, respectively.

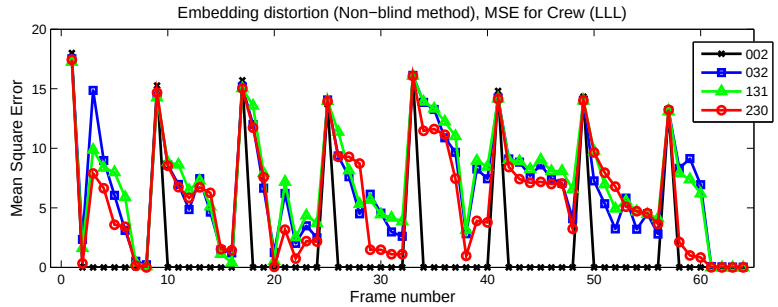

(a)

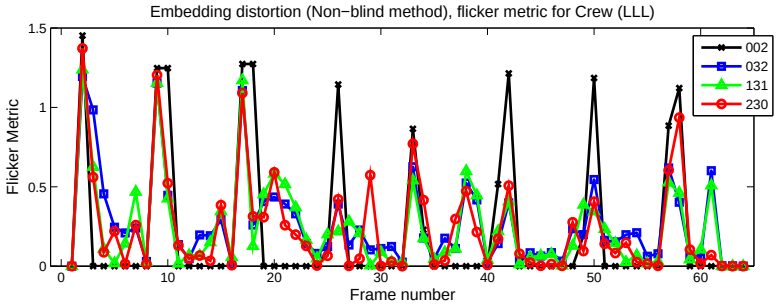

(b)

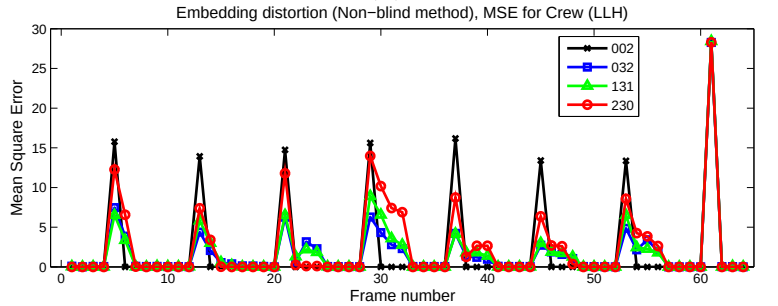

(c)

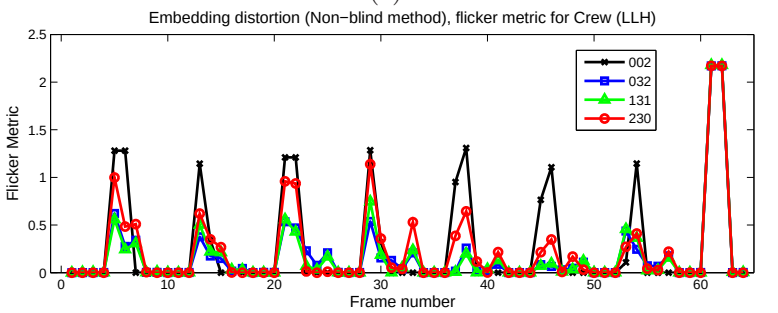

(d)

Figure 7.14: Embedding distortion performance for non-blind watermarking on LLL and LLH temporal subbands for *Crew* sequence. a) and c) represents MSE and b) and d) represents Flicker metric for LLL and LLH, respectively.

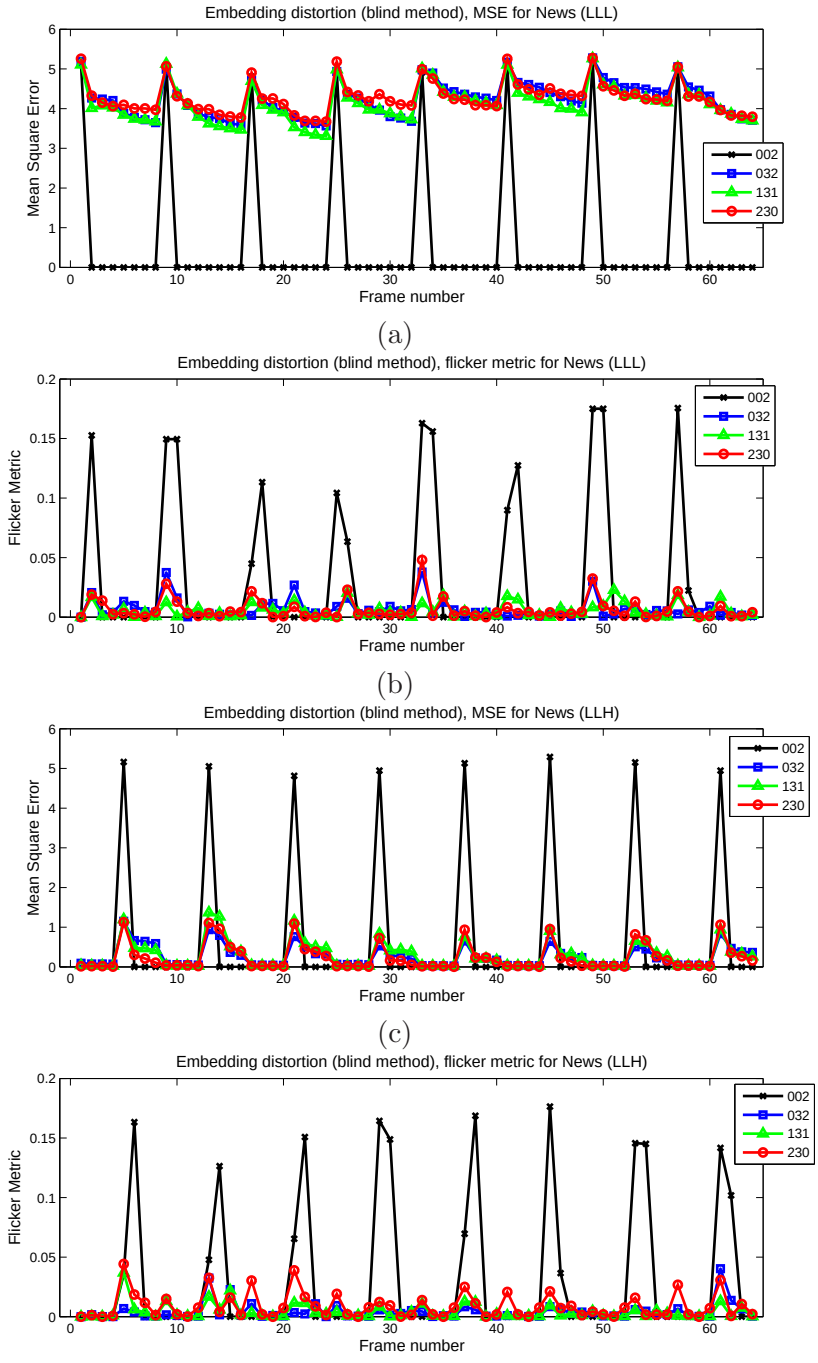

Figure 7.15: Embedding distortion performance for blind watermarking on LLL and LLH temporal subbands for *News* sequence. a) and c) represents MSE and b) and d) represents Flicker metric for LLL and LLH, respectively.

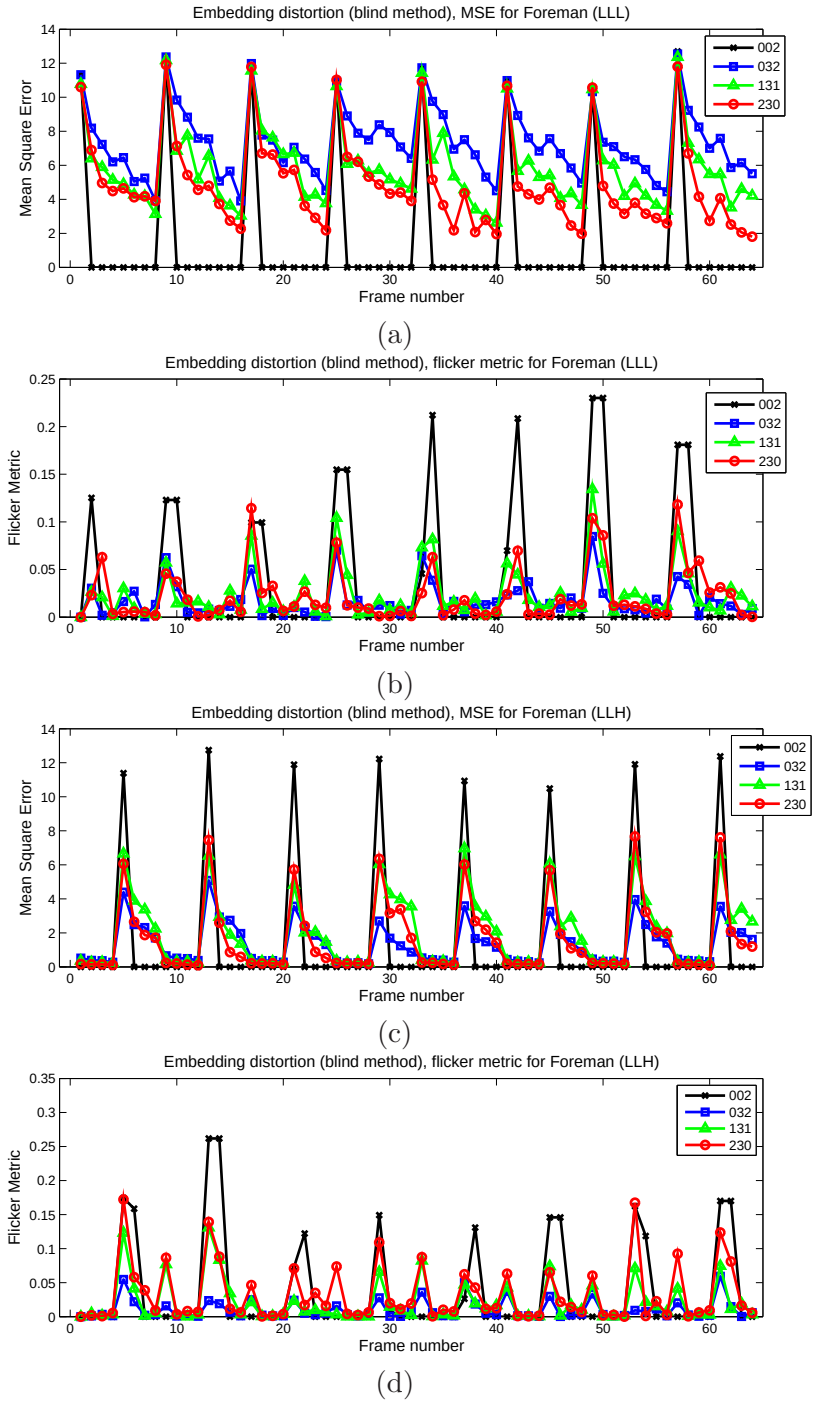

Figure 7.16: Embedding distortion performance for blind watermarking on LLL and LLH temporal subbands for *Foreman* sequence. a) and c) represents MSE and b) and d) represents Flicker metric for LLL and LLH, respectively.

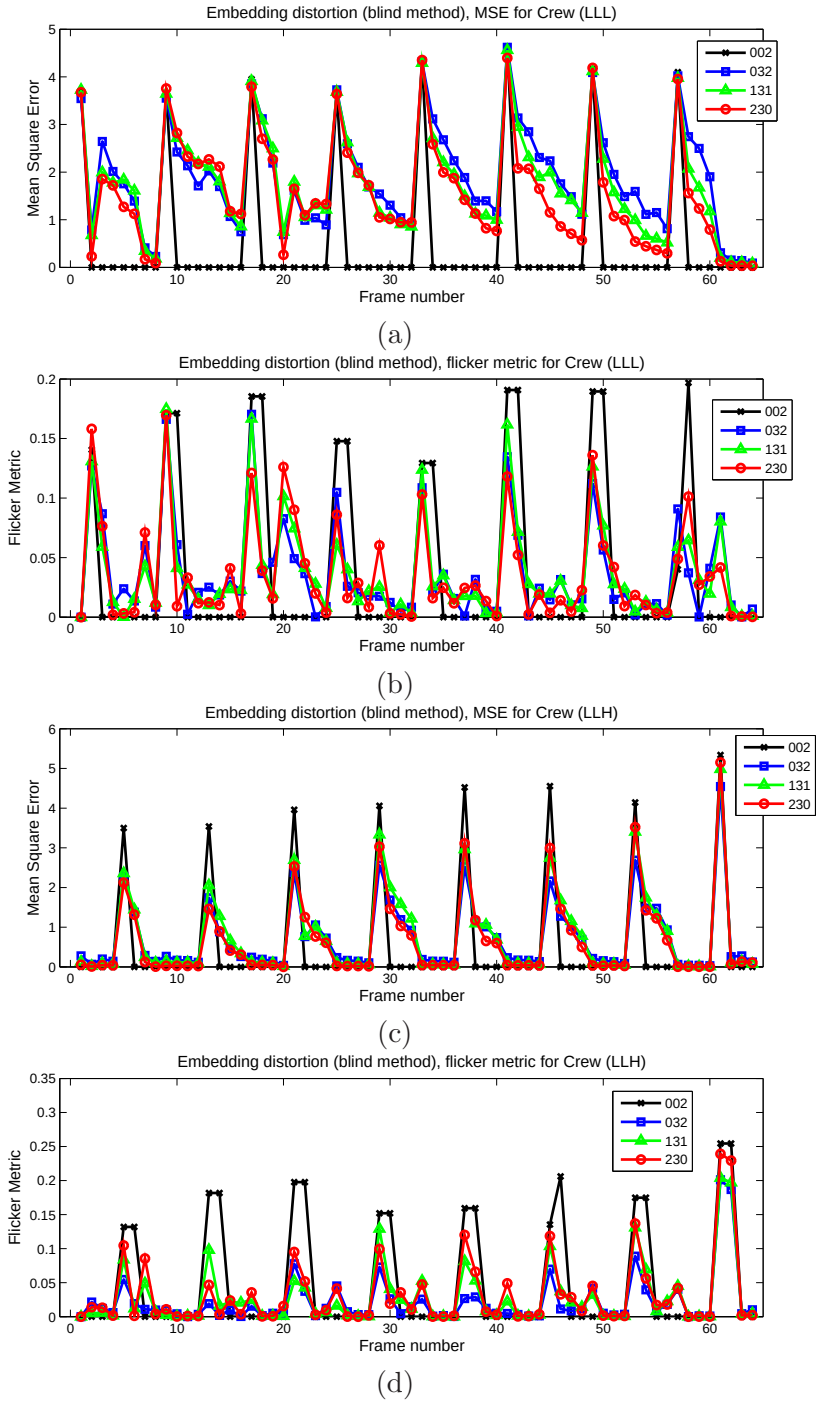

Figure 7.17: Embedding distortion performance for blind watermarking on LLL and LLH temporal subbands for *Crew* sequence. a) and c) represents MSE and b) and d) represents Flicker metric for LLL and LLH, respectively.

7.4.2 Robustness performance evaluation

This experimental set up reports the results for robustness of the proposed scheme against various scalable content adaptation of video. The robustness results for the non-blind watermarking method are shown in Figure 7.18, Figure 7.19 and Figure 7.20 for *Crew*, *Foreman* and *News* sequences, respectively. The x-axis represents the compression ratio (Motion JPEG 2000) or video bit rates (MC-EZBC) and the y-axis shows the corresponding Hamming distances. *Column 1) & 2)* show the results for the LLL and LLH frame selections, respectively. The preliminary robustness results against H.264-SVC are shown in *Appendix A*. The robustness performances shows that any combination of temporal filtering on spatial decomposition (*i.e.,* (131) and (230)) outperforms a conventional t+2D based scheme.

The experimental robustness results for blind watermarking method are shown in Figure 7.21, Figure 7.22 and Figure 7.23 for *Crew*, *Foreman* and *News* sequences, respectively. The left hand column shows results for the LLL temporal subband while results for LLH are shown in the right hand column. The rows represent various scalability attacks, Motion JPEG 2000 and MC-EZBC, respectively. In this case the motion information is obtain from the watermarked test video and based on motion retrieval analysis in Section 7.3.2.2, the motion parameters are set to the macro block size of 8×8 with a ± 16 search window. Similar to the non-blind watermarking, any combination of temporal filtering on spatial decomposition (*i.e.,* (131) and (230)) outperforms a conventional t+2D based scheme.

We now analyze the obtained results by grouping it by selection of temporal subband, *i.e.,* LLL and LLH; by embedding method, *i.e.,* non-blind and blind; and by compression scheme, *i.e.,* Motion JPEG 2000, MC-EZBC and H.264/SVC.

Selection of temporal subband:
The low frequency temporal subband (LLL) offers better robustness in comparison to high frequency LLH subband. This is due to more energy concentration in LLL subband after temporal filtering. Within the temporal subbands, in LLL subband various spatio-temporal combinations performs equally as the energy levels are nearly equal for 032, 131 and 230. However 230 performs slightly better due to lesser motion related error in spatially scaled subband. On the other hand for LLH subband, the robustness performance can be ranked as $230 > 131 > 032$ as a result of the energy distribution ranking of these combinations in Section 7.3.2.1.

Embedding method:
In the experimental set up we have used two different watermarking schemes: 1) Non-blind and 2) Blind. For a non-blind case, the watermark extraction is performed using the original host video and hence the original motion vector is available at the extractor which makes this scheme more robust to various scalable content adaptation. On the other hand as explained before, the blind watermarking scheme neither have any reference to original sequence nor any reference motion vector. The motion vector is estimated from the watermarked test video itself which results in comparatively poor robustness. The effect of motion related error is more visible in LLH subband as the motion compensated temporal high pass frame is highly sensitive to motion estimation accuracy and so the robustness performance. As discussed in Section 7.3.2.2 in case of a 2D+t (*i.e.,* 230) the error due motion vector is lesser compared to t+2D scheme and hence offers better robustness ($230 > 131 > 032$).

Compression scheme:
We have evaluated the proposed algorithm against various scalable video compression scheme, *i.e.,* wavelet based Motion JPEG 2000, MC-EZBC and H.264/SVC. First two video compression schemes are based on wavelet technology where more recent H.264/SVC uses layered scalability using base layer coding of H.264/AVC.

In Motion JPEG 2000 scheme, the coding is performed by applying 2D wavelet transform on each frames separately without considering any temporal correlation between frames. In the proposed watermarking scheme, the use of 2D wavelet transform offers better association with Motion JPEG 2000 scheme and hence provides better robustness for 2D+t combination for LLL and LLH. Also in the case of LLH subband a better energy concentration offers better robustness to Motion JPEG 2000 attacks. The robustness performance against Motion JPEG 2000 can be ranked as $230 > 131 > 032$.

MC-EZBC video coder uses motion compensated 1D wavelet transform in temporal temporal filtering and 2D wavelet transform in spatial decomposition. In compression point of view MC-EZBC usually encodes the video sequences in t+2D combination due to better energy compaction in low frequency temporal frames. But in watermarking perspective, higher energy in high frequency subband can offer better robustness. The argument is justified from the robustness results where results for LLL subbands are comparable, but a distinctive improvement is observed in LLH subband and based on the results the robustness ranking for MC-EZBC can be done as $230 > 131 > 032$.

Finally the robustness of the proposed scheme is evaluated against H.264/SVC, which uses inter/intra motion compensated prediction followed by an integer transform with

similar properties of DCT transform. Although the watermarking and video coding scheme does not share any common technology or transform, the results provide acceptable robustness. However for a blind watermarking scheme in LLH subband, proposed schemes performs poorly due to blind motion estimation. Similar to previous robustness results, based on energy distribution and motion retrieval argument, here the spatio-temporal combinations can be ranked as $230 > 131 > 032$. In a specific example case H.264/SVC usually gives preference to intra prediction to the sequences with low global or local motion, as in *News* sequence and hence exception in robustness performance to H.264/SVC is noticed for the proposed scheme.

Based on the above discussion, due to the close association between the proposed scheme and MC-EZBC, the robustness of the proposed scheme offers best performance against MC-EZBC based content adaptation. To conclude this discussion, we suggest that, a choice of 2D+t based watermarking scheme improves the imperceptibility and the robustness performance in a video watermarking scenario for a non-blind as well as a blind watermarking algorithm. In the next section we extend the image watermarking robustness model into video watermarking framework to propose watermarking with enhanced robustness against scalable compression.

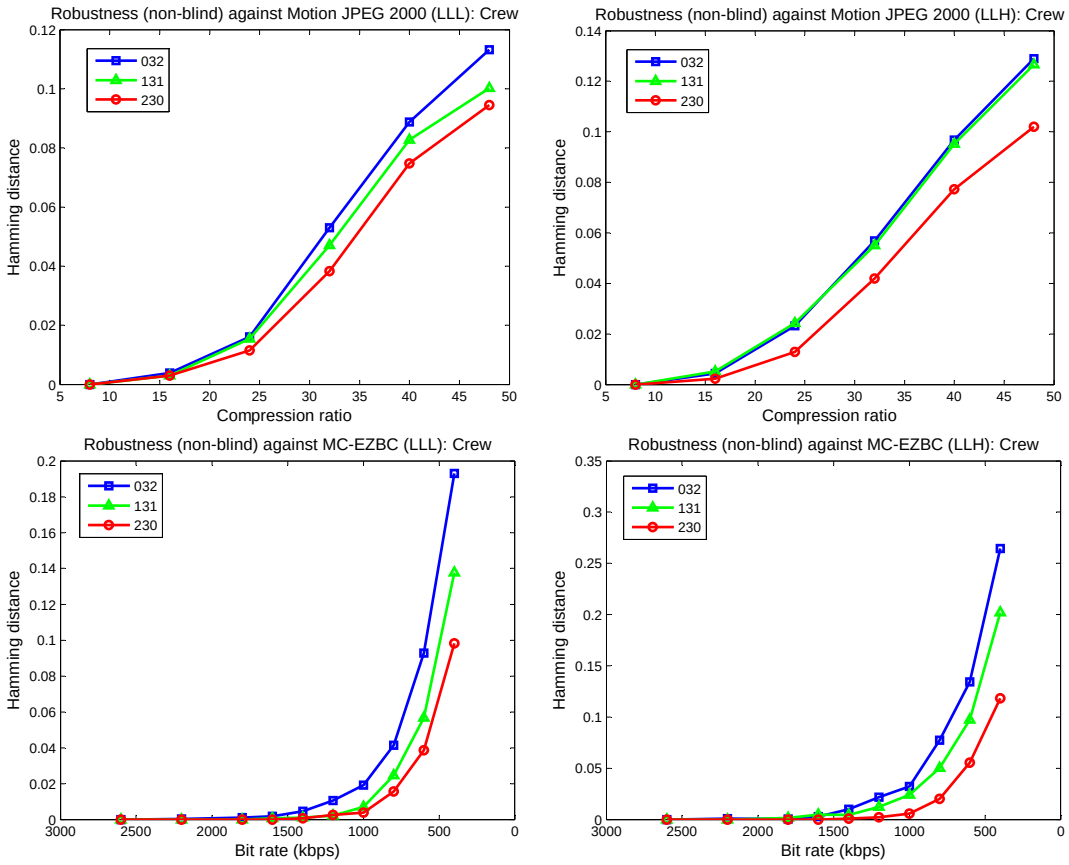

Figure 7.18: Robustness performance of non-blind watermarking scheme for *Crew* sequence. *Row 1) & 2)* show robustness against Motion JPEG 2000 and MC-EZBC, respectively. *Column 1) & 2)* represents the embedding on temporal subbands LLL & LLH, respectively.

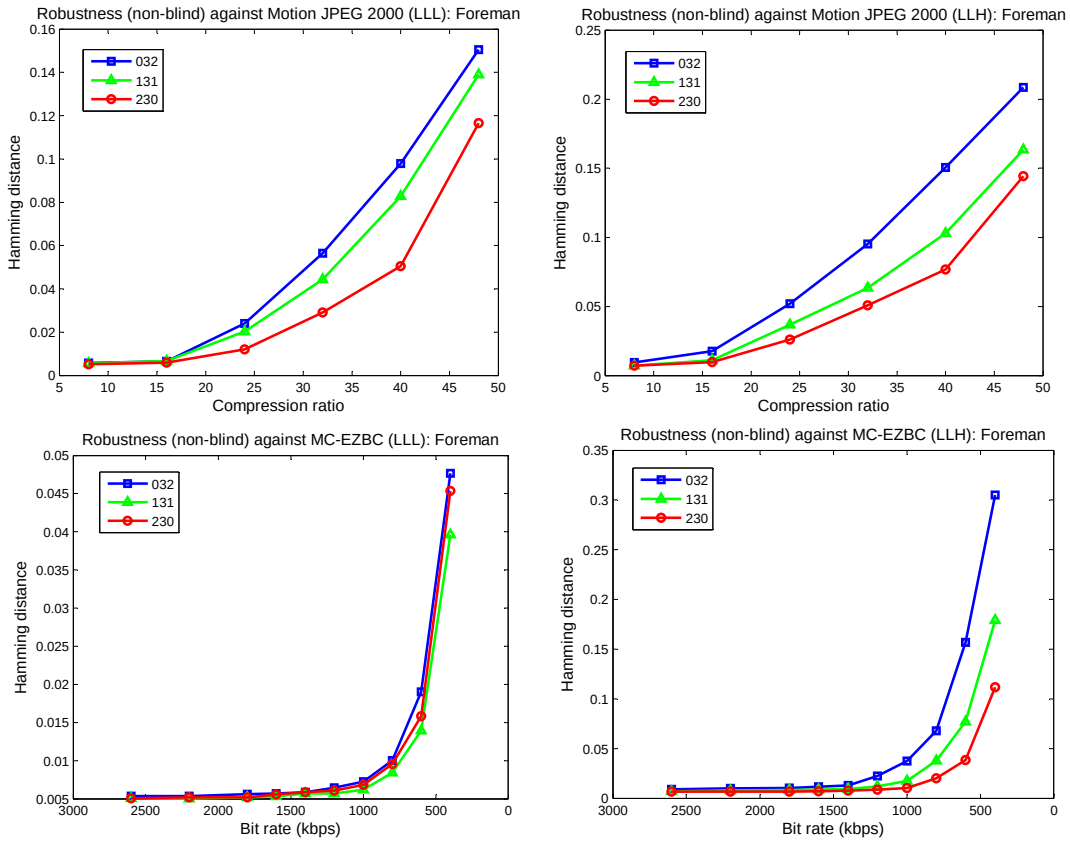

Figure 7.19: Robustness performance of non-blind watermarking scheme for *Foreman* sequence. *Row 1) & 2)* show robustness against Motion JPEG 2000 and MC-EZBC, respectively. *Column 1) & 2)* represents the embedding on temporal subbands LLL & LLH, respectively.

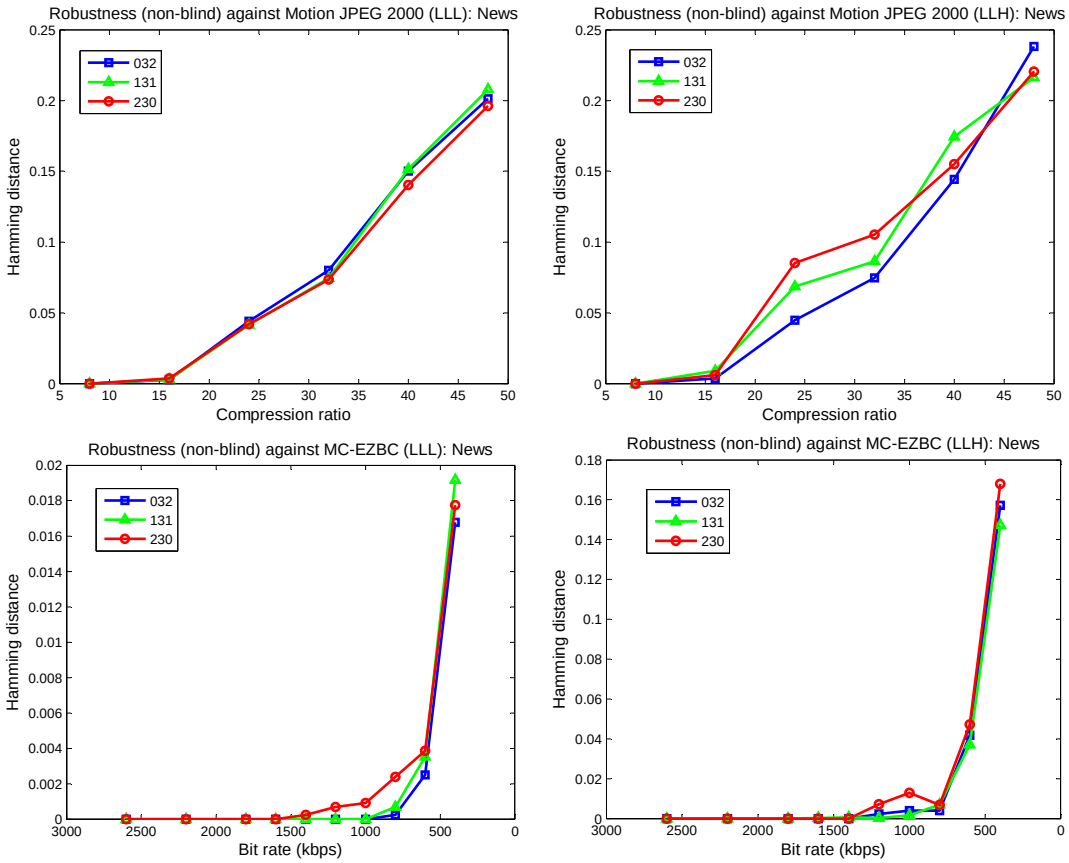

Figure 7.20: Robustness performance of non-blind watermarking scheme for *News* sequence. *Row 1) & 2)* show robustness against Motion JPEG 2000 and MC-EZBC, respectively. *Column 1) & 2)* represents the embedding on temporal subbands LLL & LLH, respectively.

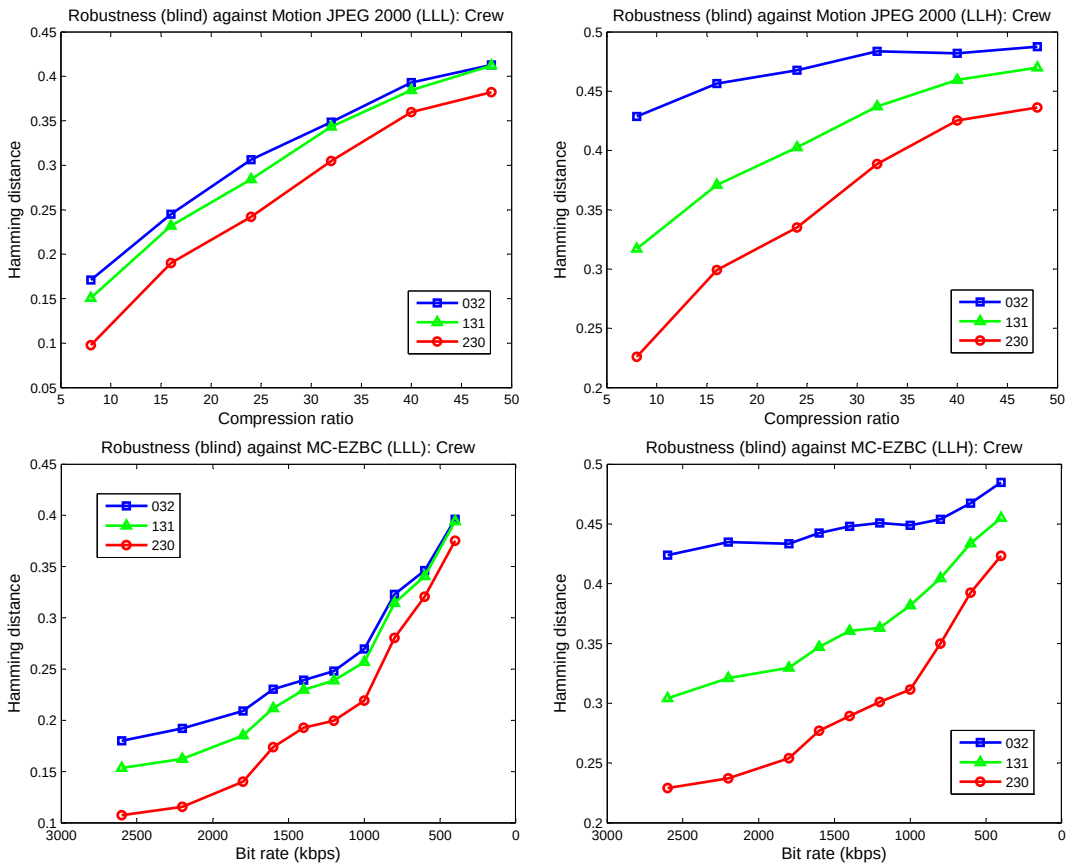

Figure 7.21: Robustness performance of blind watermarking scheme for *Crew* sequence. *Row 1) & 2)* show robustness against Motion JPEG 2000 and MC-EZBC, respectively. *Column 1) & 2)* represents the embedding on temporal subbands LLL & LLH, respectively.

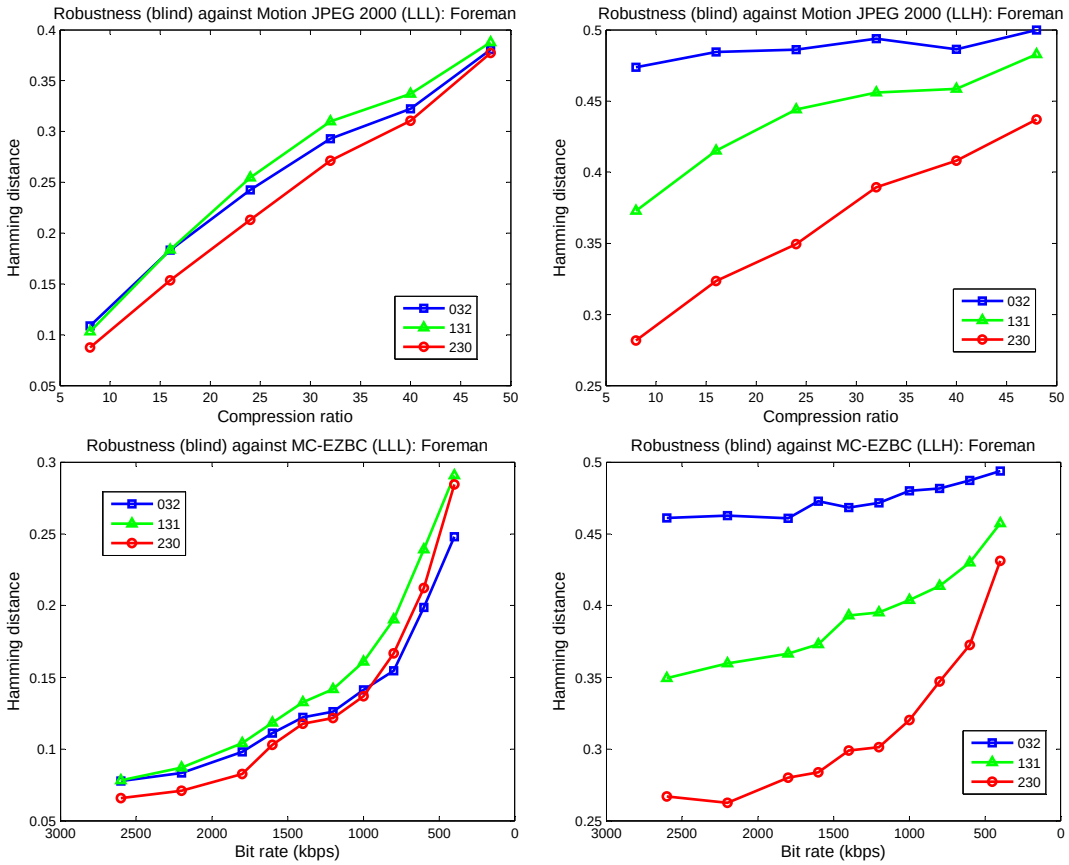

Figure 7.22: Robustness performance of blind watermarking scheme for *Foreman* sequence. *Row 1) & 2)* show robustness against Motion JPEG 2000 and MC-EZBC, respectively. *Column 1) & 2)* represents the embedding on temporal subbands LLL & LLH, respectively.

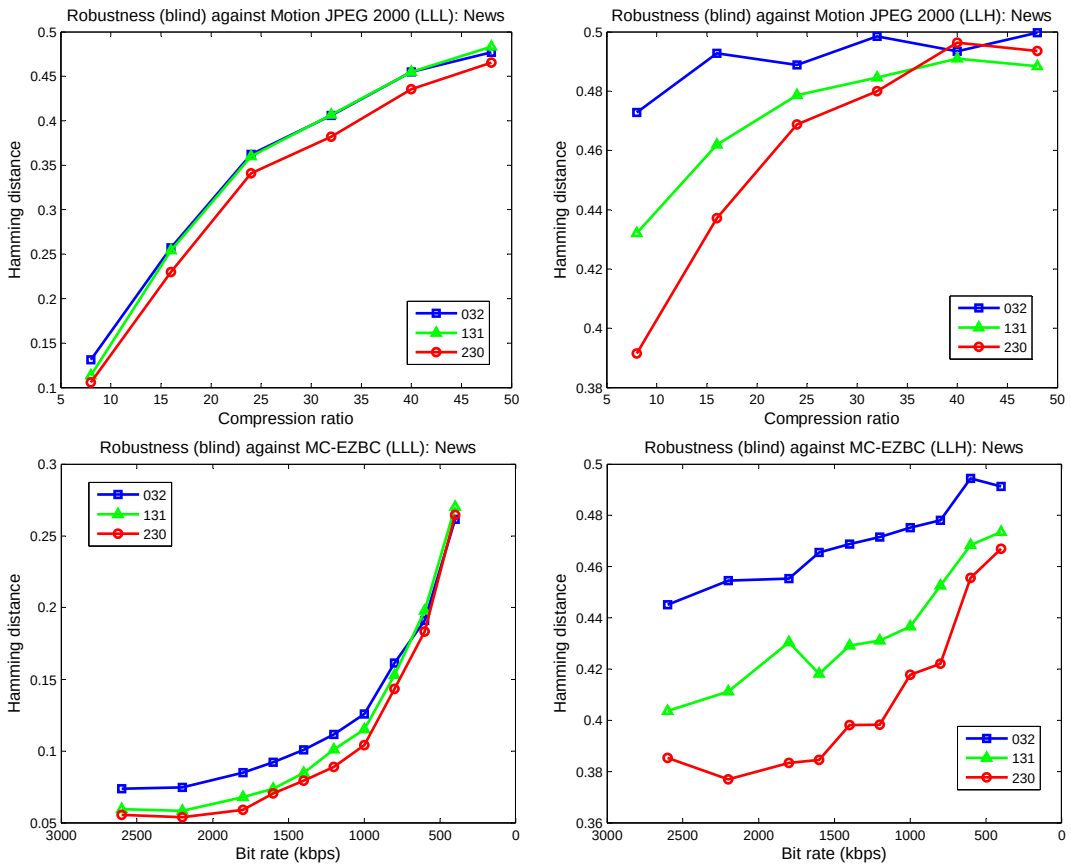

Figure 7.23: Robustness performance of blind watermarking scheme for *News* sequence. *Row 1) & 2)* show robustness against Motion JPEG 2000 and MC-EZBC, respectively. *Column 1) & 2)* represents the embedding on temporal subbands LLL & LLH, respectively.

7.5 Adopting robustness model in video watermarking

7.5.1 Robust video watermarking

So far in this chapter we have proposed and comprehensively evaluated the performances of video watermarking schemes using a generic MCTF based 2D+t+2D framework. The 2D+t spatio-temporal decomposition based watermarking outperformed traditional t+2D decomposition based watermarking schemes. Now at this point we aim to enhance the watermarking robustness further by adopting the image robustness models, as proposed in Chapter 6, into the 2D+t+2D framework. One of the major reasons for this adaptation is that, similar to JPEG 2000, the quality scalable compression within Motion JPEG 2000 and MC-EZBC can also be modeled by the bit-plane discarding based quantization as described in Section 6.2. Therefore, the proposed combined video watermarking scheme can offer an enhanced robustness against quality scalable content adaptation for video.

7.5.2 Experimental results

In the experimental set up the robustness model is adopted during the watermark embedding after 2D+t+2D decomposition. For the comparison purpose we have chosen the 2D+t, 230 subband for non-blind and blind case. The comparison is made between the cases, without using the model and using the model considering 5 bit plane discarding ($N = 5$). Other experimental parameters are kept same as in the previous section. In these cases the normalization on spatio-temporal decompositions are included. The weighting parameter are set to 0.1 in both cases. For the non-blind method, coefficients are selected in LLH subband in a raster scanning order with a data capacity of 2000 bits, while for the blind method one in every three coefficients of the selected subband (LLL here) are considered to embed the watermark with a data capacity of 2112 bits. The robustness results against various scalable compressions are shown in Figure 7.24 and Figure 7.25 for non-blind and blind method, respectively. In both the figures three test sequences *Crew*, *Foreman* and *News* are used and the robustness against Motion JPEG 2000 and MC-EZBC are compared.

It is evident from the results that the image robustness model works successfully for video watermarking techniques by improving the robustness of 2D+t embedding scheme. However the robustness model can also be applied for other combinations in 2D+t+2D framework. In a non-blind method due the availability of original sequence,

the motion vector was unaffected by the robustness model and hence outperformed the cases which did not consider the model. On the other hand, in a blind case, the use of robustness model increases the embedding distortion (as described in Chapter 6) resulting in distortion in motion vector too, which in turn, reduces the robustness improvement in this case. Ideally, the robustness model assumes same spatio-temporal decomposition parameters in embedding as well compression algorithm, where in this experimental set, the embedding scheme is used independent of the compression algorithms. Therefore we can conclude that the robustness enhancement model can perform more efficiently when used within the compression algorithms, which uses bit plane discarding model and preserve motion vector information.

7.6 Conclusions

In this chapter, a flexible generalized motion compensated temporal-spatial subband decomposition scheme, based on the MMCTF for video watermarking is presented. The MCTF was modified by taking into account the motion trajectory into obtaining an efficient update step. The embedding distortion performance evaluated using both MSE and flicker difference metric, shows superior performance for the MMCTF driven 2D+t+2D subband domain watermarking as opposed to frame-by-frame 2D wavelet domain watermarking which does not take motion into account. The proposed subband decomposition also provides low complexity as MCTF is performed only on subbands where the watermark is embedded. The robustness performance against scalable coding based compressions attacks, including Motion JPEG 2000, MC-EZBC and preliminary results for H.264-SVC (scalable extension), are also evaluated. The proposed 2D+t based video watermarking scheme within 2D+t+2D filtering framework outperforms conventional t+2D watermarking schemes in a non-blind as well as a blind watermarking scenario. This video watermarking technique is further extended using the image robustness model to enhance the robustness against scalable compression.

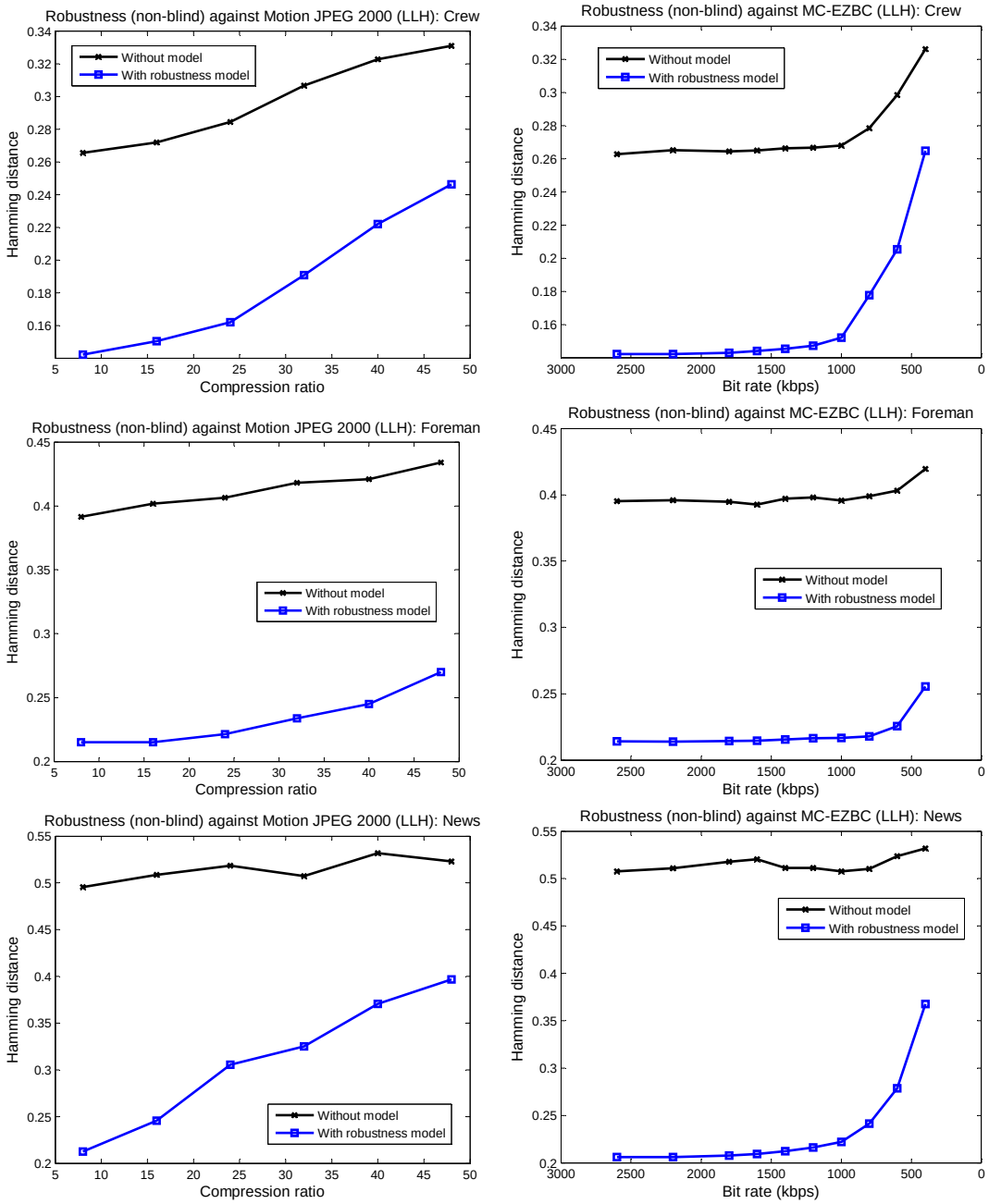

Figure 7.24: Robustness performance enhancement using bit plane discarding model ($N = 5$) of non-blind watermarking scheme for LLH subband. *Column 1) & 2)* show robustness against Motion JPEG 2000 and MC-EZBC, respectively. *Row 1), 2) & 3)* represents the test sequences, *Crew*, *Foreman* & *News*, respectively.

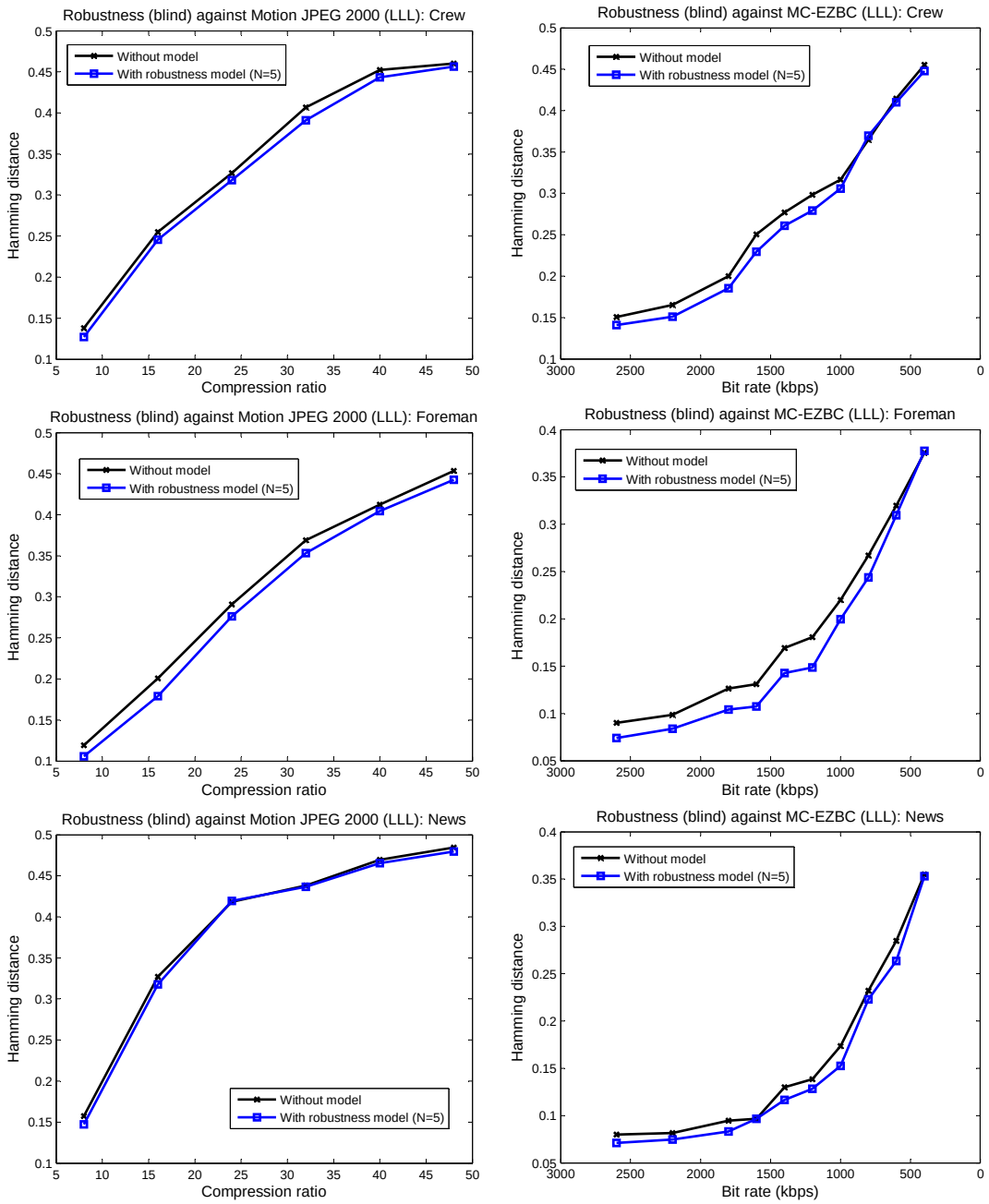

Figure 7.25: Robustness performance enhancement using bit plane discarding model ($N = 5$) of blind watermarking scheme for LLL subband. *Column 1) & 2)* show robustness against Motion JPEG 2000 and MC-EZBC, respectively. *Row 1), 2) & 3)* represents the test sequences, *Crew*, *Foreman* & *News*, respectively.

Chapter 8

Distortion Constrained Robustness Scalable Watermarking

In the previous chapters of this thesis we discussed about the embedding distortion and the robustness to quality scalable image and video coding, which are two complementary watermarking requirements. In this chapter we introduce a novel concept of scalable blind watermarking to generate a distortion-constrained robustness scalable watermarked image code-stream which consists of hierarchically nested joint distortion-robustness coding atoms.

8.1 Introduction

Inspired by image coding standard JPEG2000 and video coding scheme MC-EZBC, this work addresses two long due watermarking questions: *1) Can we define a watermark embedding-rate vs. overall embedding-distortion curve?* and *2) Can we formulate a scalable embedding-robustness relationship graph which can provide hierarchically improved robustness against an image or video processing or compression scheme?* In answering these questions, we recall the state of the art analysis in Chapter 3, where various traditional wavelet based image and video watermarking schemes are generalized and dissected into a set of processes. The performance metrics are defined into two categories: 1) Embedding performance (measured by data-capacity

and embedding-distortion such as PSNR) and 2) Robustness (measured by similarity correlation or Hamming distance (Bit Error Rate)). In these traditional watermarking methods, these metrics are often mutually exclusive and therefore measured and represented separately. On the contrary these metrics influence each other's performance and in this chapter we aim to combine them to propose a distortion constrained robustness scalable watermarking scheme. Therefore it is also important to formulate a common mutually inclusive space for the performance measures.

The concept of scalable watermarking is particularly useful for watermarking for scalable coded image and video where the watermark can also be scaled according to the heterogenous network capacity and end user's requirement for a target application. For example, for a high bandwidth network and a high resolution display, highly imperceptible but less robust watermarked image or video can be transmitted, as in this scenario, highly imperceptible media is desirable and the watermark can be extracted reliably due to lesser compression, whereas, for a low capacity network and low resolution display, the distribution server can choose highly robust watermarking stream, where, due to higher compression the watermarking imperceptibility is less important but high robustness is required for a reliable watermark extraction. Similarly, based on any other combinations of the network's capability and user's requirement, the scalable watermarked media code-stream can be truncated and distributed accordingly.

With the increased use of scalable coded media, such scalable watermarking concept is very important, but a little or no work has been proposed so far in the current literature. Available most common such algorithms are proposed either as joint progressive scalable watermarking and coding scheme [34, 35] or efficient coefficient selection methods which are robust against resolution or quality scalable attacks [36,37]. These algorithms primarily focused on two main robustness issues [38]: 1) detection of watermark after acceptable scalable compression and 2) graceful improvement of extracted watermark as more quality or resolution layers received at the image decoder.

On the contrary, we propose a novel scalable watermarking concept, based on distortion constrained watermarked code-stream to generate watermarked image / video with desired distortion robustness requirements. This work addresses the tow-fold problem of 1) obtaining the least distortion at a given watermark embedding rate and 2) achieving the best robustness in a scalable fashion by hierarchically encoding lower and higher embedded code-atoms, respectively. In designing the algorithm, we have considered the propositions for embedding distortion in Chapter 5, *i.e.,* in order to minimize the distortion, the coefficient modification must be minimized; and the concept of quality scalability using bit plane discarding model (as discussed in Chapter 6) in order

to improve the robustness against scalable content adaptation. The objectives of the proposed scheme, are:

- Creating a common performance metric to represent data-capacity and embedding distortion.
- Proposing a new watermarking algorithm which incorporates the bit plane discarding model, used in quality scaling based content adaptation in scalable coded image and video.
- Obtaining best robustness at a given embedding distortion rate.
- Scalable embedded code-stream generation using hierarchically nested joint distortion-robustness coding atoms.
- The code-stream should be allowed to be truncated at any distortion-robustness atom level to generate the watermarked image with the desired distortion-robustness requirements.

To fulfill the requirements of the said objectives, we introduced a new wavelet domain binary tree guided rules-based blind watermarking algorithm. The universal blind extractor of this algorithm is capable of extracting watermark data from the watermarked images, created using any truncated code-stream. The code-stream mentioned in this chapter refers to the joint watermarked wavelet coefficient stream.

As no such idea has been explored yet in the literature, in order to quantify the work in this chapter we have introduced a new embedding distortion metric and reported the robustness results in a hierarchical fashion to support the claim. However, further evaluation can be done in future according to the potential applications such as in authentication of multimedia streaming.

8.2 Scalable watermarking

In this section, the design and development of the proposed scalable watermarking scheme is discussed. Firstly, the new wavelet domain binary tree guided watermarking algorithm is discussed and then it is used in developing the scalable watermarking system.

8.2.1 Proposed algorithm

In proposing the new algorithm we aim to address two issues related to the main theme of the thesis, robust watermarking techniques for scalable coded image and video: 1) a robust watermarking technique which considers bit plane discarding model in scalable compression and 2) scalability of the watermarking. As discussed earlier the traditional watermarking algorithms fail to comply with the design requirements of the proposed scalable watermarking scheme. Therefore we introduce a new watermarking algorithm which satisfies the above mentioned requirements by creating watermarked image / video code-stream atoms and allows quantitative embedding-distortion measurement at individual atom level.

The proposed wavelet-based algorithm follows a similar system block diagrams as shown in Figure 3.1. The watermark embedding is performed on the coefficients generated after FDWT. The embedding algorithm follows a non-uniform quantization based index modulation. The embedding process is divided into two parts: 1) Quantized binary tree formation and 2) Watermark embedding by index modulation.

8.2.1.1 Tree formation

In this step, all selected coefficients are recursively quantized to form a binary tree. Firstly the selected wavelet coefficient (C) is indexed (b_i) as 0 or 1 using an initial quantizer λ:

$$b_i = \left\lfloor \frac{|C|}{\lambda/2^i} \right\rfloor \%2, \quad i \in 0, 1, 2, 3..., \tag{8.1}$$

where % denotes the modulo operation.

Assuming $n = \left\lfloor \frac{|C|}{\lambda} \right\rfloor$, we can identify the position of C between the quantized cluster (n) and ($n+1$) which can alternatively described as bit plane clusters as shown in Figure 8.1. The selected coefficient C is then further quantized more precisely within a smaller cluster using a smaller quantizer $\lambda/2$ and corresponding index is calculated as: $b_1 = \left\lfloor \frac{|C|}{\lambda/2} \right\rfloor \%2$. The index tree formation is continued recursively by scaling λ value by 2, until $\lambda/2^i \geq 1$. During this tree formation process the *Sign* of the coefficients are preserved separately.

Now based on the calculated index value at various quantization step a binary tree

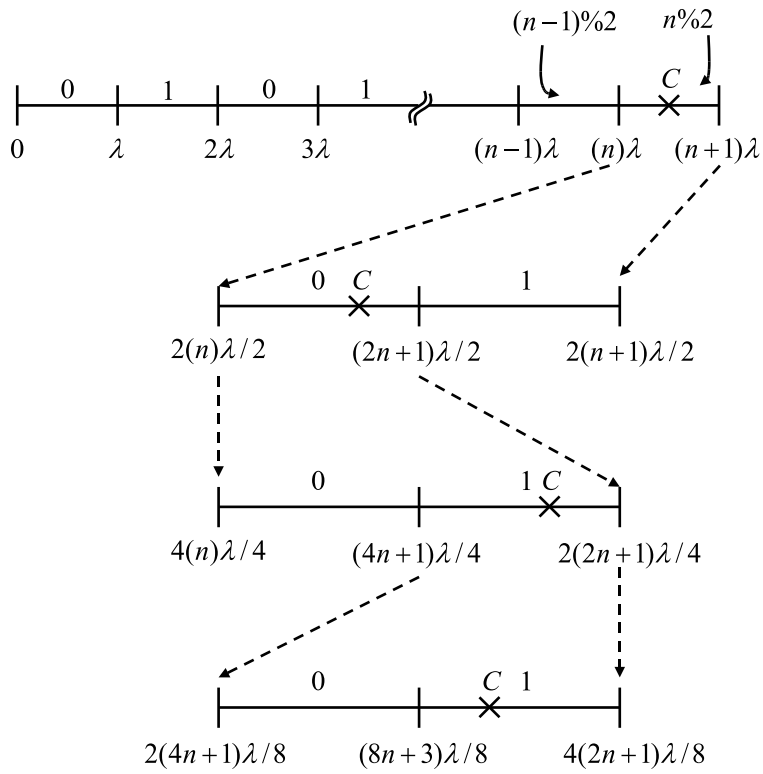

Figure 8.1: Non-uniform hierarchical quantizer in formation of binary tree.

$(b(C))$ of each selected coefficient is formed as follows:

$$b(C) = (b_0)(b_1)....(b_{i-1})(b_i), \tag{8.2}$$

where $(b_0), (b_1)...(b_i)$ are binary bits at most significant bit (MSB) to least significant bit (LSB) positions, respectively with the tree depth $i+1$. For example if $C = 135$ and initial $\lambda = 30$, the binary tree $b(C)$ will be $b(C) = 01000$. The tree formation scenario is shown in Figure 8.2. The number of tree nodes e.g. number of bits in any binary tree are decided by the initial quantizer λ and is defined as *depth* of the tree.

8.2.1.2 Embedding

The above mentioned binary tree is used to embed binary watermark information using symbol based embedding rules. To introduce the watermarking scalability, we chose 3 most significant bits which represents 8 different states corresponding to 6 different symbols. Although any other number of bits (> 1) can be chosen, the use of more number of bits (> 3) results in more states, thus increase the complexity and less

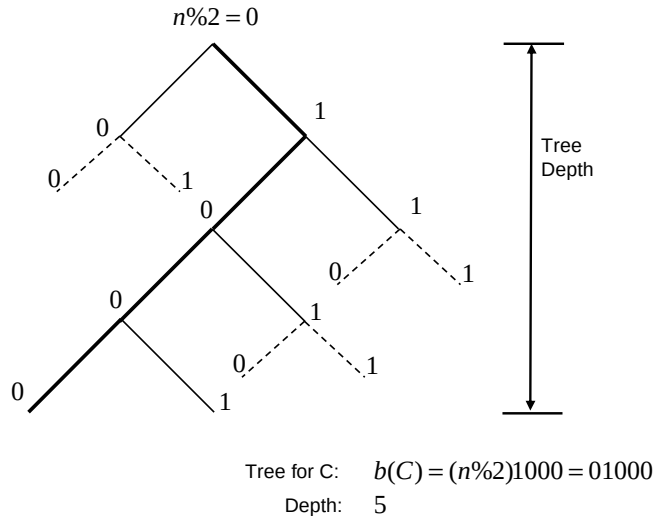

Figure 8.2: Example binary tree.

Table 8.1: Tree-based watermarking rules table

Binary tree	Symbol	Watermark Association
000xxxx	EZ	0
001xxxx	EZ	0
010xxxx	CZ	0
011xxxx	WO	1
100xxxx	WZ	0
101xxxx	CO	1
110xxxx	EO	1
111xxxx	EO	1

number of bits (< 3) reduces the watermark scalability. Now 3 most significant bits of any binary tree, represents 6 symbols (*EZ = Embedded Zero, CZ = Cumulative Zero, WZ = Weak Zero, EO = Embedded One, CO = Cumulative One and WO = Weak One*) to identify the original coefficient's association with a 0 or 1. The bits in the binary trees, symbols and corresponding associations are shown in Table 8.1 for a tree depth of 7. Now, based on the input watermark stream, if require, new association is made by altering the chosen 3 most significant bits in the tree to reach the nearest symbol as shown the state machine diagram in Figure 8.3. Assuming the current state of the binary tree is EZ, to embed watermark bit 0 no change in state is required while to embed watermark input 1, a new value of the binary tree must be assigned associated with either WO, CO or EO. However to minimize the distortion nearest state change must occur as shown in the state machine diagram. Other state changes

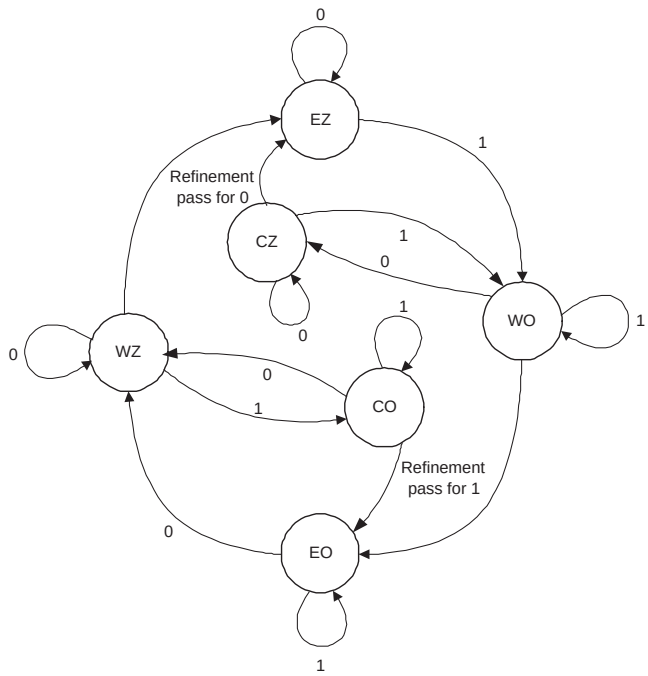

Figure 8.3: State machine diagram of watermark embedding based on tree-symbol-association model.

in the binary tree follows a similar argument. Finally the watermarked image / video is obtained by de-quantizing the modified binary tree followed by an inverse transform.

At this point we recall the issues related to embedding performance measure and propose a new metric to combine the data capacity and embedded distortion:

$$\Phi = \frac{\sum_{m=0}^{X-1}\sum_{n=0}^{Y-1}(I(m,n) - I'(m,n))^2}{L}, \tag{8.3}$$

where Φ represents embedding distortion rate, I and I' are the original and watermarked image, respectively with dimension $X \times Y$ and L is the number of watermark bits embedded, e.g. data capacity. The traditional distortion metric *PSNR* vs newly proposed Φ graphs are shown in Section 8.3.

8.2.1.3 Extraction and Authentication

A universal blind extractor is proposed for watermark extraction and authentication process. The wavelet coefficients are generated after forward transform on the test image / video followed by the tree formation process as in embedding. Based on the

recovered tree structure, symbols are re-generated to decide on a 0 or 1 watermark extraction. The extracted watermark is then authenticated by comparing with the original watermark. The authentication is done by measuring the similarity correlation or the Hamming distance (Bit Error Rate) as described in Eq. (4.2) and Eq. (4.1), respectively.

8.2.2 Scalable watermark system design

At this point we define the watermarking scalability, independent of the host image / video coding-decoding schemes. The scalability here refers to embed the watermarks in a hierarchical fashion in such a way that more embedding information leads to better robustness. In the proposed algorithm, the symbols in Table 8.1 can be ranked based on improved associated robustness. The MSB in the binary tree corresponds to coarse-grained quantization index whereas LSB represents fine-grained quantization index. It is evident that to extract the watermark bit successfully, all three MSB of any binary tree must be unaltered in case of WO, CO or WZ, CZ, whereas only two most significant bit is required to be preserved for EO or EZ. Therefore two consecutive 0s (EZ) or 1s (EO) provides strongest association with 0 or 1, respectively and so the robustness. On the other hand WO, CO and WZ, CZ offers same level of robustness and hence the robustness rank of the symbols can be defined as $EO > CO, WO$ and $EZ > CZ, WZ$. At the same time we can measure the collective embedding distortion rate as in Eq. (8.3). In this section we exploit these two property of the algorithm to design the scalable watermarking concept. The complete process is divided into three separate modules: 1) Encoding module, 2) Embedded watermarking module and 3) Extractor module.

8.2.2.1 Encoding module

The main functionality of this module is to generate a hierarchical embedded code-stream. The example scalable system model is shown in Figure 8.4. The sequential activities within the encoding module can be described in the following steps:

Step 1 (Tree formation): Binary trees are formed using the proposed algorithm for each selected coefficient to be watermarked. Every tree is now assigned a symbol according to Table 8.1.

Step 2 (Main pass): In step 2, based on the input watermark stream, we alter the trees

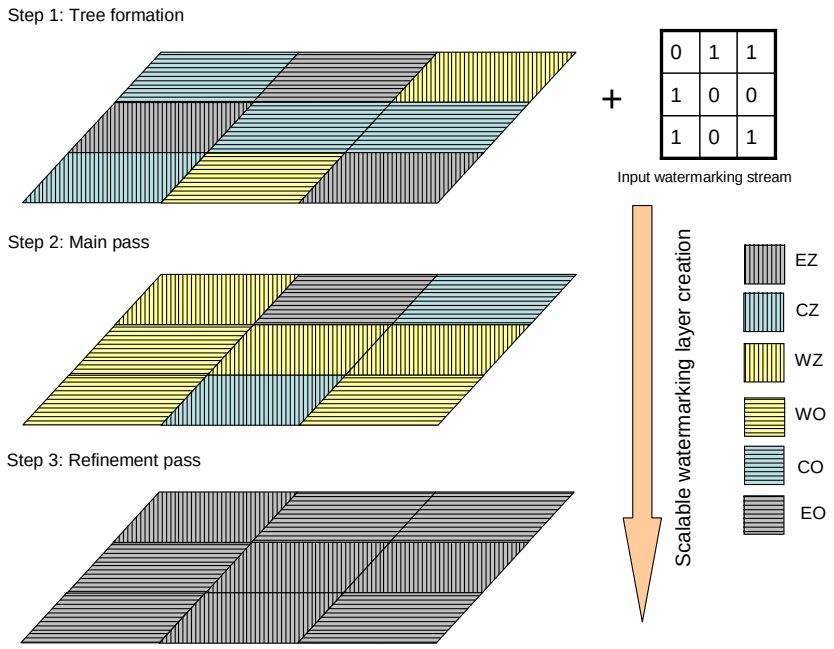

Figure 8.4: Proposed scalable watermarking layer creation.

to create right association as described in Figure 8.3 and hence all selected coefficients are rightly associated at least with basic WZ/WO symbol and thus we comfortably name it as *base layer*. The embedding distortion is calculated progressively at individual tree level.

Step 3 (Refinement pass): The main aim of the refinement passes are to increase the watermarking strength progressively to increase the robustness. The base layer provides basic minimum association with watermark bits and in this refinement pass, the watermarking strength is increased by modifying the symbols and corresponding tree to the next available level i.e. $WZ \rightarrow EZ, CZ \rightarrow EZ, WO \rightarrow EO \& CO \rightarrow EO$ as shown in the state machine diagram in Figure 8.3. At the end of this pass, all trees are modified and associated with the strongest watermark embedding EZ/EO. Similar to previous step the distortion is calculated as refinement level progresses.

Step 4 (Hierarchical atom and code-stream generation): During 2 different passes, the binary trees are modified according to the input watermark association and progressive embedding distortion is calculated at each individual tree. Here we define these individual trees or a group of trees as an *atom*. Each *atom* contains two pieces of information: 1) embedding distortion rate and 2) modified tree values. Now a code-stream is generated by concatenating these atoms as shown in Figure 8.5. One set of header information is also included in the beginning of the stream to identify the input parameters such as wavelet kernel, number of decomposition levels, depth of the binary

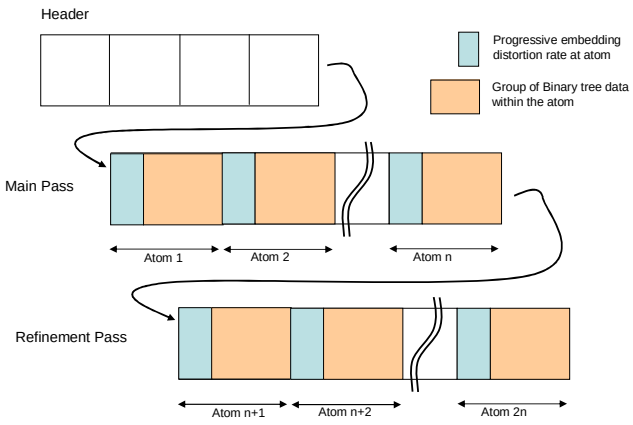

Figure 8.5: Code-stream generation.

tree etc.

8.2.2.2 Embedded watermarking module

The embedded watermarking module truncates the code-stream at any distortion-robustness atom level to generate the watermarked image with the desired distortion-robustness requirements. Inclusion of more atoms before truncation increases the robustness of the watermarked image but consumes greater embedding-distortion rate. The coed-stream truncation at atom level provides flexibility towards watermarking scalability. The truncated code-stream is then de-quantized to reconstruct the watermarked coefficients. An inverse transform on these coefficients generates the required watermarked image / video.

8.2.2.3 Extractor module

The extractor module consists of a universal blind extractor similar to the one described in Section 8.2.1.3. Any attacked or compressed test image / video is passed to this module for watermark extraction and authentication. During the extraction, forward transform is applied on the test image / video and the coefficients are used to form the binary tree. Based on the rules, stated in Table 8.1, each tree is then assigned to a symbol and corresponding association. The association of 0 or 1 indicates the extracted watermark value. The extracted watermark bits are then authenticated using a similarity correlation or Hamming distance.

The feasibility verification of this scalable watermarking concept is described in experimental results section.

8.2.3 Effect of bit plane discarding

To improve the robustness against quality scalable compression, at this point we incorporate the bit plane discarding model within the proposed algorithm by restricting the initial quantizer (λ) value to the integer power of two. Therefore the quantization cluster in tree formation (Section 8.2.1) can now alternatively described as bit plane cluster. Due to the bit plane based clustering in binary tree formation, every value in the binary tree corresponds to the bit planes of any selected coefficient. Therefore based on the depth parameter in the embedding algorithm, the selected coefficient can retain the watermark even after bit plane discarding. In this subsection we discuss the effect of bit plane discarding on extracting the watermark information.

Assuming C' and $\widehat{C}'$ as the watermarked coefficient before and after bit plane discarding, respectively, we shall examine the effect of N bit plane discarding on every bits of in the binary tree during the watermark extraction. Considering initial $\lambda = 2^M$, where M corresponds to the depth of the tree, at the extractor, using Eq. (8.1) the bit (b_i) in the binary tree can be calculated as:

$$\begin{aligned} b_i &= \left\lfloor \frac{|C'|}{2^M} \right\rfloor \%2, \\ &= k_1 \%2, \end{aligned} \tag{8.4}$$

where k_1 is the cluster index as shown in Figure 8.6. Now, using the bit plane discarding model in Section 6.2, the watermarked coefficients C' are quantized and mapped to center value $\widehat{C}'_k$ within a bit plane cluster with an index value of k_2 as shown in Figure 8.6. At this point we consider following three cases to investigate the effect of this quantization and de-quantization process:

Case 1 ($M > N$): In this case the binary tree cluster ($\lambda = 2^M$) is bigger than the bit plane discarding cluster. Hence for any bit plane discarding where $M > N$, $\widehat{C}'_k$ value remains within the binary tree cluster, $k.2^M \leq < (k+1).2^M$ as shown in Figure 8.6.a)

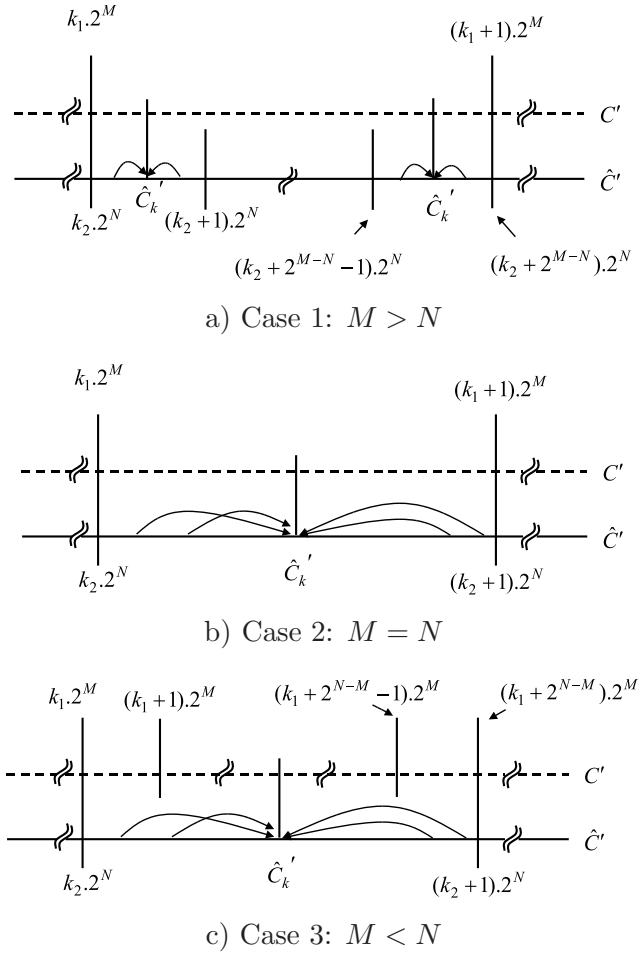

Figure 8.6: Effect of bit plane discarding in watermark extraction; $\lambda = 2^M$ and N is the number of bit plane being discarded.

and

$$\begin{aligned} b_i &= \left\lfloor \frac{|C'|}{2^M} \right\rfloor \%2, \\ &= \left\lfloor \frac{|\widehat{C}'|}{2^M} \right\rfloor \%2, \\ &= b'_i, \end{aligned} \tag{8.5}$$

where b_i and b'_i represents the bit in binary tree, without bit plane discarding and after bit plane discarding, respectively.

Case 2 ($M = N$): This case considers the same cluster size in binary tree and the bit plane discarding, and therefore $\widehat{C}'_k$ remains in the same cluster of binary tree during watermark extraction as shown in Figure 8.6.b) and hence $b_i = b'_i$.

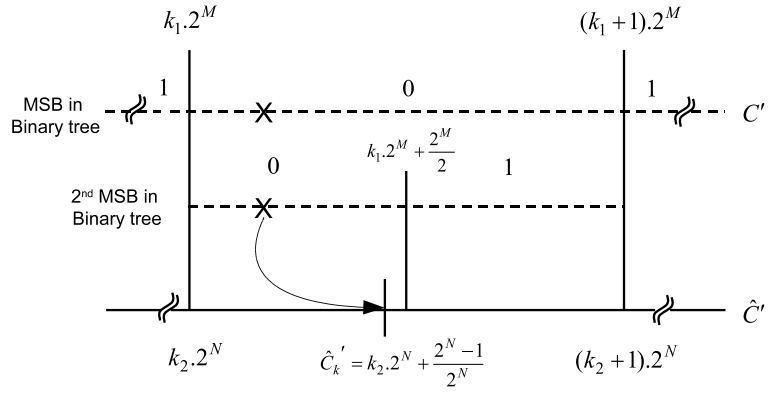

a) Case: EZ

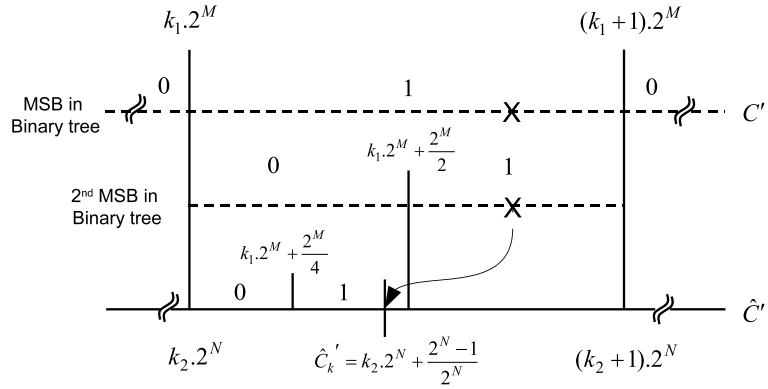

b) Case: EO

Figure 8.7: Effect of bit plane discarding in watermark extraction for special case of EZ and EO; $\lambda = 2^M$ and N is the number of bit plane being discarded.

Case 3 ($M < N$): In this scenario the number of bit planes being discarded are greater than the depth of the binary tree. Due to bit plane discarding, any watermarked coefficient (C') in the cluster ($k_2.2^N \leq C' < (k_2+1).2^N$) is mapped to the center value C'_k. In terms of the binary tree clustering this range can be defined as ($k_1.2^M \leq C' < (k_1 + 2^{(N-M)}).2^M$) where $(N-M)$ is a positive integer. Hence during watermark extraction, the index of the binary tree cluster can be changed and effectively $b_i = b'_i$ is not guaranteed.

So far we have explained the effect of bit plane discarding on individual bits of the binary tree. As the algorithm generates the watermark association symbols using the most significant three bits of the binary tree (Table 8.1) , we can define the necessary condition for the coefficients to retain the watermark as follows:

$$d \geq N + 3, \tag{8.6}$$

where d is the depth of the binary tree and N is the number of bit plane assumed to be discarded.

But, after 2nd refinement pass in the code-stream all modified coefficients are associated with either EZ and EO and in that case only most significant two bits are required to be preserved and hence when the embedding considers highest robustness criteria, Eq. (8.6) becomes:

$$d \geq N + 2. \tag{8.7}$$

However, in this case, 2nd most significant bit (MSB) in the binary tree needs not be preserved where, MSB is preserved along with the support decision from 3rd MSB, *i.e.,* EZ and EO are allowed to be extracted as CZ and CO, respectively. Now we will examine the effect of bit plane discarding in such cases when $d = N + 1$.

Case EZ:
Considering $\lambda = 2^M$, in this case after 2nd refinement pass, the coefficients (C') are associated to embedded zero (EZ→00x), *i.e.,* $k_1.2^M \leq C' < \left(k_1 + \frac{2^M}{2}\right)$ where $k_1\%2 = 0$, as shown in Figure 8.7.a). After N bit plane discarding C' is modified to the center value $\hat{C}_k = \left(k_2.2^N + \frac{2^N-1}{2}\right)$. For $M = N$ (*i.e.,* $d = N + 1$), k_2 becomes k_1 and therefore:

$$\hat{C}_k = \left(k_2.2^N + \frac{2^N-1}{2}\right) < \left(k_1.2^M + \frac{2^M}{2}\right) \Rightarrow \hat{C}_k < \left(k_1.2^M + \frac{2^M}{2}\right),$$
$$\forall \;\; k_1.2^M < \hat{C}_k < \left(k_1.2^M + \frac{2^M}{2}\right), \tag{8.8}$$

results in 2nd MSB remains 0 in the binary tree. Hence after ($d = N+1$) bit plane discarding, the coefficient association with EZ remains same and watermark information can be successfully recovered.

Case EO:
Referring Figure 8.7.b), for embedded one (EO→11x), the condition for coefficient association becomes $\left(k_1 + \frac{2^M}{2}\right) \leq C' < (k_1 + 1).2^M$ where $k_1\%2 = 1$. Similar to the previous case, after N bit plane discarding C' is modified to the center value of the corresponding cluster $\hat{C}_k = \left(k_2.2^N + \frac{2^N-1}{2}\right)$. Considering $M = N$, similar to Eq. (8.8) we can write:

$$k_1.2^M < \hat{C}_k < \left(k_1.2^M + \frac{2^M}{2}\right). \tag{8.9}$$

Therefore first two MSB of the binary tree now changed as 11x→10x. At this point we

aim to extract 3rd MSB (b') which can be retrieved as:

$$b' = \begin{cases} 0 & : \text{ if } \quad k_1.2^M \leq \hat{C}_k < \left(k_1.2^M + \frac{2^M}{4}\right), \\ 1 & : \text{ if } \quad \left(k_1.2^M + \frac{2^M}{4}\right) \leq \hat{C}_k < \left(k_1.2^M + \frac{2^M}{2}\right). \end{cases} \tag{8.10}$$

Now considering $M = N \Rightarrow \frac{2^N - 1}{2} > \frac{2^M}{4}$ and Eq. (8.9) becomes

$$\left(k_1.2^M + \frac{2^M}{4}\right) < \hat{C}_k < \left(k_1.2^M + \frac{2^M}{2}\right). \tag{8.11}$$

Combining, Eq. (8.10) and Eq. (8.11), the extracted 3rd MSB becomes $\hat{b} = 1$ and hence 11x→101. Therefore after $d = N + 1$ bit plane discarding, the coefficient association with EO becomes CO and the watermark information cam still be successfully extracted.

Combining the above mentioned cases, we can modify Eq. (8.7) and conclude that for EZ or EO the relationship between the embedding depth d and maximum number of bit plane discarding N is as follows:

$$d \geq N + 1. \tag{8.12}$$

Therefore, using the above mentioned conditions, proposed new algorithm ensures the reliable detection of watermark against quality scalable compressions which uses bit plane discarding model. We have verified these conditions using experimental simulations in Section 8.3.

8.3 Experimental results and discussion

This section provides the experimental verification of the proposed scalable watermarking scheme, for images as well as video and evaluates its robustness to scalable content adaptation attacks. As a proof of concept of the proposed scheme, firstly, we have simulated various experimental set on image watermarking and later extended it to MCTF based video watermarking.

8.3.1 Scalable watermarking for images

The experimental simulations are grouped into four sets: 1) Proof of the concept, 2) Verification of the scheme for bit plane discarding model, 3) Robustness performance against JPEG 2000 and 4) Robustness comparison with existing blind watermarking scheme. In all the experimental set, a 3 level 9/7 wavelet decomposition is performed. Then the low frequency subband has been selected to embed a binary logo based watermark. The initial quantization value λ is set to 32 resulting the tree-depth of $d = 6$. In generating the code-stream, atoms are defined by grouping every 16 consecutive binary-trees. The code-stream is generated by organizing hierarchically nested atoms, generated in 2 individual passes.

8.3.1.1 Proof of the concept

Once the code-stream is generated, set of watermarked images are produced by truncating the code-stream at different embedding-distortion rate points Φ (refer Eq. (8.3)) and the results for four test image are shown in Figure 8.8, Figure 8.9, Figure 8.10 and Figure 8.11 for *Boat*, *Barbara*, *Blackboard* and *Light House* images, respectively. As the embedding process creates hierarchical code-stream, at various Φ, watermark strength varies accordingly, *i.e.,* higher Φ corresponds to higher watermarking strength for a given data capacity. As a result with increased value of Φ high embedding distortion is introduced in the watermarked images and hence the visual image quality degrades as shown in the above mentioned figures. However with higher watermarking strength, the robustness performance improves hierarchically. The overall embedding distortion performance, measured by PSNR and the robustness performance (Hamming distance) at various Φ is shown in Figure 8.12 and Figure 8.13 for four test images. The x-axis of the graphs represents the embedding-distortion rate (Φ) and y-axis shows the related PSNR in *Row 1* and *Row 2* shows Hamming distance vs. Φ graphs.

It is evident from the results that with increasing embedding-distortion rate, *i.e.,* more watermarking strength results in a poor PSNR but offers better robustness. However a trade-off can be made based on the application scenario by selecting an optimum embedding-distortion rate to balance imperceptibility and robustness.

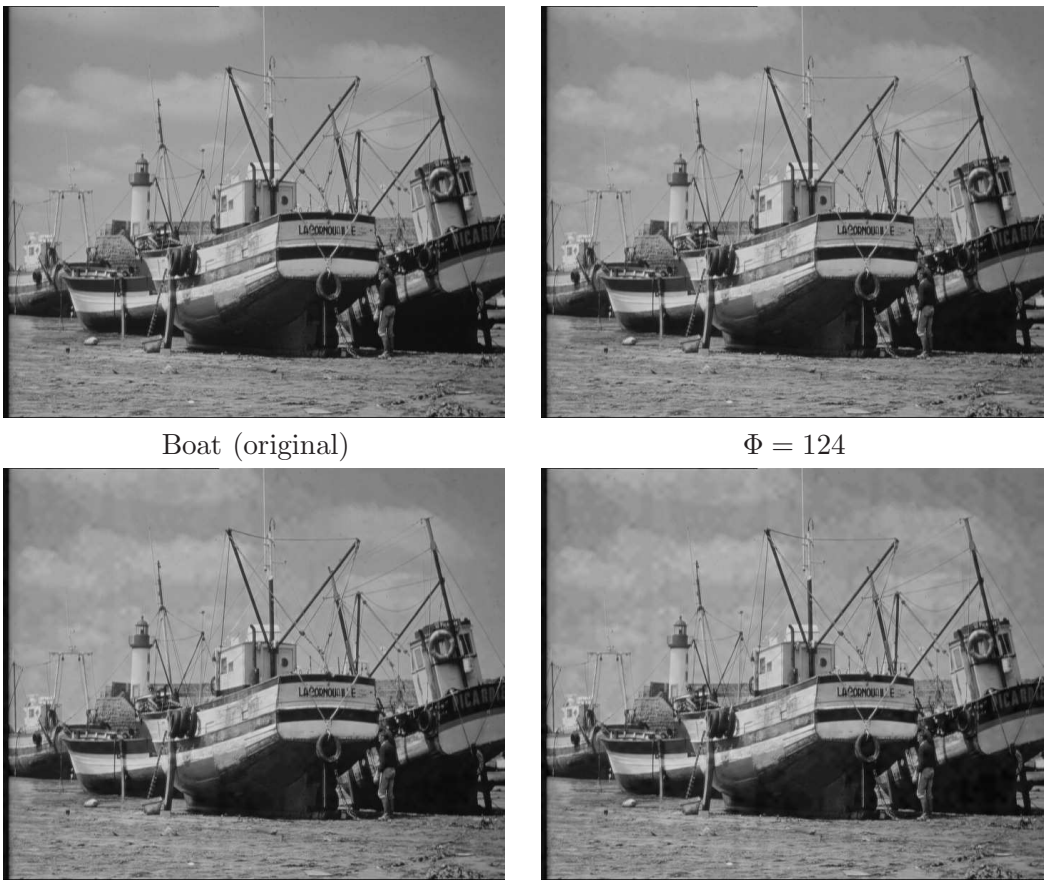

Boat (original) $\Phi = 124$

$\Phi = 867$ $\Phi = 1362$

Figure 8.8: Visual representation of watermarked images at various rate points for Boat image.

8.3.1.2 Verification of the scheme against bit plane discarding

The proposed watermarking scheme incorporates bit plane discarding model and the experimental verifications for the same are shown in Figure 8.14. The y-axis shows the robustness in terms of Hamming distance against the number of bit planes discarded (p) on the x-axis. Here different depth (d) values with minimum and maximum embedding distortion rate Φ are chosen to verify our arguments in Eq. (8.6) and Eq. (8.12). At minimum embedding rate, the condition of correct watermark extraction is given in Eq. (8.6) and the same is evident from the results shown in Figure 8.14. At maximum Φ, all coefficients are associated with EZ or EO and the necessary condition to extract watermark is discussed in Eq. (8.12), which is supported by the simulation results as shown in Figure 8.14. For example, at $d = 6$, for Φ_{min}, correct watermark extraction is possible up to $p = 3$ and for Φ_{max}, correct watermark is extracted up to $p = 5$ as shown in the said figures.

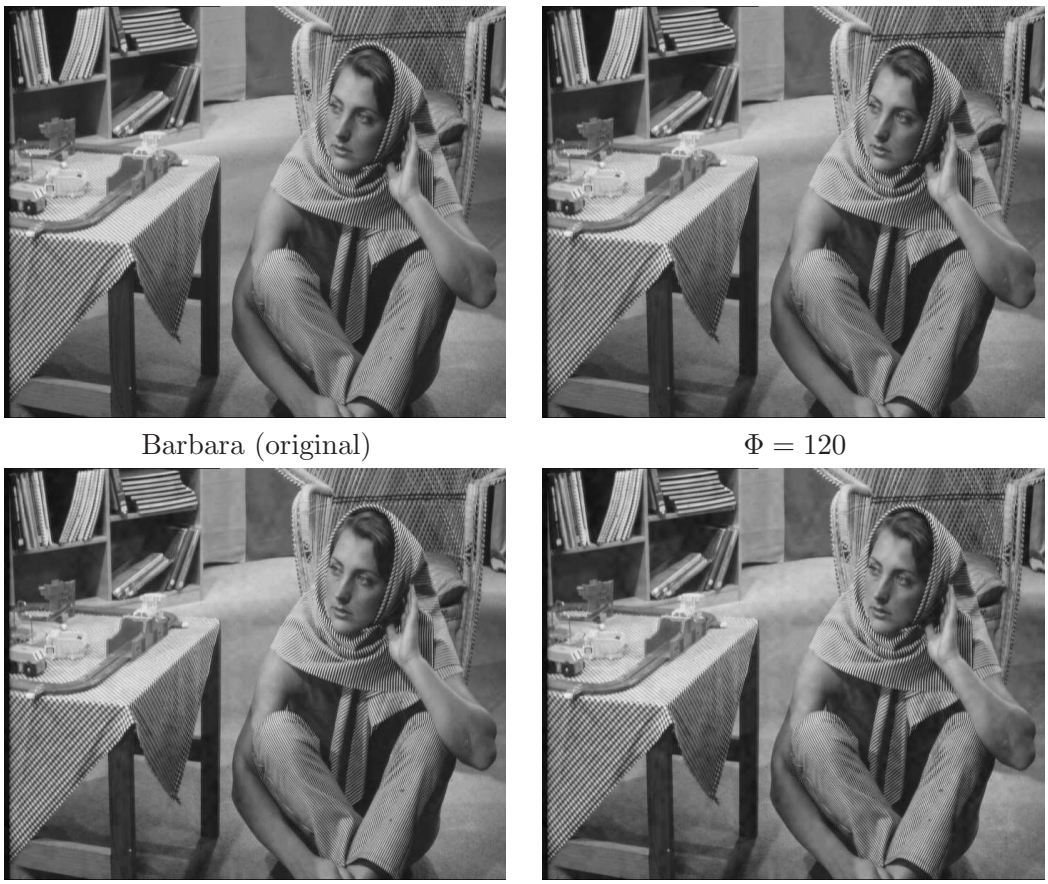

Barbara (original) $\Phi = 120$

$\Phi = 846$ $\Phi = 1330$

Figure 8.9: Visual representation of watermarked images at various rate points for Barbara image.

8.3.1.3 Robustness performance against JPEG 2000

Figure 8.15 and Figure 8.16 shows the robustness performance of the proposed watermarking scheme against JPEG 2000 scalable compression. Similar to the previous section firstly we have verified our proposed scheme's robustness against JPEG 2000 compression using different *depth* parameter d with whereas the watermark scalability at a given *depth* is shown in Figure 8.16. This results compare the robustness for various Φ for a given d. In all the figures the x-axis represents the JPEG 2000 quality compression ratio while y-axis shows the corresponding Hamming distances.

It is evident from the plots that higher depth and higher Φ in a given depth, offer higher robustness to such scalable content adaptation attacks. The watermark scalability is achieved by truncating the distortion-constrained code stream at various rate points (Φ). With increased Φ more coefficients are associated with EZ/EO and hence

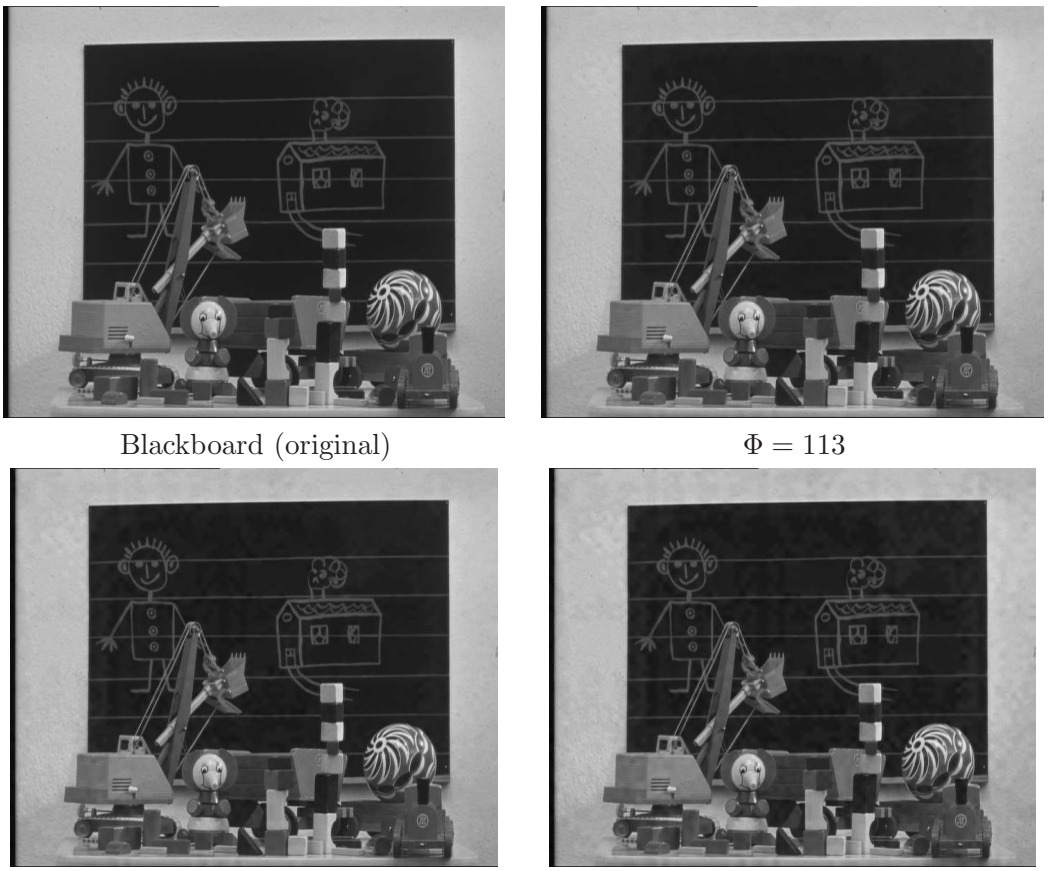

Blackboard (original) $\Phi = 113$

$\Phi = 816$ $\Phi = 1285$

Figure 8.10: Visual representation of watermarked images at various rate points for Blackboard image.

improves the robustness by successfully retaining the watermark information at higher compression rates. The results shows that more than 35% improvements in robustness is achieved when comparing two consecutive depth parameter d, whereas more than 60% improvements are reported between minimum Φ and maximum Φ at a given depth.

8.3.1.4 Robustness performance comparison with existing method

Now we compare our proposed method with the existing blind watermarking method used in this thesis. For a fair comparison, we first calculated Φ for the existing watermarking algorithm and then set the same Φ for the proposed method. The embedding performance is reported in Table 8.2 and the robustness against JPEG 2000 compression is shown in Figure 8.17.

Light House (original)

$\Phi = 121$

$\Phi = 852$

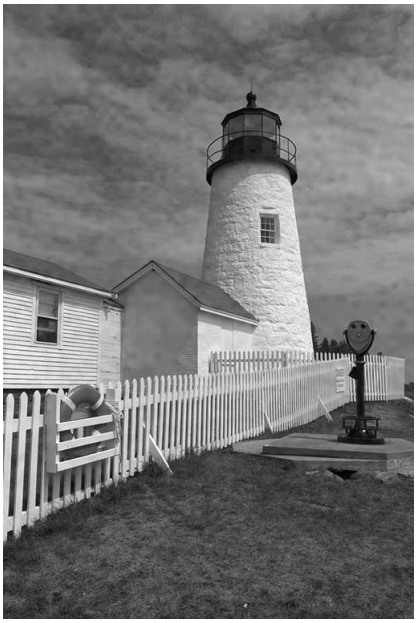

$\Phi = 1340$

Figure 8.11: Visual representation of watermarked images at various rate points for Light House image.

In embedding distortion performance comparison, at a similar embedding-distortion rate Φ, the existing method shows a better overall embedding performance PSNR. However the data capacity of the proposed algorithms are 3 times higher than the existing one. Therefore, using the new embedding-distortion metric Φ, which considers embedding distortion and data capacity into a single metric, we can fairly compare

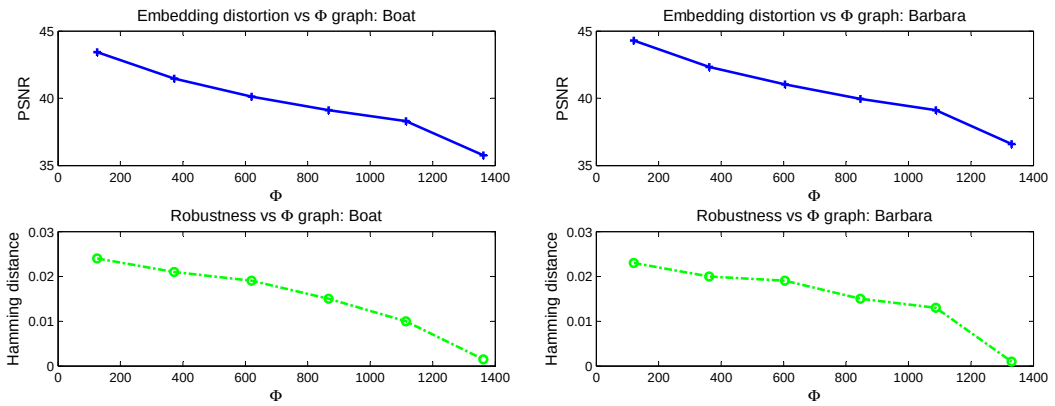

Figure 8.12: PSNR and robustness vs Φ graph. *Row 1:* Embedding distortion vs. Φ, *Row 2:* Hamming distance vs. Φ.

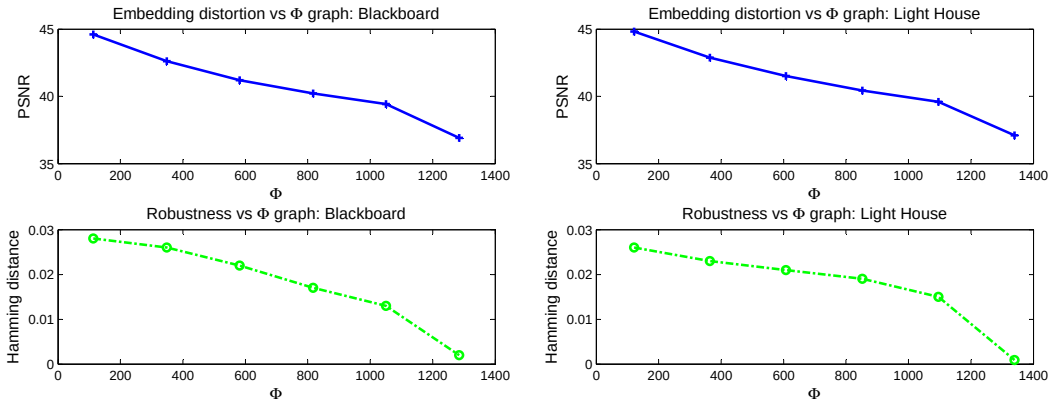

Figure 8.13: PSNR and robustness vs Φ graph. *Row 1:* Embedding distortion vs. Φ, *Row 2:* Hamming distance vs. Φ.

Table 8.2: Embedding distortion performance comparison between existing and proposed watermarking method.

	Existing algorithm			Proposed method		
	Φ	PSNR	Data Capacity	Φ	PSNR	Data Capacity
Boat	86.40	53.74	2112	84.13	47.43	6336
Barbara	80.64	55.12	2112	81.71	49.13	6336
Blackboard	69.12	56.45	2112	69.12	50.51	6336
Light House	84.48	55.36	2048	82.43	48.78	6144

the robustness performance of these two schemes and the results shows that despite of 3 times more data capacity the proposed algorithm outperforms the existing blind algorithm by an average of 20% improvement on robustness at higher compression ratio. The results also confirms that the new algorithm, based on bit plane discarding

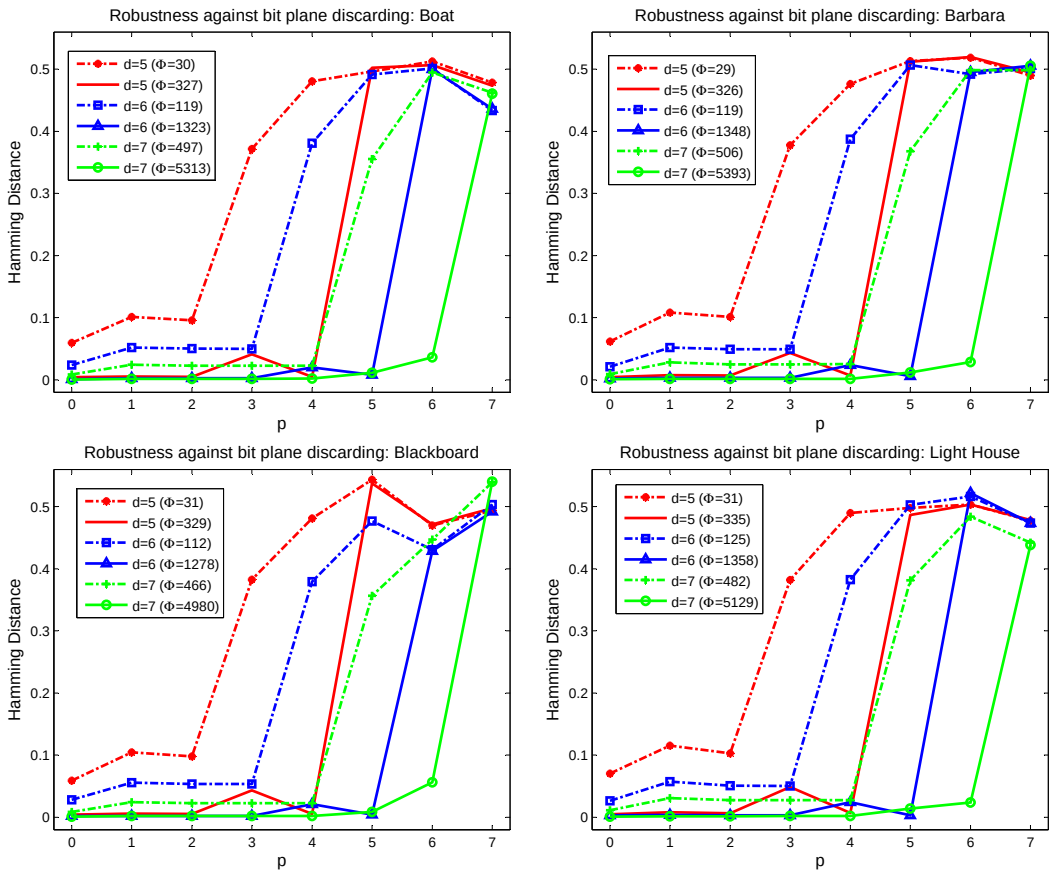

Figure 8.14: Robustness against discarding of p bit planes for various d at minimum and maximum Φ.

model, offers improvements in robustness against scalable compression over existing algorithm which does not use the model.

8.3.1.5 Application scenario of scalable watermarking

From various experimental results we can conclude that the proposed watermarking method is highly robust to scalable image compression attacks and outperforms existing methods in terms of robustness performance. At the same time it adds a new avenue to the watermarking strategies by offering flexible scalable watermarking approach. For example, to achieve the higher robustness at a high compression ratio (CR), one can choose higher Φ and the effect on embedding distortion is neutralized by compression quantization. An example is shown in Figure 8.18 for Barbara image, where we compare the embedding distortion of the watermarked image after compression. The PSNR of the watermarked and the un-watermarked images are similar at various compression

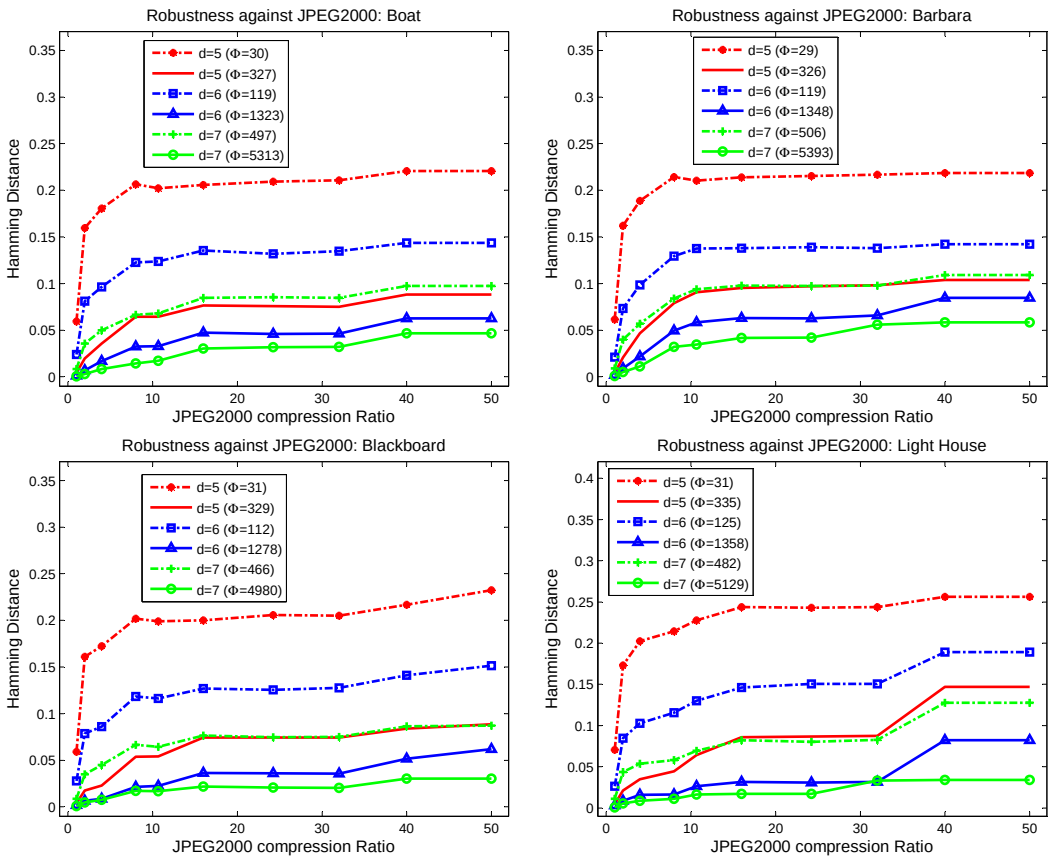

Figure 8.15: Robustness against JPEG 2000 compression for various d at minimum and maximum Φ.

points, while the watermarked image offers authenticity of the image with desired robustness, *i.e.,* Hamming distance (HD).

8.3.2 Scalable watermarking for video

In this section we have used the proposed scalable watermarking scheme for video watermarking. Here the watermarking code-stream is generated using the 2D+t+2D decomposed host video, as described in Chapter 7. In this case the binary tree is formed using the motion compensated filtered coefficients. Similar to the image watermarking of the proposed algorithm, the watermarked video is generated at a given embedding distortion rate (Φ) either at individual frame level or in every GOP. For the experimental set here we have calculated Φ for every GOP with a size of 8 frames per GOP. The watermark extraction procedure is similar to the image section. First the test video is decomposed using the 2D+t+2D frame with a blind motion estimation without any

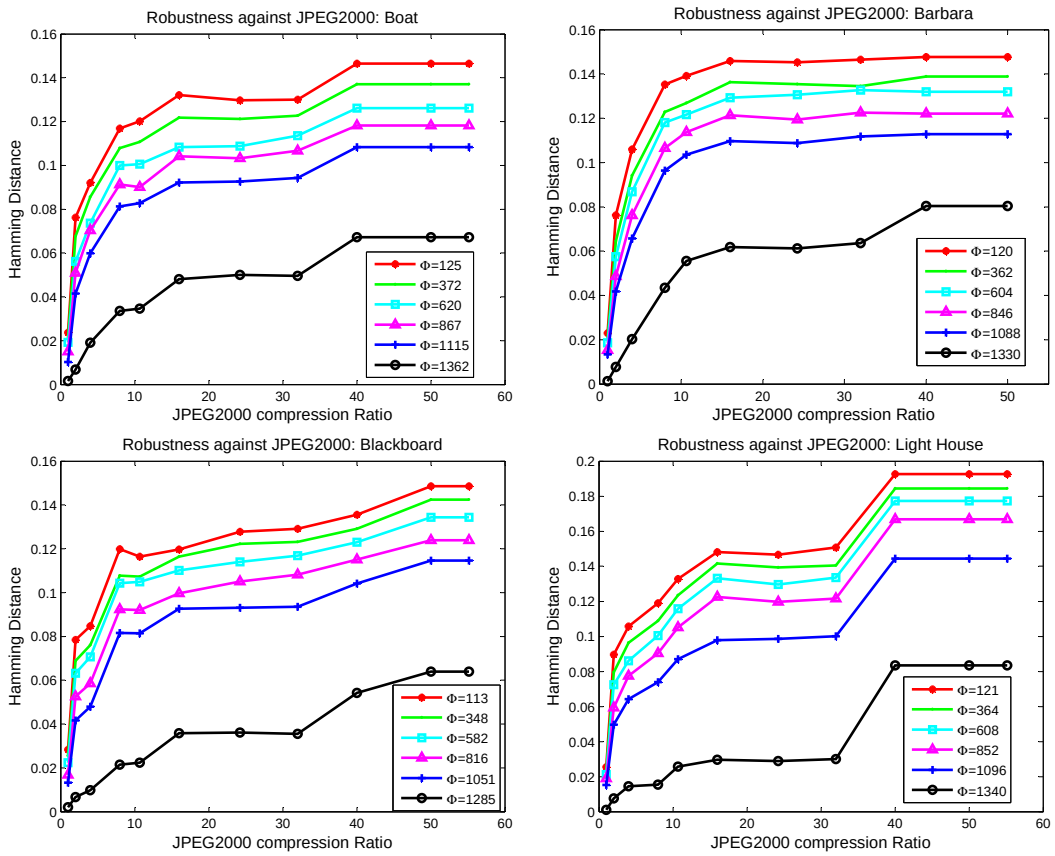

Figure 8.16: Robustness against JPEG 2000 compression for various Φ at $d = 6$.

reference to original video or motion vector and then the binary tree is formed for the selected coefficients. The watermark extraction decision is made using the association rules described in Table 8.1.

The experimental simulations here, are performed using 230 spatio-temporal subband decomposition where a 2 level 9/7 spatial decomposition is performed, followed by a 3 level MMCTF based temporal decomposition. In subband selection we used LL_s spatial subband and considered two different scenarios for temporal selection as LLL and LLH. In all the cases normalization is used during spatio-temporal decomposition. In embedding procedure, depth parameter d is set to 6 with a data capacity of 6336. The performance of the algorithm is evaluated for various Φ, by comparing the embedding distortion and robustness against scalable compressions.

The embedding distortion is measured using MSE and the results are shown in Figure 8.19 and Figure 8.20 subband for the test sequences *Crew*, *Foreman* and *News*. The x-axis represents the frame number while y-axis shows corresponding MSE. The

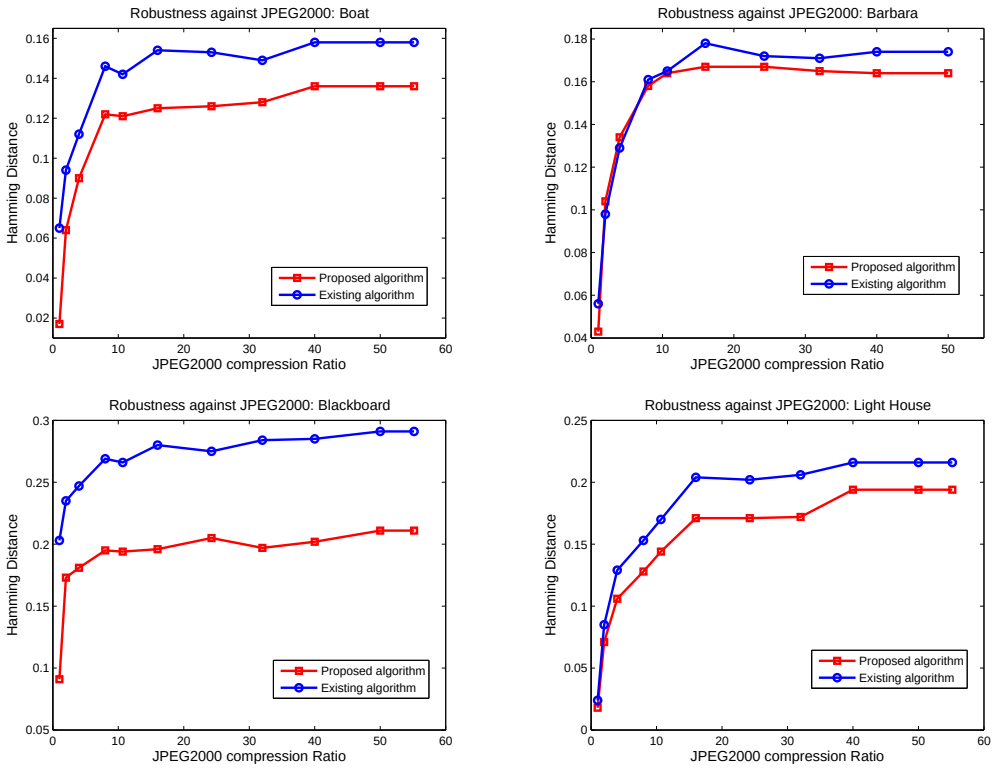

Figure 8.17: Robustness performance comparison between existing and proposed method against JPEG 2000 compression with same Φ.

robustness performance is evaluated by comparing Hamming distance against scalable compressions, *i.e.,* Motion JPEG 2000, MC-EZBC and H.264/SVC. The results are shown in Figure 8.21, Figure 8.22 and Figure 8.23 for *Crew*, *Foreman* and *News* sequences, respectively. Left hand column shows the performance for LLL subband while right hand column shows the robustness for LLL. Row 1, 2 and 3 represent the robustness performance against Motion JPEG 2000, MC-EZBC and H.264/SVC, respectively. In all the cases the x-axis shows the compression ratio / bit rates and the corresponding Hamming distances are shown in y-axis. The Hamming distances are calculated by averaging the individual frame level Hamming distances of each test sequence.

From the results it is evident that the concept of scalable watermarking is successfully realized within video watermarking framework. With the increase in embedding distortion rate Φ, the robustness performances were improved by 30% to 70% between low and high Φ, while embedding distortion is also increased with increasing Φ. Conceptually as described before, based on the end user's need, a high Φ can be chosen where high compression is expected and a low Φ can be opted for high resolution video distribution. Therefore a combined scalable watermarking and video encoding scheme

Un-watermarked: CR=2, PSNR=41.96, Φ=-, HD=-;

Watermarked: CR=2, PSNR=39.93, Φ = 120, HD=0.08;

Un-watermarked: CR=50, PSNR=21.61, Φ=-, HD=-;

Watermarked: CR=50, PSNR=21.47, Φ = 1330, HD=0.08;

Figure 8.18: Application example to use different Φ for various JPEG 2000 compression ratio to maintain embedding distortion and robustness.

can ensure secure multimedia distribution within scalable content adaptation scenario.

To conclude the discussion, we like note the limitation of this scheme. The proposed scheme does not perform well against H.264/SVC mainly due to the following reasons: 1) the proposed scheme does not follow the similar filtering and decomposition steps as in H.264/SVC coder and 2) the proposed scheme is developed on the basis of bit plane discarding model which is not followed in H.264/SVC. However for the completeness of the results we have compared the robustness performances against H.264/SVC.

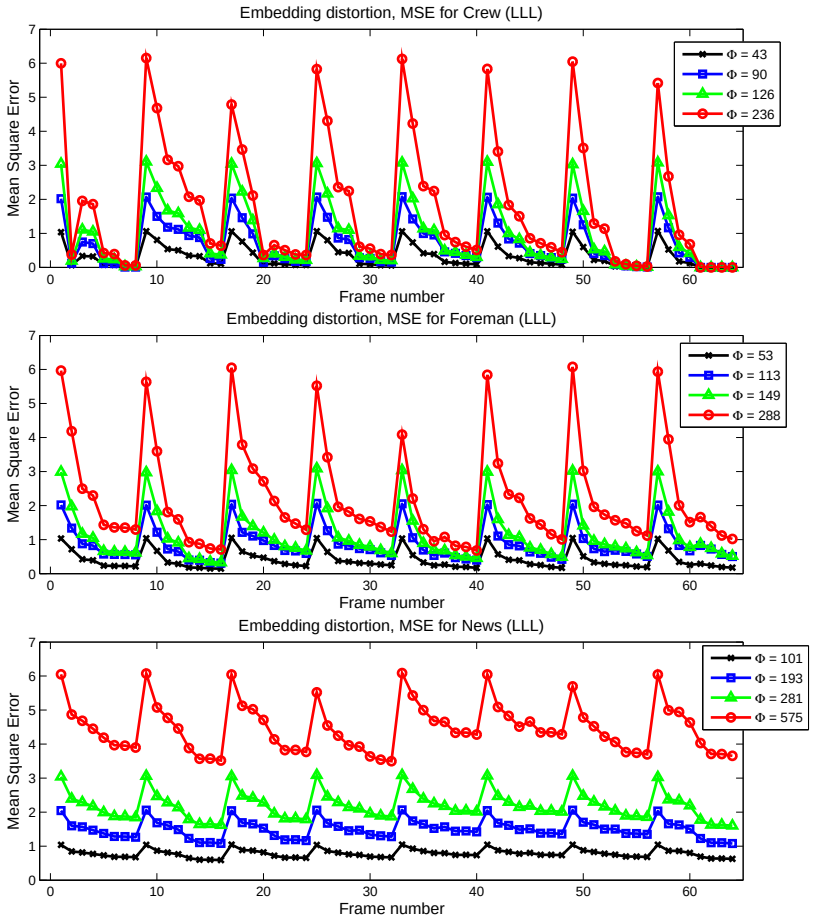

Figure 8.19: Embedding distortion performance for proposed watermarking on LLL temporal subbands for various $\Phi(d = 6)$. *Row 1), 2) & 3)* represents embedding performances for *Crew*, *Foreman* and *News* sequences, respectively.

8.4 Conclusions

In this chapter, we proposed a novel concept of scalable watermarking. Firstly a distortion constrained coed-stream is generated by concatenating hierarchically nested joint distortion robustness coding atoms. The code-stream is then truncated at various embedding-distortion rate points to create watermarked images, based on the distortion-robustness requirements. The extraction and authentication is done using a blind universal extractor. The algorithm is developed based on the bit plane discarding model and outperformed the existing blind watermarking method. The concept is experimentally verified for images and the robustness against JPEG 2000 quality scalability is tested. Finally this scheme is extended in MCTF based video watermarking scheme and the robustness is evaluated against Motion JPEG 2000, MC-EZBC and H.264/SVC. Such a scheme adds new direction in watermarking research and has many

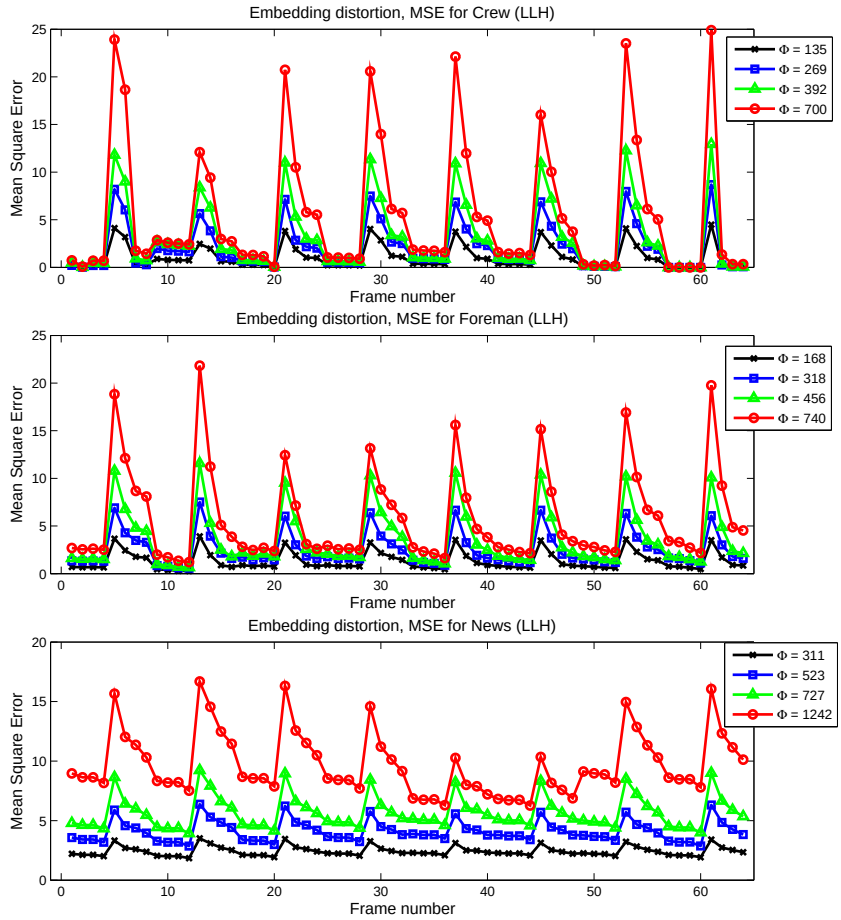

Figure 8.20: Embedding distortion performance for proposed watermarking on *LLH* temporal subbands for various Φ ($d = 6$). *Row 1), 2) & 3)* represents embedding performances for *Crew*, *Foreman* and *News* sequences, respectively.

potential watermarking applications particularly in security enabled scalable content coding.

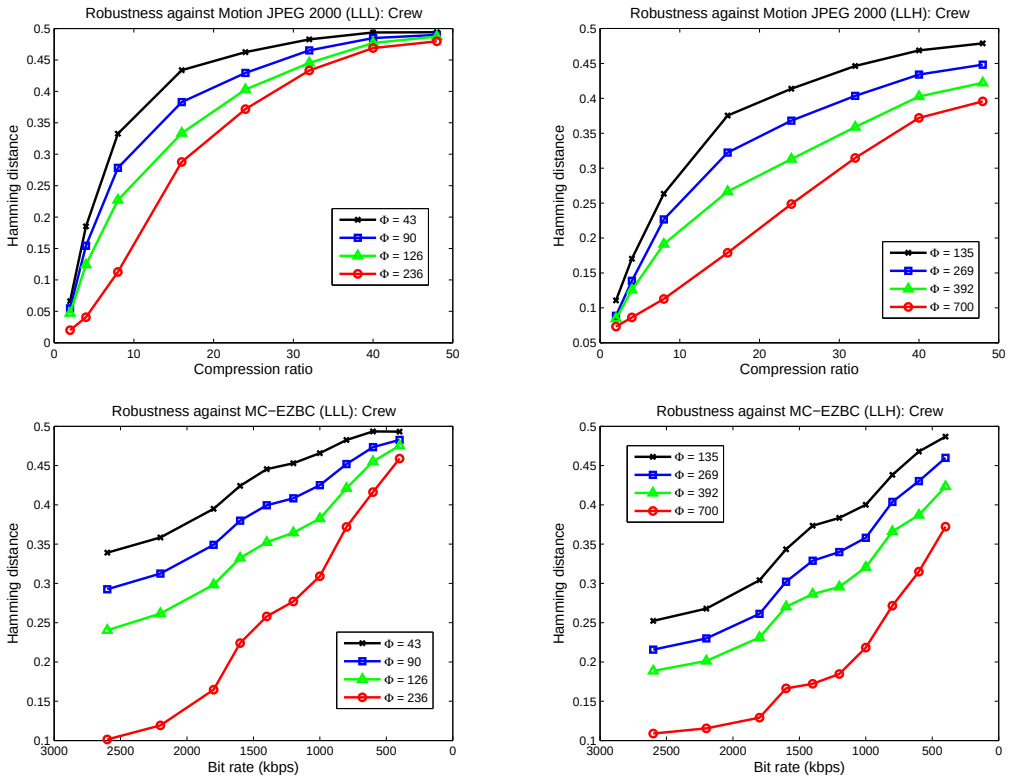

Figure 8.21: Robustness performance of proposed watermarking scheme at different Φ ($d = 6$) for *Crew* sequence. *Row 1) & 2)* show robustness against Motion JPEG 2000 and MC-EZBC, respectively. *Column 1) & 2)* represents the embedding on temporal subbands LLL & LLH, respectively.

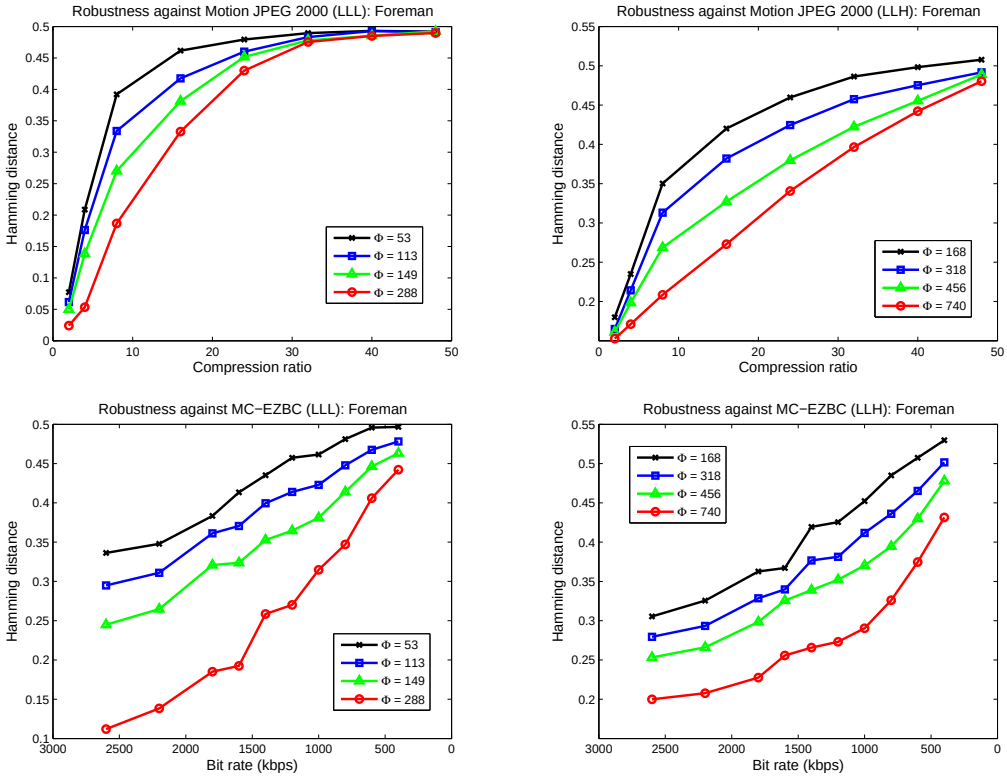

Figure 8.22: Robustness performance of proposed watermarking scheme at different Φ ($d = 6$) for *Foreman* sequence. *Row 1) & 2)* show robustness against Motion JPEG 2000 and MC-EZBC, respectively. *Column 1) & 2)* represents the embedding on temporal subbands LLL & LLH, respectively.

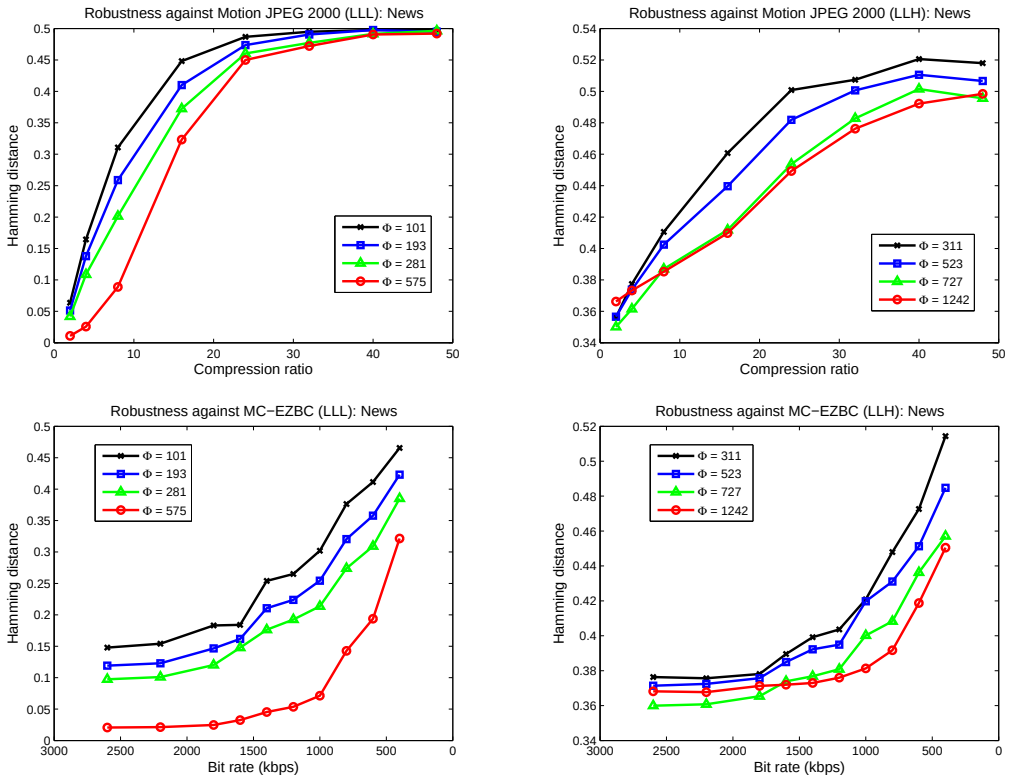

Figure 8.23: Robustness performance of proposed watermarking scheme at different Φ ($d = 6$) for *News* sequence. *Row 1) & 2)* show robustness against Motion JPEG 2000 and MC-EZBC, respectively. *Column 1) & 2)* represents the embedding on temporal subbands LLL & LLH, respectively.

Chapter 9

Conclusions and future work

The aim of this thesis was to present robust watermarking techniques for scalable coded image and video. In Section 9.1, we conclude our contributions and in Section 9.2, we suggest future research directions in this domain.

9.1 Conclusions

In order to achieve the final goal first we have generalized the image watermarking schemes related to scalable coding, *i.e.,* wavelet based algorithms. The scalable-coding based content adaptations were considered as a potential watermark attack and a content adaptation test bed framework, for evaluating the robustness of wavelet based watermarking, was presented in Chapter 4. The modular framework, Watermark Evaluation Bench for Content Adaption Modes (WEBCAM), consists of a repository of tools for emulating MPEG-21 DIA content adaptation attacks, wavelet-based watermarking, extraction and authentication. In this framework we used the parametric dissections of the wavelet based watermarking algorithms to implement the tools repository and its modular and reconfigurable wavelet-based watermarking implementation within the framework. WEBCAM provides a formal evaluation platform to compare the performances of different schemes under a controlled experimental environment for various combinations of choices for those functional submodules. It also facilitates the development of new algorithms and can also be used as an educational tool for wavelet-based watermarking algorithm design. The content adaptation tools repository provides a new set of attacks that are emerging in modern multimedia usage within the heterogeneous networks. With the use of this proposed frameworks, a comprehensive study was

carried out based on various parametric inputs such as, wavelet kernel selection, sub-band selection, embedding methods, coefficient selection etc. The robustness against scalable content adaptation was evaluated in order to identify and understand the effect of the responsible parameters.

The imperceptibility and the robustness performance are two main properties of any watermarking scheme and are complementary to each other. While focusing on robustness issues in this thesis, firstly we characterized the embedding distortion performances and categorized the responsible input parameters. In Chapter 5, a universal embedding distortion performance model was presented for wavelet based watermarking schemes. Models were proposed for orthonormal wavelet bases, which is extended to non-orthonormal wavelet kernels such as biorthogonal and non-linear wavelets. These models suggested that the MSE of the watermarked image is directly proportional to the weighted sum of energy of the modification values of the selected wavelet coefficients and this proposition is valid for orthonormal as well as non-orthonormal wavelet kernels. In the case of the non-orthonormal wavelet bases a weighting parameter is introduced and it is computed experimentally for different non-orthonormal wavelet bases whereas in the case of orthonormal wavelets, these weighting parameters are set to unity. The claims of the models were verified by extensive experimental simulations for non-blind and blind type of watermarking schemes for a wide range of wavelet kernels.

In order to propose robust watermarking techniques, in Chapter 6 we have investigated the compression process of scalable coding schemes. However within the scope of this thesis we have focused only on the quality scalability attacks. The quality scalable image coding (*i.e.,* JPEG 2000) is modeled using wavelet domain bit plane discarding to identify the effect of the quantization and de-quantization on wavelet coefficients and the data embedded within such coefficients. The relationship is then established between the watermark extraction rule, using the reconstructed coefficients, and the embedding rule, using the original coefficients, to rank the wavelet coefficients and other parameters according to their ability to retain the watermark data intact under quality scalable coding-based content adaptation. Using such relationships we have presented models for enhancing the robustness of non-blind and blind watermarking algorithms against quality scalability-based content adaptation. The proposed model for non-blind watermarking specifies the range of coefficient magnitudes that are capable of correctly extracting the embedded watermark bit under compression by considering wavelet domain bit plane discarding and ranks the coefficients accordingly. Similarly for blind algorithms, the proposed model specifies the range of magnitudes for the modified coefficient in order to extract the watermark data under compression. The simulations

showed that the proposed models outperform the robustness performance of the existing watermarking methods, where the model was not used. The high robustness of the models was experimentally verified for the JPEG 2000 quality scalability.

In the next phase of the thesis, research on video watermarking techniques were carried out. In Chapter 7, we have investigated various video watermarking schemes and proposed a novel MCTF based video decomposition architecture suitable for video watermarking techniques. The proposed scheme overcame the weaknesses (motion related flickers) of frame-by-frame video watermarking and offers improved spatio-temporal decomposition considering object motion into it. Depending on motion and texture characteristics of the video and the choice of spatial-temporal sub band for watermark embedding, MCTF has to be performed either on the spatial domain (t+2D) or in the wavelet domain (2D+t). In this work we proposed an improved video watermarking schemes by offering a generalized motion compensated 2D+t+2D framework for watermark embedding. An improved MCTF is used by modifying the MCTF update step to follow the motion trajectory in hierarchical temporal decomposition by using direct motion vector fields in the update step and implied motion vectors in the prediction step. The embedding distortion performance evaluated using both MSE and flicker difference metric showed superior performance for the MMCTF driven 2D+t+2D subband domain watermarking as opposed to frame-by-frame 2D wavelet domain watermarking which does not take motion into account. The proposed subband decomposition also provides low complexity as MCTF is performed only on subbands where the watermark is embedded. In terms of watermarking methods, we have comprehensively evaluated the performances of both non-blind and blind watermarking methods. The robustness performance against scalable coding based compressions attacks, including Motion JPEG 2000, MC-EZBC and H.264-SVC (scalable extension) were evaluated. In conclusion within the proposed 2D+t+2D filtering framework, 2D+t based video watermarking scheme outperformed conventional t+2D based watermarking schemes in a non-blind as well as a blind watermarking scenario. To offer further improvements, we have extended our robustness models for image watermarking, into the proposed video watermarking scheme, resulting in better robustness performance against various scalable compressions.

Finally, we proposed a novel concept of scalable blind image watermarking in Chapter 8. Firstly we established the concept for image watermarking and then extended the same for video watermarking. The proposed scheme generates a distortion-constrained robustness scalable watermarked media (*i.e.,* image or video) code stream which consists of hierarchically nested joint distortion-robustness coding atoms. The code stream is generated using a new wavelet domain binary tree guided rules-based blind watermark-

ing algorithm. The code stream is then truncated at any distortion-robustness atom level to generate the watermarked image / video with the desired distortion-robustness requirements. A universal blind extractor enables the extracting of watermark data from the watermarked media created using any truncated code stream. The algorithm is developed based on the bit plane discarding model and outperformed the existing blind watermarking method. The concept was experimentally verified for images and the robustness against JPEG 2000 quality scalability was tested. The scheme is further extended in MCTF based video watermarking scheme and the robustness was evaluated against Motion JPEG 2000, MC-EZBC and H.264/SVC. Such a scheme allows incorporating watermarking within scalable content coding and adds new direction in watermarking research which has many potential watermarking applications particularly in security enabled scalable media production and distribution.

9.2 Future work

The research discussed in this thesis indicates many direction to pursue further research in this domain. Here we have summarized some of them as follows:

- Modeling transmission channel related error and its effect on watermarking robustness for scalable coded media. Combining such a research with research outcomes in this thesis, can provide a complete solution to digital right management in live streaming or multimedia content sharing.
- Further improvement to WEBCAM framework to propose optimized parameter set and embedding algorithm, based on the input image or applications. This can be done by comparing the parameter sets for the given input image in order to offer best embedding performance or most robustness.
- Mathematical modeling similar to Chapter 5 between various embedding performance metrics, such as, JND, SSIM or wPSNR, and watermarking input parameters in order to obtain best parameter set which can offer improved visual quality and better robustness.
- Robust watermarking techniques for Region Of Interest (ROI) based image and video coding can provide the right balance between imperceptibility and robustness. A visual attention model based watermarking technique can be a possible way to achieve the same.
- Developing watermarking based authentication applications in JPEG 2000 streaming, *e.g.*, controlled distribution of copyrighted images to mobile, portable devices, computer

etc.

- Research on compression domain watermarking techniques for H.264/SVC. Using a similar approach presented in this thesis, a robustness model can be proposed in order to enhance the robustness against H.264/SVC based content adaptation.

- Developing real time watermarking based authentication scheme using bit stream domain watermarking for H.264/SVC etc. Such schemes are useful in multimedia content distribution including user authentication for pay-TV.

- Developing joint compression domain scalable watermarking based image and video coding schemes that offers scalability in media distribution while resolving digital right management (DRM) issues. Such an application development is possible using the scalable watermarking scheme suggested in this thesis.

Chapter 10

Appendix A

Priliminary robustness results of MCTF based video watermarking schemes against H.264-SVC scalable compression

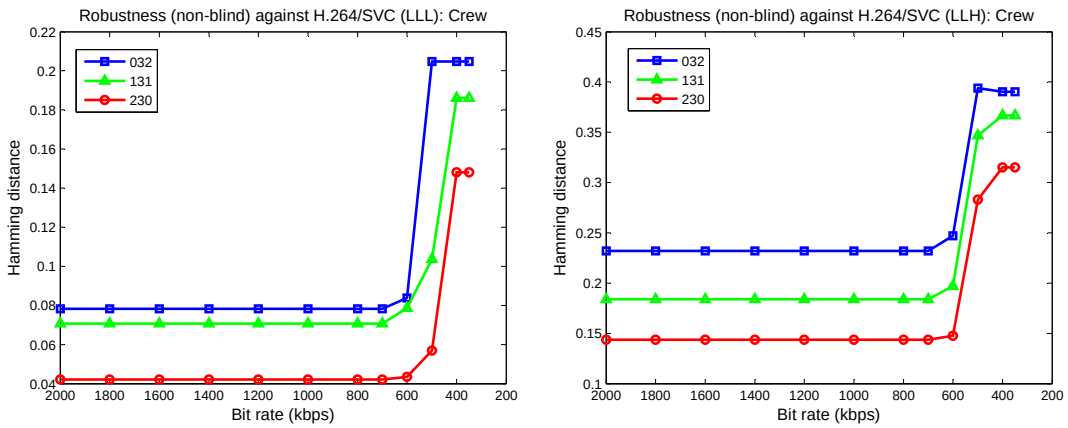

Figure 10.1: Robustness performance of non-blind watermarking scheme against H.264-SVC for *Crew* sequence. *Column 1) & 2)* represents the embedding on temporal subbands LLL & LLH, respectively.

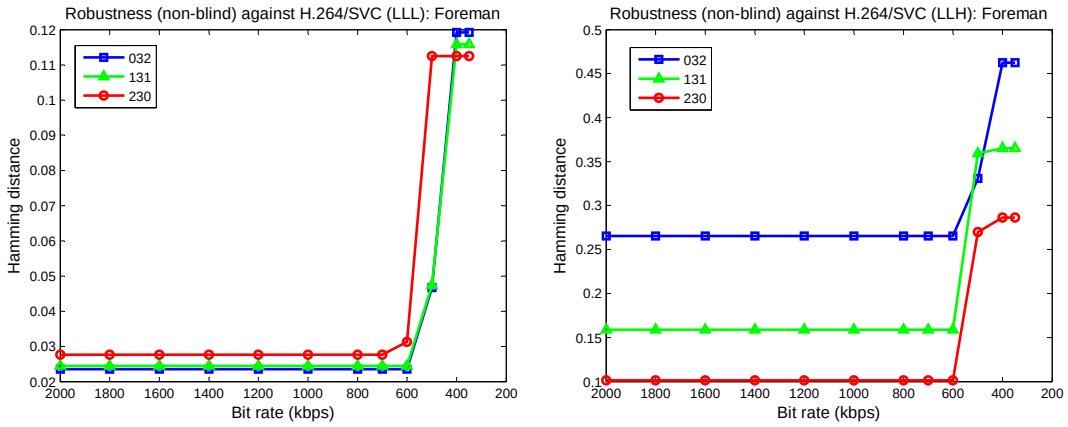

Figure 10.2: Robustness performance of non-blind watermarking scheme against H.264-SVC for *Foreman* sequence. *Column 1) & 2)* represents the embedding on temporal subbands LLL & LLH, respectively.

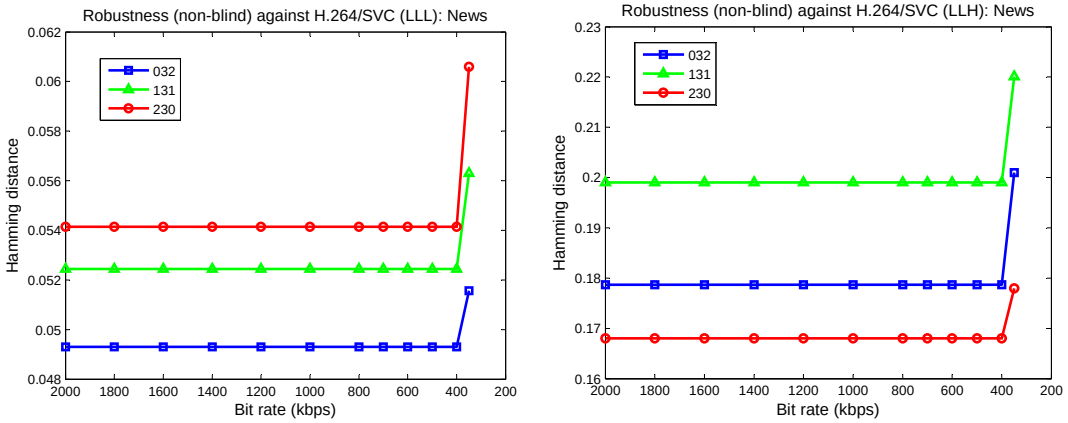

Figure 10.3: Robustness performance of non-blind watermarking scheme against H.264-SVC for *News* sequence. *Column 1) & 2)* represents the embedding on temporal subbands LLL & LLH, respectively.

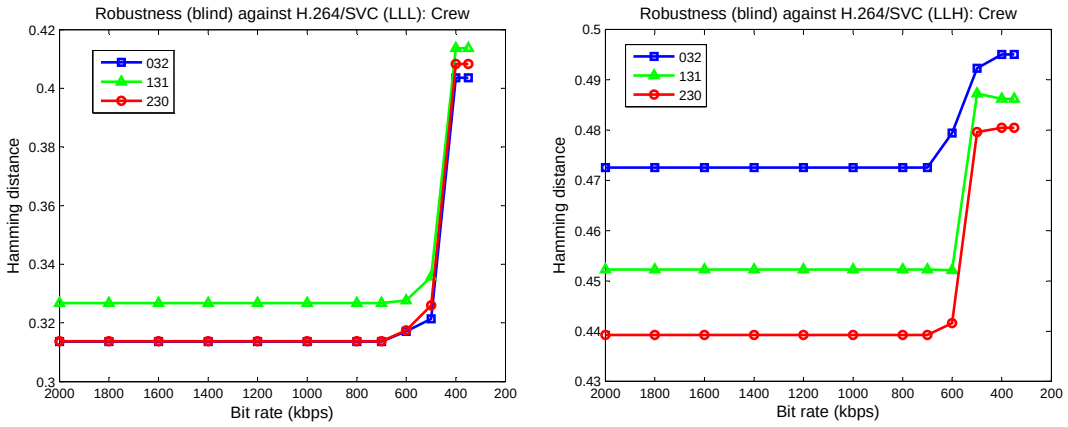

Figure 10.4: Robustness performance of blind watermarking scheme against H.264-SVC for *Crew* sequence. *Column 1) & 2)* represents the embedding on temporal subbands LLL & LLH, respectively.

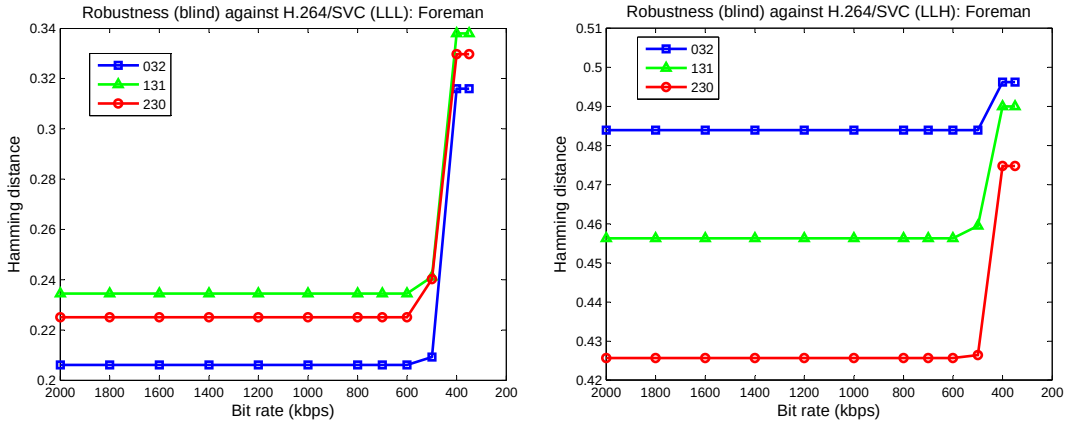

Figure 10.5: Robustness performance of blind watermarking scheme against H.264-SVC for *Foreman* sequence. *Column 1) & 2)* represents the embedding on temporal subbands LLL & LLH, respectively.

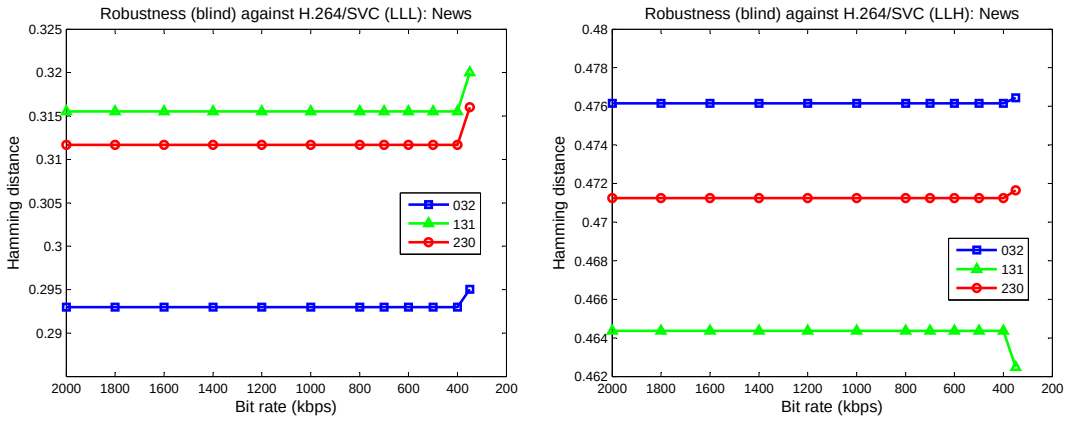

Figure 10.6: Robustness performance of blind watermarking scheme against H.264-SVC for *News* sequence. *Column 1) & 2)* represents the embedding on temporal subbands LLL & LLH, respectively.

References

[1] D. S. Taubman and M. W. Marcellin, *JPEG2000 Image Compression Fundamentals, Standards and Practice.* USA: Springer, 2002.

[2] H. Schwarz, D. Marpe, and T. Wiegand, "Overview of the scalable video coding extension of the H.264/AVC standard," *IEEE Trans. Circ. and Syst. for Video Tech*, vol. 17, no. 9, pp. 1103–1120, Sept. 2007.

[3] S. Kandadai and C. D. Creusere, "Scalable audio compression at low bitrates," *IEEE Trans. Audio, Speech, and Language Processing*, vol. 16, no. 5, pp. 969–979, July 2008.

[4] A. Vetro, "MPEG-21 digital item adaptation: enabling universal multimedia access," *IEEE Multimedia*, vol. 11, no. 1, pp. 84–87, Jan.-March 2004.

[5] L. Xie and G. R. Arce, "Joint wavelet compression and authentication watermarking," in *Proc. IEEE ICIP*, vol. 2, 1998, pp. 427–431.

[6] F. Huo and X. Gao, "A wavelet based image watermarking scheme," in *Proc. IEEE ICIP*, 2006, pp. 2573–2576.

[7] D. Kundur and D. Hatzinakos, "Digital watermarking using multiresolution wavelet decomposition," in *Proc. IEEE ICASSP*, vol. 5, 1998, pp. 2969–2972.

[8] C. Jin and J. Peng, "A robust wavelet-based blind digital watermarking algorithm," *Information Technology Journal*, vol. 5, no. 2, pp. 358–363, 2006.

[9] P. Campisi, "Video watermarking in the 3D-DWT domain using quantization-based methods," in *Proc. IEEE MMSP*, 2005, pp. 1–4.

[10] H. Tao, J. Liu, and J. Tian, "Digital watermarking technique based on integer Harr transforms and visual properties," in *Proc. SPIE Image Compression and Encryption Tech.*, vol. 4551, no. 1, 2001, pp. 239–244.

[11] X. Xia, C. G. Boncelet, and G. R. Arce, "Wavelet transform based watermark for digital images," *Optic Express*, vol. 3, no. 12, pp. 497–511, Dec. 1998.

[12] X. C. Feng and Y. Yang, "A new watermarking method based on DWT," in *Proc. Int'l Conf. on Computational Intelligence and Security, Lect. Notes in Comp. Sci. (LNCS)*, vol. 3802, 2005, pp. 1122–1126.

[13] Q. Gong and H. Shen, "Toward blind logo watermarking in JPEG-compressed images," in *Proc. Int'l Conf. on Parallel and Distributed Comp., Appl. and Tech., (PDCAT)*, 2005, pp. 1058–1062.

[14] M. Barni, F. Bartolini, and A. Piva, "Improved wavelet-based watermarking through pixel-wise masking," *IEEE Trans. Image Processing*, vol. 10, no. 5, pp. 783–791, May 2001.

[15] D. Kundur and D. Hatzinakos, "Toward robust logo watermarking using multiresolution image fusion principles," *IEEE Trans. Multimedia*, vol. 6, no. 1, pp. 185–198, Feb. 2004.

[16] Z. Zhang and Y. L. Mo, "Embedding strategy of image watermarking in wavelet transform domain," in *Proc. SPIE Image Compression and Encryption Tech.*, vol. 4551, no. 1, 2001, pp. 127–131.

[17] J. R. Kim and Y. S. Moon, "A robust wavelet-based digital watermarking using level-adaptive thresholding," in *Proc. IEEE ICIP*, vol. 2, 1999, pp. 226–230.

[18] S. Marusic, D. B. H. Tay, G. Deng, and P. Marimuthu, "A study of biorthogonal wavelets in digital watermarking," in *Proc. IEEE ICIP*, vol. 3, Sept. 2003, pp. II–463–6.

[19] T.-S. Chen, J. Chen, and J.-G. Chen, "A simple and efficient watermarking technique based on JPEG2000 codec," in *Proc. Int'l Symp. on Multimedia Software Eng.*, 2003, pp. 80–87.

[20] F. Dufaux, S. J. Wee, J. G. Apostolopoulos, and T. Ebrahimi, "JPSEC for secure imaging in JPEG2000," in *Proc. SPIE Appl. of Digital Image Processing XXVII*, vol. 5558, no. 1, 2004, pp. 319–330.

[21] Y.-S. Seo, M.-S. Kim, H.-J. Park, H.-Y. Jung, H.-Y. Chung, Y. Huh, and J.-D. Lee, "A secure watermarking for JPEG2000," in *Proc. IEEE ICIP*, vol. 2, 2001, pp. 530–533.

[22] P. Meerwald, "Quantization watermarking in the JPEG2000 coding pipeline," in *Proc. Int'l Working Conf. on Comms. and Multimedia Security*, 2001, pp. 69–79.

[23] Q. Sun and S. Chang, "A secure and robust digital signature scheme for JPEG2000 image authentication," *IEEE Trans. Multimedia*, vol. 7, no. 3, pp. 480–494, June 2005.

[24] R. Grosbois, P. Gerbelot, and T. Ebrahimi, "Authentication and access control in the JPEG2000 compressed domain," in *Proc. SPIE Appl. of Digital Image Processing XXIV*, vol. 4472, no. 1, 2001, pp. 95–104.

[25] M. A. Suhail, M. S. Obaidat, S. S. Ipson, and B. Sadoun, "A comparative study of digital watermarking in JPEG and JPEG2000 environments," *Information Sciences*, vol. 151, pp. 93–105, 2003.

[26] R. Grosbois and T. Ebrahimi, "Watermarking in the JPEG 2000 domain," in *Proc. IEEE MMSP*, 2001, pp. 339 –344.

[27] F. Hartung and B. Girod, "Watermarking of uncompressed and compressed video," *Signal Processing*, vol. 66, no. 3, pp. 283–301, 1998.

[28] G. Dorr and J.-L. Dugelay, "A guide tour of video watermarking," *Signal Processing: Image Communication*, vol. 18, no. 4, pp. 263–282, 2003.

[29] W. Zhu, Z. Xiong, and Y.-Q. Zhang, "Multiresolution watermarking for images and video," *IEEE Trans. Circ. and Syst. for Video Tech*, vol. 9, no. 4, pp. 545–550, Jun 1999.

[30] I. J. Cox, J. Kilian, F. T. Leighton, and T. Shamoon, "Secure spread spectrum watermarking for multimedia," *IEEE Trans. Image Processing*, vol. 6, no. 12, pp. 1673–1687, Dec. 1997.

[31] Y. Li, X. Gao, and J. Hongbing, "A 3D wavelet based spatial-temporal approach for video watermarking," in *Proc. IEEE Int'l Conf. on Comput. Intelligence and Multimedia App. (ICCIMA)*, 2003, pp. 260–265.

[32] S.-J. Kim, S.-H. Lee, K.-S. Moon, W.-H. Cho, I.-T. Lim, K.-R. Kwon, and K.-I. Lee, "A new digital video watermarking using the dual watermark images and 3D DWT," in *Proc. IEEE Region 10 TENCON*, vol. 1, 2004, pp. 291–294.

[33] S. Choi and J. W. Woods, "Motion-compensated 3-D subband coding of video," *IEEE Trans. Image Processing*, vol. 8, no. 2, pp. 155–167, Feb. 1999.

[34] T. P.-C. Chen and T. Chen, "Progressive image watermarking," in *Proc. IEEE ICME*, vol. 2, 2000, pp. 1025 –1028.

[35] P.-C. Su, H.-J. M. Wang, and C.-C. J. Kuo, "An integrated approach to image watermarking and JPEG-2000 compression," *The Journal of VLSI Signal Processing*, vol. 27, no. 1, pp. 35–53, Feb. 2001.

[36] D. Bhowmik and C. Abhayaratne, "The effect of quality scalable image compression on robust watermarking," in *Proc. Int'l Workshop on Digital Signal Processing*, 2009, pp. 1–8.

[37] P. Meerwald and A. Uhl, "Scalability evaluation of blind spread-spectrum image watermarking," in *Proc. Int'l Workshop on Digital Watermarking (IWDW '08), Lect. Notes in Comp. Sci. (LNCS)*, vol. 5450, 2008, pp. 61–75.

[38] A. Piper, R. Safavi-Naini, and A. Mertins, "Resolution and quality scalable spread spectrum image watermarking," in *Proc. 7th workshop on Multimedia and Security: MM&Sec'05*, 2005, pp. 79–90.

[39] N. Sprljan, M. Mrak, G. C. K. Abhayaratne, and E. Izquierdo, "A scalable coding framework for efficient video adaptation," in *Proc. Int'l Workshop on Image Analysis for Multimedia Interactive Services (WIAMIS)*, 2005.

[40] I. J. Cox, M. L. Miller, and J. A. Bloom, *Digital watermarking*. San Francisco, CA, USA: Morgan Kaufmann Publishers Inc., 2002.

[41] M. Barni and F. Bartolini, *Watermarking Systems Engineering (Signal Processing and Communications, 21)*. Boca Raton, FL, USA: CRC Press, Inc., 2004.

[42] S. P. Mohanty, "Digital watermarking : A tutorial review," Available: http://www.cse.unt.edu/ smohanty/research/OtherPublications/MohantyWatermarkingSurvey1999.pdf [Accessed: Apr. 2010]., University of North Texas, Texas, USA, Tech. Rep., 1999.

[43] J. Fridrich, M. Goljan, and A. C. Baldoza, "New fragile authentication watermark for images," in *Proc. IEEE ICIP*, vol. 1, 2000, pp. 446 –449.

[44] C. Y. Lin and S. F. Chang, "Semifragile watermarking for authenticating JPEG visual content," in *Proc. SPIE Security, Steganography, and Watermarking of Multimedia Contents*, vol. 3971, no. 1, 2000, pp. 140–151.

[45] M. Barni, F. Bartolini, and T. Furon, "A general framework for robust watermarking security," *Signal Processing*, vol. 83, pp. 2069–2084, Oct. 2003.

[46] F. Cayre, C. Fontaine, and T. Furon, "Watermarking security: theory and practice," *IEEE Trans. Signal Processing*, vol. 53, no. 10, pp. 3976 – 3987, Oct. 2005.

[47] A. Adelsbach, S. Katzenbeisser, and A. R. Sadeghi, "Cryptography meets watermarking: Detecting watermarks with minimal or zero knowledge disclosure," in *Proc. European Signal Processing Conference (EUSIPCO)*, vol. 1, 2004, pp. 446–449.

[48] O. Kwon and C. Lee, "Objective method for assessment of video quality using wavelets," in *Proc. IEEE Int'l Symp. on Industrial Electronics (ISIE 2001).*, vol. 1, 2001, pp. 292–295.

[49] Z. Wang, A. C. Bovik, H. R. Sheikh, and E. P. Simoncelli, "Image quality assessment: from error visibility to structural similarity," *IEEE Trans. Image Processing*, vol. 13, no. 4, pp. 600–612, April 2004.

[50] A. B. Watson, "Visual optimization of DCT quantization matrices for individual images," in *Proc. American Institute of Aeronautics and Astronautics (AIAA) Computing in Aerospace*, vol. 9, 1993, pp. 286–291.

[51] H. G. Koumaras, "Subjective video quality assessment methods for multimedia applications," Geneva, Switzerland, Tech. Rep. ITU-R BT.500-11, april 2008.

[52] M. Ramkumar, A. N. Akansu, and A. A. Alatan, "A robust data hiding scheme for image using DFT," in *Proc. IEEE ICIP*, 1999, pp. 211–215.

[53] J. L. Dugelay and S. Roche, "Fractal transform based large digital watermark embedding and robust full blind extraction," in *Proc. IEEE int'l conf. on Multimedia & Computing Systems (ICMCS)*, vol. 2, 1999, pp. 1003–1004.

[54] A. Bors and I. Pitas, "Image watermarking using DCT domain constraints," in *Proc. IEEE ICIP*, 1996, pp. 231–234.

[55] M. A. Suhail and M. S. Obaidat, "Digital watermarking-based DCT and JPEG model," *IEEE transactions on instrumentation and measurement*, vol. 52, no. 5, pp. 1640–1647, Oct 2003.

[56] J. R. Hernandez, M. Amado, and F. Perez-Gonzalez, "DCT-domain watermarking techniques for still images: detector performance analysis and a new structure," *IEEE Trans. Image Processing*, vol. 9, no. 1, pp. 55 –68, jan 2000.

[57] P. Vinod and P. K. Bora, "Motion-compensated inter-frame collusion attack on video watermarking and a countermeasure," *IEE Proceedings on Information Security*, vol. 153, no. 2, pp. 61 – 73, June 2006.

[58] G. Strang and T. Nguyen, *Wavelets and Filter Banks*, 2nd ed. USA: Wellesley-CambridgePress, 1997.

[59] M. Vetterli and J. Kovačevic, *Wavelets and subband coding.* Upper Saddle River, NJ, USA: Prentice-Hall, Inc., 1995.

[60] I. Daubechies and W. Sweldens, "Factoring wavelet transforms into lifting steps," *Journal of Fourier Anal. Appl.*, vol. 4, no. 3, pp. 245–267, 1998.

[61] H. Heijmans and J. Goutsias, "Nonlinear multiresolution signal decomposition schemes: Part II: Morphological wavelets," *IEEE Trans. Image Processing*, vol. 9, no. 11, pp. 1897–1913, Nov. 2000.

[62] F. J. Hampson and J.-C. Pesquet, "A nonlinear subband decomposition with perfect reconstruction," in *Proc. IEEE ICASSP*, vol. 3, 1996, pp. 1523–1526.

[63] G. C. K. Abhayaratne and H. Heijmans, "A novel morphological subband decomposition scheme for 2D+t wavelet video coding," in *Proc. Int'l Symp. on Image and Signal Processing and Analysis*, vol. 1, 2003, pp. 239–244.

[64] J.-R. Ohm, "Three-dimensional subband coding with motion compensation," *IEEE Trans. Image Processing*, vol. 3, no. 5, pp. 559 –571, Sep. 1994.

[65] P. Campisi, A. Neri, and M. Visconti, "Wavelet-based method for high-frequency subband watermark embedding," in *Proc. SPIE Multimedia Sys. and Appl. III*, vol. 4209, 2001, pp. 344–353.

[66] P. Meerwald and A. Uhl, "A survey of wavelet-domain watermarking algorithms," in *Proc. SPIE Security and Watermarking of Multimedia Contents III*, vol. 4314, 2001, pp. 505–516.

[67] D. Bhowmik and C. Abhayaratne, "Morphological wavelet domain image watermarking," in *Proc. European Signal Processing Conference (EUSIPCO)*, 2007, pp. 2539–2543.

[68] F. Hartung and M. Kutter, "Multimedia watermarking techniques," *Proceedings of the IEEE*, vol. 87, no. 7, pp. 1079 –1107, Jul 1999.

[69] T. Kalker, G. Depovere, J. Haitsma, and M. J. Maes, "Video watermarking system for broadcast monitoring," in *SPIE Conference Series*, vol. 3657, 1999, pp. 103–112.

[70] H. Inoue, A. Miyazaki, T. Araki, and T. Katsura, "A digital watermark method using the wavelet transform for video data," in *Proc. IEEE ISCAS*, vol. 4, Jul 1999, pp. 247–250.

[71] G. Depovere, T. Kalker, J. Haitsma, M. Maes, L. de Strycker, P. Termont, J. Vandewege, A. Langell, C. Alm, P. Norman, G. O'Reilly, B. Howes, H. Vaanholt, R. Hintzen, P. Donnelly, and A. Hudson, "The VIVA project: digital watermarking for broadcast monitoring," in *Proc. IEEE ICIP*, vol. 2, 1999, pp. 202–205.

[72] M. P. Mitrea, T. B. Zaharia, F. J. Preteux, and A. Vlad, "Video watermarking based on spread spectrum and wavelet decomposition," in *Wavelet Applications in Industrial Processing II*, vol. 5607, no. 1. SPIE, 2004, pp. 156–164.

[73] S. N. Merchant, A. Harchandani, S. Dua, H. Donde, and I. Sunesara, "Watermarking of video data using integer-to-integer discrete wavelet transform," in *Proc. IEEE TENCON*, vol. 3, 2003, pp. 939 – 943.

[74] F. Deguillaume, G. Csurka, J. J. O'Ruanaidh, and T. Pun, "Robust 3D DFT video watermarking," in *Proc. Security and Watermarking of Multimedia Contents, SPIE*, vol. 3657, no. 1, 1999, pp. 113–124.

[75] J. H. Lim, D. J. Kim, H. T. Kim, and C. S. Won, "Digital video watermarking using 3D-DCT and intracubic correlation," in *Proc. SPIE Security and Watermarking of Multimedia Contents III*, vol. 4314, no. 1, 2001, pp. 64–72.

[76] D.-W. Xu, "A blind video watermarking algorithm based on 3D wavelet transform," in *Proc. Int'l Conf. on Computational Intelligence and Security*, vol. 0, 2007, pp. 945–949.

[77] Z. Huai-yu, L. Ying, and W. Cheng-ke, "A blind spatial-temporal algorithm based on 3D wavelet for video watermarking," in *Proc. IEEE ICME*, vol. 3, 2004, pp. 1727 – 1730.

[78] P. Campisi and A. Neri, "Video watermarking in the 3D-DWT domain using perceptual masking," in *Proc. IEEE ICIP*, vol. 1, 2005, pp. 997–1000.

[79] P. Vinod, G. Doërr, and P. K. Bora, "Assessing motion-coherency in video watermarking," in *Proc. ACM Multimedia and Security*, 2006, pp. 114–119.

[80] P. Meerwald and A. Uhl, "Blind motion-compensated video watermarking," in *Proc. IEEE ICME*, 2008, pp. 357–360.

[81] K. Su, D. Kundur, and D. Hatzinakos, "Statistical invisibility for collusion-resistant digital video watermarking," *IEEE Trans. Multimedia*, vol. 7, no. 1, pp. 43 – 51, Feb 2005.

[82] S. J. Weng, T. T. Lu, and P. C. Chang, "Key-based video watermarking system on MPEG-2," in *Proc. SPIE Security and Watermarking of Multimedia Contents V*, vol. 5020, no. 1, 2003, pp. 516–525.

[83] E. Hauer and M. Steinebach, "Robust digital watermark solution for intercoded frames of MPEG video data," in *Proc. SPIE Security, Steganography, and Watermarking of Multimedia Contents VII*, vol. 5681, no. 1, 2005, pp. 381–390.

[84] Y. Y. Chung and F. F. Xu, "A secure digital watermarking scheme for MPEG-2 video copyright protection," in *Proc. IEEE Int'l Conf. on Video and Signal Based Surveillance, AVSS*, 2006, pp. 84 –84.

[85] J. Zhang, A. T. S. Ho, G. Qiu, and P. Marziliano, "Robust video watermarking of H.264/AVC," *IEEE Trans. Circuits and Systems II: Express Briefs*, vol. 54, no. 2, pp. 205–209, Feb 2007.

[86] M. Noorkami and R. M. Mersereau, "Compressed-domain video watermarking for H.264," in *Proc. IEEE ICIP*, vol. 2, 2005, pp. 890–893.

[87] G. Z. Wu, Y. J. Wang, and W. H. Hsu, "Robust watermark embedding/detection algorithm for H.264 video," *SPIE Journal of Electronic Imaging*, vol. 14, no. 1, p. 013013, 2005.

[88] F. Hartung and B. Girod, "Digital watermarking of MPEG-2 coded video in the bitstream domain," in *Proc. IEEE ICASSP*, vol. 4, 1997, pp. 2621 –2624.

[89] H. Liu, F. Shao, and J. Huang, "A MPEG-2 video watermarking algorithm with compensation in bit stream," in *Digital Rights Management. Technologies, Issues, Challenges and Systems*, ser. Lect. Notes in Comp. Sc. Springer Berlin / Heidelberg, 2006, vol. 3919, pp. 123–134.

[90] S. Biswas, S. R. Das, and E. M. Petriu, "An adaptive compressed MPEG-2 video watermarking scheme," *IEEE Trans. Instrumentation and Measurement*, vol. 54, no. 5, pp. 1853 – 1861, 2005.

[91] B. G. Mobasseri and M. P. Marcinak, "Watermarking of MPEG-2 video in compressed domain using VLC mapping," in *Proc. 7th workshop on Multimedia and Security: MM&Sec'05*, 2005, pp. 91–94.

[92] S. Sakazawa, Y. Takishima, and Y. Nakajima, "H.264 native video watermarking method," in *Proc. IEEE ISCAS*, 2006, p. 4 pp.

[93] L. Zhang, Y. Zhu, and L. M. Po, "A novel watermarking scheme with compensation in bit-stream domain for H.264/AVC," in *Proc. IEEE ICASSP*, 2010, pp. 1758 –1761.

[94] J. Zhang, J. Li, and L. Zhang, "Video watermark technique in motion vector," in *Proc. XIV Brazilian Symposium on Computer Graphics and Image Processing*, 2001, pp. 179 –182.

[95] Z. Liu, H. Liang, X. Niu, and Y. Yang, "A robust video watermarking in motion vectors," in *Proc. 7th Int'l Conf. on Signal Processing, ICSP*, vol. 3, 2004, pp. 2358 – 2361.

[96] K.-W. Kang, K. S. Moon, G. S. Jung, and J. N. Kim, "An efficient video watermarking scheme using adaptive threshold and minimum modification on motion vectors," in *Image Analysis and Recognition*, ser. Lect. Notes in Comp. Sc. Springer Berlin / Heidelberg, 2005, vol. 3656, pp. 294–301.

[97] N. Mohaghegh and O. Fatemi, "H.264 copyright protection with motion vector watermarking," in *Proc. Int'l Conf. on Audio, Language and Image Processing, ICALIP*, 2008, pp. 1384 –1389.

[98] W. Pei, Z. Zhendong, and L. Li, "A video watermarking scheme based on motion vectors and mode selection," in *Proc. Int'l Conf. on Computer Science and Software Engineering*, vol. 5, 2008, pp. 233 –237.

[99] D. Bhowmik and C. Abhayaratne, "A watermark evaluation bench for content adaptation modes," in *Proc. IET Int'l Conf. on Visual Media Production*, 2007, pp. 1–1.

[100] ——, "Evaluation of watermark robustness to JPEG2000 based content adaptation attacks," in *Proc. IET Int'l Conf. on Visual Info. Eng. (VIE '08)*, 2008, pp. 789–794.

[101] ——, "A framework for evaluating wavelet based watermarking for scalable coded digital item adaptation attacks," in *Proc. SPIE Wavelet Appl. in Industrial Processing VI*, vol. 7248, no. 1, 2009, p. 72480M (10 pages).

[102] ——. Watermarking Evaluation Bench for Content Adaptation Modes (WEBCAM). Available: http://svc.group.shef.ac.uk/webcam.html [Accessed: Jan. 2010].

[103] F. A. Petitcolas, M. Steinebach, F. Raynal, J. Dittmann, C. Fontaine, and N. Fates, "Public automated web-based evaluation service for watermarking schemes: StirMark benchmark," in *Proc. IEEE ICIP*, vol. 4314, 2001, pp. 575–584.

[104] S. Pereira, S. Voloshynovskiy, M. Madueno, S. M.-Maillet, and T. Pun, "Second generation benchmarking and application oriented evaluation," in *Proc. Int'l. Information Hiding Workshop, Lect. Notes in Comp. Sci. (LNCS)*, vol. 2137, 2001, pp. 340–353.

[105] V. Solachidis, A. Tefas, N. Nikolaidis, S. Tsekeridou, A. Nikolaidis, and I. Pitas, "A benchmarking protocol for watermarking methods," in *Proc. IEEE ICIP*, vol. 3, 2001, pp. 1023–1026.

[106] O. Guitart, H. C. Kim, and E. J. Delp-III, "Watermark evaluation testbed," *SPIE Journal of Electronic Imaging*, vol. 15, p. 041106 (13 pages), 2006.

[107] M. Ejima and A. Miyazaki, "On the evaluation of performance of digital watermarking in the frequency domain," in *Proc. IEEE ICIP*, vol. 2, 2001, pp. 546–549.

[108] T. Ebrahimi and R. Grosbois, "Secure JPEG 2000-JPSEC," in *Proc. IEEE ICASSP*, vol. 4, 2003, pp. 716–719.

[109] S.-T. Hsiang and J. W. Woods, "Embedded video coding using invertible motion compensated 3-D subband/wavelet filter bank," *Signal Processing: Image Communication*, vol. 16, pp. 705–724, May 2001.

[110] C. I. Podilchuk, N. S. Jayant, and N. Farvardin, "Three-dimensional subband coding of video," *IEEE Trans. Image Processing*, vol. 4, no. 2, pp. 125 –139, Feb. 1995.

[111] Y. Andreopoulos, A. Munteanu, J. Barbarien, M. van der Schaar, J. Cornelis, and P. Schelkens, "In-band motion compensated temporal filtering," *Signal Processing: Image Communication*, vol. 19, no. 7, pp. 653–673, Aug. 2004.

[112] V. G. MSU Graphics & Media Lab. MSU quality measurement tool. Available: http://www.compression.ru/video/ [Accessed: Jan. 15, 2010].